CONTROL STRATEGIES FOR FUNCTIONAL ELECTRICAL STIMULATION INDUCED CYCLING

Barry A. Stone

A thesis submitted for the degree of Doctor of Philosophy in Engineering

Department of Mechanical Engineering

University of Glasgow

November 2005

Abstract

Spinal Cord Injury can result in permanent loss of motor function below the lesion level. Electrical stimulation of the paralysed muscle can offer temporary restoration of muscular function. Functional Electrical Stimulation cycling ergometers and mobile cycling systems have been developed over a number of years to allow Spinal Cord Injured persons to exercise.

Standard able bodied exercise test are adapted and applied to paraplegic cyclists. A modified recumbent tricycle is instrumentated with an electric motor and sensors to measure cadence and the power produced by the cyclist at the crank. They are then integrated to a stimulator and a laptop computer. The tricycle is mounted on an indoor cycling trainer to provide a novel test bed for the implementation of exercise testing.

Controllers are desired to control cadence and power during cycling. Identification of input–output data for the cadence–motor loop and the power–stimulation loop is undertaken. Three muscle groups are stimulated on a paraplegic subject to produce power. Models are identified of the power and cadence systems. Thereafter controllers are designed, via polynomial methods. The results show that the controllers are robust during cadence tracking, power tracking and for disturbance rejection. The controllers can be accurately applied to exercise testing protocols.

The concept of $\dot{V}O_2$ control is introduced. $\dot{V}O_2$ is the rate of oxygen uptake during exercise. $\dot{V}O_2$–power dynamics are identified and as before a model is fitted to the measured data. Controllers are designed and further modified, as the understanding of the $\dot{V}O_2$ dynamics is developed. This is through a series of tests to improve the accuracy of the control. The results illustrate that $\dot{V}O_2$ control is a novel and practical application.

These findings develop the field of Functional Electrical Stimulation Induced Cycling within the laboratory. However further work is required to develop this application outside laboratory conditions.

Acknowledgements

So many people to thank! Where do I start?

Firstly, and I think most importantly, I have to my thank my subjects. These guys have given their time to travel through to Glasgow, every week, to participate in FES cycling. Many an hour we have spent in gym at the hospital together. They persevered with the project over the years, even with the tests that didn't work and the long hours of cycling, they kept coming back! I have to thank them for everything they gave, and I have to apologise for calling them subjects, as they are now good friends!

Next up, will have to be my supervisor Ken Hunt for his support and guidance over the years, and also a well aimed boot on occasion, to get me back on track. Alongside Ken, I have to thank Henrik, aka The MATLAB Oracle. I think I wore a hole in his door with the amount of times I went knocking next door to ask him a question.

Colleagues are next in the firing line. Most significantly I have to thank Sylvie (Pod). Sylvie and I shared an office for a few years, and with that she had to put up with my bad jokes and sometimes questionable choice in music. We had a great laugh and spent good times working and socialising together (more work than socialising, honestly!). Other colleagues (or should I say friends) include Calum (B*!*G), Lindsay (about time!), Chiara (nae more lifts to the hospital), Georg and Ben. They are all still at it and I wish them all the best with their future studies. Past colleagues I have also to thank are Thomas and Nils, who without I would never been able to conduct the work in my thesis. And how could I forget all the masters students who have come to visit us from Italy and Germany, I hope we showed you how good Glasgow, and Scotland is! Away from the academical colleagues, I have to thank all the staff in the Department of Mechanical Engineering who gave me support throughout my undergraduate degree and PhD. Most importantly I have to thank Elaine and Nicola, who sorted so much for us, and all the guys in the workshop.

From my colleagues within the Southern General Hospital I must thank Mr. Allan, Mr. Fraser and Dr. McLean who gave me the opportunity to work within the Spinal Unit. Also I would like to thank all the physiotherapists that supported us within the unit, in particular John and Willie.

From my family and friends outside the university circle I have to thank my folks. Mum, you can finally stop worrying that I will never get the PhD done, and dad you can now have peace and quiet from mum worrying! (that's until she finds a new topic to nag on) Also Ali, my sis, for being there in good and bad times during my PhD. My mates also have to get a special mention for giving me confidence and support through the years (Charlie (C-bhoy), Neil, Dougie (Slaps), Kez and Laura). I would also like to thank all the folks from "the pub".

A thanks to the EPSRC who funded my studies over the 3 years.

A final special thanks to Jude for always being there, and being there for years to come x.

Choose your future. Choose life... But why would I want to do a thing like that? .....Irvine Welsh 1993

Contents

List of Tables

List of Figures

List of Abbreviations

AB Able Bodied

ARW Anti Reset Wind-up

ARX AutoRegressive with eXogenous inputs

CP Critical Power

EMG Electromyography

FES Functional Electrical Stimulation

FES-LCE Functional Electrical Stimulation Leg Cycling Exercise

FNS Functional Neuromuscular Stimulation

GUI Graphical User Interface

HR Heart Rate

SCI Spinal Cord Injury

LT Lactate Threshold

PRBS Pseudo Random Binary Signal

SRM Schoberer Rad Messtechnik

PO Power Output

PID Proportional Integral Derivative

$\mathbf{P_c}$ Trainer Crank

$\mathbf{P_t}$ Trainer Power

WR Work Rate

Terms Glossary

Aerobic Having oxygen present, describes the metabolic process utilising oxygen.

Anaerobic Inadequate oxygen present, describes the metabolic process that does not use oxygen.

Breath-by-breath The expression of a particular physiological value averaged over on respiratory cycle.

Constant Load Test An exercise test in which the a constant power output is maintained by the subject.

Frequency The amount of times an event occurs per second.

Heart rate The rate at which the heart beats per minute

Incremental exercise test An exercise test designed to provide a gradational work rate to the subject.

Lactate threshold The exercise $\dot{V}O_2$ above which lactic acid concentration increases in the blood.

$\dot{V}O_2$ The amount of oxygen extracted from the inspired gas in a given time period.

$\dot{V}O_{2max}$ The maximum oxygen uptake that a subject can achieve.

$\dot{V}O_{2peak}$ The highest oxygen uptake achieved during exercise.

Steady State A characteristic of a physiological system in which the functional demands are being met such that its output per unit of time become constant.

Work A physical quantification of the force operating on a mass that causes it to change its location.

Power The rate at which work is performed.

1 Introduction

1.1 Introduction

The thesis is concerned with development of Functional Electrical Stimulation (FES) Cycling. Cycling systems are developed for specific exercise applications and recreation. A specific focus on its application to exercise testing is presented and its ability to improve the health of the Spinal Cord Injured (SCI) population. FES cycling should not be constrained to only the laboratory. An overriding aim is to make FES cycling enjoyable for the subjects.

This chapter provides a description of the key introductory topics of FES, SCI and FES cycling.

1.2 Spinal Cord Injury

Spinal Cord Injury (SCI) is one of the most serious injuries that can affect a human. Paralysis results from a lesion of the spinal cord. The number of new cases ranges from 8,000-10,000 per year in the USA and approximately 1200 within the UK [26]. There a number of causes of spinal cord injuries, with the most common being road traffic accidents, falls and sporting injuries, with the most common patients being young males.

The spinal cord is the signal pathway between the brain, the body's controller, and all the sensors and actuators within the body. The spine works as the main support for the spinal cord. The spine is composed of 33 bones called vertebrae and has 31

pairs of nerves, 40 muscles and numerous connecting tendons and ligaments running from the base of the skull to the waist [27]. Between the vertebrae are fibrous, elastic cartilage elements called discs. These discs are"shock absorbers" that keep the spine flexible and cushion the hard vertebrae during movement. Two pairs of nerve roots (fibre bundles) connect to the spinal cord at each vertebral level. Each pair consists of a sensory root (Dorsal) and a motor root (Ventral), which join to form a mixed spinal nerve. These pass through the vertebral column between the vertebrae, carrying sensory information from, and motor information to, the arms, legs and trunk. The afferent nerve pathways feed back information from the body to the brain, and efferent nerve pathways carry signals from the brain to the body.

The level of the injury determines the severity of the paralysis [28]. The spine is divided into five sections : the cervical, thoracic, lumbar, sacral and coccygeal, in order from the neck downward as shown in Figure 1.1. A spinal injury can be defined as complete or incomplete. This refers to how much function the patient has post injury. For example a patient could be motor complete and sensory incomplete, resulting in no motor function below the lesion, but they still experience some sensation.

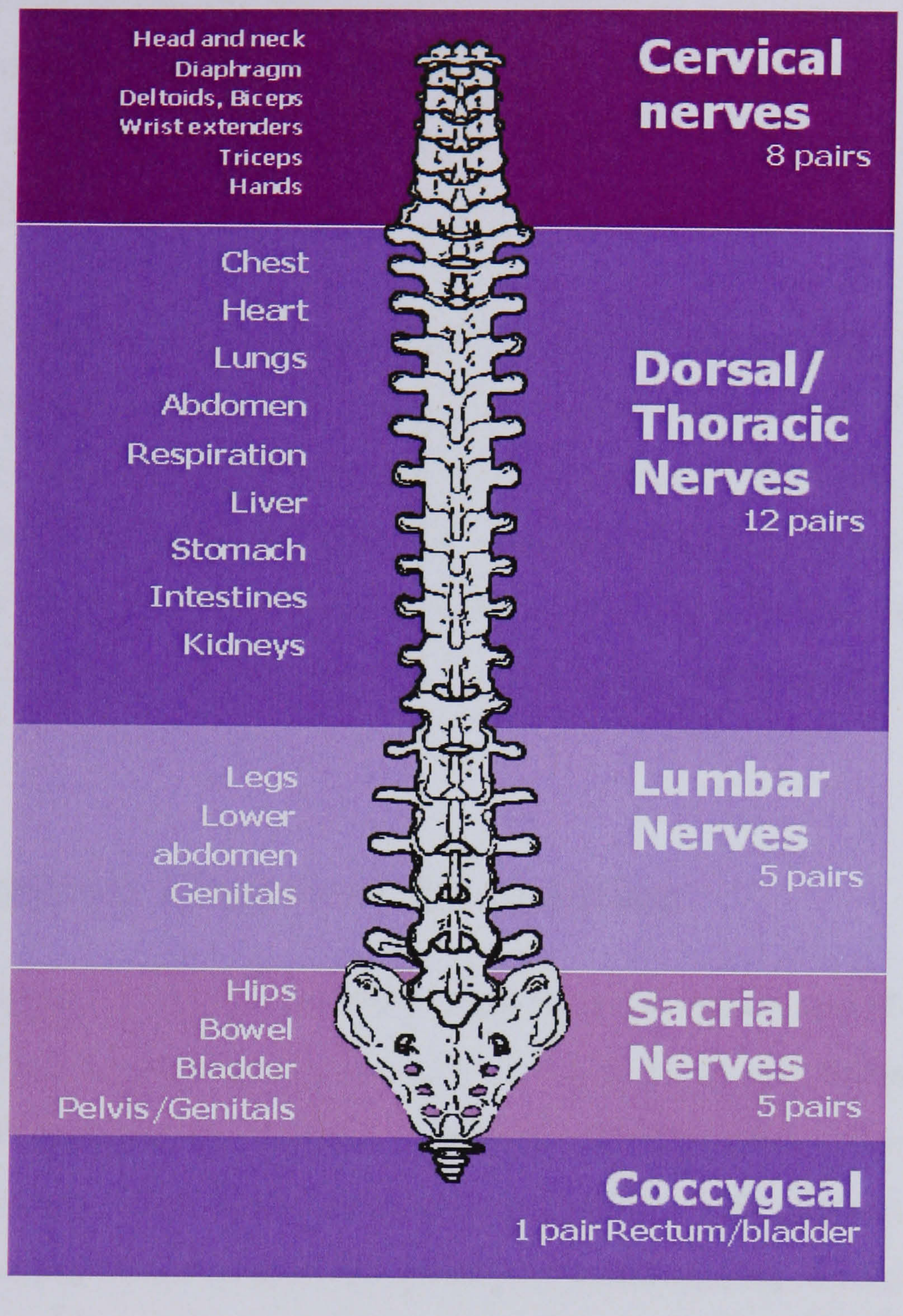

Figure 1.1: Diagram showing the regions of the spine, and the resulting paralysis from the level of the lesion. Source *www.aromacaring.co.uk/spinediagram.htm*

An injury in the Thoracic region is less common than the rest of the spine, as the rib cage protects and stabilises the trunk [40]. A lesion within this region can result in loss of muscle use below the chest muscles, paralysis or weakness of the legs, loss of sensation, sexual function and also affects bladder and bowel control. This group of SCI subjects are known as Paraplegics. Arms, hands and upper trunk functions are normally unaffected.

Spinal lesions result in numerous secondary medical conditions [53]. As the muscles below the lesion are not being exercised, they commonly lose bulk. This is known as disuse atrophy. This affects the appearance of the patient as the lower limbs lose bulk, while the upper body definition can be maintained. Other secondary conditions include pressure sores, muscular spasm, bowel problems and a decrease in cardiovascular fitness. Some of these conditions are discussed in detail in section 2.2.1.

1.3 Functional Electrical Stimulation

Functional Electrical Stimulation (FES) is the artificial stimulation of paralysed muscle, which can temporarily restore muscular function. In an able bodied (AB) person, the brain sends electrical signals down the efferent nerve pathways, via the spinal cord, to the motor nerves. This causes the muscle to contract. This pathway is blocked in a SCI person, see Figure 1.2, due to the lesion of the spinal cord. Electrical stimulation of the paralysed muscles can be performed by applying a current to the muscle's motor nerve to produce a required movement [15]. A motor nerve is an efferent nerve which innervates skeletal muscle.

FES is applied to perform a specific muscle function, e.g., contraction of the hamstring muscles. A specific muscular movement is defined and a signal is passed to a controller. The controller sends a command to a stimulator, which in turn stimulates the muscle. Sensors are then required to measure the movement and feed back to the controller that the desired task has been performed.

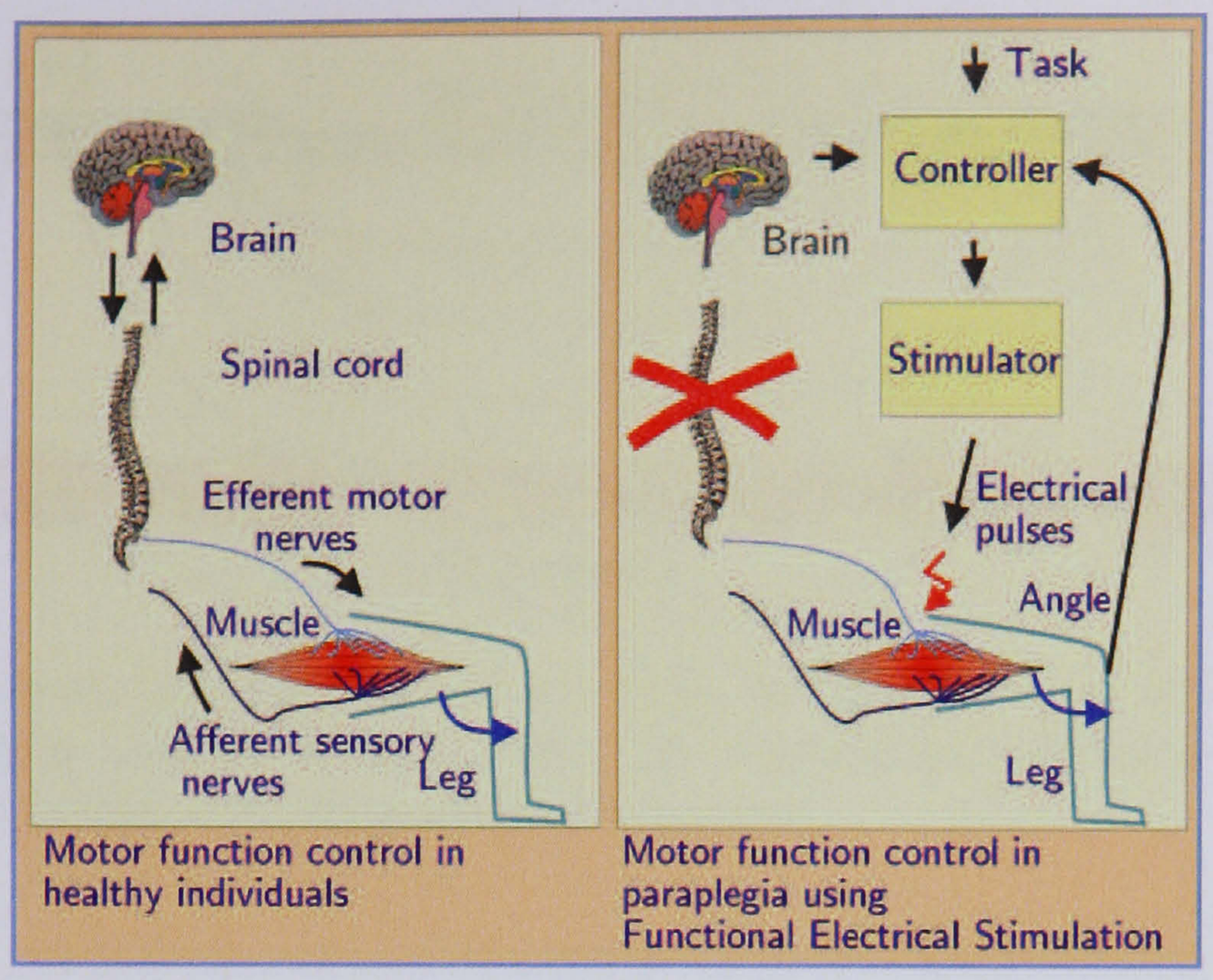

Figure 1.2: Schematic explanation of FES. This figure indicates the natural sensory pathways and the FES solution when a lesion interrupts the spinal cord.

Stimulation can be applied in three ways. Firstly is by implanted electrodes, which are surgically attached to the motor nerve, allowing for precise activation. An example of this is the LARSI system developed by Donaldson et al. [42], which is discussed in section 1.4.1; Secondly percutaneously, using needle electrodes, which penetrate the skin; Thirdly transcutaneously, via adhesive surface electrodes, see Figure 1.3. This type of electrode stimulates a large area, so therefore it is more difficult to activate a specific motor nerve. This is especially difficult if a small muscle is to be stimulated, such as the triceps. This results in a larger current being applied to penetrate the skin and subcutaneous tissue (fat), than that required for the previous two methods. However this third method is advantageous as it does not require surgery.

The stimulated muscle broadly contains 2 fibre types; Type I (Slow twitch) and Type II (Fast twitch) [64]. Which fibres are recruited determines the amount of force produced and the characteristics of the exercise. Slow twitch fibres have a slow contraction/relaxation cycle, they have high activation thresholds, tetanize at low frequencies and fatigue less rapidly. Most human striated muscles contain both types of fibres, but

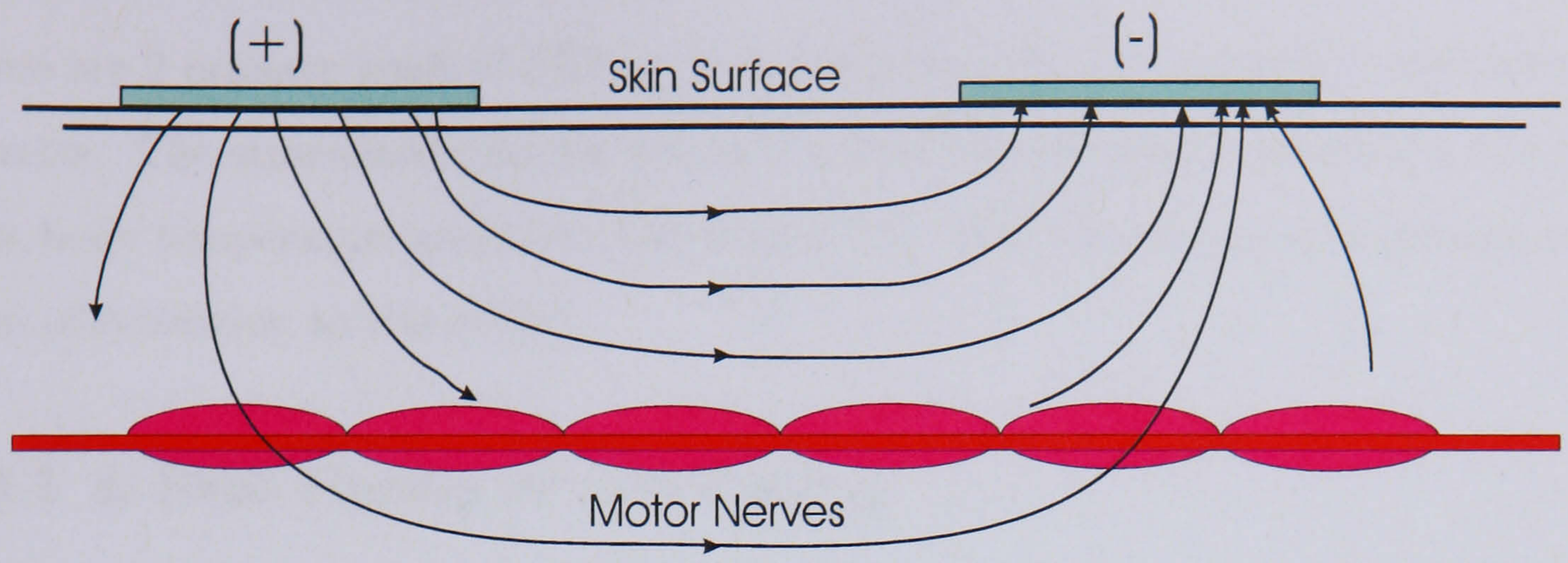

Figure 1.3: Diagram showing the electric field for muscle nerve stimulation. The graphic shows how only part of the stimulation reaches the nerve bundle, which causes the muscle to be activated.

in different proportions, which determine the colour of each muscle, with slow being white and red being fast twitch. Some show a characteristic arrangement of the fibre types within the muscle; in others the two types are randomly distributed.

Under stimulation the Type II fibers are recruited first and exert 20-30 % more force than slow fibres [54]. They produce a significantly higher force but fatigue quickly. Thereafter slow fibres are recruited. The slow fibres are more fatigue resistant, but do not generate as great an average force. An illustration of this is sprint athletes, who possess a high percentage of fast fibres. This results in maximum power for a minimum time period. An endurance athlete on the other hand will possess a high percentage of slow fibres, which exhibit lower power, but have a significantly extended time before fatigue.

1.4 FES Cycling

FES cycling ergometers and mobile cycling systems have been developed both for a commercial market and for research. Broadly, cycling systems use measurement of the pedal position to allow for stimulation of the correct muscle group to create a positive cycling action. These are discussed in detail in the thesis.

There are 2 primary goals of FES cycling; First is to give the subject a cardiovascular exercise. The stimulated muscles pump the blood to the heart, increasing the heart rate, body temperature and rate of breathing [38]. The second goal is to provide a new form of recreation to the cyclist.

1.4.1 A Brief History of FES Cycling

Petrofsky, Stacy and Phillips published a series of paper between 1983 and 2003 dealing with many aspects of FES cycling [43][44][45][46][47][48][49][50]. The earliest papers were the first published works on FES cycling. This included work on cycle ergometers, mobile cycles and the physiological responses to cycling. Some of their first work was undertaken designing an exerciser for paralysed muscle [46]. The system uses selected submaximal exercise with feedback control of leg movement to achieve a specific exercise. Stimulation of the quadriceps, by surface electrodes, is applied and the tension developed by the muscle is measured. This is used to determine the maximum isometric strength. Feedback is implemented by measuring the stimulation voltage applied to the subject's muscles, and when the maximum is reached, the programme stops. The results show an increase in muscle strength.

Petrofsky et al. investigated both stationary and mobile cycling ergometers. The mobile outdoor bicycle is a modified tricycle [45]. The modifications included the addition of a high-back seat for postural support, a potentiometer for throttle control and a potentiometer for pedal position measurement. An on board computer measures the input signals from the throttle and potentiometer to control the stimulation. Stimulation of quadriceps and gluteus maximus is applied by sequential stimulation, to reduce muscle fatigue and to improve the control of movement. Subjects were able to cycle outside for 15 minutes, however no details of speed or terrain are published. A later development was the addition of a Fatigue Meter in an attempt to quantify fatigue. The throttle output is integrated to indicate the percentage of stimulation applied. This can hence be subjectively compared to the degree of muscle fatigue. This is calibrated for each individual subject. Petrofsky concludes that a requirement for this cycle is improved

timing of the stimulation. The patterns are fixed, and therefore the stimulation timings do not alter with cadence. Hunt et al. [34] present a solution in an algorithm in their pilot study of FES cycling, where the stimulation timing is dependent on the cadence. Further work on Petrofsky's cycle was completed 10 years later [48]. A second seat was included, to allow an able bodied individual to cycle alongside a paraplegic, increasing the range of the tricycle. The able bodied cyclist can provide assistance for gradients and to overcome fatigue. Stabilizing leg bars are added to prevent movement outwith the sagittal plane. This is an indication that Petrofsky realised that FES alone may not be a sufficient propellant for mobile cycling.

Petrofsky et al. also considered stationary cycling [47]. Their device is based on a standard MONARK[1] bicycle ergometer. The ergometer is modified to give feedback of the crank position to coordinate the stimulation of the iliacus and quadriceps muscles. Training consisted of three days per week for thirty minutes. Exercise was terminated after the thirty minutes or when maximum stimulation was achieved. Exercise was with a load described as 'low'. This ergometer was used for their later work on metabolic cycling efficiencies [46]. Petrofsky and Stacy used measurements of oxygen consumption and work rates to calculate metabolic efficiency. Cyclists initially cycled at 50 rpm and 0 W for 15 minutes. Once this was possible, the work load was increased in 5 Watt increments until 15 minutes at 40 W was achieved. This took a minimum of 2 months, and a maximum of 3. Once the training was completed, each subject cycled for four minute bouts. During the fourth minute, metabolic measurements were recorded. The efficiency of the FES cyclists was 3.6%, at a work rate of 40 W. No details of the efficiency calculation are published. Efficiency of able bodied cyclists is commonly reported to be 15–27% [8] as discussed in section 2.1.

Most recently, Petrofsky [44] has developed a new algorithm to control a cycle ergometer using Electrical Stimulation (ES). Data were collected from a modified MONARK ergometer, to determine relationships between load, speed and muscle activity during

[1]Therapeutic Alliances Inc., U.S.A. http://www.musclepower.com

cycling. Petrofsky first used EMG activity to determine on/off angles for the stimulation. Loads of 0, 9.8, 19.6 and 29 N at 50 rpm and 9.8N at 30, 50, and 70 rpm were used to determine the stimulation angles. These were then implemented into the new algorithm. Their results show that paraplegic subjects, on an ERGYS system (original algorithm), could sustain 5 minutes at 9.99 $\pm$ 1.17 N (2940 $\pm$ 245 Nm min^{-1}) or 49 W. For the same subjects, with the new algorithm, the maximum load was 20.6 $\pm$ 2.94 N (5987 $\pm$ 519 Nm min^{-1}) which computes to 99.78 W. Comparing these findings to other literature, these levels of Power Output (PO) appear to be high. No details of the method of calculation are presented and doubt into the method used to compare the algorithms can be drawn. Petrofsky aimed to compare 2 algorithms for control of ES cycling. To accurately compare the 2 algorithms, the algorithms have to be the only variable. However, in this study the algorithms were implemented on different cycle ergometers.

FES cycling has been implemented in both open and closed loop. Chen et al. developed a modified cycling ergometer (MONARK) for paraplegic subjects [9]. They geometrically modelled the ergometer and derived several stimulation patterns for FES leg exercise (FES-LE). The aim of the closed loop control is to maintain a desired cycling cadence for a trained paraplegic subject. They use a fixed stimulation pattern and adjust only the gain of the stimulation intensity. A PID controller is designed for the geometric model. This PID controller is shown to be robust against stimulation disturbances and can overcome fatigue and facilitate FES-cycling exercise. Chen et al. later carried out similar work applying Fuzzy Logic Control [11], with similar results.

Similarly, Gföhler and Lugner modelled the rider/tricycle system as a planar rigid body [22]. The goal of this paper was the development of an optimized stimulation pattern of leg muscles to perform cycling. To obtain the maximum average power output with minimum muscle force, the start, duration and amplitude of the stimulation signal applied is optimized for the pedalling frequency. The modelling and simulation approach was used to determine maximum pedalling power while cycling at 35 rpm. The results show that the optimised patterns, implemented with a paraplegic subject, were able

to apply an averaged drive torque of 45 W at 35 rpm. They found that the muscle force of the hamstrings was converted to drive power with the highest efficiency. In this study a non-circular pedaling path is used. They conclude that the PO on the optimised pedalling path can be higher than circular pedalling paths, depending on the subjects leg length.

An example of implanted cycling was developed by Perkins et al.. Control of cycling used stimulation of the lumbar anterior spinal nerve roots [42], which is proven to be effective for mobile cycling. The Lumbo-sacral Anterior Root Stimulator Implant (LARSI) system consists of a R.F. coupled multiplexor receiver implanted on the right costal margin. Leading cables connect to intra-dural cuff electrodes, trapping the anterior spinal roots L2 to S2 on both sides. A female T9 paraplegic was implanted in 1994. A commercially available tricycle was adapted for FES cycling. The modifications included switches to start and stop the cycling programme, a shaft encoder to measure the crank angle and a shelf to hold the stimulator. The subject could mobile cycle for over 1 km, coping with gentle slopes, with a cadence range of 25 - 85 rpm. This subject is the first person to demonstrate FES cycling using nerve root stimulation. Static pedal reaction forces were recorded, for a range of stimulation intensities. The maximum recorded force of 150 N was found during extension phase (180 °). The lowest, 0 N, was measured when the hips were most flexed and most extended (0 °). Schutte et al. [57] suggest areas to consider for future optimization of FES technology :

- The muscle forces being generated in response to electrical stimulation.
- How these muscle forces interact with the skeletal-ergometer linkage, to power the crank.
- The metabolic energy costs of producing the crank power.

1.5 Introduction Chapter Conclusions

This chapter is used to introduce the general areas of background to the thesis; Spinal Cord Injury and FES. A brief history of FES cycling describes some of the initial

research in this area. This background and initial research will be discussed further throughout the thesis.

1.6 Thesis Outline

- **Chapter 1** provides an introduction to the topics of Spinal Injury, FES and FES cycling.

- **Chapter 2** outlines the current background knowledge which is referenced throughout the thesis. This is in the form of a description of exercise testing and a summary of the physiological factors in FES cycling.

- **Chapter 3** introduces the cycling apparatus used throughout the experimental procedures. This is followed by an introduction to the control theory which is used in the controller design process, later in the thesis. The methods employed for exercise testing are also discussed.

- **Chapter 4** introduces the motor and power control in FES cycling. A motorised FES cycle is utilised to develop controllers for exercise testing of paraplegic cyclists. Identifications are undertaken with two paraplegic subjects and results are presented for cadence tracking, power tracking and disturbance rejection tests. These controllers are then applied to exercise tests and the results are presented and discussed.

- **Chapter 5** introduces $\dot{V}O_2$ control. The reasoning for controlling $\dot{V}O_2$ is discussed in relation to $\dot{V}O_2$ throughout the literature. Before controller design, preliminary tests examine the relationship between $\dot{V}O_2$ and changes in power, allowing for the $\dot{V}O_2$ dynamics to be identified. Controllers are designed and a simulation study is undertaken. The controllers are then applied to a paraplegic subject. The controller results are analysed.

- **Chapter 6** continues the $\dot{V}O_2$ controller design from Chapter 5. The analysis from Chapter 5 is used to develop the controllers and these are tested with a paraplegic subject. The results are discussed and conclusions are drawn from these.

- **Chapter 7** reinforces the conclusions drawn from the motor, power and $\dot{V}O_2$ control. Recommendations for future work are suggested.

1.7 Thesis Contribution

Control of Power in FES Cycling. A method for the control of power during FES cycling. Robust control of a two loop control strategy is achieved. Separately identified cadence and power controllers interact to maintain a reference power and cadence. The design is based on models identified from measured input-output data. Thereafter RST controllers are designed via polynomial methods, to a specified controller structure. The results show the design method, controller structure and application to be a robust design.

Development of Exercise Testing Protocols. Utilisation of the power and cadence control allows for the development of a test bed for paraplegic exercise testing. Established exercise testing procedures are translated into requirements for the control strategy. The results show that accurate exercise tests can be implemented. Small changes in power are achieved during incremental exercise tests, allowing for the maximum amount of steps to be implemented within the limited FES cyclists power range. Alternatively during constant load tests, the power and cadence levels can be maintained for extended periods accurately. The control strategy allows for negative power levels to be included within the exercise test, thus extending the cyclists power range.

Control of $\dot{V}O_2$. The feasibility of $\dot{V}O_2$ control is demonstrated. A novel FES cycling cascade control structure is presented to control $\dot{V}O_2$ responses during cycling. $\dot{V}O_2$ dynamics are measured for various cycling power levels before an identification PRB-signal is developed. Input and output dynamics are measured to develop a model of the $\dot{V}O_2$-power system. As with the power and motor control, controllers are developed via polynomial methods.

Prior to implementation of the controllers with the paraplegic subject, the controllers are simulated. The controllers are shown to be accurate and robust for these simulations. The controllers are tested and developed for the paraplegic subject. The results show that $\dot{V}O_2$ control is a feasible concept with practical

implementations for exercise testing, for both the able bodied and paraplegic populations.

These results are a major novel contribution to the literature and represents the main contribution of this thesis.

1.8 Publications

1. Stone, B., 'A preliminary study of control and optimisation of electrical stimulation induced cycling in paraplegia', Proc. UKACC Postgraduate Symposium, Sheffield, 2002.

2. Hunt, K.J., Stone B., Negäard, N.O., Schauer T., and Fraser M.H., 'FES cycling with electric motor assist', Proc. 1st FESnet Conference, Glasgow, September 2002.

3. Hunt, K.J., Cathcart, A.J., Ferrario, C., Stone, B., Grant, S., Ward, S.A. and Fraser, M.H., 'Workrate and cadence control for exercise testing in FES cycling', Proc. 8th Annual Conference Int. Functional Electrical Stimulation Society, Queensland, Australia 2003.

4. Stone, B., Ferrario, C., Hunt, K.J. and Fraser, M.H., 'An overview of functional electrical stimulation (FES) induced cycling', Proc. 2nd IEEE EMBSS UKRI PG Conf. Biomed. Eng. Med. Phys., Birmingham, 2003.

5. Hunt, K.J., Stone B., Negäard, N., Schauer, T., Fraser, M.H., Cathcart, A.J., Ward, S.A. and Grant, S. 'Control strategies for integration of electric motor assist and functional electrical stimulation in paraplegic cycling: utility for exercise testing and mobile cycling', IEEE Transactions on Neural Sys. and Rehab. Eng, Vol. 12, pages 89 - 101 March, 2004.

6. Ferrario, C., Stone, B., Hunt, K.J., Ward S.A., McLean, A.N. and Fraser, M.H., 'Oxygen cost of different stimulation patterns for FES cycling', Proc. 9th Annual Conference Int. Functional Electrical Stimulation Society, Bournemouth, England 2004.

7. Hunt, K.J., Ferrario, C., Grant, S., Stone, B., McLean, A.N., Fraser, M.H. and Allan, D.B., 'Comparison of stimulation patterns for FES-cycling using measures of oxygen cost and stimulation cost', Medical Engineering and Physics, In press, 2005.

2 Background

This section details the background and prior knowledge required before experimental procedures are undertaken. The basic physiology of SCI and summary of FES was discussed in the Chapter 1. This chapter introduces the additional background required for the thesis. The topic of exercise testing is introduced in relation to the measurement of power, energy expenditure and efficiency. The methods of exercise testing are discussed in detail in Section 3.4.2. Thereafter the literature regarding the physiological aspects of FES cycling is presented.

2.1 Exercise Testing

Physiologists undertake exercise tests on subjects to measure improvements in cardiovascular fitness over a defined training period [64]. Defined simply, the body is an input (fuel) - output (useful work) system. An increase in cardiovascular fitness may correspond to an increase in the efficiency of this transition.

2.1.1 Power, Energy Expenditure and Efficiency

The human body converts chemical energy, which we intake from food, to mechanical energy which we exert in everything we do as humans. Like any machine, the body is not 100% efficient. Efficiency is dependent on what task the body is undertaking, i.e. recumbent cycling maybe more efficient than walking.

Power is used to express the magnitude of work done per unit of time, measured in Watts (W) or Joules per second (Js^{-1}). Power describes the rate at which work is

being performed, which is the intensity level of the exercise [54].

Energy expenditure during exercise can be measured via 2 methods: Direct and Indirect Calorimetry. Direct calorimetry involves the measurement of heat production during exercise, and uses this as an indication of metabolic rate [64]. Indirect calorimetry estimates the metabolic rate via measurement of oxygen consumption. The indirect method is the most practical, of the 2 as it does not incur the large costs and space from construction of a temperature controlled chamber, required for direct calorimetry.

A known relationship between oxygen consumed and the amount of heat produced provides an estimate of the metabolic output. The calorific values of the substrate (fat, carbohydrates and proteins) being 'burnt' by the muscle when exercising is known and estimated as 21 kJ per litre of O_2 consumed [64]. The O_2 consumed is measured by means of spirometry. The inspired O_2 which is approximately 21 % of atmospheric air has the expired O_2 subtracted to give the total oxygen uptake by the body (VO_2). The rate of uptake is known as $\dot{V}O_2$.

From the measurement of the power and the energy expenditure, the net efficiency of the exercise can be defined by,

$$\text{efficiency}_{\text{net}}(\%) = \frac{\text{Energy Output}}{\text{Energy expenditure above rest}} \text{ x } 100\% \tag{2.1}$$

Typical efficiencies for cycling ergometry ranges from 15–27 % [8]. The subject of efficiency is discussed in relation to the power output in section 4.1.1

2.2 International Research

FES cycling has developed over a number of years and a number of papers have been published focusing on different aspects of cycling. The significant papers and authors in a range of topics are reviewed and are related back to the overall topic of power output and power control. The reviewed literature is presented throughout the thesis,

where it is deemed most relevant. A historical development of FES cycling is presented in the introduction, through the work started by Petrofsky (section 1.4.1) and the advancement to motor integration and assisted cycling (section 4.1.2). A specific focus on Power Output (section 4.1.1) is presented when the topic of power and motor control is discussed. Prior to the advancement of controlling $\dot{V}O_2$, the reasoning behind the concept is discussed in reference to the literature (section 5.1). Physiological aspects (section 2.2.1) and fatigue (section 2.2.2) are presented to provide some additional background knowledge.

2.2.1 Physiological Literature Review

The potential benefits of FES are numerous, and could be seen as an additional method of rehabilitation. However the implementation of FES cycling is not commonplace within this process. The physiological aspects are illustrated to show why lower limb exercise is beneficial for paraplegics.

A study by Janssen et al. [38] summarizes research findings of FES lower limb training, with respect to the effects on health, fitness and function. The review considers a number of key issues which are summarised in the thesis. No reference to papers cited by Janssen are given: only their conclusions and findings are presented.

- **Muscular performance for FES-induced exercise:** several weeks of FES training has induced hypertrophy and increased both strength and endurance. Results show that improved performance from the muscle elicits an increase in magnitude of metabolic and cardiopulmonary responses.

- **Muscle size:** it was found that Functional Electrical Stimulation Leg Cycling Exercise (FES-LCE) exercise training appeared to reverse or retard disuse atrophy of the paralysed muscle and that bulk and appearance of the lower limbs had greatly improved.

- **Range of motion (ROM):** SCI can limit the ROM and may hinder activities, such as transfers. Transfers are when he patient moves from their wheelchair. There is evidence in the literature that FES can increase the ROM.

- **Spasticity:** spasticity is characterised by hypertonia and velocity dependent hyperflexia, which causes discomfort and disruption of daily activities. Spasticity can be controller by means of medication and passive stretching to reduce the levels of spasm. The authors conclude that most FES users experience a temporary reduction in spasticity on the day of exercise. They report that due to the increased muscle bulk that the severity of the spasm can increase, but they occur less frequently. This finding has been commented on by our subjects, but is unpublished.

- **Skeletal System:** after SCI, the greatest bone loss occurs in the first 2 years post injury. They state that available data suggests that FES exercise may help in retarding osteoporosis progression, especially in the acute and rapid loss of the first 2 years.

- **Cardiopulmonary Fitness:** studies indicate that FES-LCE exercise imposes relatively high magnitudes of aerobic metabolic and cardiopulmonary responses. These high levels could not be achieved by arm ergometry. They state that power output achieved by SCI subjects after several weeks of exercise training, provides $\dot{V}O_2$ levels equivalent to walking (1.0 $l.min^{-1}$). Significant gains in peak $\dot{V}O_2$, heart rate (HR), Stroke Volume (SV) and Cardiac Output (CO) are reported.

- **General Findings:** the results found that subjects had an improved self image, they felt stronger and more energetic, less fatigued and they had an increased feeling of overall well being. The findings also suggest that mood disorders, common to the SCI population may be improved with FES exercise.

This article gives a comprehensive overview, providing a strong argument for FES and its therapeutic benefits. It is noted that for FES to be at its optimal effectiveness it has to be part of the patient's lifestyle. This paper is an excellent reference for the

advantages of FES implementation.

FES has been applied to a number of rehabilitation methods. In studies, [15],[18], FES has been used for muscle strengthening, before undergoing a specific task. By stimulating individual muscles groups, training of the muscle can be achieved. Sipski et al. [60] conducted a questionnaire for 47 patients who participated in a clinical electrical stimulation ergometer programme. Their findings are listed below:

- 62% of paraplegics, 65% quadriplegics reported improved endurance.
- 62% of paraplegics and 56% quadriplegics reported improved self image.
- 54% of paraplegics and 77% quadriplegics reported their appearance was better.

Interestingly, six out of nine patients who had a history of neurogenic pain noted an increase in pain, causing them to leave the programme. They also noted a significant increase in oxygen uptake and increased heart rate while using the ergometer. They state that FES should be only used for patients who understand the possible health benefits and the risks, and the cost effectiveness of such a programme should be considered.

Phillips et al. [51] examined the muscular, respiratory and cardiovascular responses of FES cycling in tetraplegic subjects. When referring to Petrofsky's work on outdoor FES cycling [45], they comment on the complexity of measuring the cardiopulmonary effects of such exercise, due to varying grades and terrains. This was in 1989, and the advancement in technology, such as telemetry and mobile breath by breath measurement systems, can now make this possible. They also identified parameters that could be used as indicators of the effect of FES cycling. These included the length of time the subject could cycle as a measure of endurance, the increase in Forced Vital Capacity (FVC) post training and an increase in cardiac output. All results were compared with the increase from resting recorded values.

Consistent reports in the literature note an increase in heart rate [16],[31],[32],[6] and an increase in Bone Mineral Density (BMD)[30],[4], following FES cycling.

2.2.2 Fatigue

The factor of fatigue plays a major role in the successful operation of FES cycling. The rapid onset of muscle fatigue is one of the major problems when using electrical stimulation to restore functional movement in individuals with a neurological deficit. Binder and Scott [7] describe muscle fatigue as the temporary loss in the force-generating ability of a muscle because of prior activation.

Fatigue is a difficult factor to measure, detect or predict. Fatigue rate will differ for each subject, and could be dependent on the level of training and fitness prior to injury. Tepavac and Schwirtlich suggest a possible method of monitoring the onset of fatigue [62]. The method was to use surface electromyography (sEMG) signals and torque measurement curves. These curves were used to establish a relationship that can be used for detection of the decrease of the force associated with FES-induced muscle fatigue. Their findings suggest that it is possible to use processed sEMG as a 'trigger' signal to alter the stimulation pattern. A similar study was conducted by Cifrek et al., using surface myoelectric (ME) signals to evaluate muscle fatigue, by analysing changes in the power spectrum median frequency (MPF) [12].

A study by Binder-Macleod and Scott compared the levels of fatigue produced by various electrical stimulation trains [7]. They examined the effect on peak force and force-time integral during knee extension with able bodied subjects, when three different stimulation trains were applied:

- VFT's – Variable Frequency Trains
- CFT's – Constant Frequency Trains
- DFT's – Doublet Frequency Trains

They found that DFT's produced the greatest peak forces and force time integrals. Results suggest that clinical applications to activate muscles may require a combination of train types to optimize stimulation.

Chen and Yu [10] investigated the fatigue characteristics of paralysed muscles during dynamic FES cycling. For direct measurement of muscle force as a fatigue index, response EMG was investigated. They state that it is difficult to model and that a complete explanation of the effect of muscle contraction velocity on stimulus evoked EMG requires a more physiological study.

2.3 Conclusions from Literature

Overall the literature discussed gives a broad overview of the initial work on FES cycling, with the studies of Petrofsky, up to the current work, considering the physiological measurements and the advancements in FES technology. A number of techniques are employed which have similar outcomes and responses from the cyclists.

After examination of the published literature and background, the area of accurate power control becomes apparent as a crucial requirement to be investigated. Exercise testing protocols state that accurate power control is required, therefore controllers should be designed for these specific tests.

Also, FES cycling is advanced to the stage that it is moving from the laboratory environment to a realistic mobile solution. For this step to occur optimization of the power produced during cycling is required. The levels of output power by the cyclists (10-40 W), is not sufficiently high to cope with variations in terrain and slope. The addition of motor integration is a possible solution. The motor assistance increases the range of the cyclist and can compensate for slope, wind and fatigue. However, it is at the expense of increasing both the weight and the overall cost of the mobile cycle.

The ideal situation for power control is to produce the maximum power for the minimum stimulation pulsewidth input. Throughout the tests discussed within this thesis, stimulation pulsewidth is varied and both stimulation charge and amplitude remain constant.

The area of accurate exercise testing is also open for investigation. Increasing the accuracy of the power control is a possible avenue, but an alternative is to examine if the $\dot{V}O_2$ can be controlled during exercise.

2.4 Background Chapter Conclusions

This chapter developed the background presented within the introductory chapter and focused on the health benefits of FES. The concept of exercise testing was introduced and is discussed further in the following chapters. A focus of the experimental work presented in this thesis is development of FES cycling for exercise testing. The health benefits of FES cycling are presented from the literature to indicate that there is both physiological and scientific benefits.

3 Materials and Methods

This chapter serves the purpose of introducing the experimental setup that is utilised throughout this thesis. The problem of accurate power measurement is addressed, as this is a key factor to exercise testing. Thereafter the protocols for exercise testing are described, for both constant and incremental tests. The details of the paraplegic subjects that have participated in the experimental procedures are given. Finally the control theory that is utilised within the experimental work is presented.

3.1 Apparatus

A standard recumbent tricycle (ICE[1]) is adapted for FES cycling, see Figure 3.1. The primary mechanical additions are ankle orthoses and an electric motor. The trike has a low centre of gravity, which is essential for stability during cycling and for stable patient transfer. The customised ankle orthoses are fixed to standard pedals, stabilising the ankle joint and constraining the legs to motion in the sagittal plane only. This trike was developed from a trike discussed by Hunt et al. [34].

An auxiliary electric motor is mounted behind the seat and is powered by two 12 V batteries, positioned either side of the motor. The motor is connected via gearing and chain drives to the rear (drive) wheel of the trike, which is also coupled to the pedals. This enables both the motor and pedal power to be combined to produce the total Power Output (PO). Additionally the motor can be utilised to perform zero stimulation cycling. Zero stimulation cycling is the case when only the motor is used to perform cycling and no stimulation is applied.

[1]Inspired Cycle Engineering Ltd., http://www.ice.hpv.co.uk

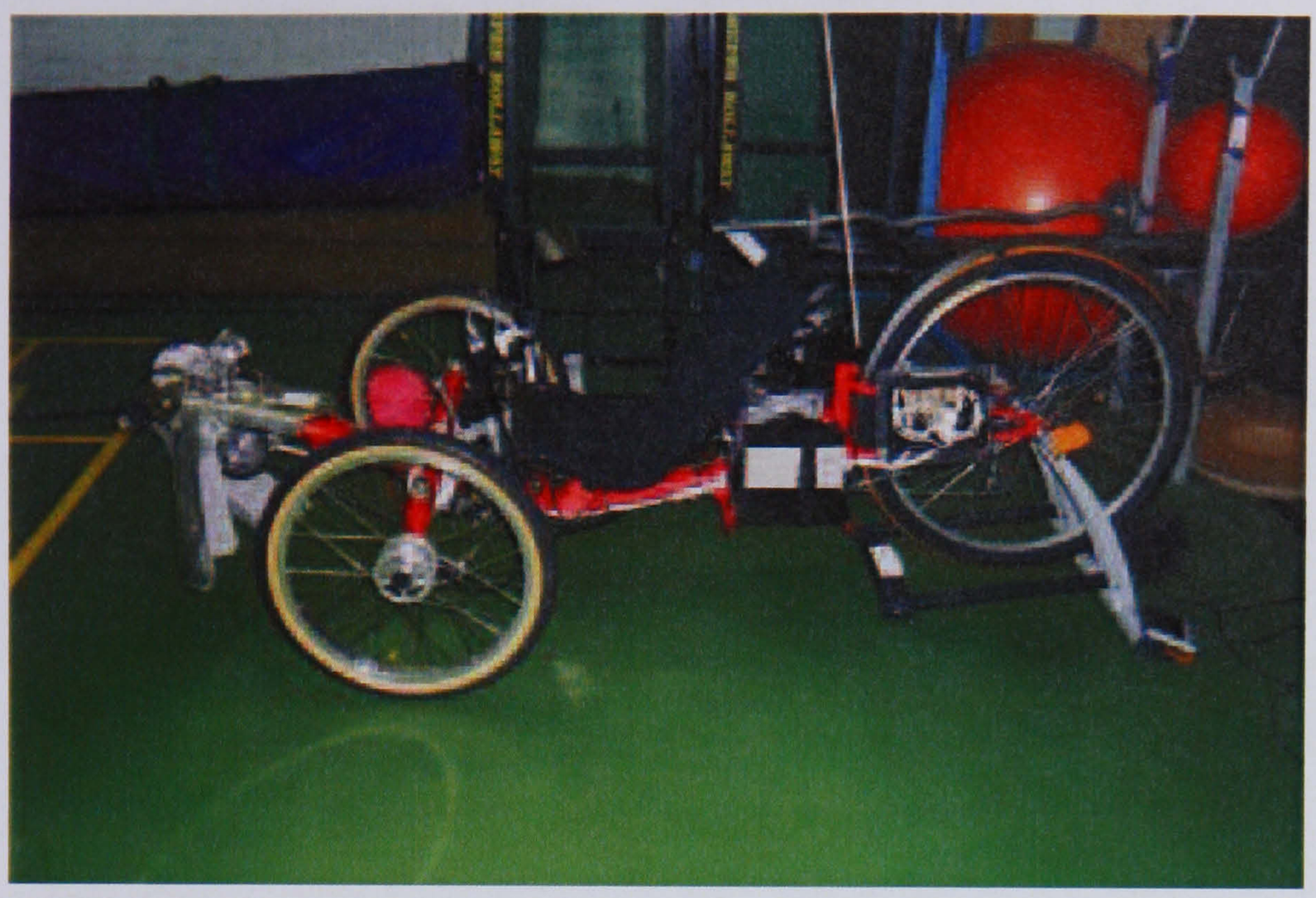

Figure 3.1: Motor trike mounted on the TACX ergometer.

3.2 Instrumentation

The trike is equipped with a 10-bit shaft encoder, which is attached to the pedals via a small cog and a chain drive. The encoder measures the crank angle, which is differentiated to give the rotational velocity (cadence) at the pedals.

A throttle is mounted on the right hand side handlebar. The throttle can be configured to control 2 outputs, depending on the software implemented: the motor input signal which allows open loop control of the motor speed, and the stimulation pulsewidth in open loop control. The throttle can also be used as a safety measure during testing. If a controller becomes unstable, the software can be switched from closed to open loop, and the test can continue with manual control of stimulation.

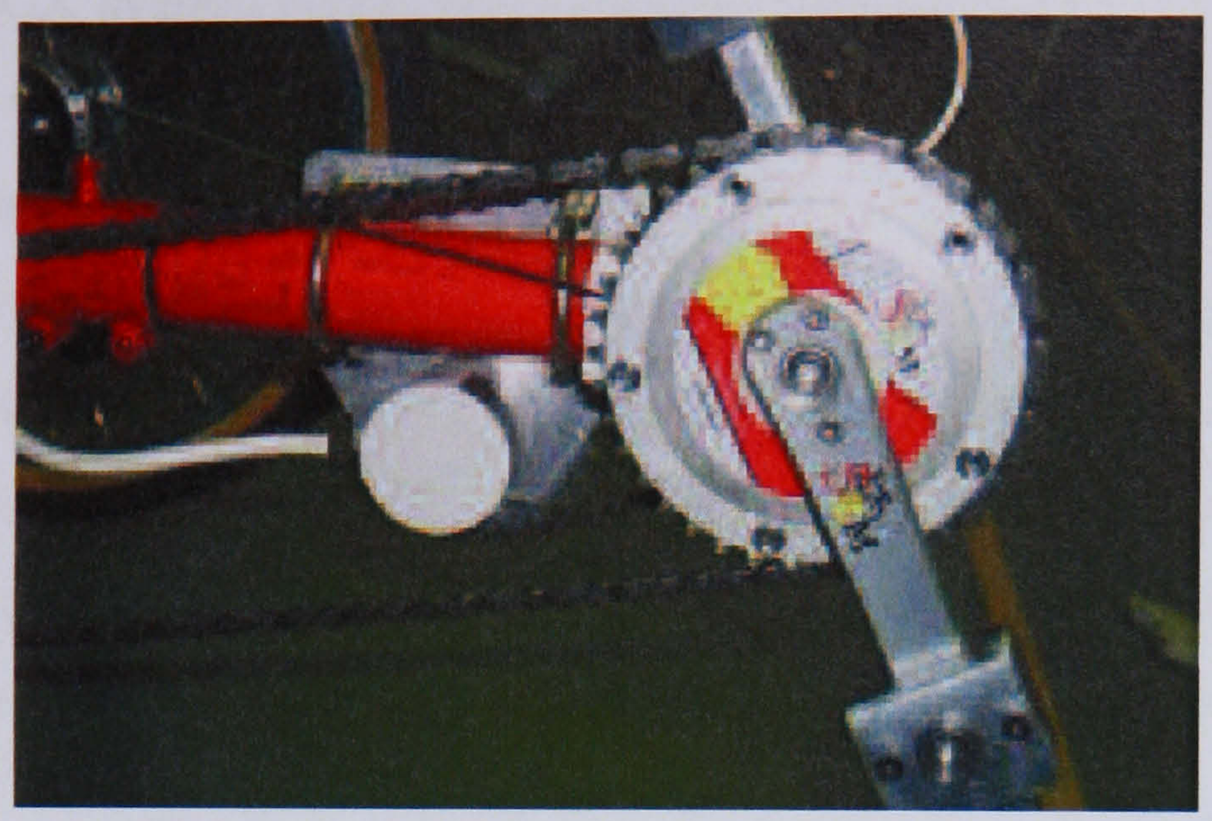

Figure 3.2: SRM sensor replaces the right crank on the trike. To the left of the SRM sensor the shaft encoder can be seen below the trike boom.

3.2.1 Power Measurement

Power can be measured via 2 methods: a SRM sensor (P_c) and a Tacx trainer (P_t). The two systems are discussed in later in the thesis. The right hand crank is replaced with the torque measuring sensor, called a SRM [2] Crank, see Figure 3.2. This sensor measures the torque produced in the crank, with an accuracy of $\pm$ 2.5 %, by means of 4 strain gauges in a Wheatstone Bridge configuration. The torque (T), in conjunction with the angular speed ($\dot{\theta}$), enables the calculation of the instantaneous power from,

$$\text{Power} = \text{P} = \text{T}\dot{\theta} \tag{3.1}$$

The SRM specifications state that there is an operational power range of 0-4800 W, with an accuracy of 2.5 %. This degree of accuracy corresponds to 0.5 W variation, when cycling at 20 W, and the operating cadence is in the range 20-255 rpm. The SRM system is calibrated using known weights. The advantage of the SRM sensor is that it measures only the power generated by the stimulated muscles at the crank (P_c).

The tricycle system, in Figure 3.1, is mounted on a cycle trainer (TACX[3]) for indoor

[2]Schoberer Rad Messtechnik (SRM), http://www.srm.de
[3]http://www.tacx.nl

cycling. The TACX system is an electronically controlled brake, which applies resistance to the rear wheel. The trainer can control, via a hand held user interface, speed, power and resistance. The desired power output is entered into a hand held control pad and the actual power (P_t) produced is then measured. The electric brake automatically adjusts to maintain the reference power. However this configuration is not used in the experiments described in this thesis. The trainer has an operating range of 2-999 W, with no documentation of measurement accuracy. Through correspondence with the manufacturers, they state that accuracy is increased when operating above 100 W.

This system allows for simulations of different conditions such as slope and wind resistance. When a disturbance is applied the system can measure the total PO at the rear wheel of the trike. The resistance of the trainer can be adjusted by means of a screw, which pushes a roller against the rear tyre. The manufacturers suggest that for accuracy this should be set between 1 and 3 turns of the screw. By means of a simple test, 2 turns has been shown to be most accurate for a tyre pressure of 60 psi. Measuring the power at the rear wheel indicates the combined power of stimulated muscles and the motor.

The disadvantages the TACX system has for FES cycling is that it only allows steps in power of 10 W. Taking into account the relatively small power range that the average FES cyclist can produce (0-25 W), this would not be appropriate for small increments. Berkelmans et al. [6] in a recent study used a TACX trainer to implement exercise testing. They found difficulties in accuracy of the power measurement, when operating in the power range of 63 - 141 W.

A simple test was carried out to determine the difference between the 2 systems. By cycling at a specific power at the trainer, the SRM power was measured. A cyclist cycled until the desired power on the trainer was achieved. The cyclist maintained this level for one minute and the SRM power was recorded. The test was repeated 5 times for each power level. The motor was not utilised in this test. The results are shown in Table 3.1.

Trial	*Trainer (W)*	*SRM (W)*					*SRM Average(W)*	*Difference*
1	40	29	34	27	29	33	30.4	9.6
2	60	49	47	50	49	50	49.2	10.8
3	80	70	65	63	64	70	66.4	13.6
4	100	88	91	88	87	90	88.8	11.2
5	120	108	114	105	106	113	109.2	10.8
6	140	139	n/a	135	n/a	131	135	5

Table 3.1: Comparison of SRM and TACX Measurements.

The results indicate that there is a difference of approximately 10 Watts between the SRM and the trainer. The 2 results for the SRM sensor that are marked not applicable (n/a) occurred as the SRM sensor failed to correctly record the power on these occasions. This result is surprising as intuition suggest that the SRM power should be higher than the TACX, due to power losses throughout the system. The SRM sensor measures the power produced by the stimulated muscles at the pedals. Therefore any power losses will be minimal. The TACX power measurement is not used during testing, but is used as an indication of combined power and to simulate terrain changes, during static cycling.

3.2.2 Power Levels

Throughout the remainder of the thesis different power levels are referred to. These levels are described below;

Negative Power When the cyclists legs are rotated by only the motor, the weight of the provides a resistive torque against the motor. This can be measured as negative power at the crank.

Zero Watts This is when the cyclist legs are stimulated during cycling so that the stimulation overcomes the weight of the cyclists legs.

Passive Cycling Passive cycling is the state when only the motor is used to rotate the cyclists legs. No stimulation is applied.

3.2.3 Data Acquisition

The torque measurement, the digital signal from the angle and throttle signal are interfaced to a laptop computer via a data acquisition card. The signals are imported into MATLAB [4], Simulink, where they are measured and control signals are produced. The signals are sampled at 20 Hz via the Real Time Toolbox.

3.3 Stimulation Parameters

The output of the control software is the command signal to an 8 channel stimulator [5]. The stimulation pulsewidth is modulated, with the applied frequency ($20Hz$) and current, to each muscle group, fixed. The current is different for each muscle group: quadriceps, hamstrings and gluteal muscles are stimulated up to 120 mA, in 10 mA increments. Typically these values are in the range of 90 - 120 mA. The pulsewidth is adjusted, either manually or under closed loop control, in the range of 0 - 700 μs. A schematic representation of the pulsewidth can be seen in Figure 3.3.

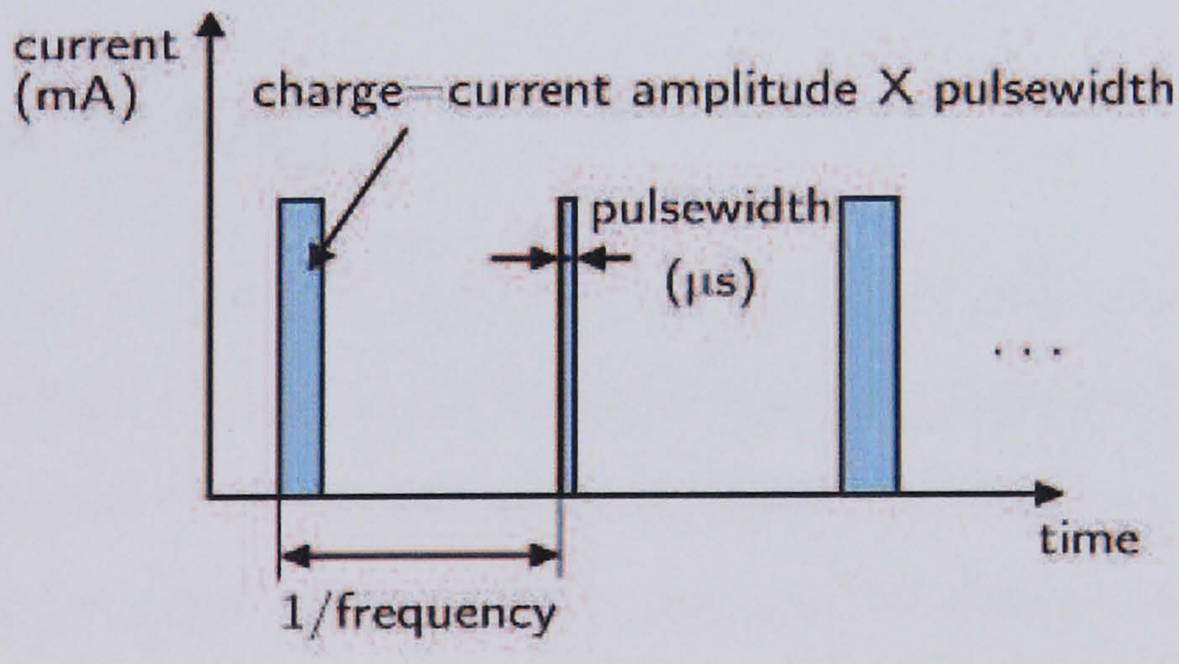

Figure 3.3: The current and frequency of stimulation are constant, and the pulsewidth is changed either via the throttle or the power controller.

The crank angle is used to switch on and off the desired stimulated muscle (see Figure 3.4). The arc over which the muscle is stimulated is determined statically, where

[4]The MathWorks Inc., http://www.mathworks.com
[5]Stanmore Stimulator, Salisbury, UK

the stimulated muscle produces an active, positive torque. These static patterns are shifted proportionally to the cycling cadence, typically 50 rpm. This is in order to compensate for the dynamic response of the stimulated muscle, i.e. the time taken for the muscle to produce force so that it is applied at the correct point in the pedalling action.

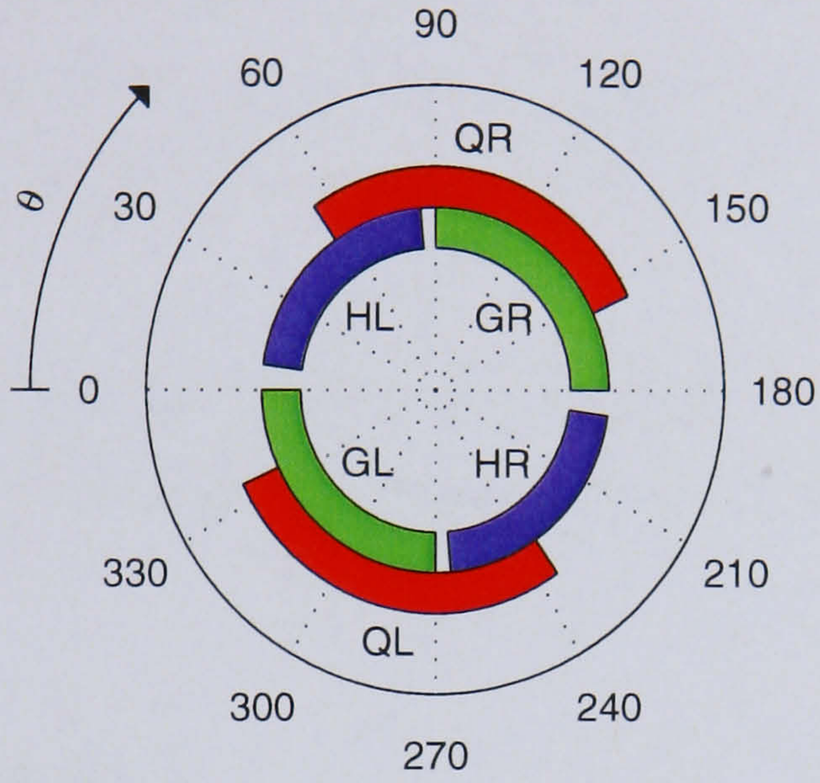

Figure 3.4: The figure shows the arcs over which the 3 muscle groups are stimulated. The speed correction is applied in the opposite direction to that of the angle (θ). H-hamstrings, Q-quadriceps, G-gluteal, R-right and L-left.

3.4 Exercise Testing

Exercise Testing can be used to measure a number of physiological responses from a subject. By the means of measuring the cardiovascular and ventilatory systems of a subject during exercise, the subjects exercise limits can be determined. Two types of exercise testing protocols are commonly used on AB athletes; Constant Load and Incremental tests. These test have been developed over a number of years by sports physiologists and they use gas exchange to monitor the subjects exercise tolerances.

3.4.1 Gas Exchange Monitoring

A portable breath by breath, cardiopulmonary exercise system is used to monitor the physiological responses to FES cycling. The system directly measures O_2 and CO_2 concentrations of the inspired/expired air. The subject wears a facemask, covering both the mouth and nose. The mask has a volume transducer (turbine, with accuracy of 2 %) fitted, with gas sample lines. The gas analysers have an accuracy of 0.1 % and a response time of 100 ms. The system used for gas monitoring is via a MetaMax 3B Breath by Breath Gas Analyser (Cortex Biophysik GmbH, Germany).

Gas monitoring has been integrated into the Simulink models, allowing for synchronised measurement of cardiorespiratory responses and the trike apparatus.

3.4.2 Testing Protocols

In this section the protocols for incremental and constant loading testing are described. The aims of the tests are described, and the desired outcomes are stated. In Chapter 4 these protocols are applied to SCI subjects. During exercise testing specific power and cadence requirements are required to successfully undertake the exercise test [35]. This section outlines the general prerequisite conditions required before and during testing and also the profile of the power control required.

Prerequisite conditions to testing are required which are common to both test types. To minimise the influences of extraneous factors, during different tests and across different test days, subjects are instructed to adhere to several criteria prior to each testing session:

1. Good health at the time of testing.
2. No strenuous exercise in the 24 hour period before testing.
3. No alcohol to be consumed in the 24 hour period prior to testing.
4. No caffeine ingestion during the 4 hour period prior to testing.

5. Similar meals on test day prior to testing, with no food consumption for 2 hours preceding test

In addition, standard, "non threatening" laboratory conditions must be created. The aim is to create an essentially stimulus free environment, thus ensuring the recorded responses relate to the metabolic challenge and are not "contaminated" by unrelated environmental factors.

Incremental Test

An incremental test is designed to provide gradational stress to the subject. The work rate is increased over uniform periods of time, or continuously as a ramp. Typically metabolic measurements are recorded with the patient at rest, during a period of low intensity work (zero stimulation) and then while the work rate increases in steps [64].

Measurements are recorded while the work rate is increased, until the subject is unable to continue, or the stimulation has saturated and the desired work rate can no longer be maintained. At this point the subject will continue to cycle without any load. An electric motor is used to rotate the rear wheel to provide a zero stimulation warm down. This is to prevent the steep fall in blood pressure that is occasionally experienced when vigorous exercise is abruptly terminated.

A schematic representation of an incremental test is shown in Figure 3.5.

(a) Warm-up of 7 minutes stimulated cycling at 0 W.

(b) 10 minutes of rest (not attached to facemask).

(c) At least 3 minutes of recorded rest.

(d) At least 4 minutes of passive cycling.

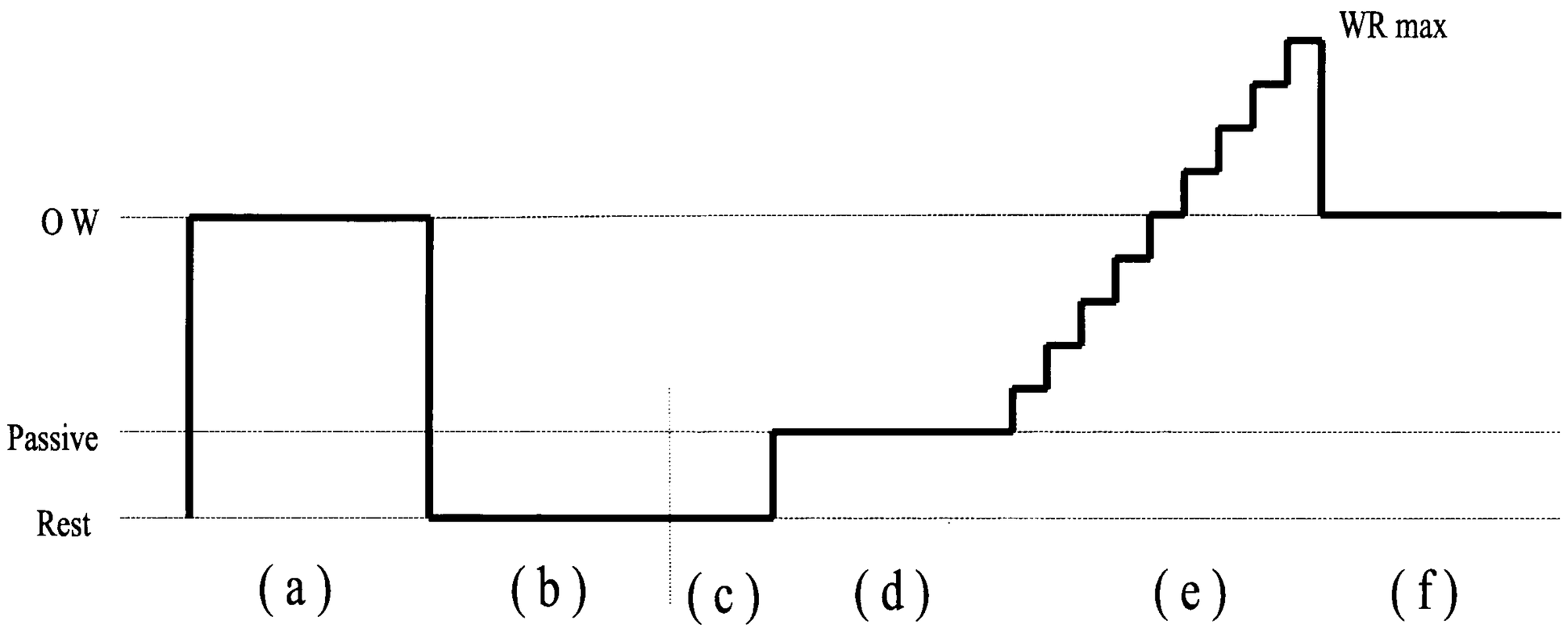

Figure 3.5: Schematic representation of incremental exercise test.

(e) Work-rate increased by 1 W/min until saturation limit is reached. Work-rate should be increased or decreased depending on the subjects' abilities.

(f) 6 minutes stimulated cycling at 0 W for recovery.

Constant Load (Step) Test

A constant load exercise is one in which a constant power output is maintained by the subject. Constant work rate tests can be useful in determining $\dot{V}O_2$ rates and measuring gas exchange dynamics [54].

A schematic representation of a constant load step test is shown in Figure 3.6.

(a) Warm-up of 7 minutes simulated cycling at 0 W.

(b) 10 minutes of rest (not attached to facemask).

(c) At least 3 minutes of recorded rest.

(d) At least 4 minutes of passive cycling.

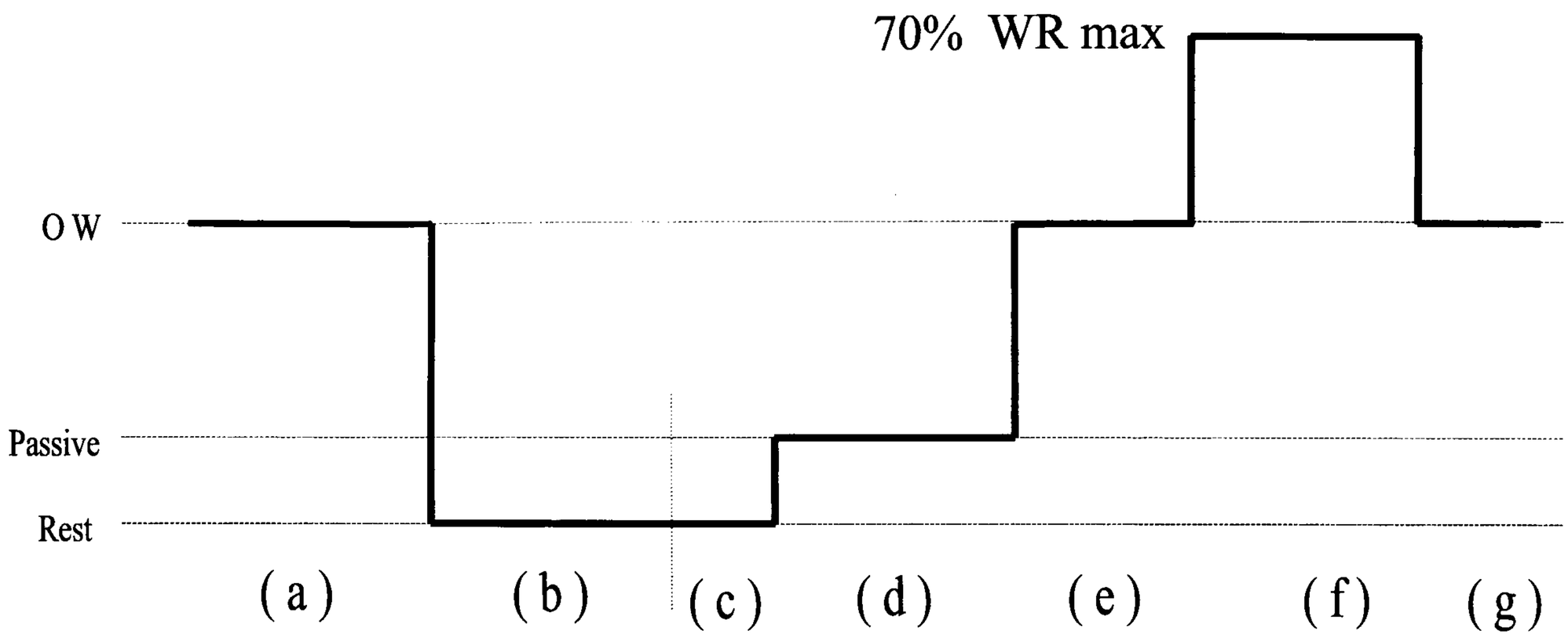

Figure 3.6: Schematic representation of constant load exercise test.

(e) 8 minutes of 0 W stimulated cycling.

(f) 20 minutes (or the limit of tolerance) at 70 % of the maximum work-rate measured via an incremental exercise test.

(g) 8 minutes stimulated cycling at 0 W for recovery.

3.5 Subjects

Subject 1 participated in both the power/motor control study and the $\dot{V}O_2$ control study and is a motor-complete, sensory incomplete (see section 1.2), T8/9 spinal cord injured paraplegic. The subject had been participating in FES cycling for approximately 2 years prior to these tests. He was 3 year post injury at the start of cycling.

Subject 2 participated in only the power/motor control study and is a motor and sensory complete, T10 spinal cord injured paraplegic. The subject had also been participating in FES cycling for approximately 2 years and was 3 years post injury at the start of cycling.

The details of the training and cycling sessions are detailed in Hunt et al [34]. Training consisted of cycling once a week for 1 hour. The 1 hour session consisted of 3 bouts of 20 minutes cycling. The cyclists had been participating in FES cycling for approximately 2 years prior to the commencement of these experiments. All procedures were approved by the Southern General Hospital Ethics Committee. The subjects provided informed written consent prior to participation.

3.6 Control Theory

The control background is now presented, detailing sensitivity analysis and RST controllers. The RST controller development contains a number of equations. The application of these equations is used throughout the controller design work. It is intended to be used as a reference, and is referred to throughout the experimental work, results and discussion. The control structures in which the RST controllers are applied are shown in Chapters 4 and 5.

Stability and Robustness

To analyse the properties of a closed loop system, consider the generic feedback loop [19], in Figure 3.7.

The plant (P) is the identified model of the system that is to be controlled, by controller (C). The reference (r) is the input to the system, at which the operator desires the system to be controlled to. u is the control signal from the controller. The effect of disturbances (d), and measurement noise (n), are added to the system. Disturbances can be the form of vibrations or friction, whereas measurement noise is the noise that emanates from the sensors in the system. The closed loop equation for the system is given in Equation (3.2).

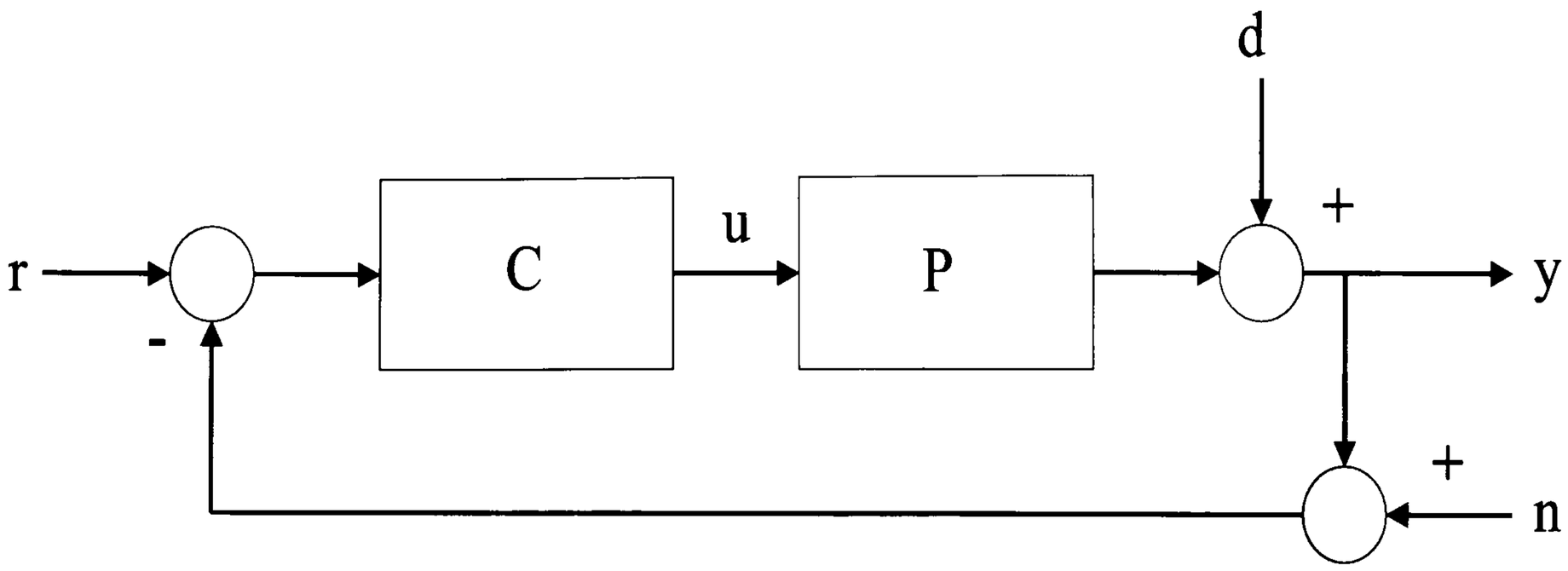

Figure 3.7: Generic control loop structure.

$$y = \frac{CP}{1+CP}r + \frac{1}{1+CP}d - \frac{CP}{1+CP}n \tag{3.2}$$

The sensitivity function (S) and complementary sensitivity function (T) are defined as,

$$S = \frac{1}{1+CP} \tag{3.3}$$

$$T = \frac{CP}{1+CP} \tag{3.4}$$

S determines the disturbance rejection properties of the loop, while T defines the tracking response to the input signal, and the effect of measurement noise. In the frequency domain, the smaller $|S(j\omega)|$ is the greater the system's ability to attenuate disturbances, at the frequency ω. Any peaking of S should be avoided so as to not amplify any disturbances. Ideally T should be equal to 1 over the bandwidth f the plant. T should be small at high frequencies to avoid exceeding the plant capacity, adverse effects of measurement noise and loss of robustness at high frequencies. In the crossover region, peaking of both S and T should be avoided to prevent overly large sensitivity to disturbances, increased influence of measurement noise and loss of robustness.

These points can be summarised as design requirements for S and T;

S should be small at low frequencies to achieve :

- Good disturbance attenuation,
- Satisfactory command response,
- Robustness of closed loop stability against perturbations in the inverse loop gain.

T should be small at high frequencies to achieve :

- Avoiding exceeding plant capacity,
- Avoiding unwanted effects of measurement noise,
- Robustness of closed loop stability against perturbations in the loop gain.

Trade-offs in these conditions are required due to the constraint that,

$$S + T = 1 \tag{3.5}$$

RST-type Controller

The control structure of an RST controller can be seen in Figure 3.8. This configuration of controller gives the designer 2-degrees of freedom. Firstly $T(q^{-1})$, in the forward loop can be in the form of a pre-filter, from the reference signal $r(t)$. Secondly in the return path of the closed loop, $S(q^{-1})$, where the feedback characteristics can be determined.

Integral action is implemented in the forward path of the closed loop, and is taken as part of the plant in the controller design. This explained later in Eqn. (3.32), where S_d is set to be an integrator and in Figure 3.8 where the integrator term is $\frac{1}{1-q^{-1}}$. The purpose of integral action is to decrease the size of the steady state error. A drawback of this decrease in the error is that it is at the expense of a more oscillatory response, due to an increase in the gain. The employment of integral action will effect the steady state properties of the feedback system. This can make the system less sensitive to parameter change in the controller and the plant. This is important when you consider that the plant is a human body, whose condition changes daily.

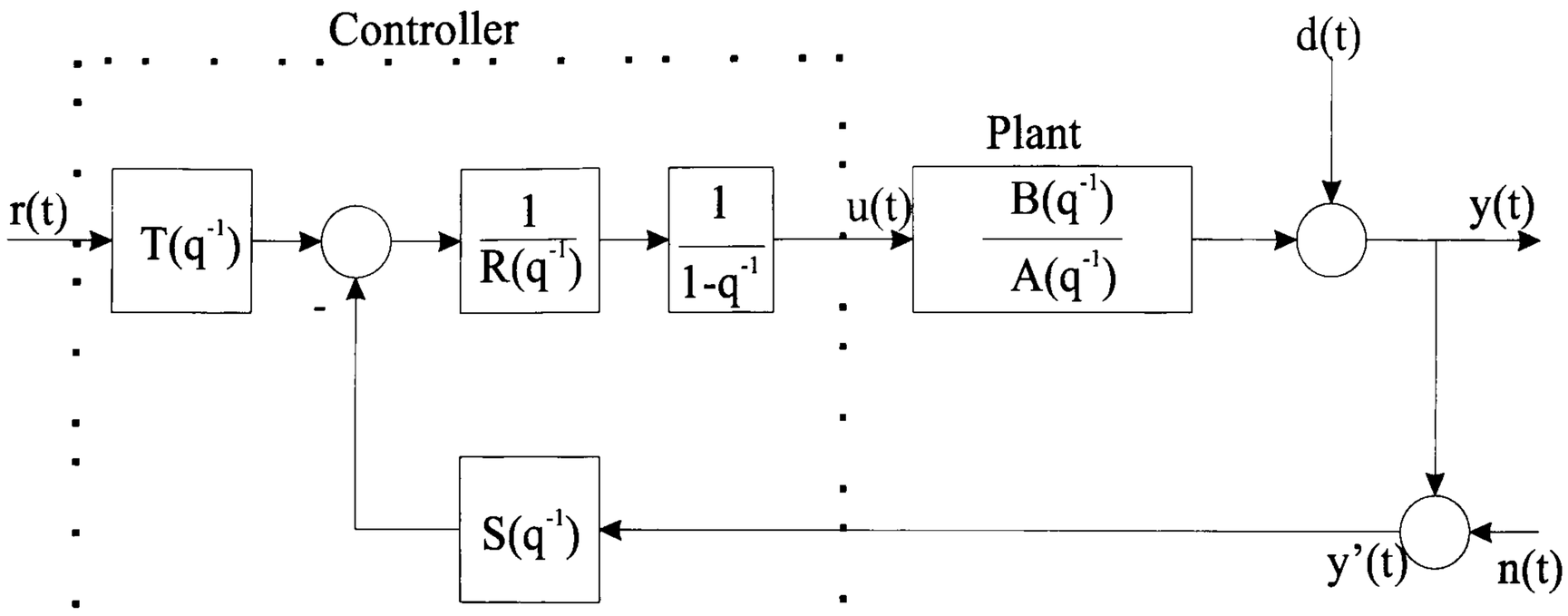

Figure 3.8: Generic feedback RST control loop structure. This figure is taken and modified from [33].

A controller that includes integral action, can become saturated by a large control error and will remain saturated even if the process output is changed. As the integrator is unstable, it will integrate up to a up to a very large value, and may take considerable time to reduce to a normal value. This is called integrator windup. When the plant is saturated, an extra feedback loop tries to make the error signal equal to zero. This is known as antireset windup [19].

Pole Placement Design

The pole placement approach to controller design is developed below. Pole placement refers to the fact that the design is formulated in terms of obtaining a closed loop system with specified poles. This method is based on prior knowledge of both the plant and a specified closed loop response, with the controller polynomials being the only unknown. If the plant has a transfer function $P = \frac{B}{A}$, and the compensator $C = \frac{Y}{X}$, then the closed loop characteristic equation is,

$$AX + BY = C_p \tag{3.6}$$

Where X and Y are the only unknowns and C_p is the desired closed loop poles.

The closed loop response can be specified most simply as a step, in the form of a standard second order differential equation, where the ω_n and ζ are defined by the designer :

$$\frac{\omega_n^2}{s^2 + 2\zeta\omega_n s + \omega_n^2} \tag{3.7}$$

For the design of an RST-type controller, a rise time, observer rise time and antireset windup (ARW) rise time can be specified by the designer. Also specific poles, with desired chacteristics, such as an integrator, can be designed into the controller.

3.7 Diophantine Equation

The development of the Diophantine equation is taken from an explanation given by Åstrom and Wittenmark [61].

The system has one control variable, u, and one measured output, y, which are related by the input-output model, see Figure 3.8

$$y(t) = \frac{B(q^{-1})}{A(q^{-1})}u(t) + d(t) \tag{3.8}$$

A general linear controller can be represented by,

$$R(q^{-1})u(t) = \frac{T(q^{-1})r(t) - S(q^{-1})y'(t)}{\frac{1}{1-q^{-1}}} \tag{3.9}$$

The integrator term seen in the denominator of Equation 3.9 is not carried through the derivation as it is taken as part of R.

Where the feed-forward pulse transfer function is $H_{ff} = \frac{T(q^{-1})}{R(q^{-1})}$ and the feedback pulse transfer function is $H_{fb} = \frac{S(q^{-1})}{R(q^{-1})}$, Eliminating $u(t)$ gives the equation,

$$(A(q^{-1})R(q^{-1}) + B(q^{-1})S(q^{-1}))y'(t) = B(q^{-1})T(q^{-1})r(t) \tag{3.10}$$

Characteristic polynomial of the closed loop system is,

$$A_{cl}(q^{-1}) = A(q^{-1})R(q^{-1}) + B(q^{-1})S(q^{-1}) \tag{3.11}$$

Which is simply an equation in the form of Eqn. 3.6. As $A_{cl}(q^{-1})$, $A(q^{-1})$ and $B(q^{-1})$ are known, the pole placement design simplifies to finding polynomials $R(q^{-1})$ and $S(q^{-1})$, such that the degree of $S(q^{-1}) \leq R(q^{-1})$.

The characteristic polynomial, $A_{cl}(q^{-1})$ can be factorised as,

$$A_{cl}(q^{-1}) = A_c(q^{-1})A_0(q^{-1}) \tag{3.12}$$

Where A_c is the controller polynomial and A_0 is the observer polynomial.

And, $T(q^{-1}) = t_o A_0(q^{-1})$, where $t_0 = \frac{A_c(1)}{B(1)}$. This condition of t_0 is chosen to obtain the static gain of the system, in this case to have unit gain and low frequency gain matching.

3.7.1 Cancelation of poles and zeros

It is possible to cancel poles and zeros that are well damped, in the controller design process. The polynomials A and B are factored as,

$$A = A^+ A^- \tag{3.13}$$

$$B = B^+ B^- \tag{3.14}$$

where A^+ and B^+ are the factors that can be cancelled, and are chosen to be monic. The polynomials A^+ and B^+ must have all their roots inside the unit circle. It follows that R, S and T have the structure,

$$R = B^+ \bar{R} \tag{3.15}$$

$$S = A^+ \bar{S} \tag{3.16}$$

$$T = A^+ \bar{T} \tag{3.17}$$

Which results in the characteristic equation,

$$A_{cl} = A^+ B^+ (A^- \bar{R} + B^- \bar{S}) = A^+ B^+ \bar{A}_{cl} \tag{3.18}$$

The polynomials A^+ and B^+ which are cancelled, become factors of the characteristic equation, A_{cl}. This can be factorised as,

$$A_c = B^+ \bar{A}_c \tag{3.19}$$

$$A_0 = A^+ \bar{A}_0 \tag{3.20}$$

So that, (as in Equation 3.12)

$$A_{cl} = A_c A_0 \tag{3.21}$$

Cancelling the common factors in Equation 3.18, we find,

$$A^- \bar{R} + B^- \bar{S} = \bar{A}_{cl} = \bar{A}_c \bar{A}_0 \tag{3.22}$$

Let the desired response to command signals to be given by,

$$y_m = (\frac{B_m}{A_m})r \tag{3.23}$$

By introducing,

$$R = A_m B^+ \bar{R} \tag{3.24}$$

$$S = A_m A^+ \bar{S} \tag{3.25}$$

$$T = \bar{B}_m \bar{A}_0 \bar{A}_c A^+ \tag{3.26}$$

It follows that the Diophantine equation is,

$$\bar{A}_0 \bar{A}_c = A^- \bar{R} + B^- \bar{S} \tag{3.27}$$

The Diophantine Equation can be solved using methods such as the Euclid's Algorithm or by the use of the Sylvester Matrix. However within polynomial toolbox in MATLAB, there is a function for solving this equation.

Degree Condition:

$$\deg A_{cl} = 2\deg A + \deg A_m + \deg R_d + \deg S_d - 1 \tag{3.28}$$

If polynomials $R_d(q^{-1})$ and $S_d(q^{-1})$, which specify given factors of $R(q^{-1})$ and $S(q^{-1})$, are introduced to the control, i.e. integral action and a notch filter, then the Diophantine Equation (Eqn. 3.27) becomes,

$$\bar{A}_{cl} = A^- R_d \bar{R} + B^- S_d \bar{S} \tag{3.29}$$

The controller is given by,

$$Ru = Tr - Sy' \tag{3.30}$$

Where,

$$R = A_m B^+ R_d \bar{R} \tag{3.31}$$

$$S = A_m A^+ S_d \bar{S} \tag{3.32}$$

$$T = \bar{B}_m A^+ \bar{A}_{cl} \tag{3.33}$$

$$B_m = \bar{B}_m B^- \tag{3.34}$$

and the closed loop characteristic equation is,

$$A_{cl} = A^+ B^+ A_m \bar{A}_{cl} \tag{3.35}$$

Which results, after simplification, in the degree condition given in Eqn. 3.28

3.7.2 ARX Models

The plant shown in Figure 3.8 ($\frac{B(q^{-1})}{A(q^{-1})}$) will be implemented in the form of an ARX model. The ARX model is identified from system identification data measured from the plant. System Identification methods build mathematical models of a dynamic system based on measured data. The System Identification Toolbox, within MATLAB, is utilised for identification of models, which result from sampled input/output (i-o) data [6]. A specific model structure is assumed, and the parameters in this structure are estimated using the data. Within a Graphical User interface (GUI), the order of the desired model can be selected, or multiple model orders can be identified and compared. It is important to remember that any estimated model is only a simple

[6]MATLAB Version 6.5, Release 13.

reflection of the actual system.

The models of the plant are created from"Working Data". The working data can be the entire recorded i-o, or a specific section of the data. The working data is then used to design the model, which is validated against the whole data set. For accuracy the validation data should be different from the working data. Ideally two identical identifications should be undertaken to design one model. The transfer function identified as the model is compared against the validation data, and is typically expressed as a percentage fit to that data. In the ARX case, the estimation involves an iterative, numerical search for the best fit. The ARX model structure is in the form :

$$A(q^{-1})y(t) = B(q^{-1})u(t - nk) + d(t)$$

The parameters are estimated using a prediction error method. The model orders are specified in the form $[n_a n_b n_k]$, where :

$n_a : A(q^{-1}) = 1 + a_1 q^{-1} + ... + a_{na} q^{-nb}$

$n_b : B(q^{-1}) = b_1 + b_2 q^{-1} + ... + b_{nb} q^{-nb+1}$

$n_k =$ the pure time delay

The structure is defined by the three integers n_a, n_b, and n_k. n_a is equal to the number of poles and n_b is the number of zeros. For a system under sampled data control, n_k is typically equal to 1, if there is no dead time. These integers are defined during the model design process and various combinations of structures can be examined.
Model selection compares the complexity of the model to the percentage fit of the model to the validation data. A trade off has to be made between an increase in percentage fit to an increase in model complexity. For example a second order model has a 57 % fit and a fifth order model has a 60 % fit. The increase in complexity of the fifth order model would outweigh the 3 % increase in fit and therefore the second order model would be chosen to design a controller.

reflection of the actual system.

The models of the plant are created from"Working Data". The working data can be the entire recorded i-o, or a specific section of the data. The working data is then used to design the model, which is validated against the whole data set. For accuracy the validation data should be different from the working data. Ideally two identical identifications should be undertaken to design one model. The transfer function identified as the model is compared against the validation data, and is typically expressed as a percentage fit to that data. In the ARX case, the estimation involves an iterative, numerical search for the best fit. The ARX model structure is in the form :

$$A(q^{-1})y(t) = B(q^{-1})u(t - nk) + d(t)$$

The parameters are estimated using a prediction error method. The model orders are specified in the form $[n_a n_b n_k]$, where :

$n_a : A(q^{-1}) = 1 + a_1 q^{-1} + ... + a_{na} q^{-nb}$

$n_b : B(q^{-1}) = b_1 + b_2 q^{-1} + ... + b_{nb} q^{-nb+1}$

$n_k =$ the pure time delay

The structure is defined by the three integers n_a, n_b, and n_k. n_a is equal to the number of poles and n_b is the number of zeros. For a system under sampled data control, n_k is typically equal to 1, if there is no dead time. These integers are defined during the model design process and various combinations of structures can be examined.
Model selection compares the complexity of the model to the percentage fit of the model to the validation data. A trade off has to be made between an increase in percentage fit to an increase in model complexity. For example a second order model has a 57 % fit and a fifth order model has a 60 % fit. The increase in complexity of the fifth order model would outweigh the 3 % increase in fit and therefore the second order model would be chosen to design a controller.

4 Power and Motor Control

This chapter details the motor and power control during FES cycling. The control of an electric motor is an established concept which is applied to many everyday applications. In comparison, the introduction of an electric motor in conjunction with FES power control is a relatively new concept.

In this chapter the literature is discussed which relates to the measurement of power, the control of power and the methods used to incorporate an auxiliary power source into FES cycling. Thereafter, the control system for motor and power control is presented. This work focuses on the design of the controllers for both the motor and power control loops. Results are presented where these controllers have been applied for exercise testing. The power controller work is supplemented with a section investigating possible new methods for controlling power in FES cycling.

4.1 Power Control in FES Cycling Literature

Throughout many studies the power output from FES cycling has been measured and used as measure of increased performance. Few papers attempt to control power. Instead a stimulation level is maintained and the resulting power recorded. The literature discussed in the next section identifies the key studies that have measured and compared power results.

4.1.1 Power Output During FES Cycling

Theisen et al. [63] analysed external power output (PO) changes during cycling with FES. Measurements of physiological responses in 5 paraplegic subjects during 40 minutes of FES cycling were also recorded. Subjects cycled under constant stimulation amplitude (140 mA) and a constant pedalling rate of 50 rpm. A customised MOTOMed Viva cycle ergometer[1], which calculates the power by the negative motor current resulting from the torque exerted on the crank, was utilised. The protocol states that the first 5-10 revolutions were performed with no stimulation, to take into account the effects of leg weight in the power calculations.

Theisen comments on previous studies where the power output is not a well controlled variable, as the cycling resistance is adjusted to maintain a reference cadence of 35-50 rpm. As the cadence varies, the power varies in direct proportion. The results show that PO demonstrated a strong time related dependency and showed significant changes even under constant stimulation. After 2 minutes, PO reached a maximum, followed by a sharp drop after 6 minutes. It then rose again to a level below the maximum after 19.5 minutes. The efficiency after 6 minutes was 3.3 ± 1.1 % and had a significant increase to 4.7 ± 1.2 % after 19.5 minutes.

Theisen concluded that external power output production during prolonged FES cycling is highly variable, despite constant electrical stimulation and $\dot{V}O_2$. However it is important to note that no attempt was made to control the power produced. A decrease in PO output at 2-6 minutes was suggested to be due to maximum stimulation intensity being achieved and no further muscle fibres being recruited. Also, antagonistic muscle stimulation through increased stimulation during the initial phase, may decrease PO and hence efficiency. Furthermore, they conclude that $\dot{V}O_2$ increases linearly with work intensity, such that pulmonary $\dot{V}O_2$ is linearly related to absolute mechanical PO. This study clearly indicates the low power levels achieved for metabolic energy expended, and hence low metabolic efficiencies.

[1]MOTOMed, Reck, Germany

Glaser et al. compared the efficiency of Functional Neuromuscular Stimulation (FNS) leg cycle ergometry with SCI and leg cycling with able bodied (AB) cyclists [24]. 20 SCI and 20 AB subjects cycled on a ERGYS 1 system for 5 minute bouts, followed by 5 minutes rest, at increments of 6 W. The cadence remained constant at 50 rpm. The efficiency of the exercise was calculated in four ways:

1. Gross Efficiency - no baseline correction
2. Net Efficiency - resting metabolism as baseline correction
3. Work Efficiency - unloaded cycling metabolism baseline correction
4. Delta Efficiency - metabolism at a lower PO as baseline correction

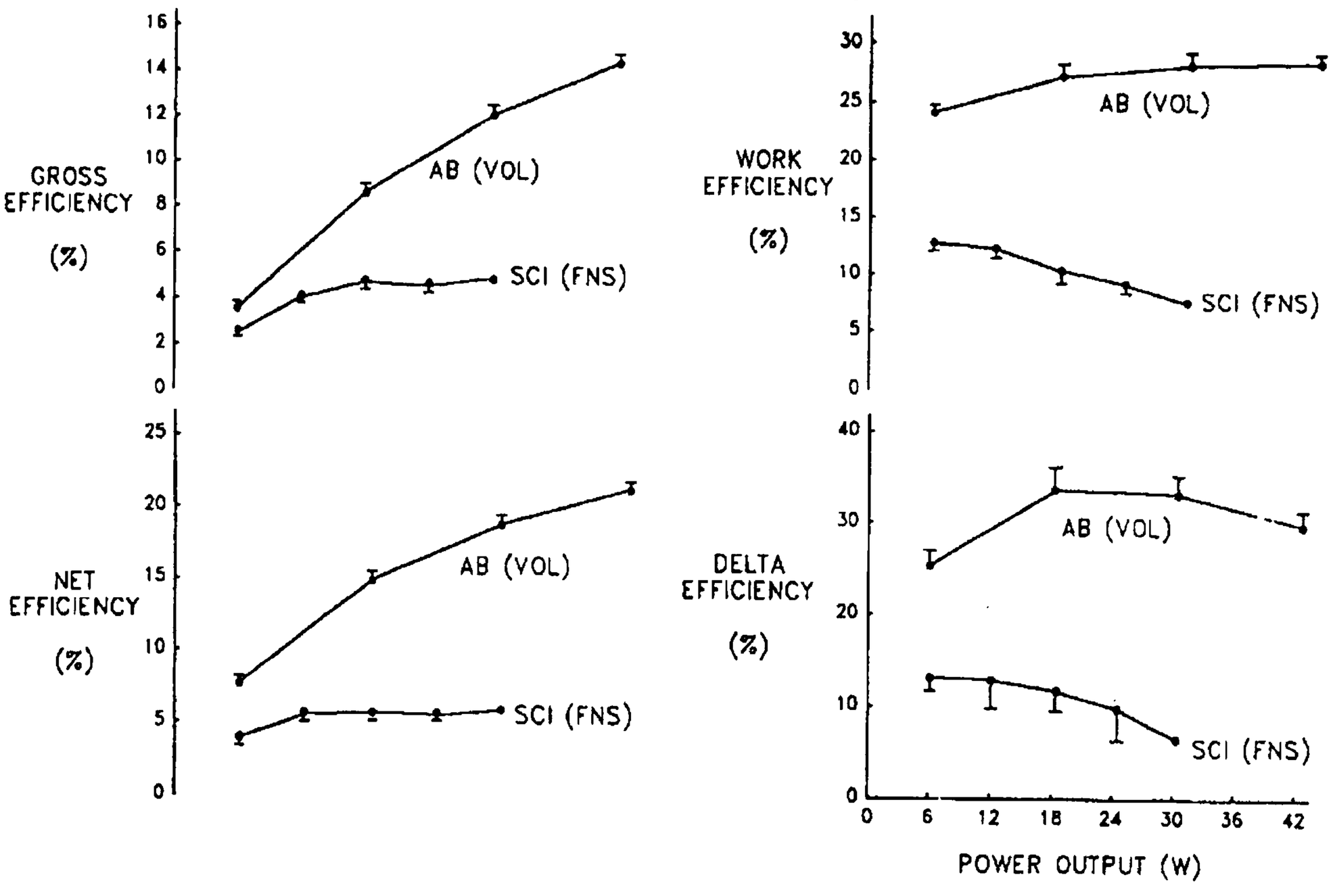

Figure 4.1: The four different methods of measuring efficiency are shown: Work, Gross, Delta and Net efficiency. The difference between Able bodied and SCI efficiency can be seen clearly. This figure is reproduced from [24].

Each baseline correction results in a different efficiency value. These can be seen in Figure 4.1. In [63], Theisen et al. determine the gross efficiency, with comparable efficiency results for the SCI subjects. The efficiency calculations indicate the significant

differences in AB and SCI efficiencies for cycling.

When Oxygen Uptake is plotted against PO for these experiments (see Figure 4.2), the oxygen uptake can be seen to be higher in the SCI, compared to the AB subjects. These findings are supported by a previous study, by the same authors [23], where significantly higher levels of HR and $\dot{V}_E$ are reported for SCI compared to AB subjects, over a similar power range. $\dot{V}_E$ is the volume of expired air during exercise. The authors conclude that even though this highlights the inefficiencies in FNS cycling, it can actually be desirable due to the high metabolic and cardiopulmonary responses, at relatively low power levels. The functionality of FES cycling could be considered when deciding on what level of efficiency is required. For example, for mobile cycling, a higher efficiency would be desirable, to extend the range of cycling, whereas, for an exercise, a short, inefficient strategy may be more acceptable to illicit higher levels of metabolic work.

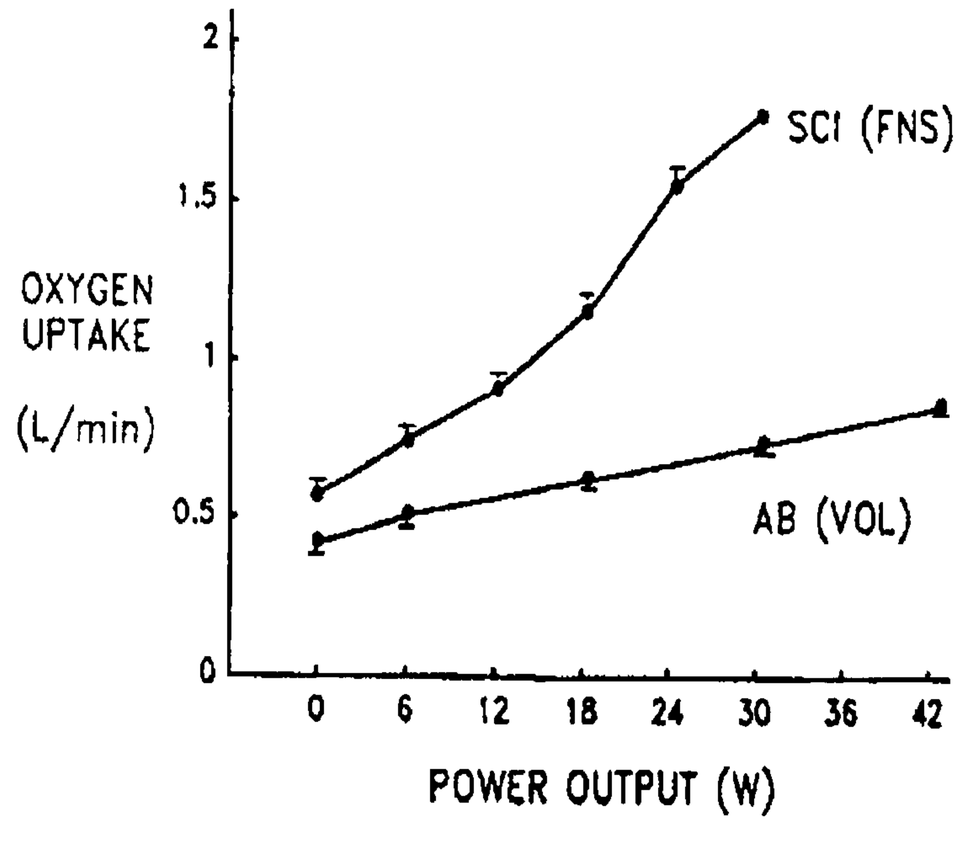

Figure 4.2: Mean oxygen uptake of SCI and AB subjects during steady state-rate cycle ergometer exercise at various PO levels. Figure reproduced from [24].

Eser et al. [14] examined the relationship between PO and the stimulation frequency of paralysed muscle during cycling. Their aim was to determine whether stimulation frequencies higher than 30 Hz would increase PO for a cycling period of 30 minutes.

Cycling was implemented on a Stim Master[2] system and PO was logged every minute and averaged over the 30 minute period.

The mean power output was 12.1, 14.2 and 14.8 W for 30, 50, and 60 Hz respectively. The maximum power produced was 29.5 W, at 60 Hz stimulation. This maximum power was recorded in the first and second minute, which corresponds to results found by Theisen [63]. The authors suspect that power output maybe related more to physical activity level before injury and thickness of subcutaneous fat layer, than to lesion level. It was also noted that power output at the end of the sessions was higher than the average power output of the whole session, which suggests that no fatigue is detected at the end of the session. They conclude that a higher PO is achieved by using a stimulation frequency of 60 compared to 30 Hz, and that a higher stimulation frequency should be used for FES cycling.

Kjær et al. [39] investigated cardiovascular and ventilatory responses to electrically induced cycling with complete epidural anaesthesia in AB subjects. Cycling was conducted on a ERGYS I system. While subjects cycled without anaesthesia and stimulation cardiovascular and respiratory responses were measured, including Heart Rate (HR), $\dot{V}O_2$, Mean Arterial Pressure (MAP) and Cardiac Output (CO).

The subjects then cycled under anesthesia via FES, which caused cutaneous sensory anaesthesia below T8-T9 and complete paralysis of the legs, also resulting in absence of both central command and neural feedback from the contracting muscle. PO was measured and compared for both situations, from an ERGYS system. The power produced was markedly lower by a factor of approximately one third under stimulation (see Figure 4.3). Minute Ventilation ($\dot{V}E$), the volume of air taken into or exhaled from the body, was higher under FES.

Stimulation of the 3 muscle groups by FES is intended to represent the natural cycling action. These results indicate that there is a high inefficiency in the stimulation of

[2]www.stimmaster.com

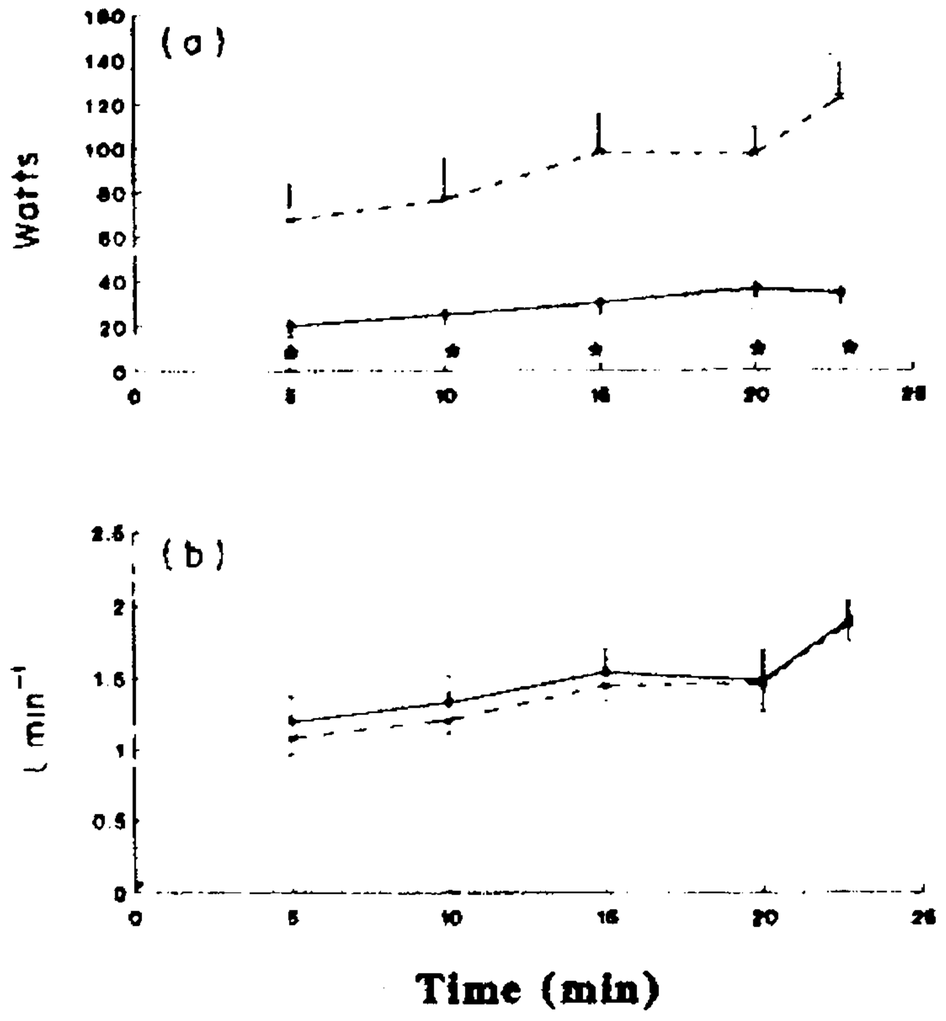

Figure 4.3: The power produced under voluntary cycling is represented by the dashed line and with FES by the solid line in part (a). The power (Watts) is plotted against time (min). Part (b) shows the $\dot{V}O_2$ uptake for both cases. The $\dot{V}O_2$ uptake is similar for both voluntary and FES cycling. This figure is reproduced from [39].

muscle. The stimulated muscle in this study has not atrophied, as it would be in an SCI person. The power output of an SCI person would be significantly lower due to the poor condition of the atrophied muscle, depending on the time post injury. This study questions both the efficiency and techniques of FES cycling.

Power Output (PO) has also been measured in a seated posture. Ragnarrson et al. [55] showed a PO increase of 50%, during 1 week of FES knee extension training programme. At the start of training the subjects trained against a resistance of 25N, which increased to 37 N at the end of the 4^{th} week. At this point the subjects progressed to cycling on an ERGYS 1 System. They state that all quadriceps muscles (19 subjects), no matter how weak initially, gained both strength and endurance with training.

Sinclair et al. [59] recorded pedal forces during FES cycling in paraplegics, on an ERGYS I System, and compared them to able-bodied subjects cycling at the same work rate. Results show that paraplegic subjects applied significantly larger peak forces than

the able bodied subjects because of the short duration of neuromuscular stimulation. Able bodied subjects were able to achieve the same average workload by applying a smaller force over each revolution. It is suggested that these large forces contribute to the low efficiencies measured by Petrofsky [49]. Sinclair et al. further conclude that if the muscle was stimulated over a wider range of angles, then it may be possible to reduce the peak force. This is not possible on the ERGYS I system, due to fixed on/off angles. A study by Ferrario et al. investigated this [17]. It was found that increasing the stimulation arc reduces the efficiency of the stimulation applied to the muscle to force relationship. It is also observed that the oxygen cost at constant power FES cycling can be influenced by the stimulation arcs employed.

4.1.2 Assisted Cycling

The concept of assisted cycling was first introduced by Petrofsky, as discussed earlier (Section 1.4.1), but motor assisted FES cycling is an area where only a relatively small amount of work has been published, compared to traditional FES cycling. Two groups have employed a motor during FES cycling.

Gföhler and Lugner have published a number of papers [1],[20],[22] describing a tricycle configuration and optimized stimulation pattern. In [21], an electric motor is utilised in order to reduce muscle spasm, allowing for passive movement of the lower extremities before FES is initiated. Results show that the patients have fewer spasms when cycled passively by the motor before FES is applied. The motor was implemented in a feed-forward manner, and was employed to overcome gradients. The stimulation time was also shortened to overcome spasm during cycling. They state that paralysed muscles are mostly atrophied and only a limited number of effective leg muscles can be reached by surface electrodes. It is therefore important to convert the generated muscle force into drive power with highest possible efficiency.

Gföhler and Lugner utilised an adapted FES cycling ergometer to optimize the stimulation and pedalling pattern. They developed a three bar linkage [20], to optimize

the pedal path. The linkage consisted of a wing, coupler and crank, and makes the pedal move along a non-circular path. A force-measurement crank was also developed and integrated, measuring the force which is transferred from the crank to the torque measuring shaft, via the chain, by means of 4 strain gauges. The force developed by the muscle is determined by subtracting the measured passive power from the power measured with stimulation. This force measuring system is similar to the SRM[3] sensor employed in our studies. The SRM sensor is detailed in Section 3.2.1 and in [35].

A study by Pons et al. [52] developed a four wheel mobile 'paracycle'. An electric motor was provided to drive the pedals at a speed suitable for passive cycling and to accelerate the vehicle from rest. The motor was also used as a brake to slow the paracycle. A motor power of 5 W was used when training with paraplegic subjects. This power addition was used to compensate for losses in the gearing, rather than to drive the pedals. As Gföhler et al., the motor was implemented in a feedforward manner.

The stimulation strategies for this study were determined by means of EMG measurements. EMG of 5 healthy subjects was recorded while cycling. These strategies were then modified until the 'smoothest action' was found. Smoothness was evaluated subjectively. Poor correlation was found between the expected stimulation sequence (EMG) and the sequence finally chosen. In section 1.4.1, it was discussed how Petrofsky used EMG to determine on/off stimulation [44]. Petrofsky does not discuss if a good correlation was found.

We have developed our own motor assisted FES tricycle, which is discussed in detail in [35] and in the sequel. In comparison to the papers by Gföhler and Pons our system utilises the motor as a propulsion aid. The motor is part of a 2-loop integrated control strategy, which combines the motor and stimulated leg power, to produce a combined output power. The addition of the motor is also a highly useful aid for metabolic exercise testing as the cadence and power can be independently controlled.

[3]Schoberer Rad Messtechnik(SRM) http://www.srm.de

Various other groups have discussed the idea of assisted wheelchair propulsion. Glaser et al, [25] demonstrated an FES propulsion system for a wheelchair. By means of a linkage system and stimulation of the quadriceps muscles, a footplate is moved driving a ratchet and pawl, which elicits forward propulsion of the chair. This system demonstrated, in 1983, that this addition to a wheelchair was a feasible concept. A similar system has been developed more recently by James et al. [37]. Using knee angle, the quadriceps and hamstring muscles are stimulated, generating propulsion via a similar mechanism. These concepts have been developed to be included in a cycling system, notably by Berkelmans et al. [5] and the development of the Berkel Bike. The Berkel Bike is a hybrid FES tricycle. A hand crank and FES cycling mechanism is added to a conventional wheelchair. The hand cranking is used to passively rotate the legs before stimulation is applied to the quadriceps, hamstrings and gluteal muscles. Thereafter the hand cranking provides additional propulsion to the legs. A further study [6] showed a significant increase in power output (86-96 W) and an increase of $\dot{V}O_{2peak}$ (25.7-28.1 ml/min/kg), after a 4 week training period.

4.2 Cadence and Power Control

This section describes the control of power and cadence for FES cycling. The control structure is firstly discussed, followed by how the power and cadence loop interact to produce a total power output at the rear wheel. The identification of the power and cadence dynamics are presented, followed by the design and development of the controllers. The controllers are tested and results from both constant load and incremental tests are presented. This will indicate practical applications for these controllers.

4.2.1 Control Structure

The control structure employed to simultaneously control leg power and cycling cadence is shown in Figure 4.4. The two control loops are designed independently but act together to produce a positive cycling action.

In the first loop, the cadence of the pedals is controlled via an electric motor. The motor input signal (%) is adjusted to maintain a reference cadence. The cadence is measured via the shaft encoder on the pedals. The motor is used to maintain a constant cadence, while overcoming factors such as slope, friction and fatigue.

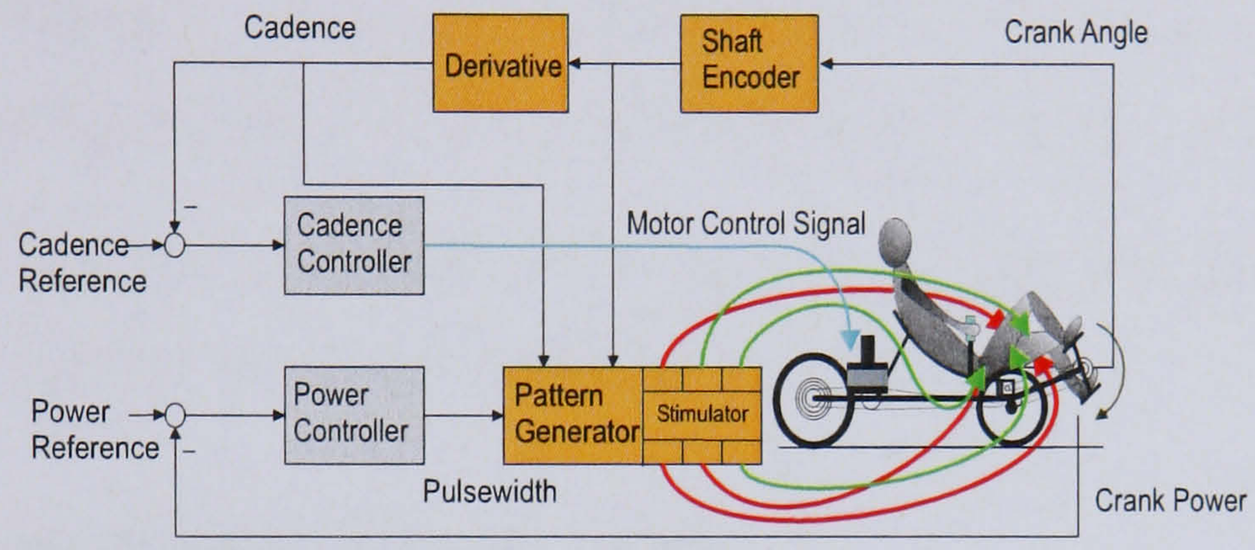

Figure 4.4: Integrated closed loop control scheme. One loop automatically adjusts the motor input to maintain a reference cadence. The second loop automatically adjusts the stimulation pulsewidth to keep the leg power close to an arbitrary reference value.

The second loop provides feedback control of leg/muscle power. As previously discussed (Section 3.2.1), the power produced at the cranks is measured via the SRM sensor. The stimulation pulsewidth is automatically adjusted to maintain a reference power level. This control structure allows for independent control of 2 variables, which combine to produce the total mechanical output power and a smooth cycling action. For example, if the power reference is increased, the speed at which the pedals are rotating will tend to increase. This results in the motor input signal automatically decreasing to maintain the reference cadence.

4.2.2 Identification of Motor Dynamics

The open loop dynamics of the electric motor-cyclist system are identified initially, a model is identified and a controller is designed. The system identification and controller design steps consists of the following steps.

- Open Loop PRBS Test: The subject sits on the tricycle with their legs secured in the orthoses. The motor input signal is increased via the throttle until a mean value is reached, where a PRBS signal is applied. The resulting cadence is measured via the shaft encoder. No stimulation is applied at this stage. The PRBS is designed using prior knowledge of the cyclists abilities and the cadence at which they are comfortable cycling.

- Model Identification: A transfer function model is estimated to the input-output data (motor input-cadence). The model is assessed against validation data.

- Controller Design: A controller is designed using the pole placement method, with a specified closed loop rise time and damping.

Input-Output Identification Data for Subject 1

The open loop identification data for the motor cadence/loop are shown in Figure 4.5 for subject 1. The sample frequency (Ts) is 20 Hz. The total data set is shown in Figure 4.5(a), while the zoomed plot of Figure 4.5(b) focuses on part of the data used for estimating the model. The motor input signal is shown in the lower part of the graphs. The measured cycle cadence is the solid line in the upper part of the graphs. The high-frequency ripple in the measured output is caused by the weight of the legs during each cycle (the frequency of the ripple is twice that of the cycling cadence). This input-output data is used to identify linear models, and it was found that a second-order linear transfer function was sufficient for good approximation. The second-order model was simulated with the PRBS input which was applied to the physical system, using a short sequence from the overall data set. The simulated output is plotted as the dashed line in the upper graphs of Figure 4.5(a) (best seen in the zoomed plot of Figure 4.5(b)). A number of model orders were estimated, but as discussed in section 3.7.2 a second order model was the best trade off between percentage fit and model complexity. It is seen that the model captures the dominant dynamic response of the motor loop. For the purposes of control design, it is unnecessary for the model to capture the high-frequency gravitational effects of the legs acting on the pedals, since it is not desirable for the controller to try and counteract these effects.

The identified model has the transfer function;

$$\frac{0.004769z^{-3}}{1 - 1.923z^{-1} + 0.8871z^{-2}} \tag{4.1}$$

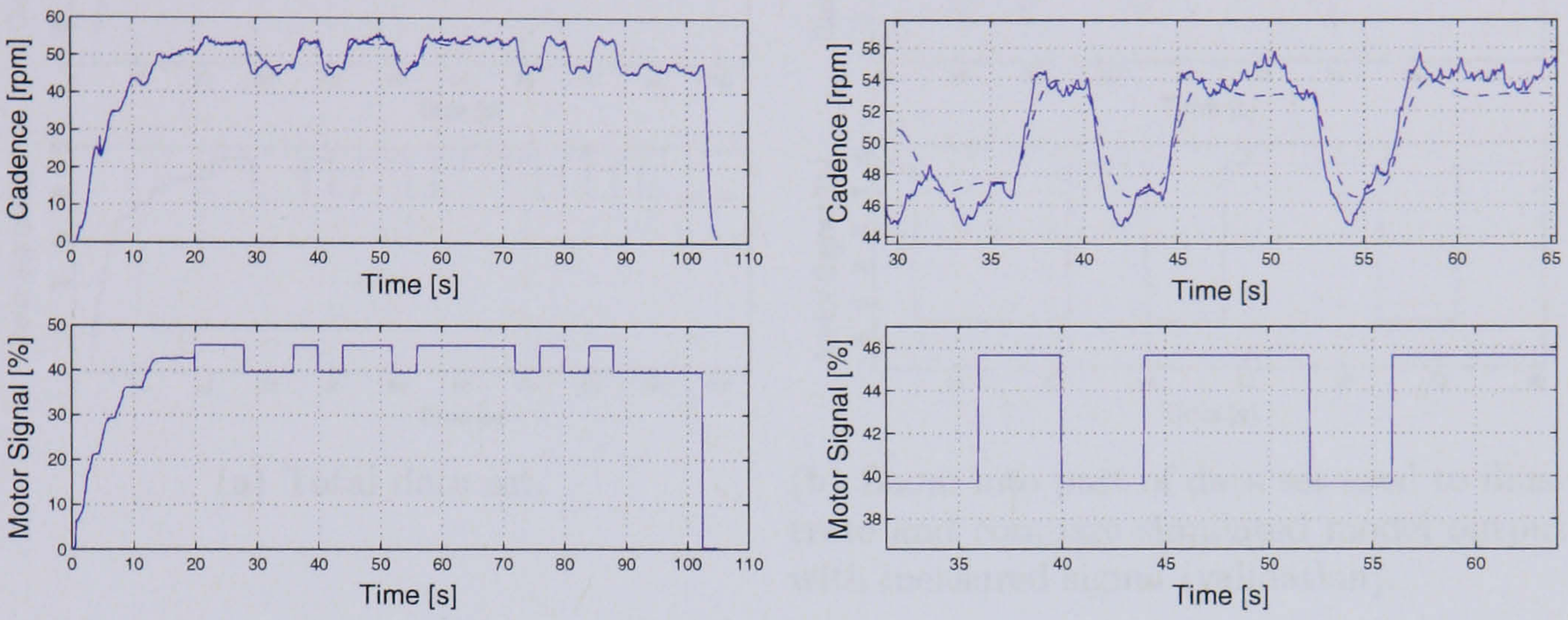

(a) Total data set.

(b) Zoom into part of data set used to illustrate and compare simulated model output with measured signal (validation).

Figure 4.5: Identification of motor input - cadence system for Subject 1. The normalised motor input signal is shown in the lower graphs. The upper graphs show the corresponding cycle cadence (solid line). The dashed line in the upper graphs is the output of the identified model.

Input-Output Identification Data for Subject 2

Similarly, the process is repeated for Subject 2, as shown in Figure 4.6. The identified model has the transfer function;

$$\frac{0.001245z^{-3}}{1 - 1.876z^{-1} + 0.8871z^{-2}} \tag{4.2}$$

Motor Controller Design

The identified models' transfer functions are used to design controllers. The RST controller is designed as discussed in section 3.6. The ARX structure and rise-times of the motor controllers are shown in Table 4.2.

The motor controller for Subject 1 has transfer function,

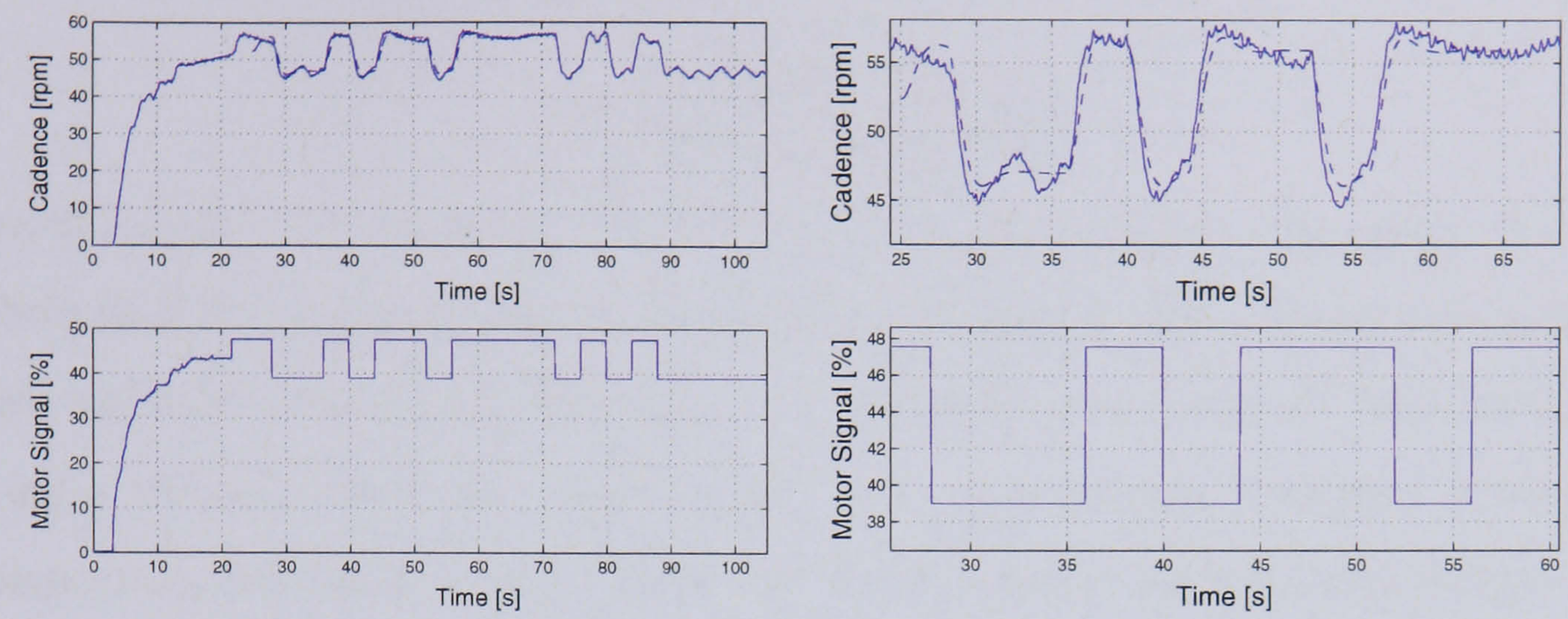

(a) Total data set.

(b) Zoom into part of data set used to illustrate and compare simulated model output with measured signal (validation).

Figure 4.6: Identification of motor input - cadence system for Subject 2. The normalised motor input signal is shown in the lower graphs. The upper graphs show the corresponding cycle cadence (solid line). The dashed line in the upper graphs is the output of the identified model.

ARX Structure	[2 1 3]
Controller T_R	3 s
Observer T_R	1.5 s
ARW T_R	10 s
Ts	0.05 s

Table 4.1: Rise times and Controller structure for the Motor Controllers

$$\frac{0.004164z^{-3}}{1 - 1.715z^{-1} + 0.9604z^{-2}} \tag{4.3}$$

and the motor controller for Subject 2 has transfer function,

$$\frac{0.004269z^{-3}}{1 - 1.871z^{-1} + 0.8799z^{-2}} \tag{4.4}$$

Figure 4.7 shows the sensitivity functions for the motor loops. The plots of $|S|$ and $|T|$ show that the gravitational leg ripple has a frequency well outside the bandwidth of both loops (it is (50 rpm)/(60 s·min^{-1}) = 0.833 Hz, or 5.2 rad/s). This means that the ripple will not affect the control signal, i.e. that neither controller attempts to attenuate this disturbance (since $|S| \approx 1$ at this frequency for both controllers).

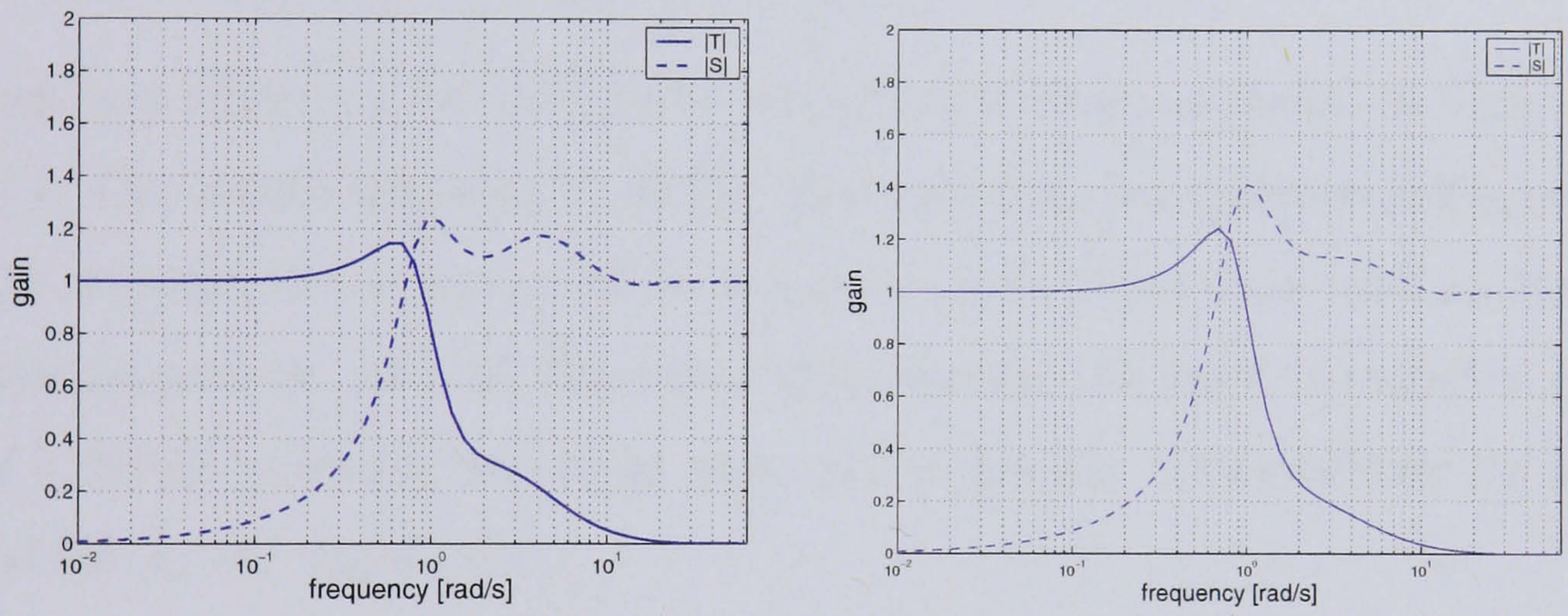

(a) Magnitude of closed loop sensitivity and complimentary sensitivity for Subject 1.

(b) Magnitude of closed loop sensitivity and complimentary sensitivity for Subject 2.

Figure 4.7: Sensitivity Functions for the Motor Loop.

4.2.3 Identification of Power Dynamics

The open loop dynamics of the stimulation-power system are identified initially, a model is identified and a controller is designed. The system identification and controller design steps consist of the following;

- Open Loop PRBS Test: The subject sits on the tricycle with their legs secured in the orthoses. The motor is controlled to a constant cadence of 50 rpm. The stimulation input signal is increased via the throttle until a mean value is reached, where a PRBS signal is applied. The resulting power is measured via the SRM sensor.The PRBS is designed using prior knowledge of the cyclists abilities and the power at which they are comfortable cycling.

- Model Identification: A transfer function model is estimated to the input-output data (stimulation - power). The model is assessed against validation data.

- Controller Design: A controller is designed using the pole placement method, with a specified closed loop rise time and damping.

Input-Output Identification Data for Subject 1

The open loop identification data for the stimulation/power is shown in Figure 4.8 for subject 1. The sample frequency is 20 Hz. The total data set is shown in Figure 4.8(a), while the zoomed plot of Figure 4.8(b) focuses on part of the data used for the model identification process. As with the motor identification the input stimulation is in the form of a PRBS, shown in the lower parts of the graphs. The resulting leg power is the solid line in the upper plots.

During the identification the motor controller was used to maintain a constant cycling cadence of 50 rpm. A first order model was found to model the dynamics, and the model output is simulated (dashed line) in the upper part of Figure 4.8(b).

The identified model has the transfer function;

$$\frac{0.002202z^{-3}}{1-0.9834z^{-1}} \tag{4.5}$$

Input-Output Identification Data for Subject 2

Similarly, the process is repeated for Subject 2, as shown in Figure 4.9. In this figure the power increases in the initial 10 s of the identification, with no stimulation applied.

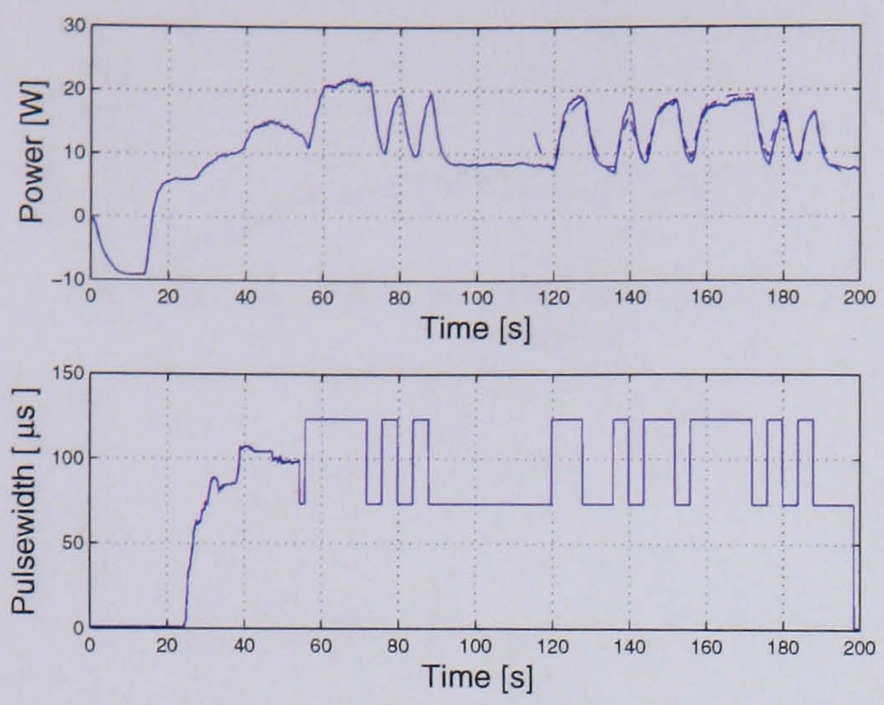

(a) Total data set.

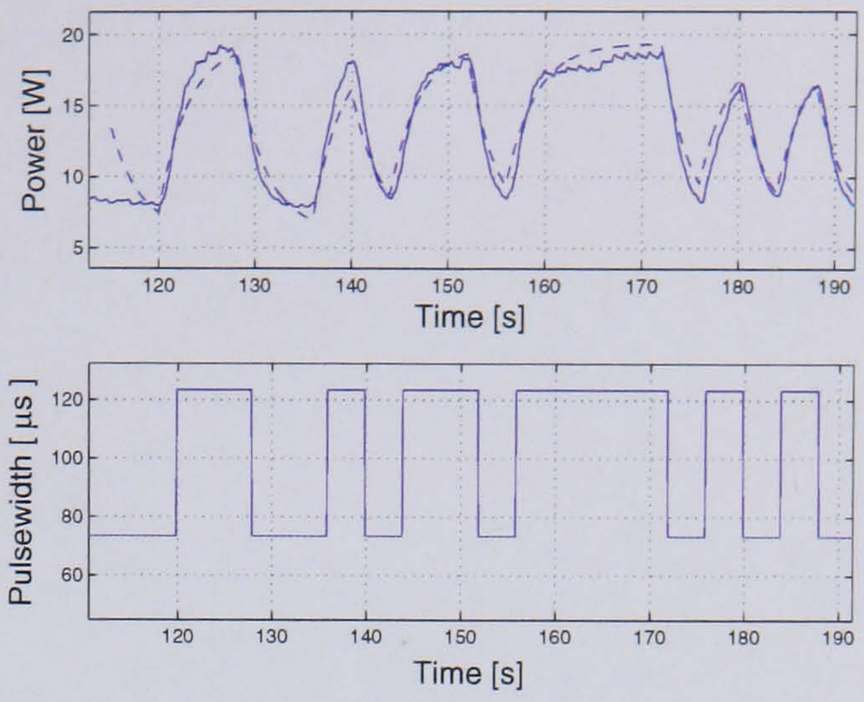

(b) Zoom into part of data set used to illustrate and compare simulated model output with measured signal (validation).

Figure 4.8: Identification of stimulation - leg power system for Subject 1. The pulsewidth input signal is shown in the lower graphs (PRBS signal). The upper graphs show the corresponding leg power (solid line). The dashed line in the upper graphs is the output of the identified model.

This is due to the experimenter rotating the pedals to aid the start-up of cycling.

The identified model has the transfer function;

$$\frac{0.00264z^{-3}}{1-0.9853z^{-1}} \tag{4.6}$$

Power Controller Design

The identified model's transfer functions are used to design controllers. The RST controller is designed as discussed in section 3.6 The ARX structure and rise-times of the power controllers are shown in Table 4.2.

ARX Structure	[1 1 3]
Controller T_R	10 s
Observer T_R	15 s
ARW T_R	15 s
Ts	0.05 s

Table 4.2: Rise times and Controller structure for the Power Controllers

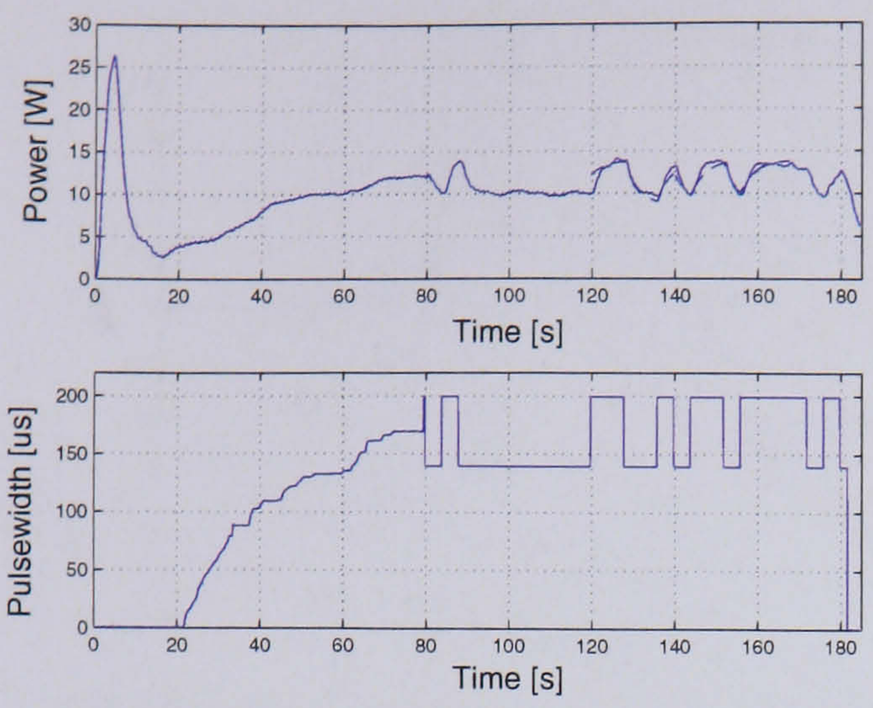

(a) Total data set.

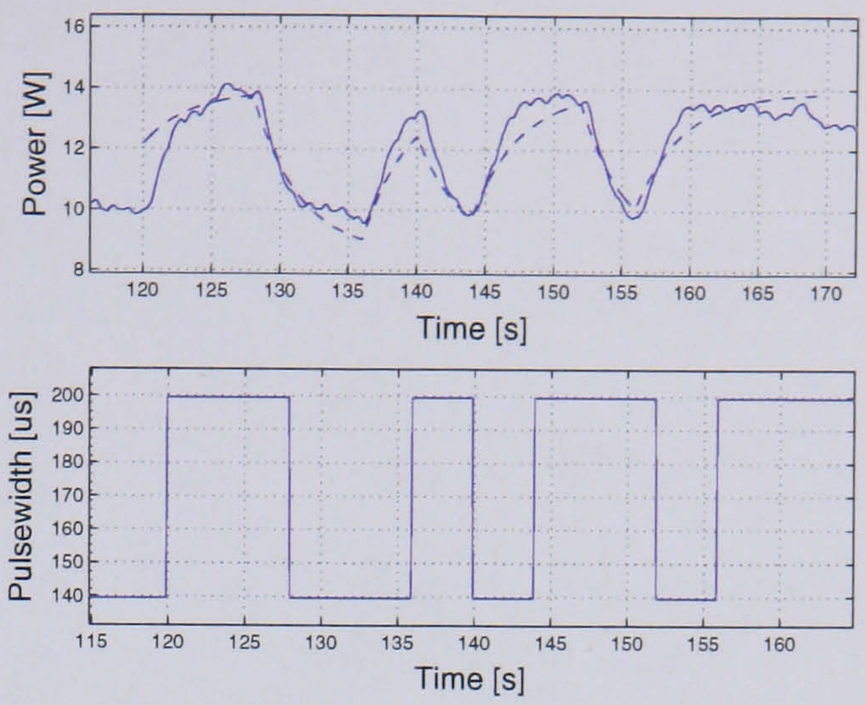

(b) Zoom into part of data set used to illustrate and compare simulated model output with measured signal (validation).

Figure 4.9: Identification of stimulation - leg power system for Subject 2. The pulsewidth input signal is shown in the lower graphs (PRBS signal). The upper graphs show the corresponding leg power (solid line). The dashed line in the upper graphs is the output of the identified model.

The power controller for Subject 1 has transfer function,

$$\frac{0.001102z^{-3}}{1 - 1.934z^{-1} + 0.9354z^{-2}} \tag{4.7}$$

and the power controller for Subject 2 has transfer function,

$$\frac{0.004952z^{-3}}{1 - 1.956z^{-1} + 0.9564z^{-2}} \tag{4.8}$$

Figure 4.10 shows the sensitivity functions for the power loops.

4.2.4 Controller Performance Results

3 tests are undertaken to assess the performance of the controllers. The tests are detailed below;

Cadence Tracking The reference cadence is changed in a step-wise manner, while the reference power remains constant.

Power Tracking The reference power is changed in a step-wise manner, while the reference cadence remains constant.

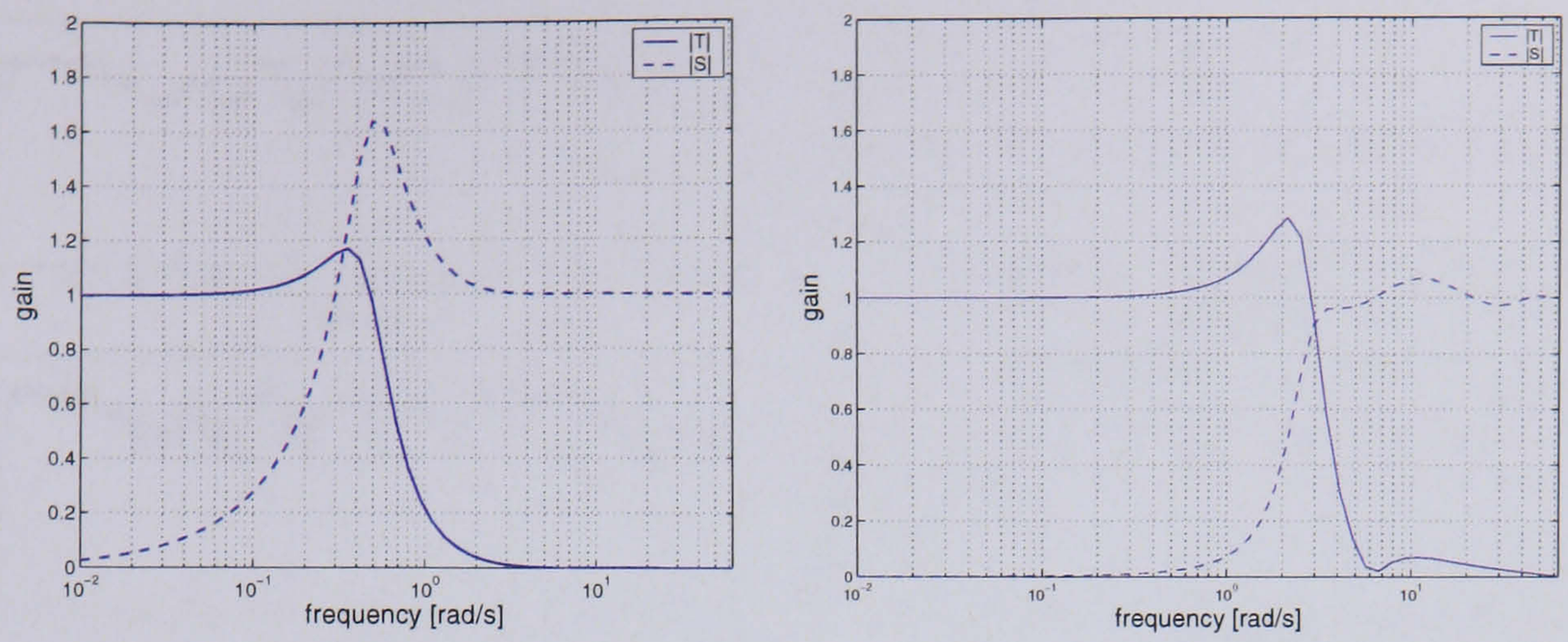

(a) Magnitude of closed loop sensitivity for Subject 1.

(b) Magnitude of closed loop sensitivity for Subject 2.

Figure 4.10: Sensitivity Functions for the Power Loop.

Disturbance Rejection The power and the cadence reference values are held constant, while the resistance at the rear wheel is changed to simulate a disturbance such as slope or air resistance.

It is desired that both the cadence and power will track their corresponding reference levels within an error band of 10 %.

Cadence Tracking

Figures 4.11 and 4.12 show the cadence tracking results for Subject 1 and Subject 2 respectively. In both upper parts of Figures 4.11(a) and 4.12(a), the cadence (solid line) is seen to track well to the reference level (dotted line). The motor input signal in the lower part of these figures is seen to change when the reference cadence is altered.

The corresponding power responses are shown in the upper part of Figures 4.11(b) and 4.12(b). The power reference (dotted line) was held constant at 10 W for Subject 1 and 12 W for Subject 2. Subject 2 has a higher reference power level due to a higher power level used during training sessions. The actual power (solid line) tracks well to the reference following an initial transient. The initial transient in the actual power (in the first 10 s of the test) results from the experimenter manually rotating the pedals.

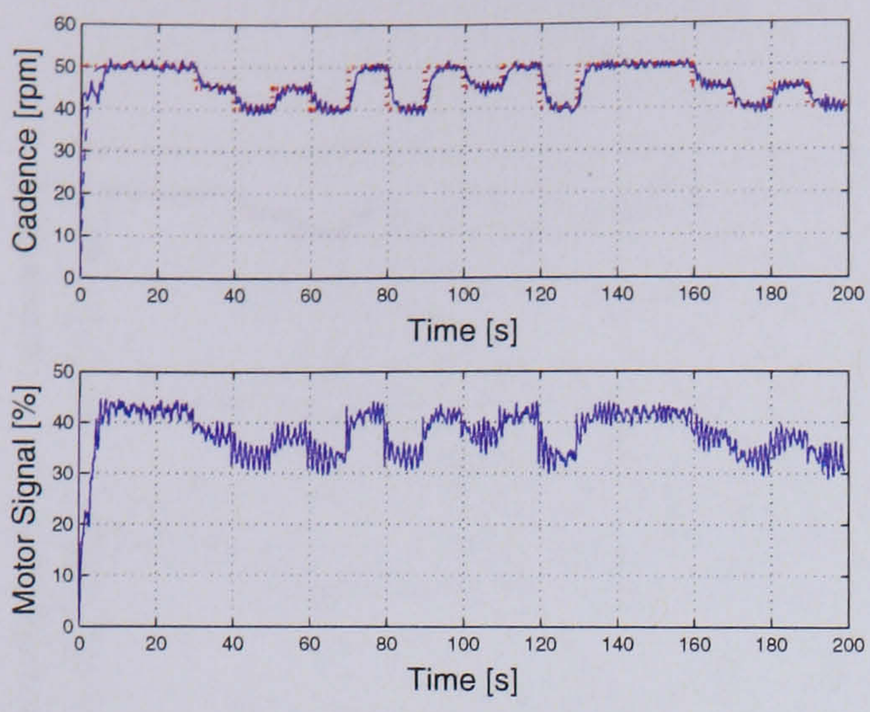

(a) Motor loop response. The upper graph shows the reference cadence (dotted line), the measured cadence (solid line), and the ideal cadence response (dashed line). The lower plot shows the motor input signal.

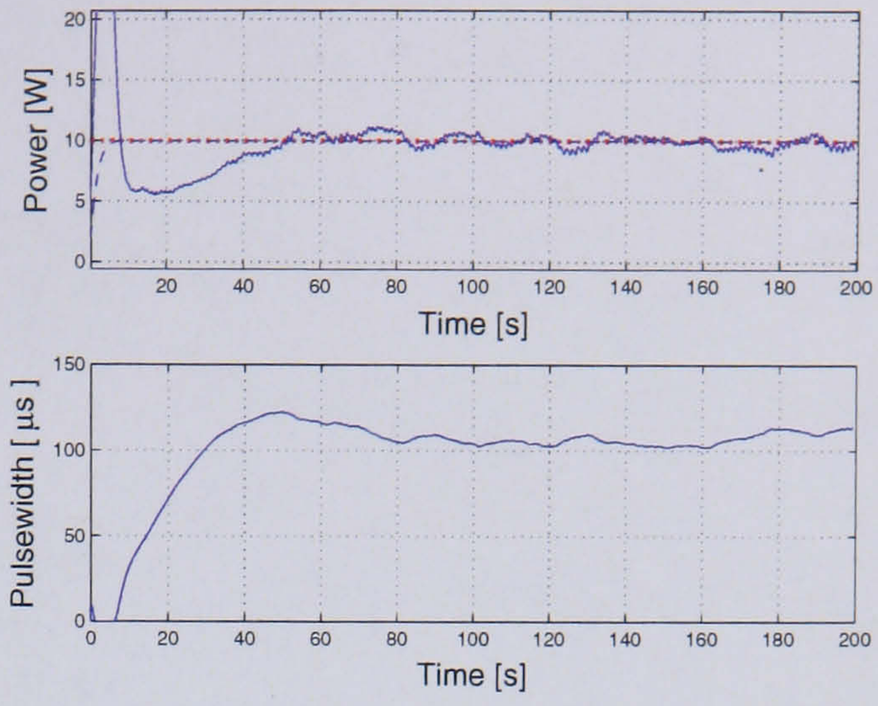

(b) Stimulation loop response. The upper graph shows the controlled leg power (solid line), and the ideal power response (dashed line). The reference leg power is constant at 10 W (dotted line). The lower plot shows the stimulation pulsewidth.

Figure 4.11: Subject 1 - Cadence Tracking

The power tracks close to the reference despite the changes in the reference cadence.

The stimulation signal is smooth in both tests.

Power Tracking

The results of the power tracking test for subjects 1 and 2 are shown in Figures 4.13 and 4.14 respectively. During this test the motor controller reference is set at a constant 50 rpm, and is shown in Figures 4.13(a) and 4.14(a). This cadence is chosen as it is the cadence at which the cyclists train at. Again the cadence tracks well to the reference value as the power reference is changed.

The upper parts of Figures 4.13(b) and 4.14(b) show the power response. The reference value (dotted line) is changed between 10 and 15 W and the power (solid line) tracks well to the reference, following closely to the ideal response (dashed line). As in the Cadence Tracking there is an initial transient due to the input from the experimenter.

The lower parts of Figures 4.13(b) and 4.14(b) show the corresponding stimulation

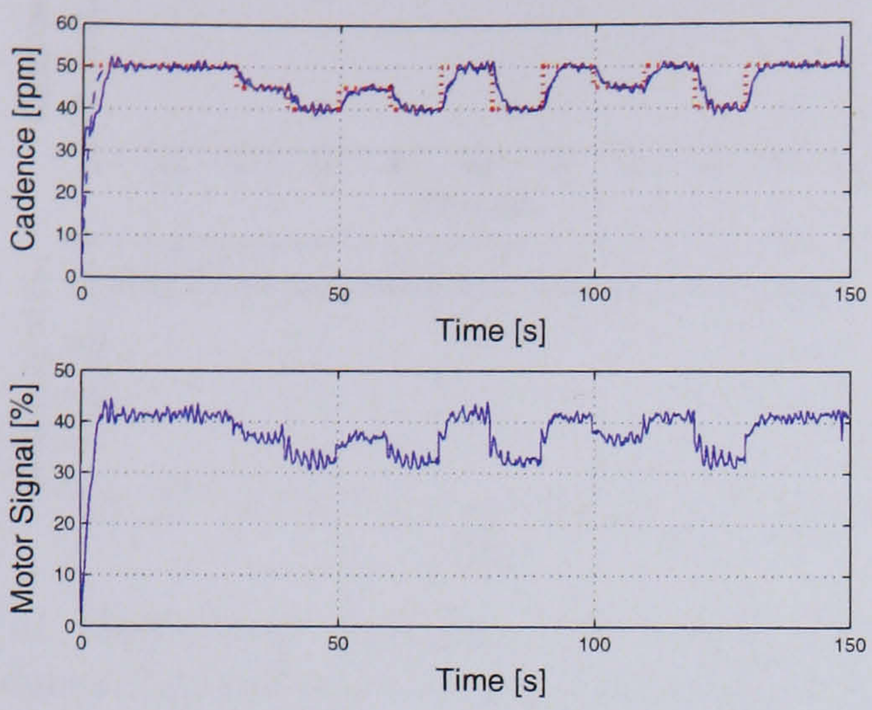

(a) Motor loop response. The upper graph shows the reference cadence (dotted line), the measured cadence (solid line), and the ideal cadence response (dashed line). The lower plot shows the motor input signal.

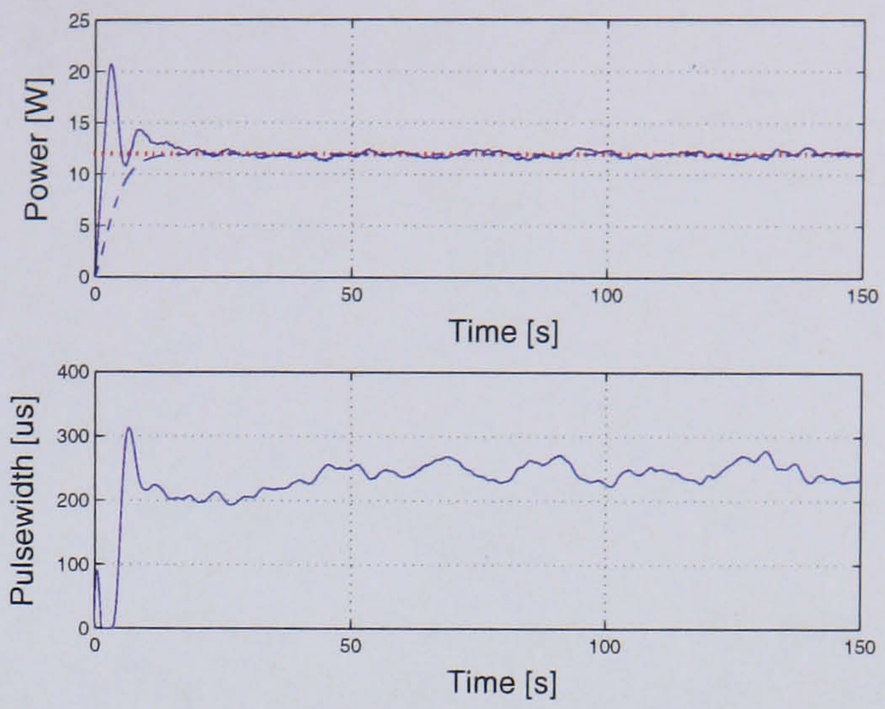

(b) Stimulation loop response. The upper graph shows the controlled leg power (solid line), and the ideal power response (dashed line). The reference leg power is constant at 12 W (dotted line). The lower plot shows the stimulation pulsewidth.

Figure 4.12: Subject 2 - Cadence Tracking

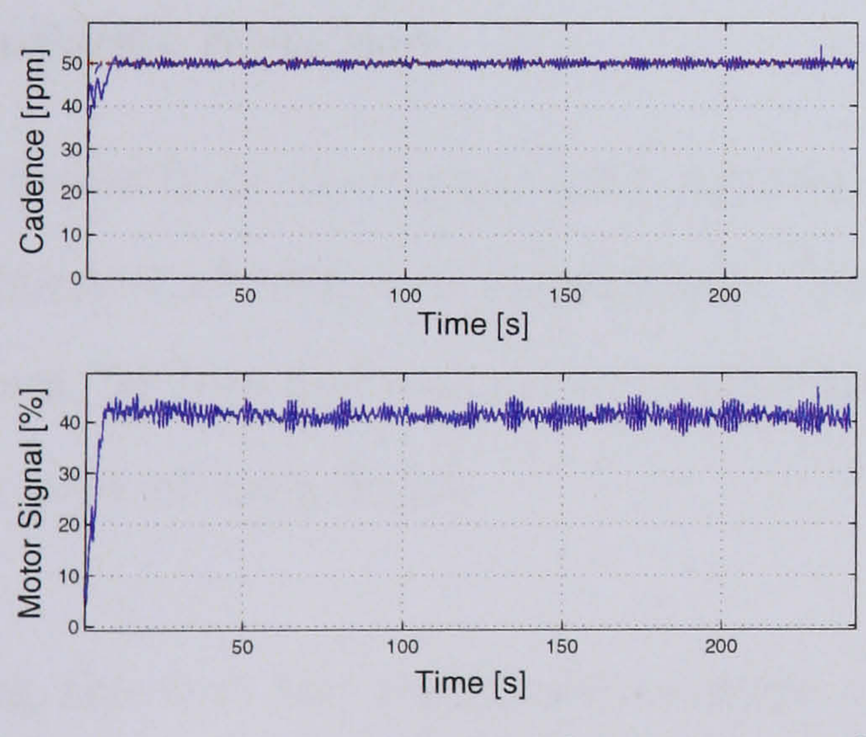

(a) Motor loop response. The upper graph shows the reference cadence (dotted line), the measured cadence (solid line), and the ideal cadence response (dashed line). The lower plot shows the motor input signal.

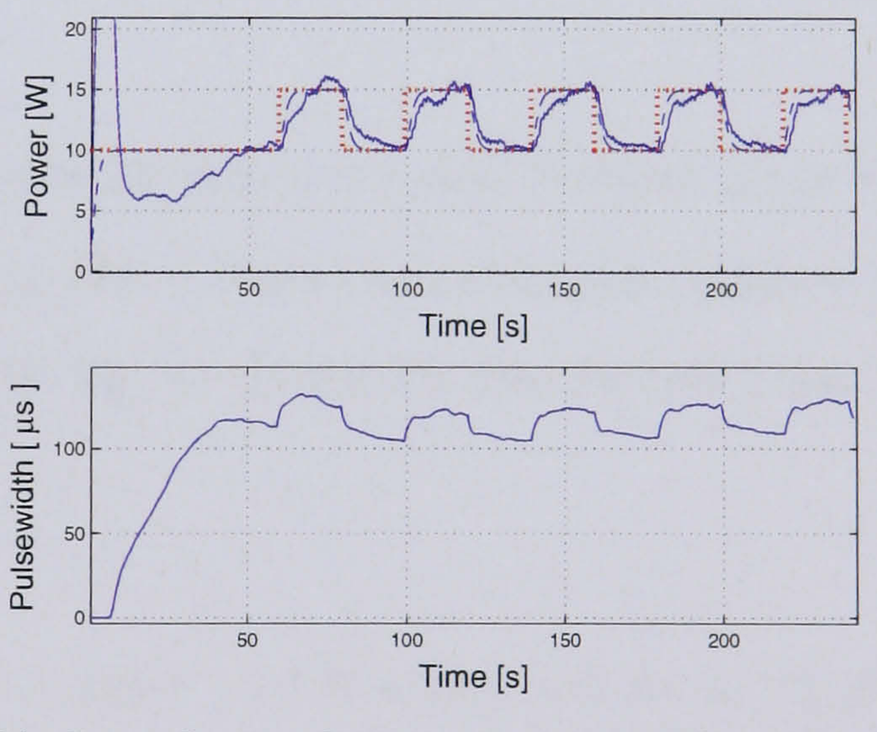

(b) Stimulation loop response. The upper graph shows the controlled leg power (solid line), and the ideal power response (dashed line). The reference leg power changes between 10 W and 15 W (dotted line). The lower plot shows the stimulation pulsewidth.

Figure 4.13: Subject 1 - Power Tracking

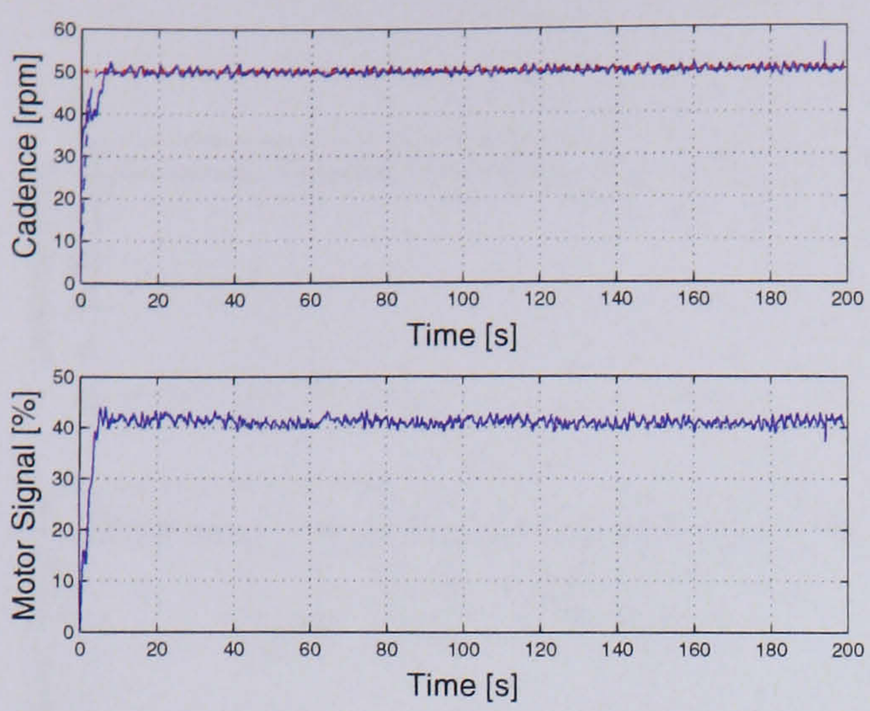

(a) Motor loop response. The upper graph shows the reference cadence (dotted line), the measured cadence (solid line), and the ideal cadence response (dashed line). The lower plot shows the motor input signal.

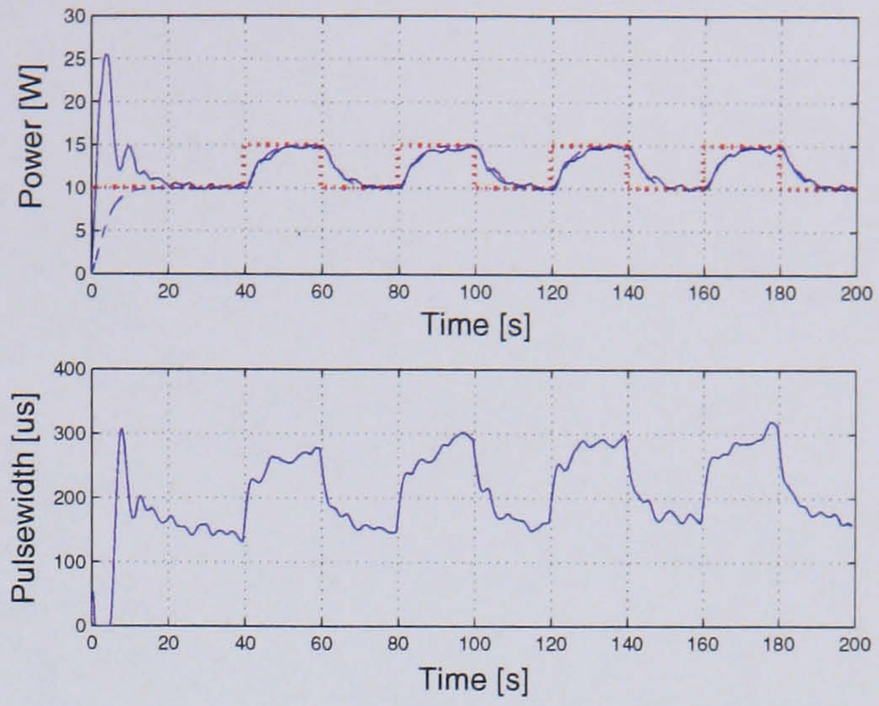

(b) Stimulation loop response. The upper graph shows the controlled leg power (solid line), and the ideal power response (dashed line). The reference leg power shanges between 10 W and 15 W (dotted line). The lower plot shows the stimulation pulsewidth.

Figure 4.14: Subject 2 - Power Tracking

applied to the muscles. The plots show the stimulation changing in response to the change in reference power.

Disturbance Rejection

The results from the disturbance rejection tests for Subject 1 and Subject 2 are shown in Figures 4.15 and 4.16 respectively. During these tests the reference cadence was a constant 50 rpm and the power a constant 10 W, as shown by the dotted lines in the upper part of each figure.

During the test the resistance between the trainer and the rear wheel is varied between maximum and minimum levels. The effect of varying the resistance results in a change in the total output power between 15 and 49 W. In all plots the effects of the disturbance is negligible, and both the cadence and leg power output are close to the reference values.

The disturbance is applied after 50 s and held for 20 s for Subject 1 (Figure 4.15).

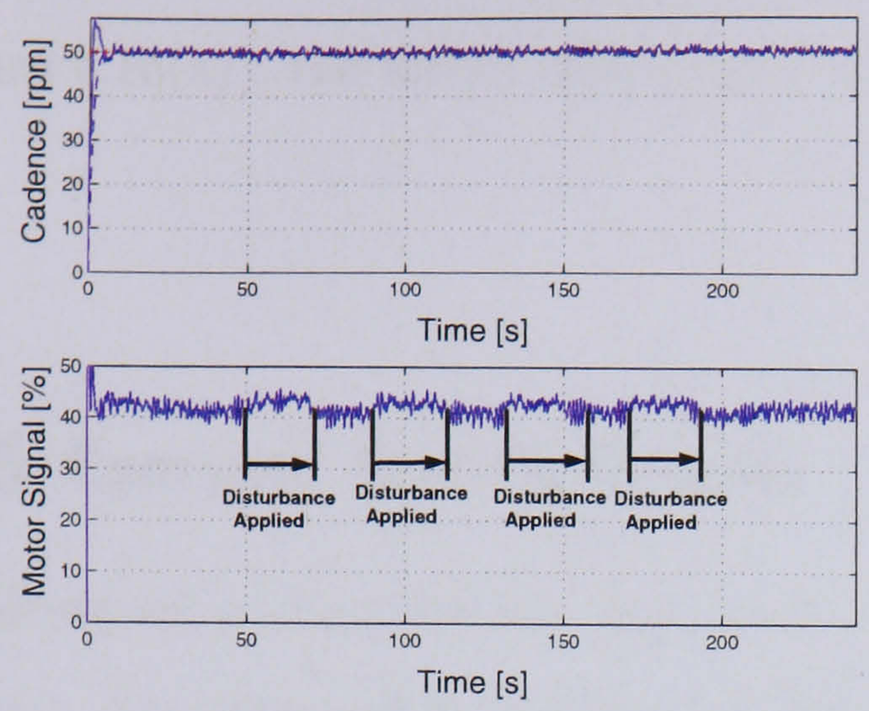

(a) Motor loop response. The upper graph shows the reference cadence (dotted line), the measured cadence (solid line), and the ideal cadence response (dashed line). The lower plot shows the motor input signal.

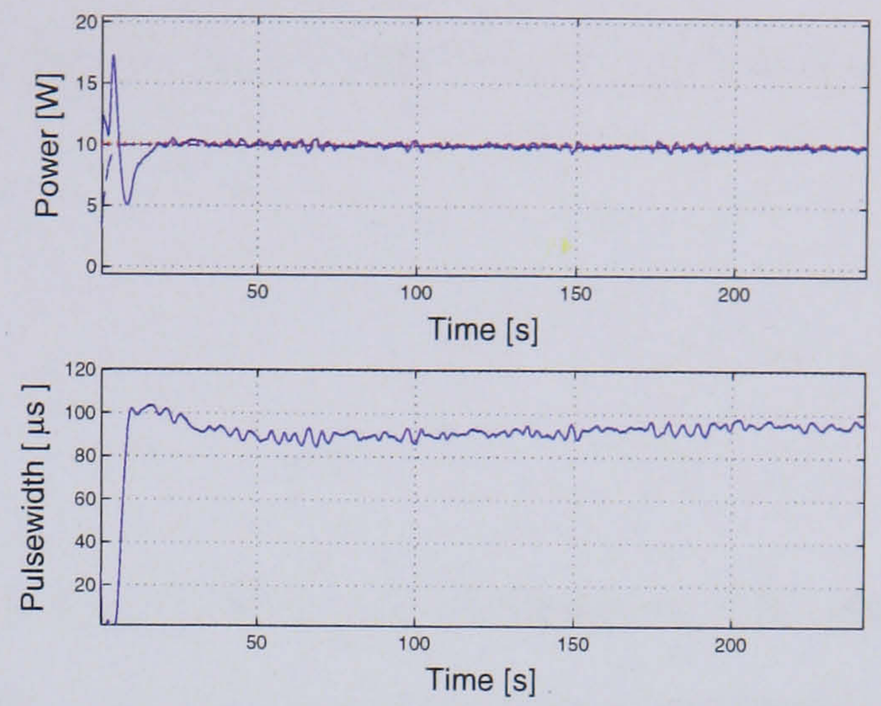

(b) Stimulation loop response. The upper graph shows the controlled leg power (solid line), and the ideal power response (dashed line). The reference leg power is constant at 10 W (dotted line). The lower plot shows the stimulation pulsewidth.

Figure 4.15: Subject 1 - Disturbance Rejection

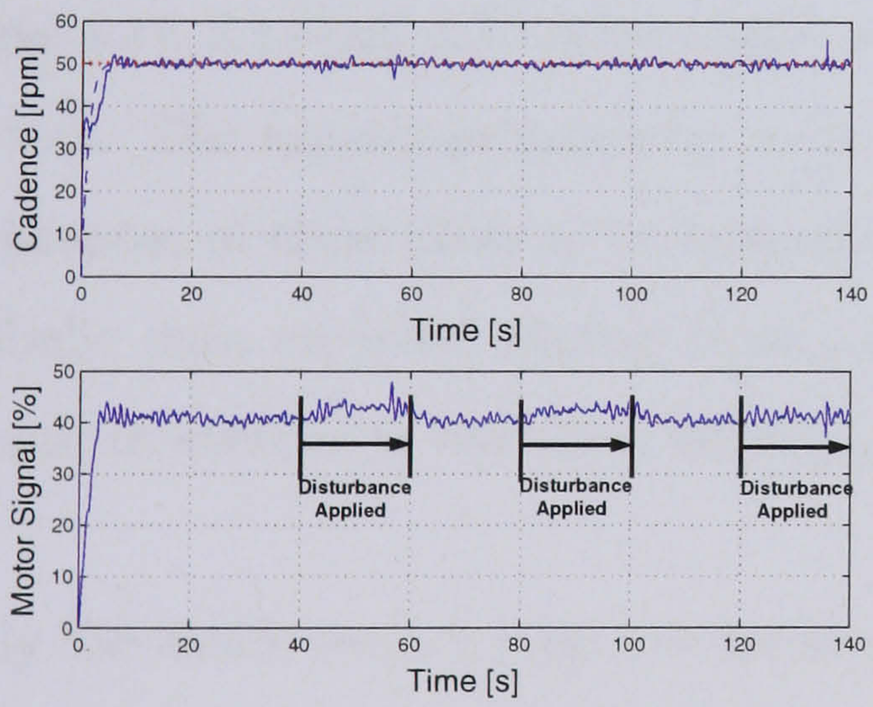

(a) Motor loop response. The upper graph shows the reference cadence (dotted line), the measured cadence (solid line), and the ideal cadence response (dashed line). The lower plot shows the motor input signal.

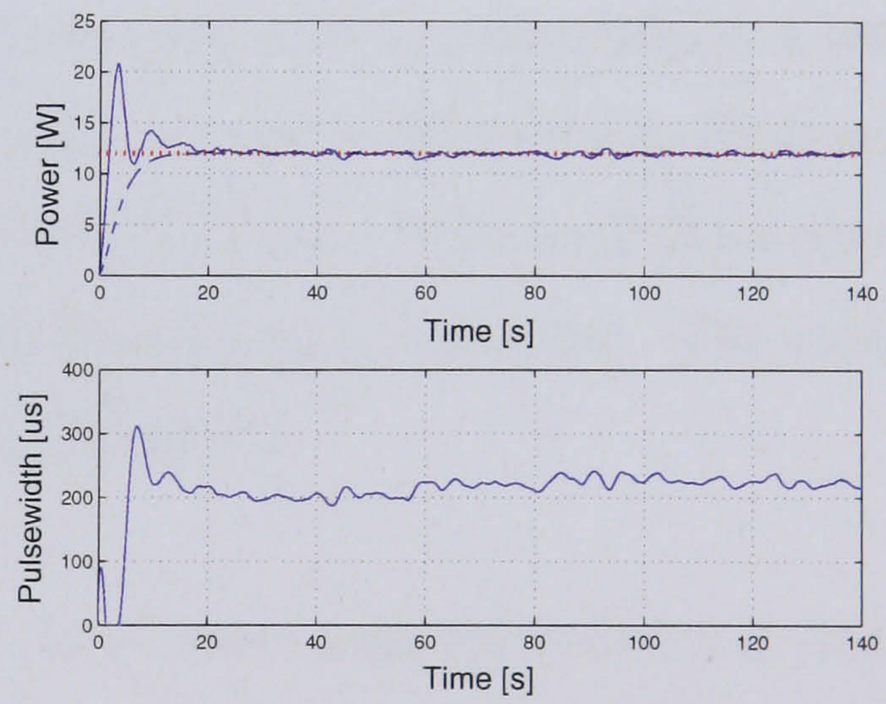

(b) Stimulation loop response. The upper graph shows the controlled leg power (solid line), and the ideal power response (dashed line). The reference leg power is constant at 12 W (dotted line). The lower plot shows the stimulation pulsewidth.

Figure 4.16: Subject 2 - Disturbance Rejection

Thereafter it was applied/released in steps of 10 s. The effect of this on the motor input signal can be seen in the lower part of Figure 4.15(a). Similarly for Subject 2 (Figure 4.16(a)), the motor input signal can be seen to change every 20 s starting from 40 s.

4.2.5 Exercise Testing Results

The designed controllers are now used in a more practical application, i.e. exercise testing. As discussed in section 3.4.2 there are two exercise testing protocols commonly undertaken : Constant Load Tests and Incremental Tests. The performance of the controllers is discussed for both cases.

The results presented are for Subject 1 only as Subject 2 discontinued FES cycling due to unrelated medical reasons.

Constant Load Exercise Test

Figures 4.17, 4.18 and 4.19 demonstrate the application of the controllers to a constant load test. The typical protocol for a constant load test is described in Section 3.4.2. The purpose of these plots is to demonstrate the function of the controllers only. The metabolic data recorded during these experiments is not presented. The metabolic response to exercise is discussed throughout Chapter 5.

Firstly the motor control loop is considered. In all three tests the cadence is controlled to a nominal value of 50 rpm. The upper parts of Figures 4.17(a), 4.18(a) and 4.19(a) show the measured cadence from the shaft encoder and the lower parts show the motor input signal. The motor controller holds the cadence well at a mean 50 rpm, but the controller is always working to maintain this value. The cadence does not vary significantly during the test. When a small change from the reference occurs the controller acts quickly to correct itself. The motor input signal varies according to changes in the

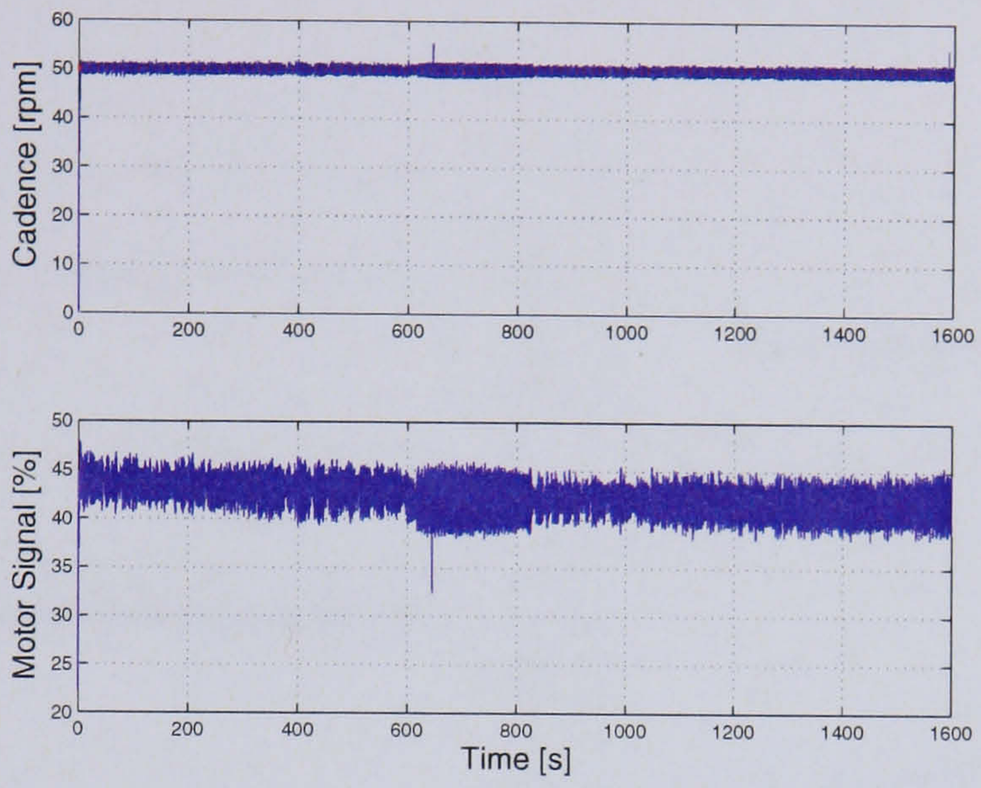

(a) Motor loop response. The upper graph shows the reference cadence (dotted line) and the measured cadence (solid line). The lower plot shows the motor input signal.

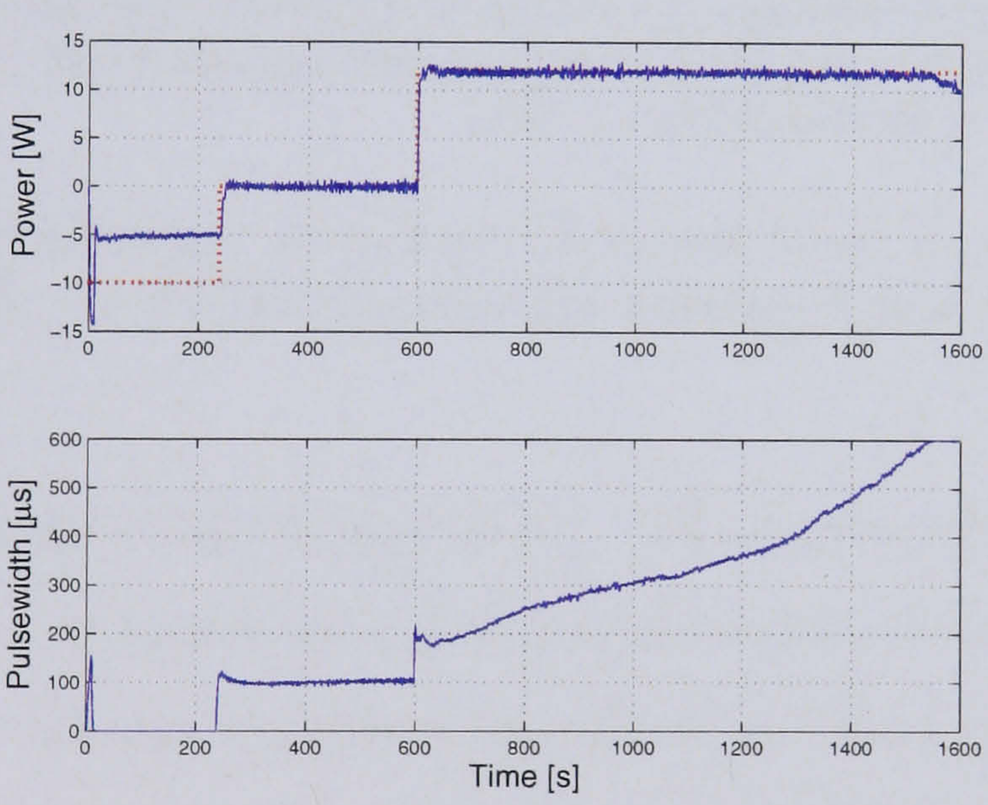

(b) Stimulation loop response. The upper graph shows the reference power (dotted line) and the controlled leg power (solid line). The lower plot shows the stimulation pulsewidth.

Figure 4.17: Power and Cadence plots from Constant Load Test 1. In all graphs the reference is the dotted line and the measured data the solid line.

cadence, therefore it appears"noisy" like the cadence signal.

In Figures 4.18(a) and 4.19(a) spikes can be seen in both the cadence and motor input plots. These spikes are due to momentary losses of power, in the electric motor.

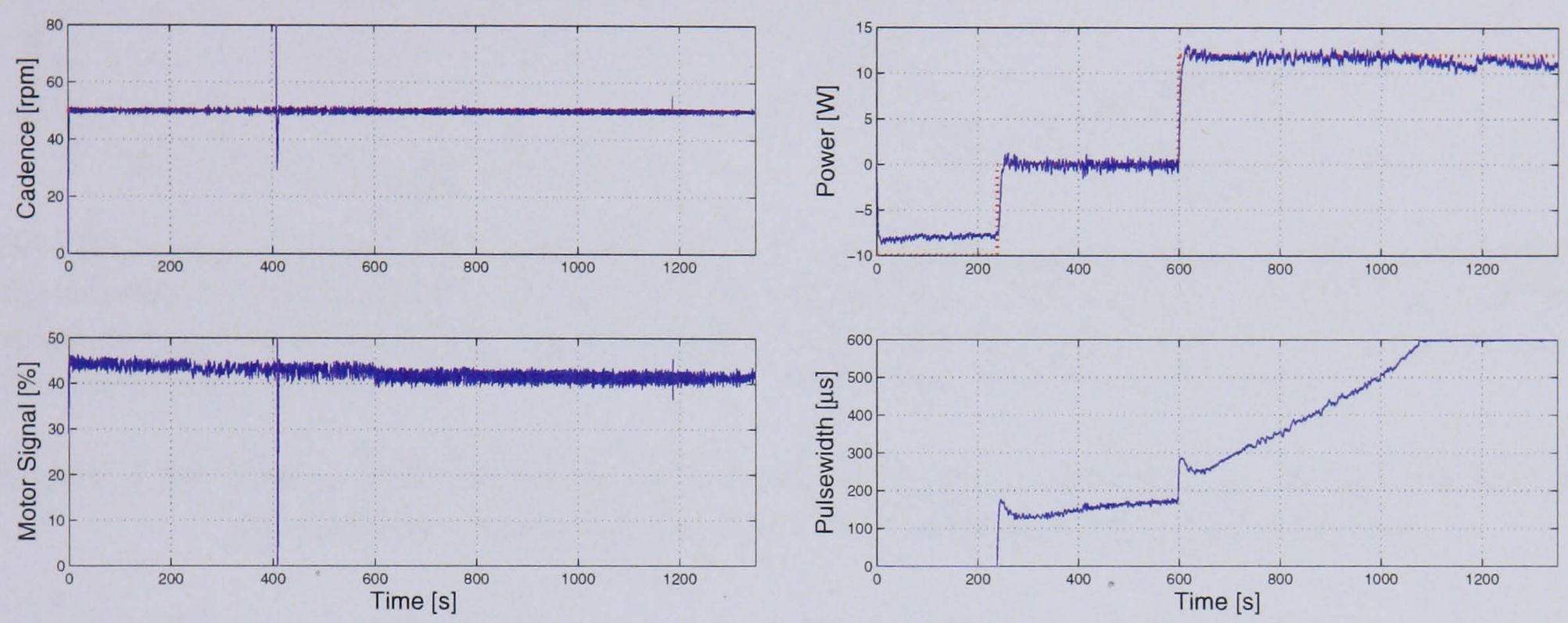

(a) Motor loop response. The upper graph shows the reference cadence (dotted line) and the measured cadence (solid line). The lower plot shows the motor input signal.

(b) Stimulation loop response. The upper graph shows the reference power (dotted line) and the controlled leg power (solid line). The lower plot shows the stimulation pulsewidth.

Figure 4.18: Power and Cadence plots from Constant Load Test 2. In all graphs the reference is the dotted line and the measured data the solid line.

Secondly, the power control loop is considered. The upper parts of Figures 4.17(b), 4.18(b) and 4.19(b) show the power and the lower parts show the stimulation pulsewidth applied to the muscles. Initially the power level is set to a level at which no stimulation is applied. This allows only the motor to turn the legs before stimulation is applied. The power is then increased so that the muscles are stimulated slightly, before the reference power is increased to the constant load level desired for the test. The power is seen to be well controlled under all 3 references throughout the test period.

The resulting stimulation plots are shown in Figures 4.17(b), 4.18(b) and 4.19(b). The maximum stimulation in these experiments is set to 600 μs for tests 1 and 2, and 650 μs for test 3. In all 3 tests the stimulation follows a similar profile. When the reference power is changed to 12 W, the stimulation increases gradually. As the subject begins

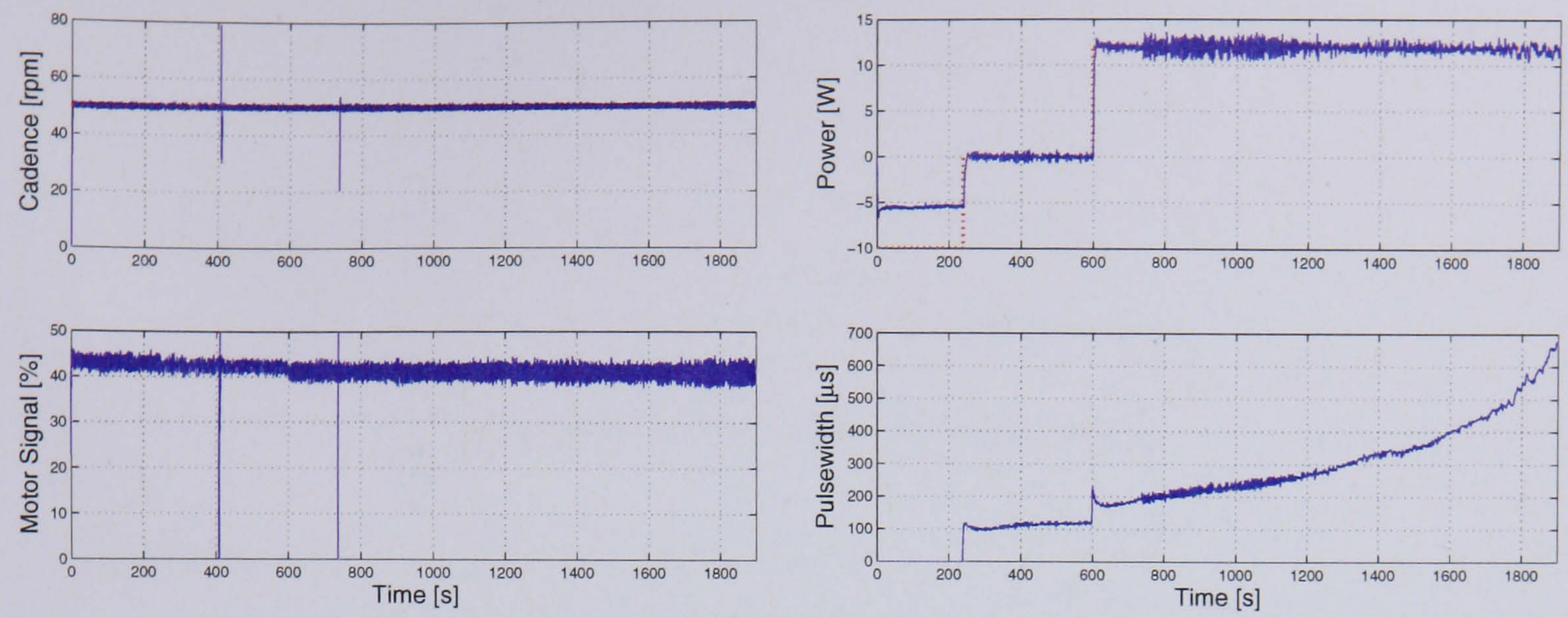

(a) Motor loop response. The upper graph shows the reference cadence (dotted line) and the measured cadence (solid line). The lower plot shows the motor input signal.

(b) Stimulation loop response. The upper graph shows the reference power (dotted line) and the controlled leg power (solid line). The lower plot shows the stimulation pulsewidth.

Figure 4.19: Power and Cadence plots from Constant Load Test 3. In all graphs the reference is the dotted line and the measured data the solid line.

to fatigue, in the last 200 s, the stimulation increases exponentially until the maximum is achieved.

Incremental Exercise Test

Figures 4.20, 4.21 and 4.22 are the results from 3 incremental exercise tests. The typical protocol for an incremental exercise test is discussed in section 3.4.2. As with the Constant Load Tests, only the control results are presented.

In these experiments the cadence is held at a constant 50 rpm. As with the constant load test this is achieved well. During the low power warm-up the stimulation and power is shown to spike on 3 occasions (Figure 4.20(b)). This is due to the cyclist experiencing a muscle spasm during the onset of stimulation. The motor control signal in the lower parts of Figures 4.20(a), 4.21(a) and 4.22(a) is shown to only slightly decrease as the power levels increase towards the end of the test. This indicates that the 2 loops are working well together to maintain a constant output at the rear wheel. As in the constant load test, Figures 4.20(a) and 4.22(a) show the motor input signal

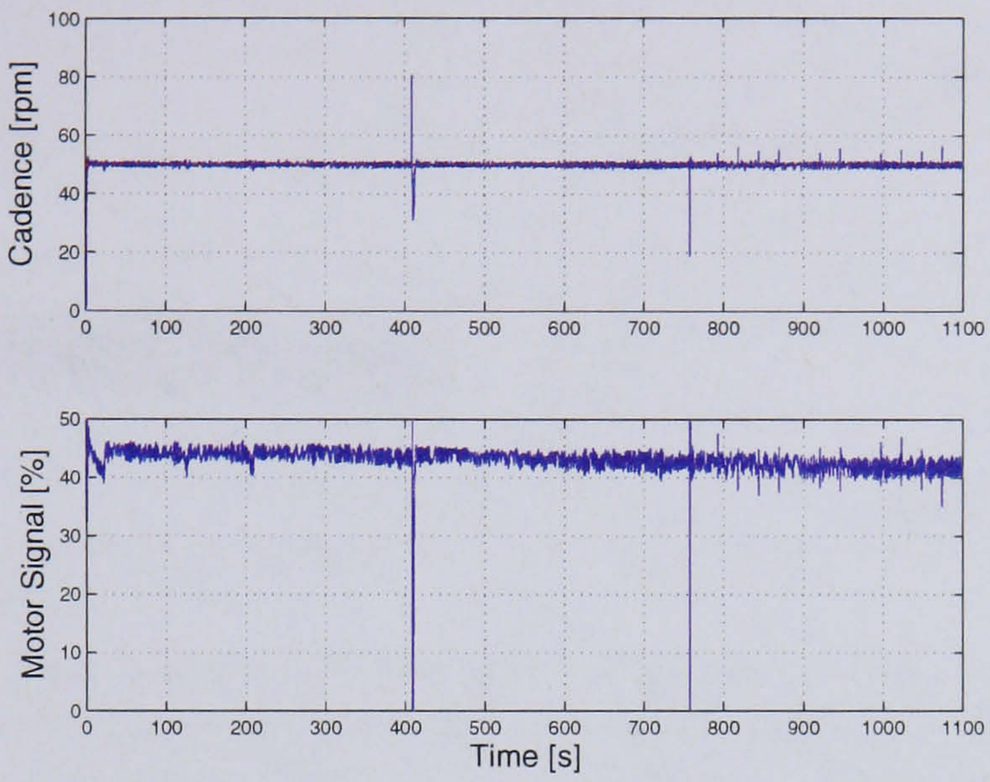

(a) Motor loop response. The upper graph shows the reference cadence (dotted line) and the measured cadence (solid line). The lower plot shows the motor input signal.

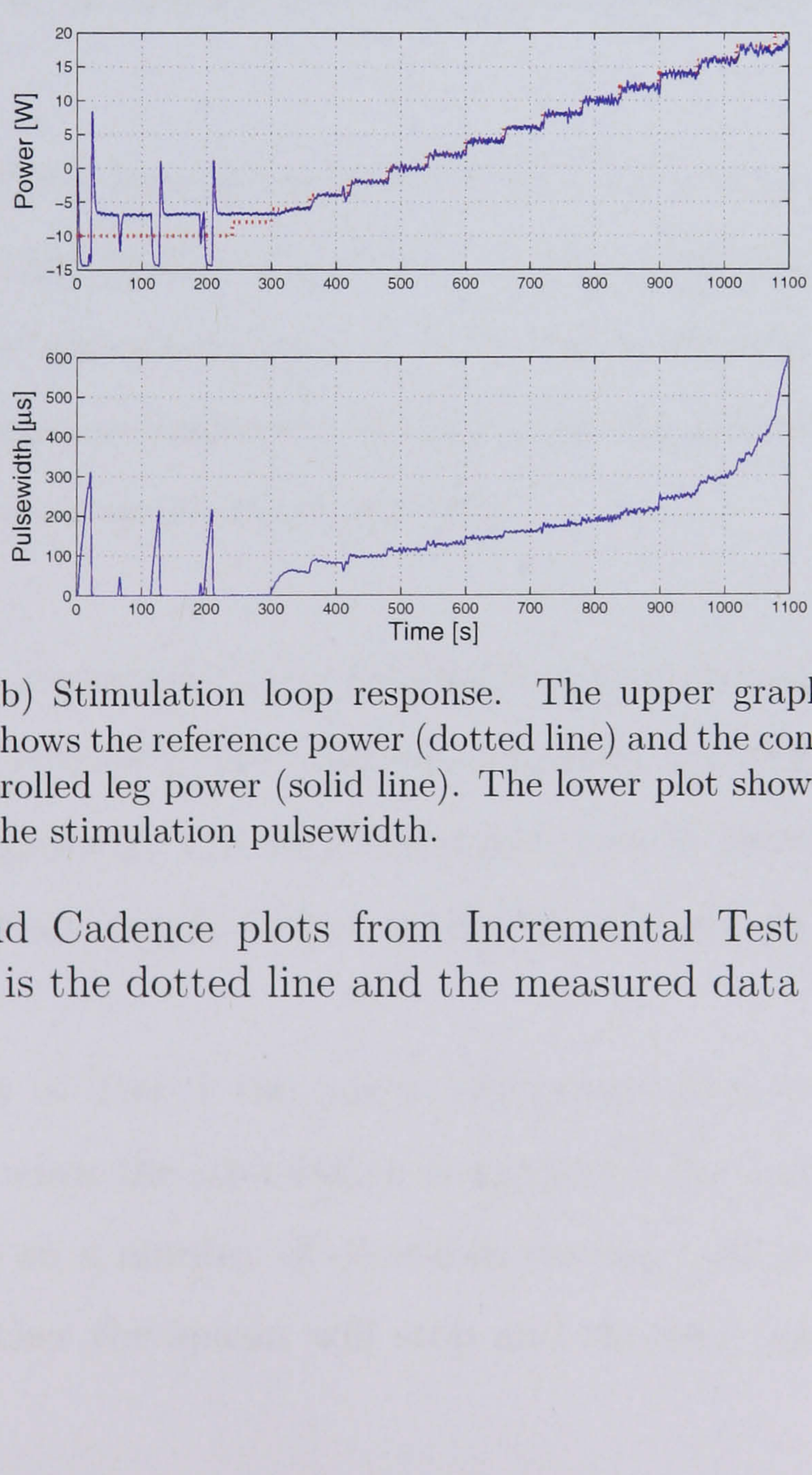

(b) Stimulation loop response. The upper graph shows the reference power (dotted line) and the controlled leg power (solid line). The lower plot shows the stimulation pulsewidth.

Figure 4.20: Power and Cadence plots from Incremental Test 1. In all graphs the reference is the dotted line and the measured data the solid line.

spiking as there is a momentary loss in the motor power.

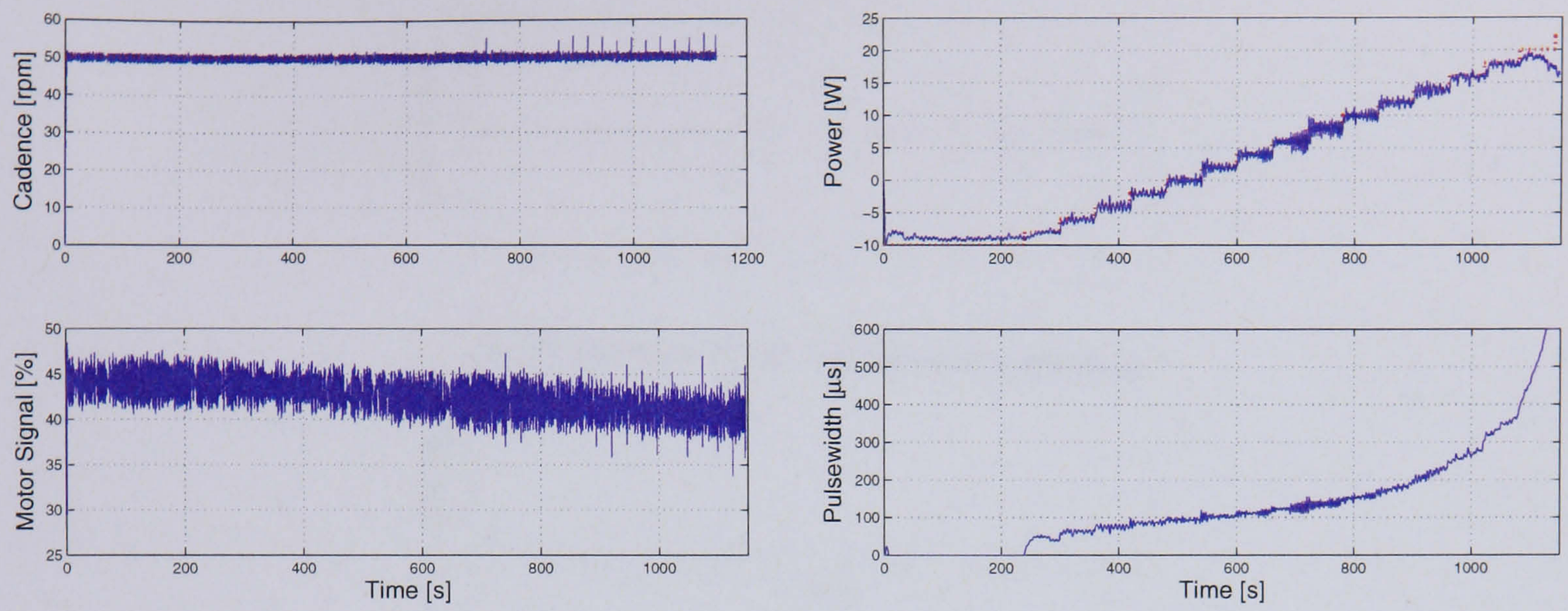

(a) Motor loop response. The upper graph shows the reference cadence (dotted line) and the measured cadence (solid line). The lower plot shows the motor input signal.

(b) Stimulation loop response. The upper graph shows the reference power (dotted line) and the controlled leg power (solid line). The lower plot shows the stimulation pulsewidth.

Figure 4.21: Power and Cadence plots from Incremental Test 2. In all graphs the reference is the dotted line and the measured data the solid line.

In an incremental exercise test the power control loop is especially of interest. The power reference is initially held at a low level so that stimulation applied to the muscles is zero. Thereafter the stimulation is increased in steps of 2 W every 60 s, until the maximum stimulation is achieved. At this point the stimulation is turned off and the subjects' legs are rotated by the motor only.

At all power levels the measured power oscillates around the reference value. The controller is continuously working to maintain the reference, therefore the controller adjusts the stimulation appropriately. The oscillations are seen to increase about a higher reference levels. The test are stopped when maximum stimulation level is reached.

During the first 220 s of Test 1 the power and stimulation is seen to spike (Figure 4.20(b)). This occurs when the stimulation is applied to the muscles and they begin to spasm. This occurred on a number of occasions during cycling training. This subject is able to decide whether the spasm will stop and the test can continue, or that the

test must end.

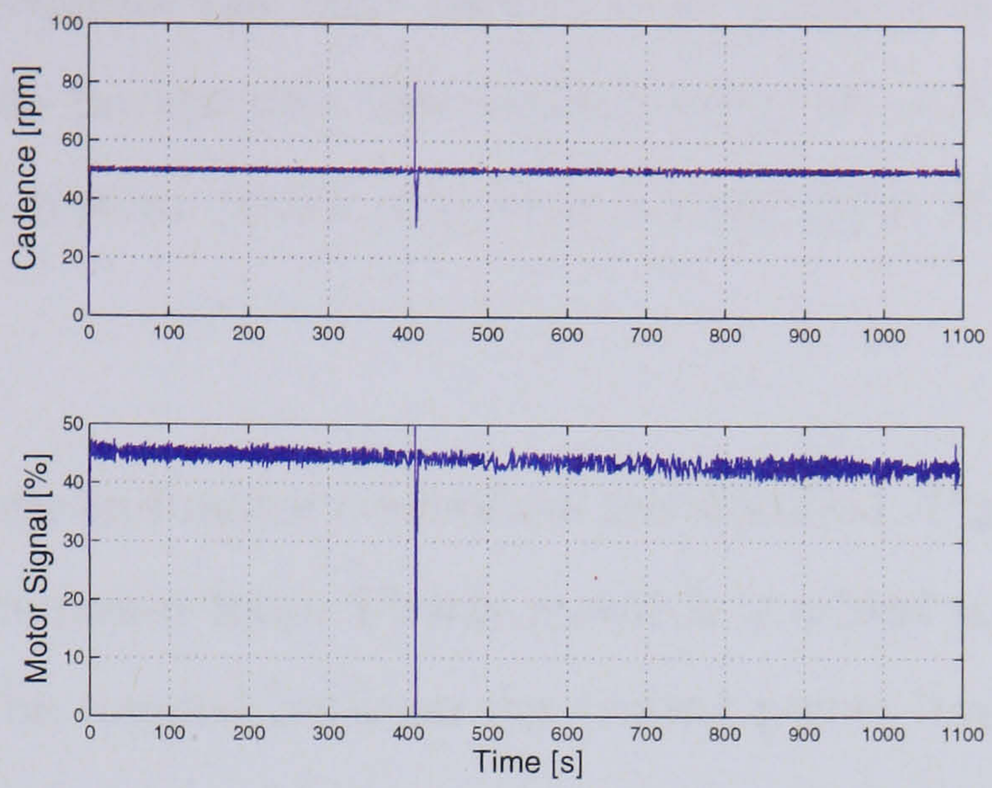

(a) Motor loop response. The upper graph shows the reference cadence (dotted line) and the measured cadence (solid line). The lower plot shows the motor input signal.

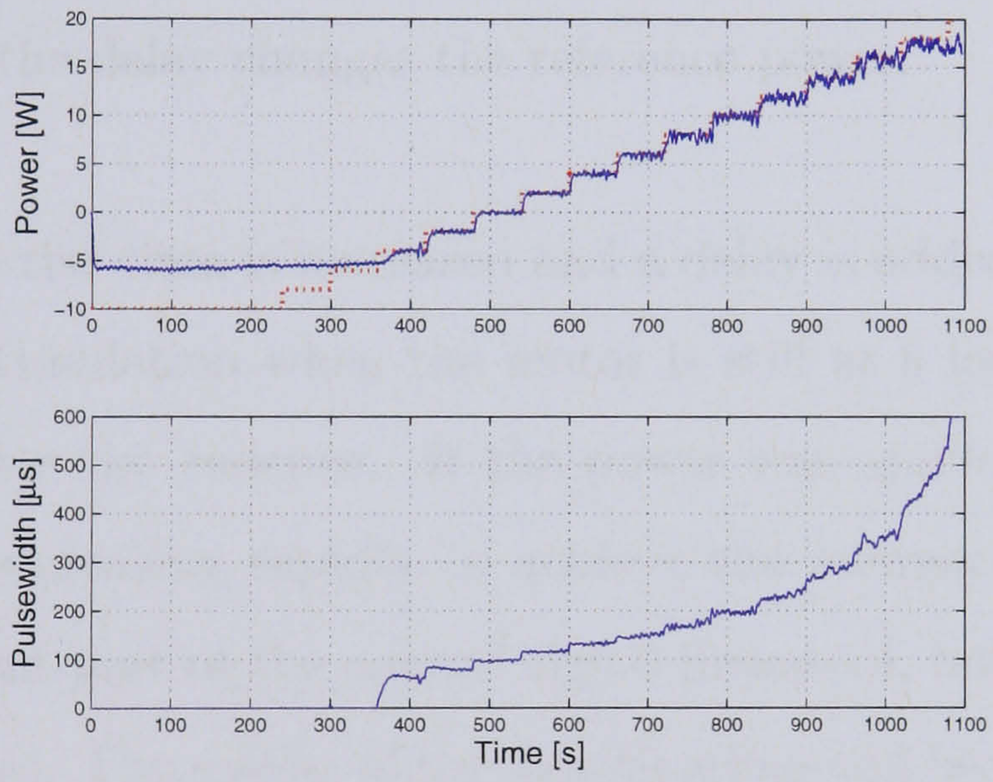

(b) Stimulation loop response. The upper graph shows the reference power (dotted line) and the controlled leg power (solid line). The lower plot shows the stimulation pulsewidth.

Figure 4.22: Power and Cadence plots from Incremental Test 3. In all graphs the reference is the dotted line and the measured data the solid line.

It is useful to note that these tests were undertaken over a long time period. Controller design was undertaken only once and therefore robustness is shown in the controller design against any possible changes in the plant over time.

4.2.6 Controller Modifications

These exercise tests highlighted the requirement for the motor controller to have a slower rise time. The current rise time results in a "jerky" start to cycling. Considering this in relation to paraplegics, the sudden onset of cycling may induce heavy loading on the skeletal system, which may have a lower Bone Mineral Density (BMD) [4].

Therefore both the power and motor controllers are modified. Figure 4.23 demonstrates the modifications to the power loop. Firstly a switch is added to the control system to allow the reference to be toggled between the testing power level and the warm down level. Secondly, as discussed, a delay is added to the control system. Figure 4.24(b) shows the result of this. The power reference is set to a level below that of minimum stimulation for the cyclist. As the cadence increases to 50 rpm, the stimulation remains at 0μs for 15 s before the delay changes the reference power.

The motor controller's rise time is increased and a delay is added to the power loop to prevent the onset of stimulation when the motor is still at a low cadence. The delay is acts as dead zone for the cadence. If the power was applied as before, it would result in stimulation increasing rapidly to achieve the reference cadence and power. Not only is the transient part of the control signal improved, but also the steady-state part is a smoother signal. The results of the modifications can be seen in Figure 4.24(a).

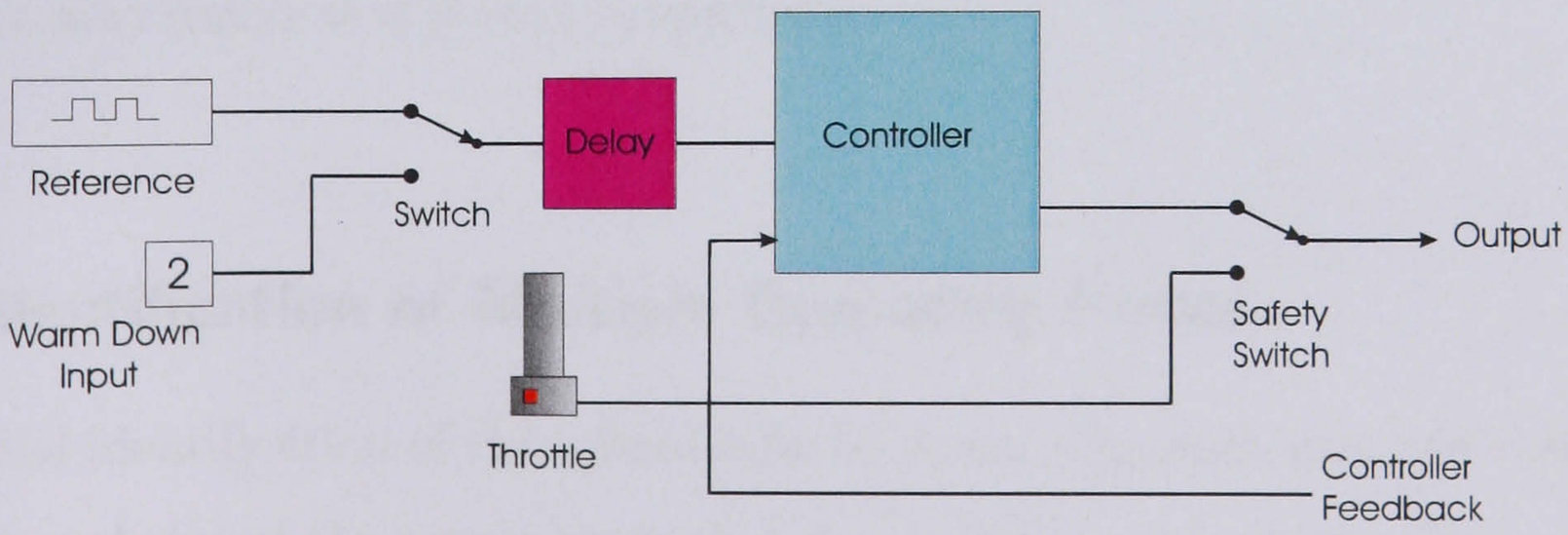

Figure 4.23: Schematic representation of modifications to the controller structure.

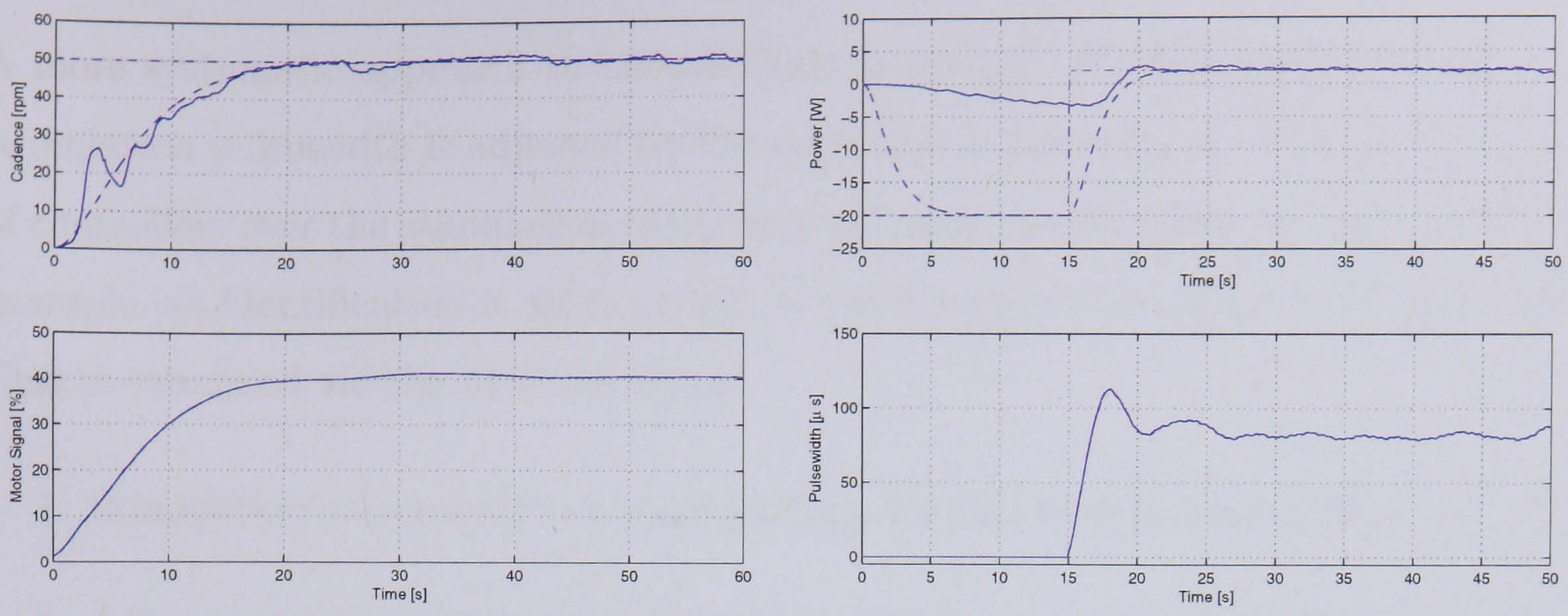

(a) Motor loop response. The upper graph shows the reference cadence (dash-dot line), the measured cadence (solid line), and the ideal cadence response (dashed line). The lower plot shows the motor input signal.

(b) Stimulation loop response. The upper graph shows the controlled leg power (solid line), the ideal power response (dashed line) and the reference leg power (dash-dot line). The lower plot shows the stimulation pulsewidth.

Figure 4.24: Part 4.24(a) shows the slow rise time of the motor controller and Figure 4.24(b) shows the delay of the onset of the stimulation. As the cadence increases, the stimulation remains at zero until the time is 15 s.

4.3 The Power-Stimulation Relationship

An observation from the incremental exercise tests is how the controller performs at different power levels. For example, in Figure 4.21(b), the measured power level oscillates more around different power levels. In particular this can be seen at the power levels between 6, 8 and 10 W. Two possible causes of this phenomenon are that the controller's performance is reduced at this power level or that these oscillations correspond to the onset of fatigue. A small study is proposed to investigate how stimulation and power are related at different magnitudes.

4.3.1 Identification of Multiple Operating Points

The original identification of the stimulation to power dynamics was undertaken based on prior knowledge of the power levels that the cyclists could achieve. The stimulation was increased to a level at which the cyclist was comfortable and the stimulation / power was relatively stable, before a PRBS was applied.

A more systematic approach to identification is desired. As discussed previously the stimulation pulsewidth is adjusted by the controller in the range 0 - 700 μs. A number of controllers over the stimulation range may be more suitable than one controller. For example, an identification in steps of 100 μs could result in 7 models and 7 controllers. This is examined via the protocol below:

1. Stimulation is increased to a predefined pulsewidth level in steps of 50 μs [50, 100, 150.....350 μs]

2. After a set time period (settling time) a PRBS is added to the stimulation input.
   The PRBS is identical for each identification, as is the settling time.

3. The input stimulation and output power are recorded.

4. The identification lasts for 2 minutes.

5. 5 minutes of rest between each identification

This protocol is repeated twice for Subject 1, detailed in section 3.5.

Identification Results

Figures 4.25 and 4.26 show the results from the identifications at the 7 levels of stimulation. Figures 4.25(a) and 4.26(a) show the PRBS stimulation input and Figures 4.25(b) and 4.26(b) the resulting power output.

4.3.2 Discussions of the Power-Simulation Relationship

The results from these identifications highlight a number of possibilities for further identifications. Both sets of results show that the Point 2 (100 μs) produces the largest changes in power. In Figure 4.25 the power ranges from -3 to 10 W and in Figure 4.26 from -2 to 15 W. This suggest that 100 μs may be an optimal level for identification for this subject. The 3^{rd} level identification (150 μs) also produces a large change in power, and in Identification 1 it produces a maximum power of 18 W and a near maximum in

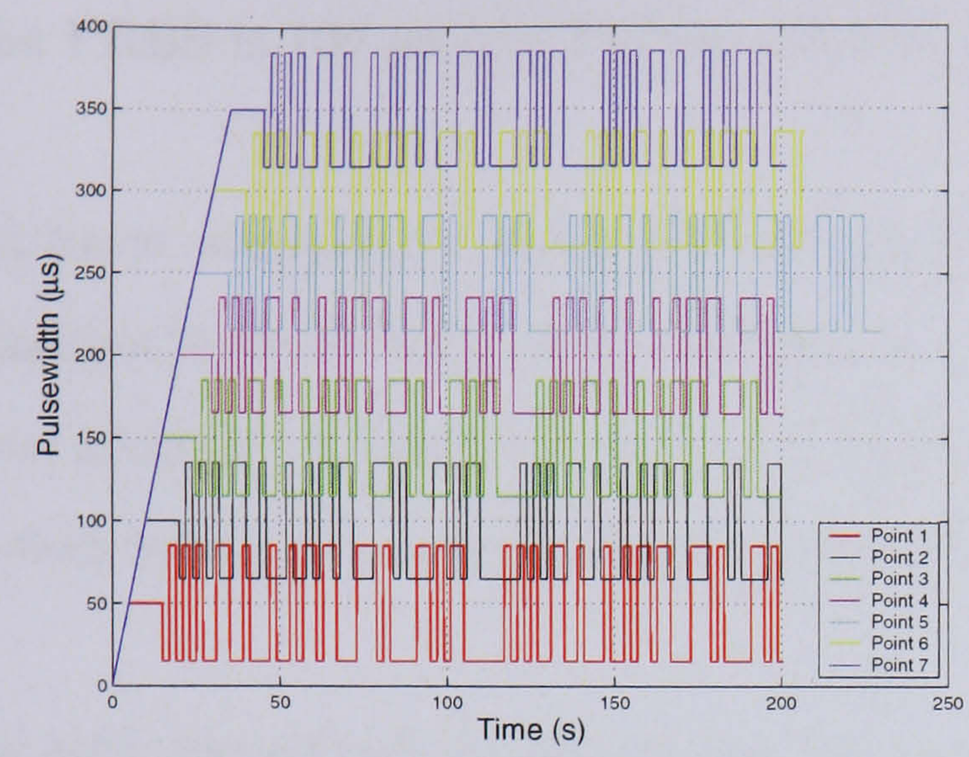

(a) Input PRBS for each operating point.

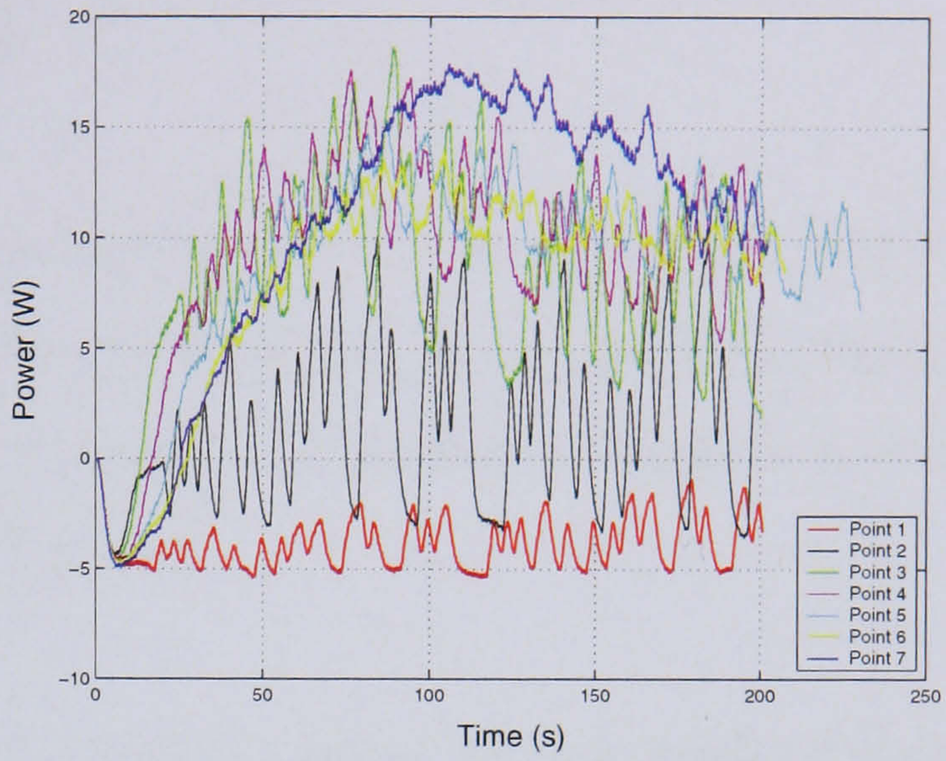

(b) Resulting output power for identification 1.

Figure 4.25: Identification 1.

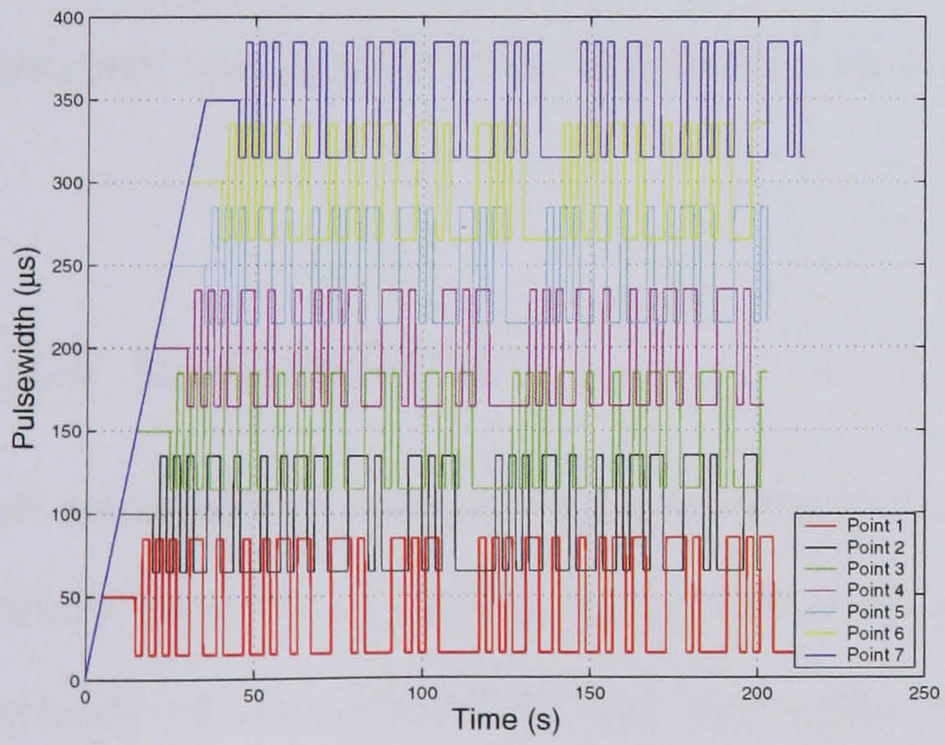

(a) Input PRBS for each operating point.

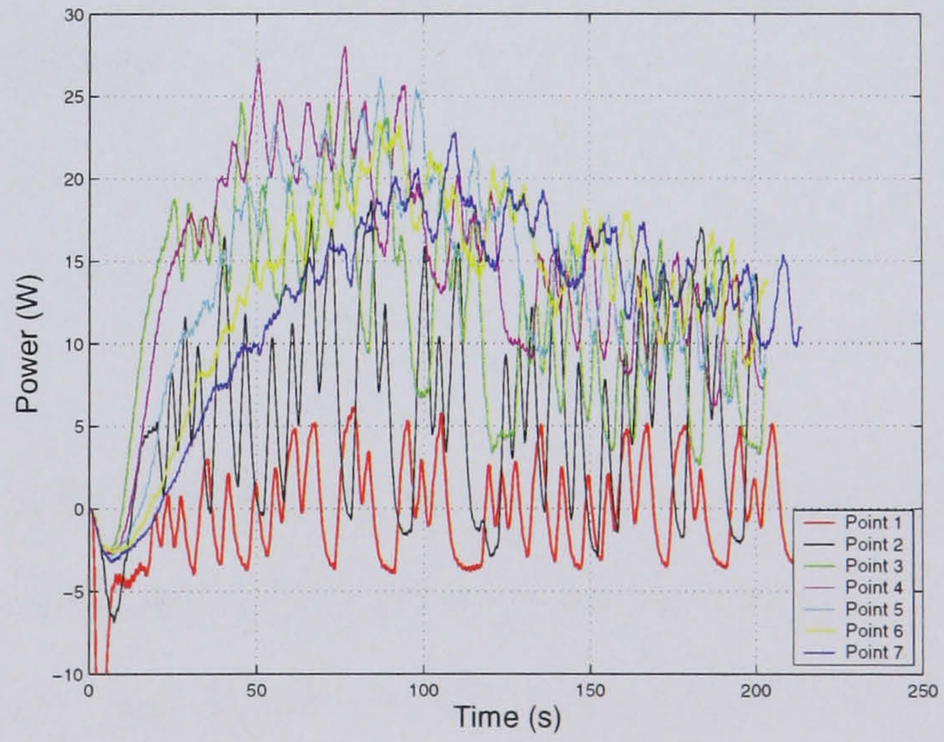

(b) Resulting output power for identification 2.

Figure 4.26: Identification 2

Identification 2 of approximately 26 W.

Referring to the power controllers designed previously, the average stimulation level of the PRBS is 100 μs (see Figures 4.8 and 4.9).

At lower stimulation levels (50 μs) the power can be seen to change clearly with the changes in the PRBS. An identification at this low level may prove useful if a strategy was adopted to create a warm-up or start-up controller. Therefore at negative and low power levels the control of power could be improved.

In both identifications fatigue can be seen to affect the power at high levels of stimulation. It is interesting to note that initially fatigue is noticeable at levels below the maximum that can be delivered from the stimulator (700 μs). From Point 4 onwards (in both identifications), as the stimulation is increased, the power increases to maximum before it falls to a similar level. In Identification 1 this level is in the region of 10 W and 12 W in Identification 2. These levels are similar to the maximum power levels that are achieved at 100 μs. The shape of the power data, at these high stimulation levels, does not lend itself to the identification of models, as the changes in the stimulation is not reflected in the power data. This suggest that identifications at high stimulation levels are not suitable for the design of controllers.

4.3.3 Conclusions

The methods presented for the design and implementation of power and motor controllers have been shown to be effective in facilitating accurate exercise testing. The methods of identification and controller design are shown to be straightforward, easily implemented and rely on standard design techniques. The controllers and control structure are shown to be effective when the loops are implemented in the two loop control strategy. They are shown to track changes in both the cadence and power, as well as minimising the effect of disturbances. The disturbance test results suggest that this control strategy will adapt well to outdoor cycling. The applied disturbances

reflect those that may be encountered during outdoor cycling, such as slope or wind. However these results are gained on an exercise trainer. During mobile cycling the total inertia of the body would alter the dynamics of the motor and the cadence. The consequences of this would have to be investigated.

The controllers were designed on the test day prior to the commencement of testing. These controllers have been proved to be robust over time and against small changes in the subject's physiology. Power controllers performed well over a number of weeks, therefore identifications and controller design are not required at each test.

The addition of an effective electric motor assist allows for cycling to commence before stimulation is applied. The motor can increase the cadence gradually as the stimulation is applied. This can also be applied to new FES cyclists. In the early stages of FES cycling training the stimulated muscles will fatigue quickly or not even be capable of producing any significant force. The electric motor can be utilised to rotate the legs while a low level of stimulation is applied to slowly train the muscles.

With reference to exercise testing protocols the ability to use the negative power levels greatly extends the power levels available for exercise testing. The relatively low levels of power that are achieved by FES cyclists result in a narrow band of power that is available for exercise testing. By using the negative power region, the power range used in exercise testing can be increased.

The controllers are shown to achieve the small changes in power required for incremental testing and also the constant levels required for constant load tests. A closer look at the stimulation - power loop suggests that further work could be researched into the power controller. For example an adaptive scheme may be employed where various controllers operate at corresponding power levels. This may increase the accuracy of the power control, the length of time a cyclist is able to maintain cycling (by increasing the efficiency of the exercise) and the maximum power possible.

5 $\dot{V}O_2$ Identification and Initial Controller Design

5.1 Why control $\dot{V}O_2$?

The title of this section is a simple question of why we might want to control a FES cyclist's $\dot{V}O_2$? $\dot{V}O_2$ is the rate of oxygen uptake during exercise [64]. There are two answers : One that an engineer would give, and one that an exercise physiologist may give. As an engineer, the simple answer may be that the $\dot{V}O_2$ is a measurable output from a system which has a known input, the power. Therefore it presents some engineering problems: "Can this system be modelled?" and "Can it be controlled?" From a physiology standpoint the reasoning must be what benefits this control would have for the efficacy of exercise training programmes and exercise testing procedures. Currently, in exercise testing, a power level is defined, but could it be possible that defining a $\dot{V}O_2$ level could be a more effective method? Would $\dot{V}O_2$ control be more precise?

$\dot{V}O_2$ is known to be related linearly to power for able bodied subjects up to (and beyond) the lactate threshold [64]. The maximum value of $\dot{V}O_2$ ($\dot{V}O_{2max}$) can be found via an incremental exercise test, as described in section 3.4.2. $\dot{V}O_{2max}$ is defined as "the $\dot{V}O_2$ at which performance of increasing levels of work rate exercise failed to increase $\dot{V}O_2$, by 150 ml/min despite an increase in work rate" [64]. One of the criteria for reaching $\dot{V}O_{2max}$ is that the power is seen to increase while the $\dot{V}O_2$ plateaus. In FES cycling $\dot{V}O_{2max}$ is rarely, if ever, achieved. More often the maximum stimulation level is reached first, thereafter the power produced either plateaus or drops. This $\dot{V}O_2$

level is known as $\dot{V}O_{2peak}$, the highest $\dot{V}O_2$ achieved during a test. There are equations which allow extrapolation of the $\dot{V}O_2$ to calculate the $\dot{V}O_{2max}$, from the last completed work rate. Similarly $\dot{V}O_{2max}$ can be estimated from the heart rate (HR) response to sub-maximal exercise. Extrapolating the HR to the age adjusted maximum (220 - Subject's Age), gives an estimate of $\dot{V}O_{2max}$, through a similar linear relationship (for the general AB population). This relationship may not apply in the SCI, where a so called "blunted heart-rate response" can be observed (generally T5 lesions and above) [2].

The $\dot{V}O_2$ response during incremental exercise can be divided into 2 parts: Aerobic and Anaerobic exercise. Aerobic simply means "in the presence of oxygen" [54]. The muscles use the oxygen to burn the fuel, adenosine triphosphate (ATP). During exercise, when the required O_2 amount is not met, the subjects enters an Anaerobic state, "without oxygen". This state is when the fuel is burned without oxygen and a by-product of this is an increase in expired CO_2. The subject is said to reach the lactate threshold (LT) at the transition between the aerobic and anaerobic phases, as shown in Figure 5.1. Lactic acid is an end product of this anaerobic state, produced when there is the condition of inadequate oxygen supply to the muscles. The lactic threshold can be identified by either blood sampling or from gas exchange data. For example by looking for an increase of gradient in the $\dot{V}CO_2$ versus $\dot{V}O_2$ slope (See Figure 5.1). When training, it is more beneficial to train in an aerobic state. The LT corresponds to a certain level of $\dot{V}O_2$ and it may be desirable to control the $\dot{V}O_2$ to a level below this. Therefore the subject will exercise aerobically for a prolonged period.

The linear relationship between HR and $\dot{V}O_2$ [64] could also be exploited as a controllable output during FES cycling. HR monitors are easily affordable when compared with a breath by breath gas exchange measurement system. These can cost tens of thousands of pounds. However the control of HR is restricted in two ways. HR monitors output a radio frequency signal, which through experience, can be interfered with when a electric motor is running on the trike. This has been seen during physiological measurements with this apparatus. Secondly, and more significantly, SCI subjects

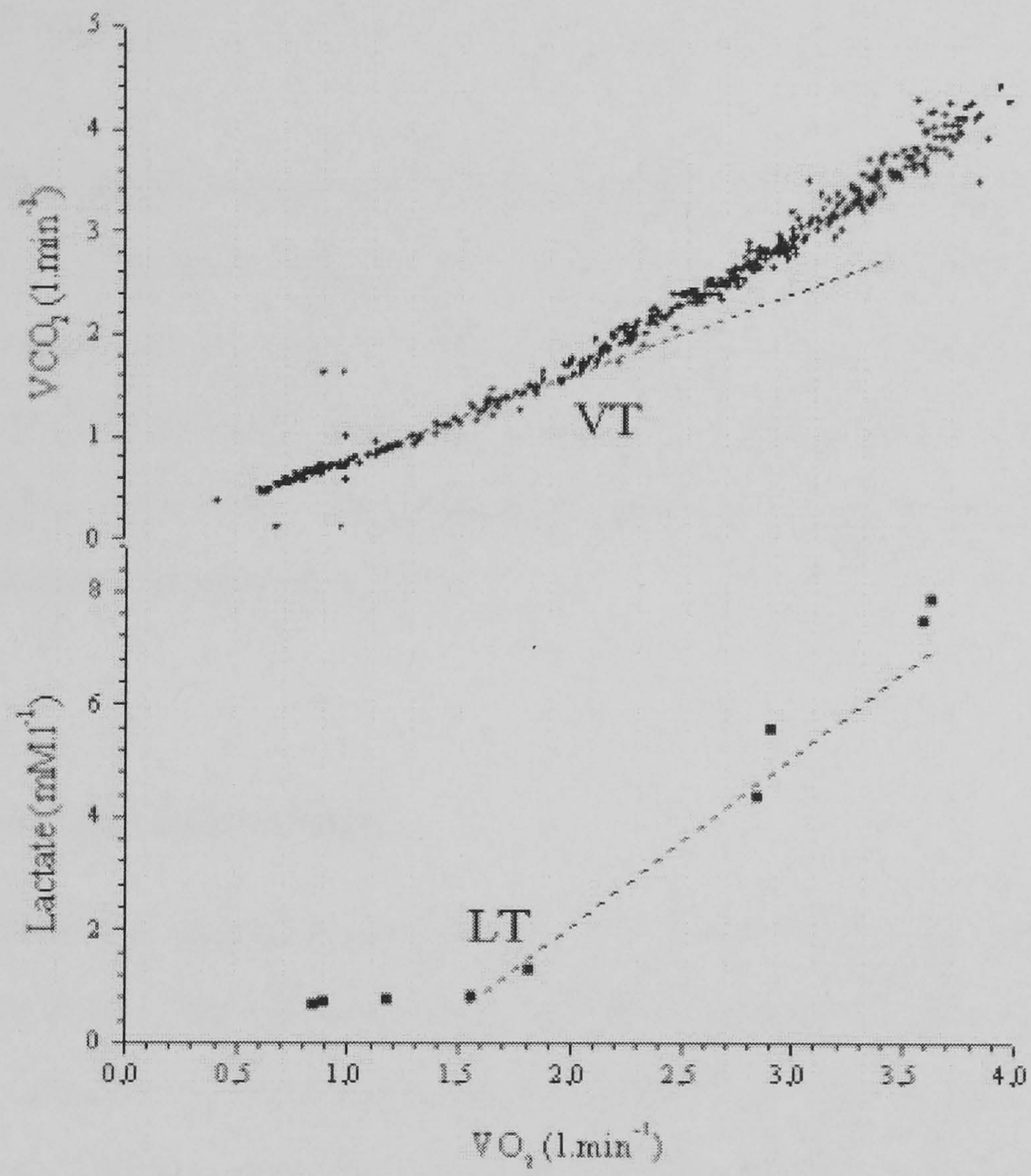

Figure 5.1: A representative example of ventilatory threshold (VT) and lactate threshold (LT) determination [58]. The thresholds can be seen as the gradients of the VT and LT lines increase.

with a high complete lesion (T5 and above) may experience a blunted HR [2] typically only ever reaching a maximum HR around 130 bpm. The heart has both positive and negative feedback, the sympathetic and para-sympathetic pathways respectively. In a high level lesion the sympathetic pathway to the heart is cut off, resulting in this lower maximum HR, for a high work rate. Furthermore, HR is quite variable and can be easily affected by environmental conditions (body temperature, stress and anxiety). Even with controlled environmental conditions and removal of stimulus, subjects can still be easily distracted.

HR and $\dot{V}O_2$ are linearly related up to the peak HR, but then the HR tends to plateau with SCI persons during exercise. HR is quite variable, excluding the influence of environmental variabilities, those with tetraplegia have been shown to have a highly variable HR/$\dot{V}O_2$ relationship [41]. When prescribing HR control of exercise, it is typically in the region of 60-90% of the maximum HR, but this may not be an appropriate method of exercise prescription in SCI.

5.1.1 $\dot{V}O_2$ in the Literature

In numerous studies throughout the literature $\dot{V}O_2$ has been measured as an outcome measure. Glaser et al. [26] compared AB and SCI levels of $\dot{V}O_2$ during cycling. They found that the $\dot{V}O_2$ for SCI was higher than that of AB subjects, for a specific power. The results were quite homogenous, allowing for the conclusion that $\dot{V}O_2$ may be predicted for given power levels, regardless of injury level and time post injury. They also suggest that Functional Neuromuscular Stimulation (FNS) cycling is a potential means to achieve specific rates of $\dot{V}O_2$, through training at percentage of the maximum. Glaser also recorded the HR during their experiments, and they comment that it is "quite remarkable" how precisely the HR tracks the $\dot{V}O_2$ response. They did not experience a plateau in the HR response, they only comment that it stops at approximately 135 bpm and a corresponding power of 30 W. The HR still has an upward trend at this point.

These findings, by Glaser, are supported through a study by Hooker et al. [32]. A period of neuromuscular electrical stimulation (NMES) leg cycle ergometry took place over a 19 week period, on a REGYS1 system. $\dot{V}O_2$ increased from 1.29 ± 0.30 to 1.42 ± 0.39 l/min, an increase of 10 %. This corresponded to an increase in WR of 25 %, when cycling to fatigue. No significant change in HR (−4 %) were recorded between pre and post training. In submaximal exercise it is noted that during pre-testing that the $\dot{V}O_2$ represented 77 % of the maximum, whereas post training this had decreased to 68 % of $\dot{V}O_{2max}$. This 9 % decrease in $\dot{V}O_2$ indicates that even over a 19 week period there is a change in $\dot{V}O_{2max}$, which would highlight a requirement to recalibrate the percentage of $\dot{V}O_2$ that a cyclist is using as a training level.

Through a period of chronic exercise training on a cycle ergometer with FES, Barstow et al. showed that peak $\dot{V}O_2$ and WR significantly improved with training [3]. As with Glaser, they found that $\dot{V}O_{2peak}$ significantly correlated with HR before and after training. Training consisted of 24, 30 minute sessions on a REGYS1 FES leg cycle ergometer. Incremental and constant load tests were carried out prior to and after the training period.

The results show an increase in $\dot{V}O_2$ from 1.28 ± 0.31 to 1.42 ± 0.34 (l/min), HR decreased from 134.3 ± 26.7 to 131.5 ± 23.8 bpm for a total increase of WR of 4.6 W, over the test period. Barstow [2] had previously reported a lower than expected HR response and stated that it was unclear what "the consequences of a blunted HR response to exercise would be on exercise capacity", the $\dot{V}O_2$ and the WR. They state that this reduced HR may reduce the ability of a subject to increase or sustain aerobic metabolism, as the cyclist increases to a constant submaximal exercise level. Barstow [3] states that only an 11 % increase in $\dot{V}O_2$ has been achieved, whereas previous studies have shown 22-58 % increase. However the subjects started at higher initial values. They conclude that the HR results do not change enough in this study to be classed as "significant adaptations" from training.

Returning to the work by Petrofsky, discussed previously, the investigators examined

the effect of training on endurance and cardiovascular responses [49]. On a MONARK ergometer, 8 volunteers undertook a period of cycling with intermittent exercise tests to assess any improvements. WR increased from 0 to 40 W for 30 minutes cycling, in the first 3 months. In the second 3 months this increased to 55 W for all subjects. They discovered approximate linear relationships between HR, oxygen uptake and WR. However, they found no significant increase in oxygen uptake over the 6-month period. This paper does not correlate well with the studies, previously discussed, by Barstow, Glaser and Hooker. They all demonstrated an increase in $\dot{V}O_{2max}$, over a similar, if not shorter training period.

A study by Raymond et al. [56] considered the cardiorespiratory responses to voluntary arm cranking exercise (ACE) and ES leg cycling in the paraplegic population, and their effect on $\dot{V}O_2$. They found that the combination of FES cycling and ACE elicited higher $\dot{V}O_2$ than ACE alone, but there was no significant difference in submaximal HR or power between the 2 different forms of exercise. Jacobs compared ACE and FES ambulation in a similar manner [36]. Jacobs found that peak $\dot{V}O_2$ did not differ between the 2 exercise modalities, although FES ambulation elicited significantly higher HR (191 v's 179 b/min). This study indicates that the FES ambulation may allow comparable cardiorespiratory demands as ACE. These 2 studies highlight that although the HR increases with the exercise mode, it may not increase enough to use as a control variable. They both comment that FES training may effectively increase cardiorespiratory capacity.

Assuming that an increase in $\dot{V}O_{2max}$will occur with training, training can be conducted at a percentage of this value via $\dot{V}O_2$ control. How reliable would the power-$\dot{V}O_2$ relationship be? Edwards examined the test-retest reliability of gas exchange kinetics using a PRBS exercise test. 2 PRBS tests between 25 and 85 W were conducted by 10 AB subjects over 3 300 s cycles [13]. The results show that no significant differences were found between the $\dot{V}O_2$ kinetics between the 2 tests. They state that in previous studies the AB subjects' $\dot{V}O_2$ kinetics were unaffected over a 9 month training period. However it is noted through personal clinical practice that FES cyclists can experience

a relatively severe detraining by not cycling for a period of 2 weeks (2, 1 hour cycling sessions), and Edward's study is for AB subjects. These findings suggest that models of $\dot{V}O_2$ kinetics, and their subsequent controllers, may be robust over a long time period of intensive cycling. The study concludes that $\dot{V}O_2$ kinetics are more reliable than those of $\dot{V}CO_2$, with $\dot{V}CO_2$ having a higher noise to signal ratio.

5.1.2 Critical Power

Hill [29] reviewed the concept of Critical Power (CP) within the literature. The basis of CP theory is that there is a hyperbolic relationship between power output and the time that the power output can be maintained. There are 3 mathematically equivalent models to calculate the CP :

Nonlinear power-time model CP is the asymptote to the hyperbolic curve.

(Linear power-1) / time model CP is the intercept with the y-axis.

Linear work-time model CP is the slope of the relationship.

To estimate the value of the CP, subjects undergo a series of maximal exercise tests at various work rates, but in theory only 2 tests are required for the linear models. The test is simple and only requires an ergometer and a stopwatch.

The CP was compared with the LT in 2 studies and was found to be significantly higher than the power associated with the LT (28 % and 13 %). CP was also compared with the mean anaerobic threshold (MAT). The MAT is similar to the LT, and is described as "the onset of blood lactate accumulation"[54]. The actual difference between the 2 is very small and the terms can be used interchangeably. In this case the CP was found to be 64 % and 16 % higher in the 2 studies. Therefore CP is higher than these two 'markers' for the transition between the aerobic and anaerobic states, and that the CP occurs when a the cyclist is in an anaerobic state.

The CP has been shown to increase after endurance training, and can be used to reflect aerobic fitness. It can be found simply and may have a use for the prediction and quantification of training intensity. Therefore, if identified, would the CP be an effective level for training, rather than the $\dot{V}O_2$ level associated with the LT? A second question: does the CP occur with FES cycling? As the $\dot{V}O_{2max}$ is limited by fatigue at maximum stimulation, the identification of the CP may not be possible. However, it is possible that the theory of CP could be adapted to use $\dot{V}O_{2peak}$.

5.1.3 Summary of Thoughts on $\dot{V}O_2$

As the HR response can be blunted, while the $\dot{V}O_2$ continues to increase with work rate, the $\dot{V}O_2$ becomes a more desirable variable to control. $\dot{V}O_2$ control would allow for training at a specific percentage of $\dot{V}O_{2max}$, whether it is the CP or the below the LT. However there are some practical issues that have to be considered :

Cost The Metamax system has an initial cost of approximately twenty two thousand pounds. This cost limits the system to use in a clinical environment and not in an individual's home on a regular basis.

Time The time required to calibrate and set up the Metamax system is considerable. After the 1 hour warm-up time, the system has to be calibrated. When this time is added to an hour of daily training, this would be a significant period of a cyclist's day.

Comfort Some subjects have commented on how the face mask can become uncomfortable over a long period. This may prove to be a negative factor when undertaking a long period of exercise.

Therefore a compromise may be sought, following the protocol defined below :

- $\dot{V}O_{2max}$ incremental exercise test to determine the $\dot{V}O_{2peak}$
- Select a percentage of the $\dot{V}O_{2peak}$, at the CP or below the LT.
- Perform a $\dot{V}O_2$ control test at the selected level.

- Use the controller output (power reference) as a training level for a time period of a month. This power reference would take the subject through the stages of a constant load test, warm-up, constant load and warm down.

- Repeat $\dot{V}O_{2max}$ to determine if the $\dot{V}O_{2max}$ has increased.

- Repeat process at a percentage of the new $\dot{V}O_{2peak}$.

Re-calibrating the percentage of $\dot{V}O_{2max}$ will allow for a controlled step increase in $\dot{V}O_{2max}$ over a monthly period.

Aim of $\dot{V}O_2$ Control

The aim of $\dot{V}O_2$ control therefore is to use the motor and power controllers, designed previously, to control the $\dot{V}O_2$. A reference $\dot{V}O_2$ level is applied to a $\dot{V}O_2$ controller and the power controller will adjust the power to achieve the reference via closed loop feedback control.

5.2 Preliminary Tests

5.2.1 Power and Stimulation Levels

The identification of $\dot{V}O_2$ dynamics requires a long identification time period. The length of the identification test is dictated by 2 related factors; the power level and the stimulation level. The power levels for the PRB-signal must be such that the subject does not become fatigued too quickly. Therefore the criteria for identification are that the PRBS should be as high as possible, and last for as long as possible. 3 power patterns are implemented to gain an indication of the time periods that the subject will be able to sustain. The patterns are defined below :

- Pattern 1 - Step power output between 1 and 5 W.

- Pattern 2 - Step power output between 1 and 8 W.

- Pattern 3 - Step power output between 1 and 15 W.

Results

In Figure 5.2(a) the Power and Stimulation levels are shown for Pattern 1. Steps in power of 1 to 5 Watts result in a change of stimulation between 130 and 200 μs. In Figure 5.2(b) the Power and Stimulation levels are shown for Pattern 2. Steps in power of 1 to 8 Watts result in a change of stimulation between 150 and 230 μs. In Figure 5.2(c) the Power and Stimulation levels are shown for Pattern 3. Steps in power of 1 to 15 Watts result in a change of stimulation between 180 and 700 μs. The cadence from Pattern 1 is shown in Figure 5.2(d). The cadence is controlled to 50 rpm for all 3 tests.

Conclusions

Pattern 1 does not produce a significant change in pulsewidth over the test. Pattern 3 causes the stimulation to reach the maximum level (500 μs), after only 1000 s. Pattern 2 is the most promising as the pulsewidth changes well in relation to changes in power. This level is selected to be used in the identification, but the power level is increased to change between 0 and 10 W as the subject commonly cycles about this power level.

5.2.2 Pseudo Random Binary Signal Design

A power Pseudo Random Binary Signal is applied to the plant (the cyclist). The PRBS is designed to contain time intervals that will show significant changes in the $\dot{V}O_2$ dynamics. Although the signal is "Random", characteristics can be designed into the signal, via MATLAB :

- The amplitude of the PRBS is chosen to be between 0 and 10 W.
- The length of the signal is chosen to be 1800 s.
- The time of step change is defined to be 30 s.

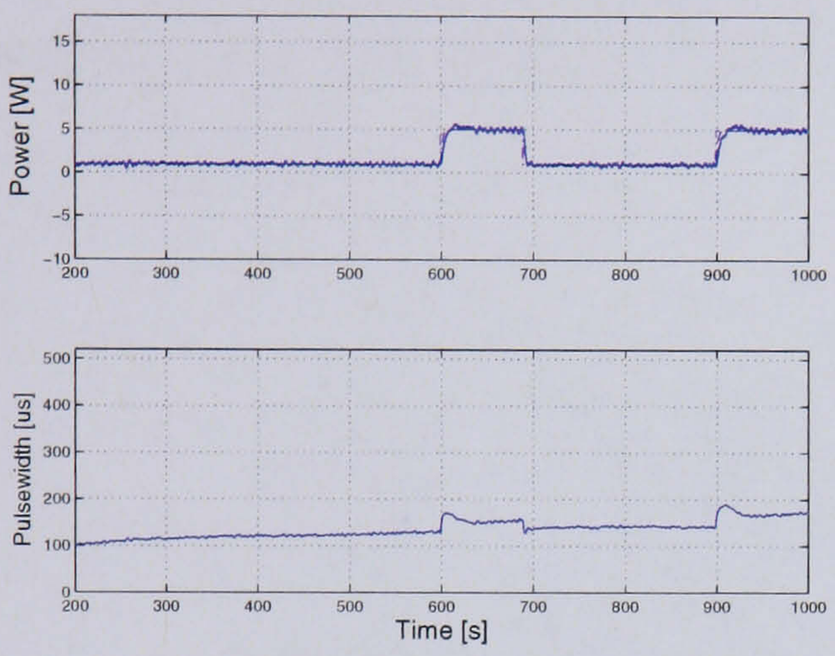

(a) PRBS Test 1 - 5 W

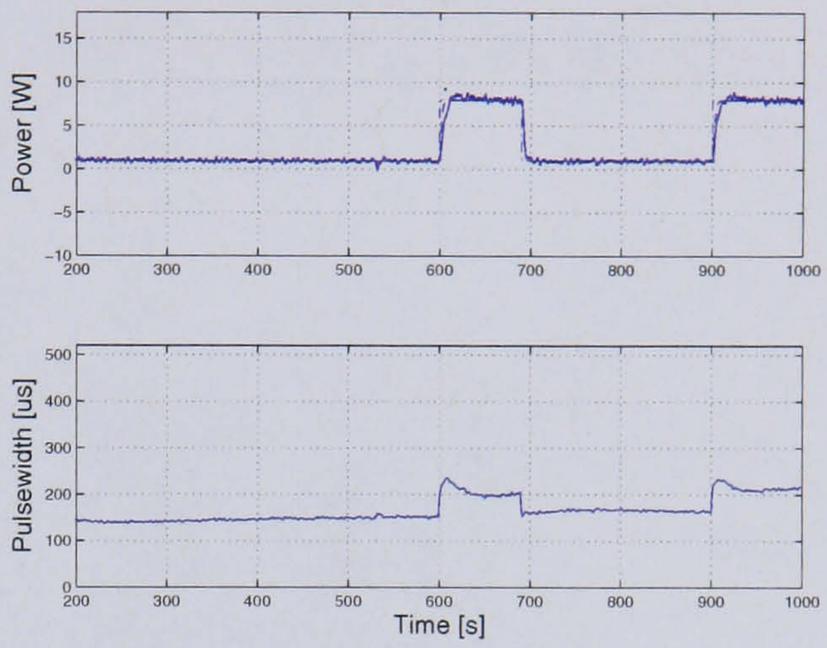

(b) PRBS Test 1 - 8 W

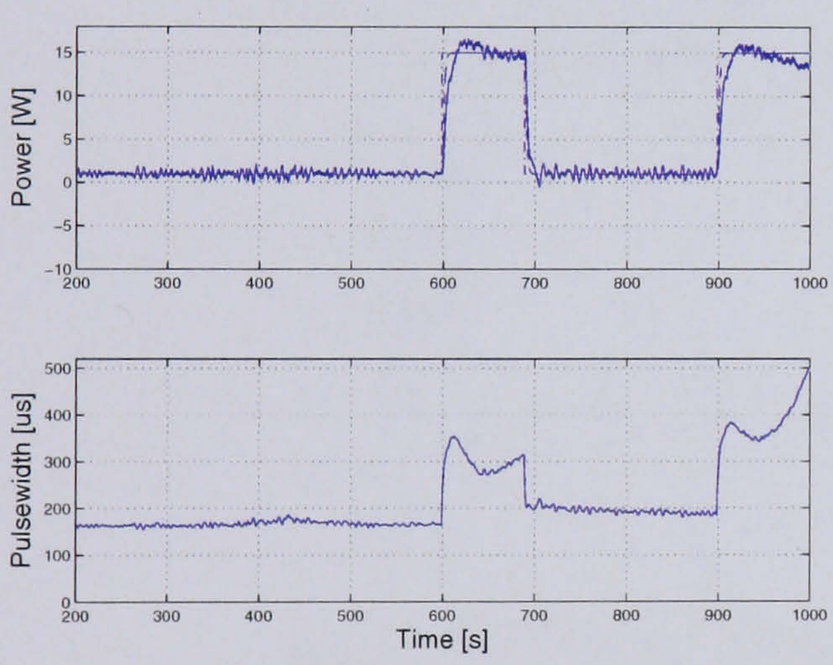

(c) PRBS Test 1 - 15 W

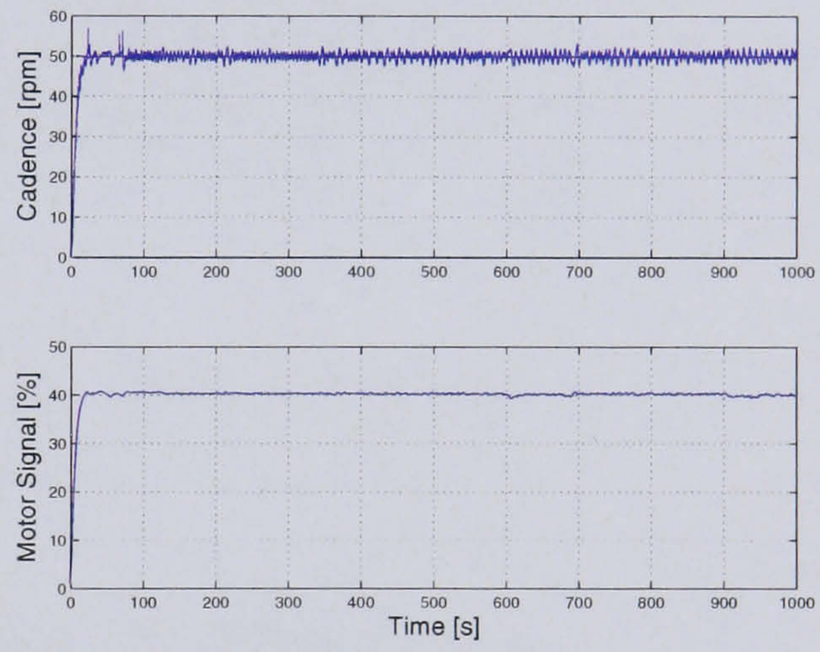

(d) Motor Control

Figure 5.2: For the power plots, the upper graph shows the controlled leg power (solid line), and the ideal power response (dashed line) and the reference leg power (dash-dot line). The lower plot shows the stimulation pulsewidth. Similarly, for the cadence plot the upper graph shows the reference cadence (dotted line), the measured cadence (solid line), and the ideal cadence response (dashed line). The lower plot shows the motor input signal.

The signal is designed to step on time multiples of 30 seconds. This is to allow resampling of the data, before the modelling process. When the controller is implemented in real-time, the metamax records on a breath by breath basis. The rate of breathing has no fixed sample rate, so an averaging algorithm is applied to average 30 seconds of $\dot{V}O_2$ data (which may contain between 5 and 8 breaths, depending on exercise level). In the modelling process, the sampling rates are required to be the same for the power signal and the $\dot{V}O_2$ data. Figure 5.3 shows the PRBS used for identification.

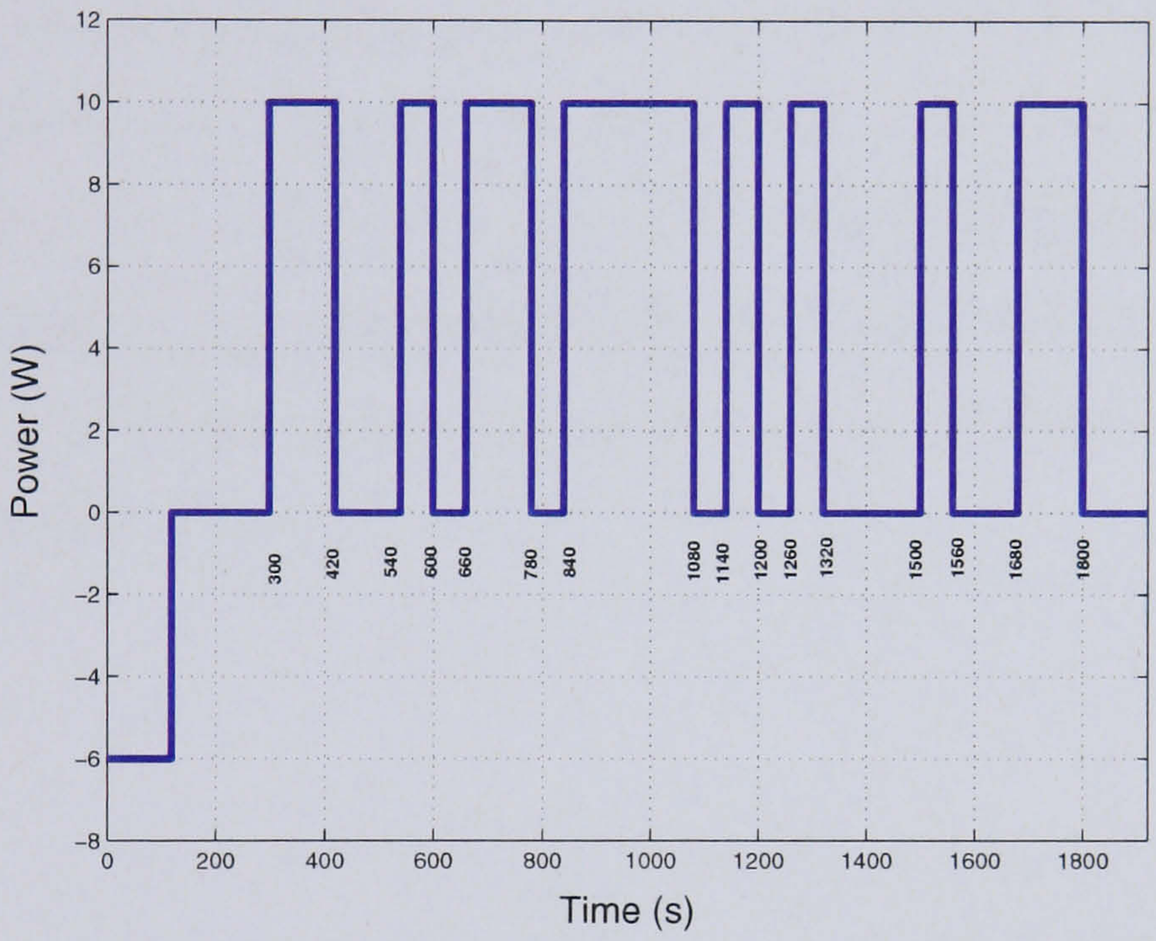

Figure 5.3: Power PRBS for $\dot{V}O_2$ Identification.

5.3 $\dot{V}O_2$ Identification

5.3.1 Test Protocol

2 separate identification tests were undertaken with Subject 1 (see Section 3.5) on separate test days. Identical equipment, set-up and protocol were used for both identifications. The test protocol is listed below :

- Warm Up - 5 Minutes, Low stimulation cycling without the mask, at -3 W.
- 10 minutes rest, without mask.

- 5 minutes rest with mask.
- 30 minutes of Cycling - PRBS identification of $\dot{V}O_2$ at a cadence of 50 rpm.
- 0 stimulation (motor assisted) cycling warm down.

The 2 identifications were undertaken on separate test days, one week apart.

$\dot{V}O_2$ Identification Results

Figure 5.4 shows the cadence and motor control results from the two identification tests. Both identifications, Figures 5.4(b) and 5.4(d), yield similar results in terms of power control. The power is controlled well to the reference, throughout the identifications. The corresponding stimulation levels are also comparable for both experiments, with a maximum stimulation pulsewidth in the region of 300μs. The resulting $\dot{V}O_2$ data is shown in Figure 5.5.

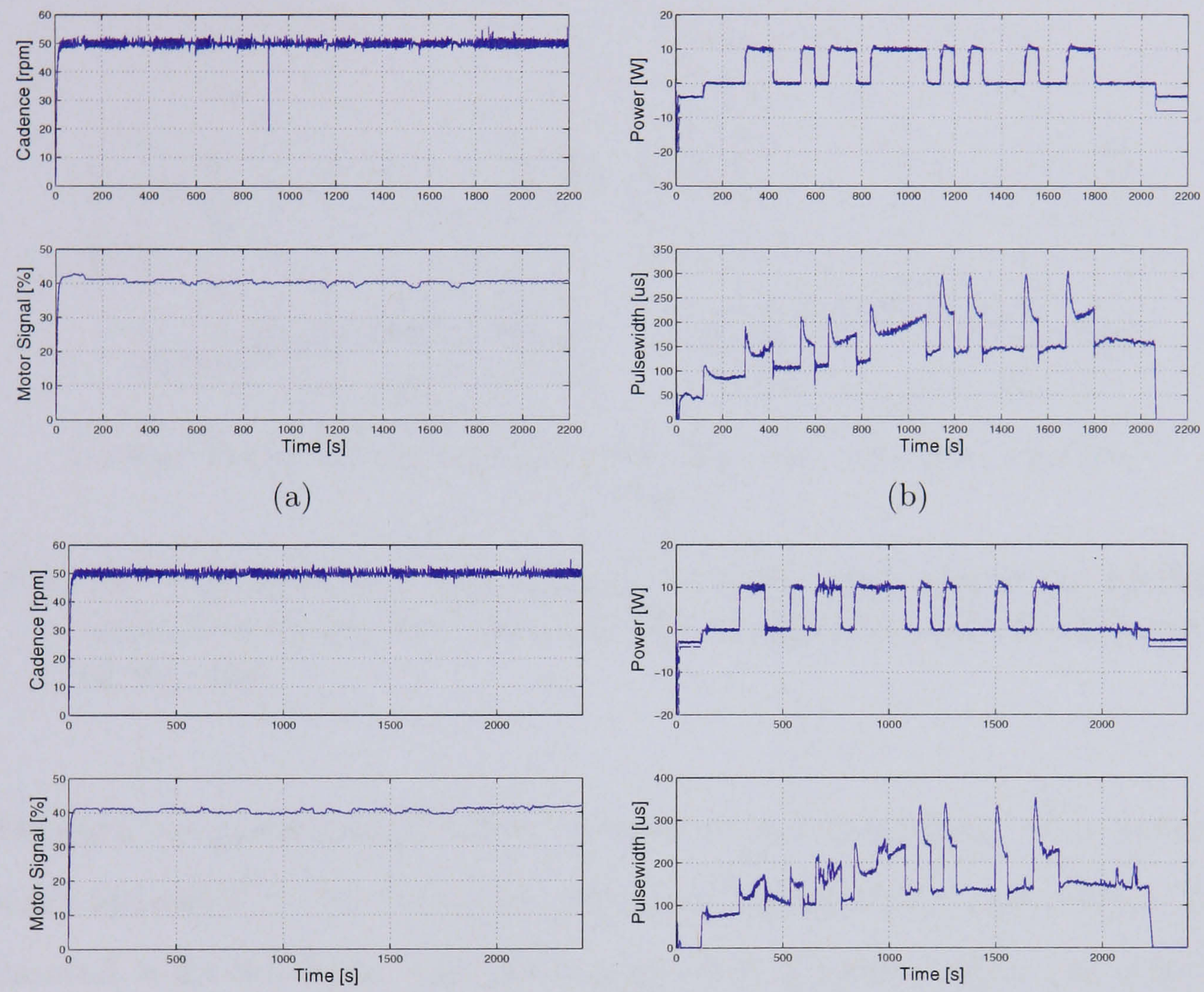

Figure 5.4: Identifications: In all graphs the reference is the dotted line, the measured data the solid line and the ideal response the dashed line. The figures show, (a) the cadence control from identification 1, (b) the power control from identification 1, (c) the cadence control from identification 2 and (d) the power control from identification 2.

5.4 $\dot{V}O_2$ Results and Preprocessing

The 2 identifications are shown in Figure 5.5. The figures are annotated to indicate the 5 phases of the identification test. The section of data that will be used for modelling is the section labelled Power PRBS.

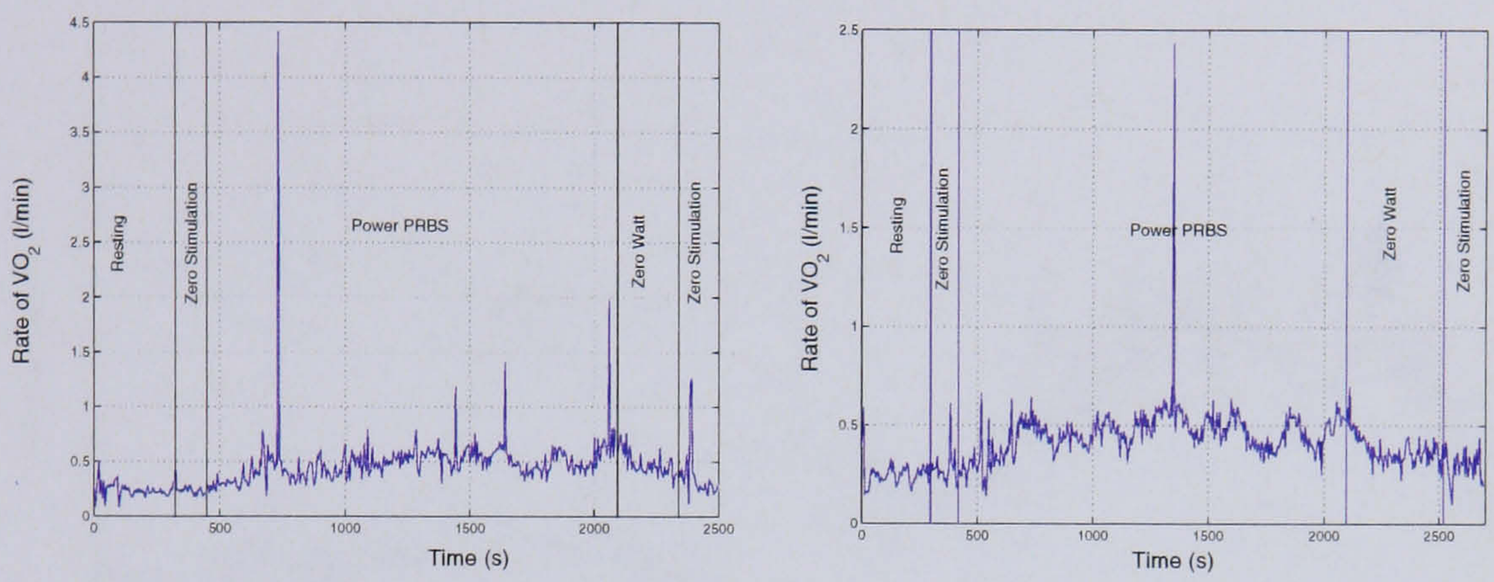

(a) Raw $\dot{V}O_2$ data from identification 1.

(b) Raw $\dot{V}O_2$ data from identification 2.

Figure 5.5: The $\dot{V}O_2$ figures are annotated to identify the phases of the identification tests. The figures show how the $\dot{V}O_2$ changes through the different phases of the tests.

The $\dot{V}O_2$ data are preprocessed before resampling and modelling. Non physiological outliers are identified in the $\dot{V}O_2$ data, shown in Figures 5.6(a) and 5.6(c). They are then removed from the data, and are re-plotted in Figures 5.6(b) and 5.6(d). The outliers are removed at this stage in the identification and modelling process, so that a more accurate model of the power-$\dot{V}O_2$ may be obtained. When a $\dot{V}O_2$ controller is implemented with a subject, not all of the outliers will be filtered out of the input $\dot{V}O_2$ data. The controller will be analysed to ensure that it is robust against large $\dot{V}O_2$ inputs.

Comparing the 2 $\dot{V}O_2$ identifications, they yield similar $\dot{V}O_2$ response profiles. Figures 5.6(b) and 5.6(d) have a similar profile. However, the first identification produces a higher maximum $\dot{V}O_2$, approximately 0.8 l/min compared with 0.7 l/min. This is an indication of the variability of $\dot{V}O_2$ between identical tests.

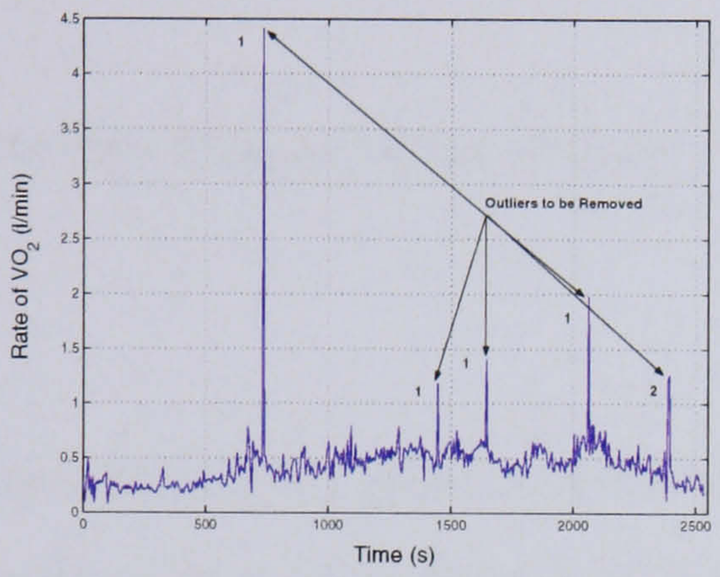

(a)

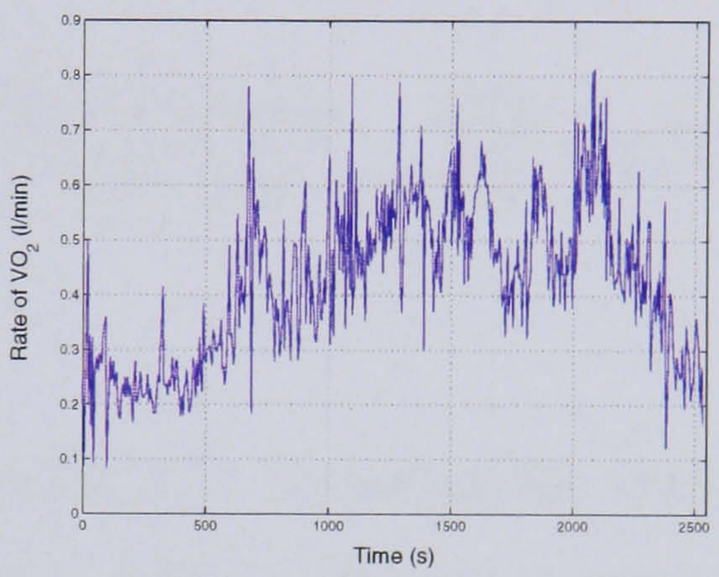

(b)

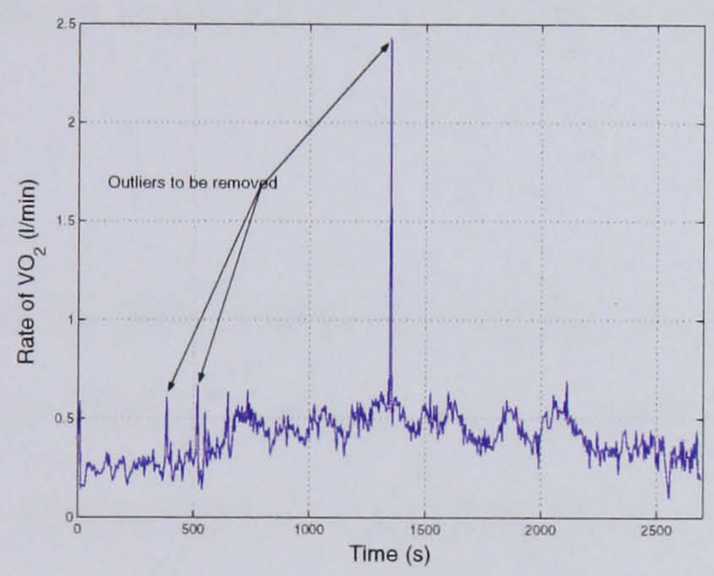

(c)

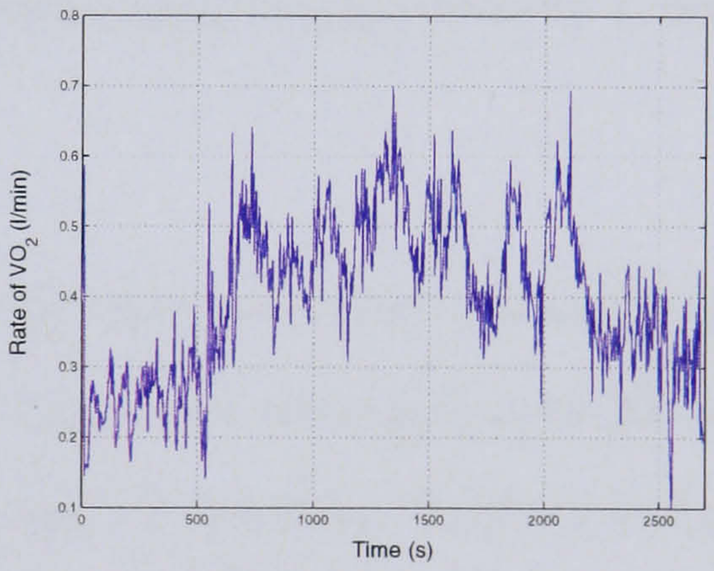

(d)

Figure 5.6: Plots 5.6(a) and 5.6(c) show the identification of the outliers that are to be removed from the $\dot{V}O_2$ for identifications 1 and 2 respectively. Figures 5.6(b) and 5.6(d) show the respective data once the outliers have been removed. The data is now shown on an smaller $\dot{V}O_2$ scale.

5.4.1 Averaging of $\dot{V}O_2$ data

All the breaths in the previous 30 seconds are found and their coinciding values of $\dot{V}O_2$ are measured. The $\dot{V}O_2$ values are summed, the maxima and minima are removed and their average is calculated. This value is then used as the $\dot{V}O_2$ value for that 30 seconds. The average time between breaths can be calculated, by taking the number of samples and the total test time:

$$\text{Average time between breaths} = \frac{\text{No. of breaths}}{\text{Total time}} = \frac{2335}{531} = 4.77\ s \qquad (5.1)$$

This value includes all the phases of the identification, including the data recorded at resting. The frequency of breaths will increase with an increase in exercise intensity, therefore within a 30 second sample of exercise data, approximately 5 breaths will be averaged.

An algorithm is developed to average the $\dot{V}O_2$ data and allow for analysis at different sample times. The algorithm allows for the data to be averaged over 30s, and then the $\dot{V}O_2$ can be outputted at intervals of 30, 20 and 10 seconds. Figures 5.7(a) and 5.7(b) show the $\dot{V}O_2$ data and averaged $\dot{V}O_2$ data from identification 1 and the averaged $\dot{V}O_2$ data alone respectively, for a 30 second output interval.

The averaged $\dot{V}O_2$ data for identification 1 is plotted with the PRBS power data in Figure 5.8. The $\dot{V}O_2$ is seen to react to changes in the power reference, after a delay. An upward trend in the $\dot{V}O_2$ is identified over the initial 1300 s of the identification. This coincides with the phases of resting, zero stimulation cycling and the first half of the PRBS identification. Prior to modelling this trend will be removed.

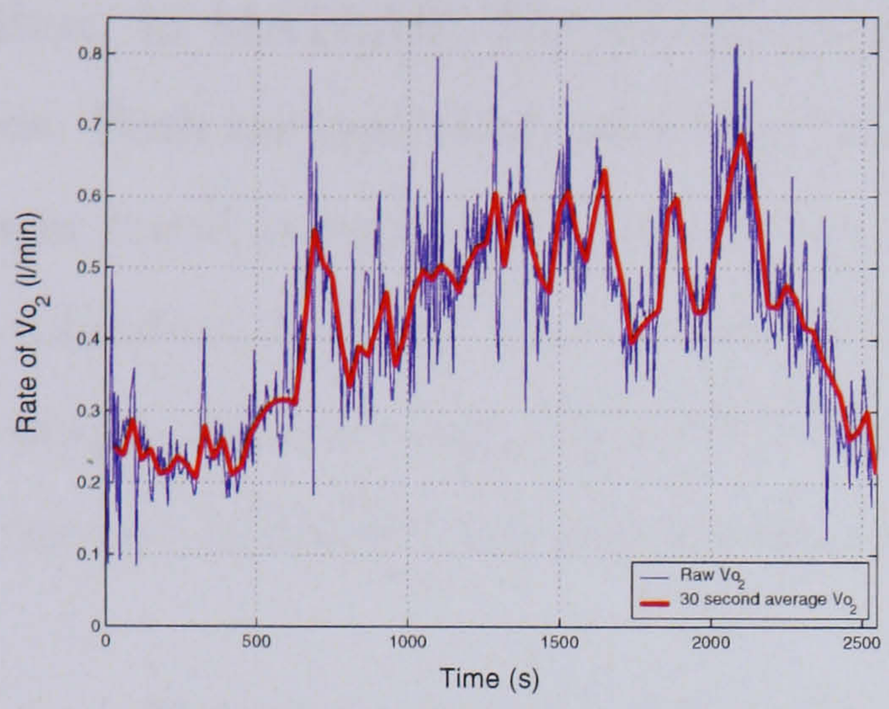

(a) Original $\dot{V}O_2$ data overlayed with the $\dot{V}O_2$ averaged over 30 s.

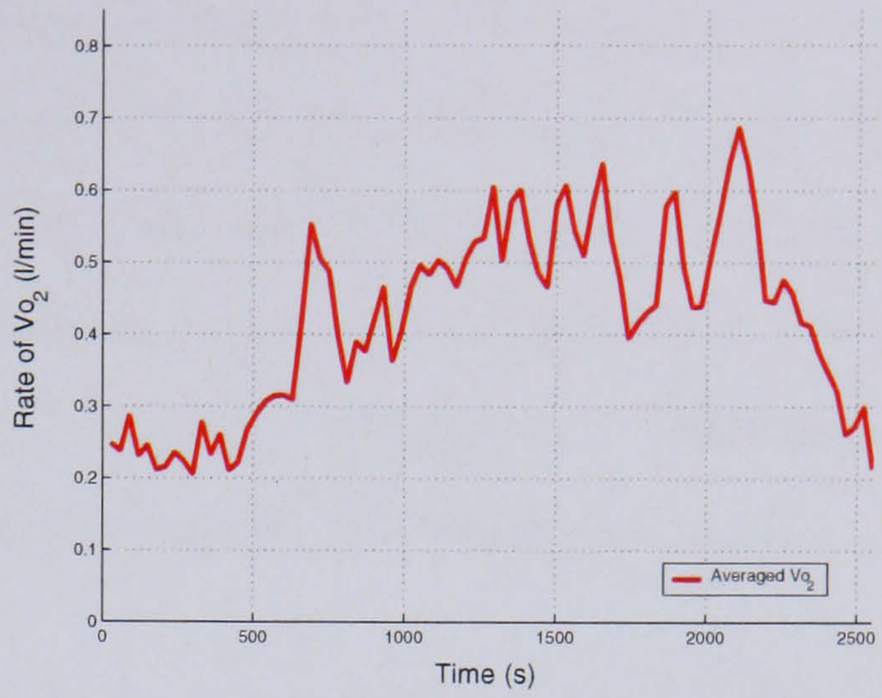

(b) $\dot{V}O_2$ averaged over 30 s.

Figure 5.7: Plots showing the averaged $\dot{V}O_2$ identification data 1.

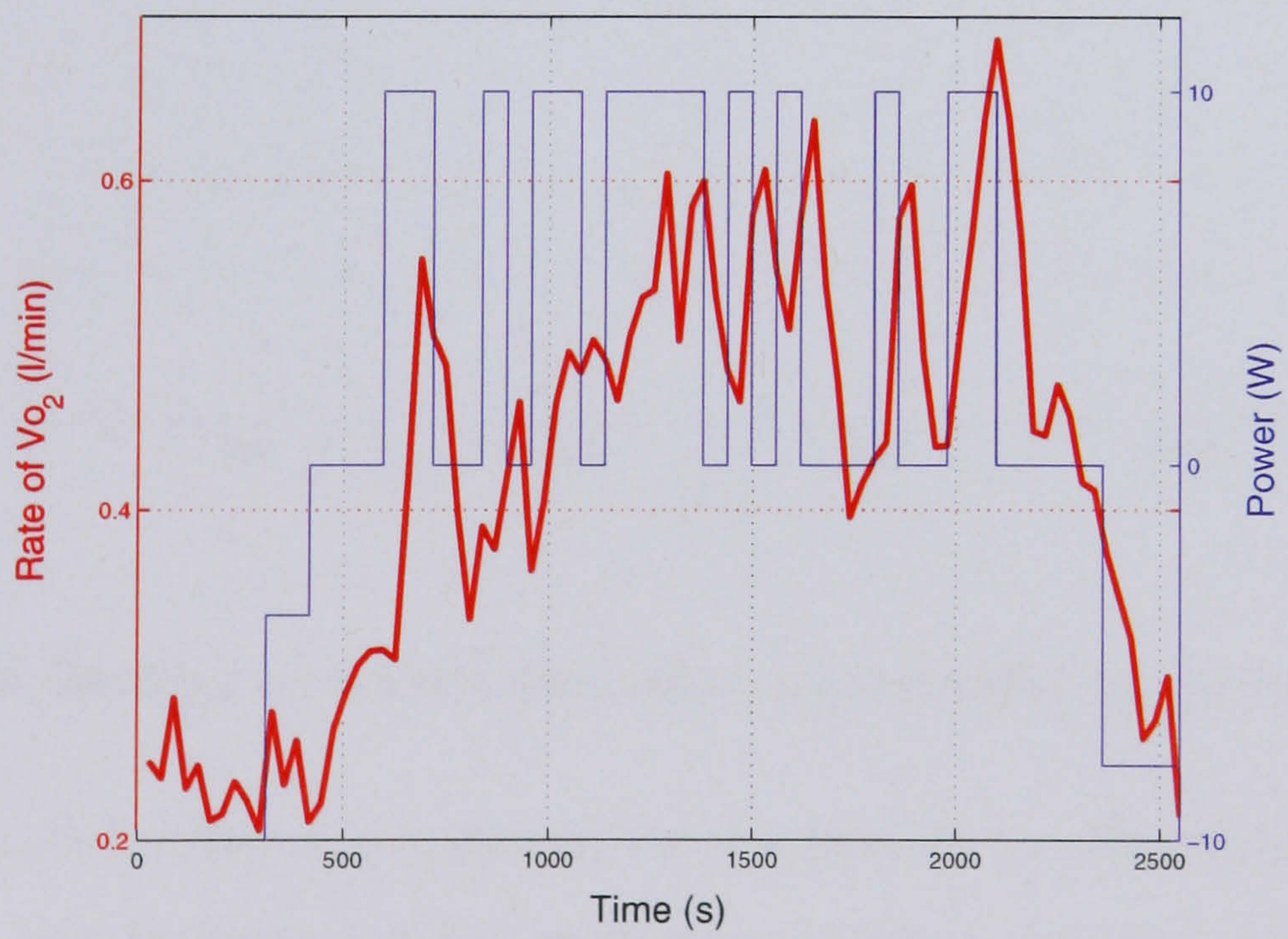

Figure 5.8: Plot showing the $\dot{V}O_2$, averaged over 30 s and the power PRBS from identification 1.

5.4.2 Modelling Data

The PRBS power (Input) and $\dot{V}O_2$ (Output) data are imported into the Identification Toolbox, in MATLAB. The data is preprocessed firstly by removing the mean and trends. Both the input and output sequences have their mean values removed, and then a linear trend is estimated and removed. The data are then separated into working and validation data. An example for identification 1 is shown in Figure 5.9. The input and output data is simply divided in two, to create the working and validation. The first section is labelled the working data and the second, the validation data.

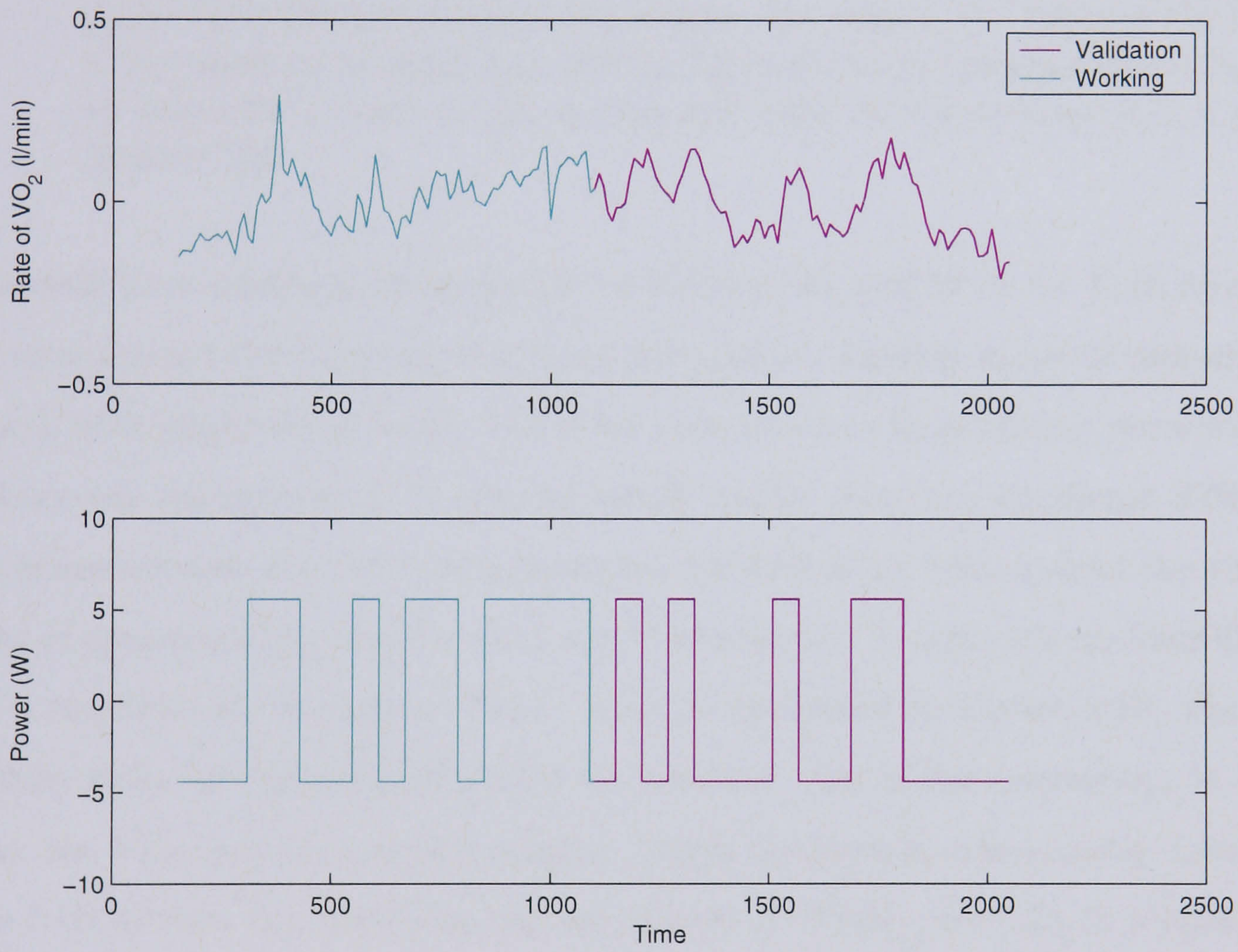

Figure 5.9: Working and Validation data, with trends and means removed.

Various ARX model orders are analysed for the best fit to the input-output data (as discussed previously in Section 3.7.2, and lowest order model. For example a 4^{th} order model may have a 45% fit, and a 1^{st} order model a 39% fit. For this case the 1^{st} order model would be chosen, as the model is significantly simpler, for a relatively small decrease in percentage fit. The models created for the 2 sets of identification and the 3 sampling rates (Ts) are summarised in Table 5.1.

	Identification 1			Identification 2		
Ts (s)	30	20	10	30	20	10
ARX Structure	131	141	121	121	111	121
Fit (%)	48.17	46.02	47.55	49.76	48.25	51.39
T_R (s)	58.97	42.87	**75.44**	108.6	129.9	**151.8**
D_C Gain	0.0142	0.0148	0.015	0.0178	0.0184	0.0219
BW	0.0390	0.0490	0.0289	0.0208	0.0169	0.0144

Table 5.1: Summary table of Identified models, for 3 sampling rates. Where T(s) is the sampling rate, Fit is the percentage fit of the model against the validation data, T_R is the rise time of the model, D_C gain is the ratio of the output of a system to its input and BW is the bandwidth, the maximum frequency at which the output of the system will track an input sinusoid in a correct manner [19].

The models have similar percentage fits of between 46 and 52 % for both identifications, even though the different structures are utilised. Further model structures were analysed, with longer delay terms, but these were found to have smaller percentage fits and hence are not presented. In the presented models there are significant differences in rise times between the the 2 identifications. Identification 1 has a short rise time, an average of approximately 59 s for the 3 model structures. In comparison, Identification 2 has a rise time on average of 130 s. This is illustrated in Figure 5.10, where the $\dot{V}O_2$ data from the two identifications are overlaid. On initial inspection, in Figure 5.10(a), the $\dot{V}O_2$ responses appear similar. When the data is subsequently zoomed, in Figure 5.10(b) then the dissimilarities are identified. Firstly the $\dot{V}O_2$ in identification 1 responds faster to a change in power, and secondly the $\dot{V}O_2$ increases to a higher value. Throughout the whole of Identification 1 the level of $\dot{V}O_2$ is consistently higher than that of Identification 2.

The difference in rise times excludes the possibility of cross identification between the two data sets. If the identified $\dot{V}O_2$s had had similar rise times then one test could have been used for working data, with the other as validation. This may have resulted in more accurate models.

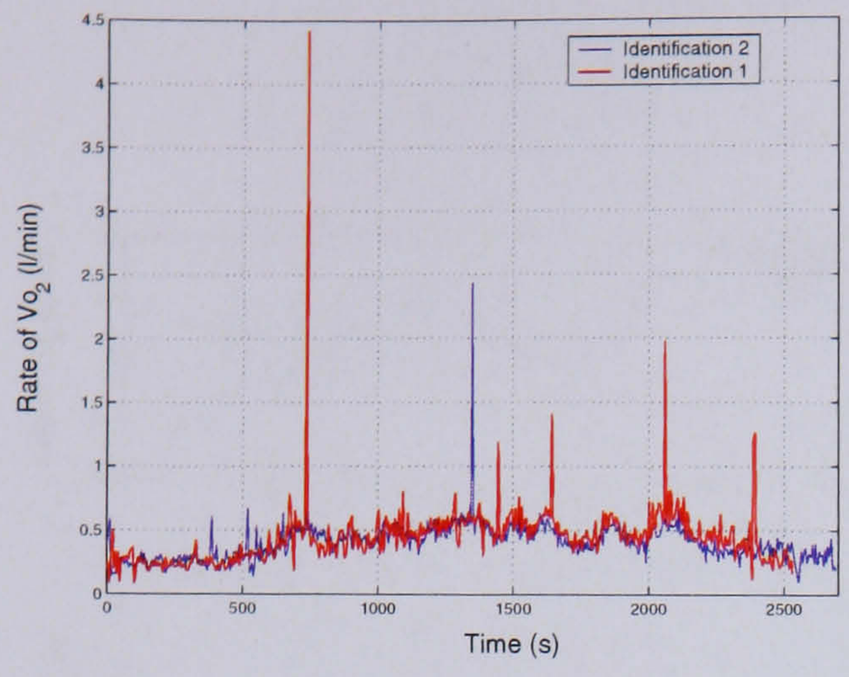

(a) $\dot{V}O_2$ identifications.

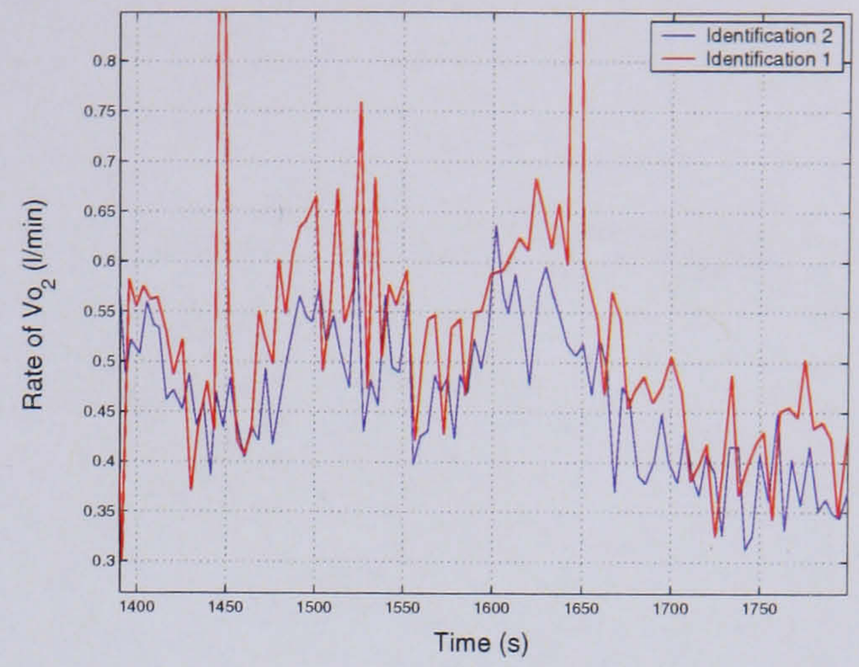

(b) Zoomed selection of the $\dot{V}O_2$ identifications.

Figure 5.10: $\dot{V}O_2$ identifications overlaid to indicate the dissimilarities in the dynamics.

A model from each identification is selected for controller design. The models have a 121 ARX structure and a sample time of 10 s from Table 5.1. The model for Identification 1 will be known as model 1, with corresponding controller 1 and similarly for Identification 2.

Model 1

Figure 5.11(a) shows the Working and Validation data for Identification 1 and the corresponding best fit model in Figure 5.11(b). The model does not fit the validation data exactly. The model can be seen to follow the general shape of the validation data but not achieve the peak levels. The transfer function for the ARX 121 structure, Model 1 is given as;

$$\frac{0.00162z^{-1} + 0.002414z^{-2}}{1 - 0.7459z^{-1}} \tag{5.2}$$

Figure 5.12 shows the normalised step response, bode plot and Pole-Zero (PZ) map for Model 1. The PZ-map shows both poles within the unit circle, with a pole at the origin.

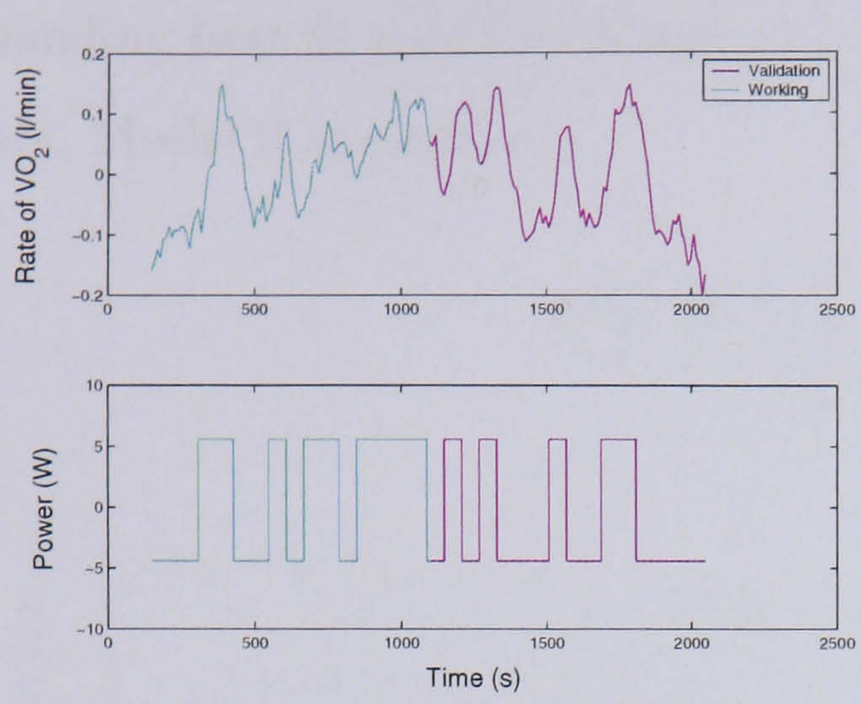

(a) Selected Working and Validation data, with trends and means removed.

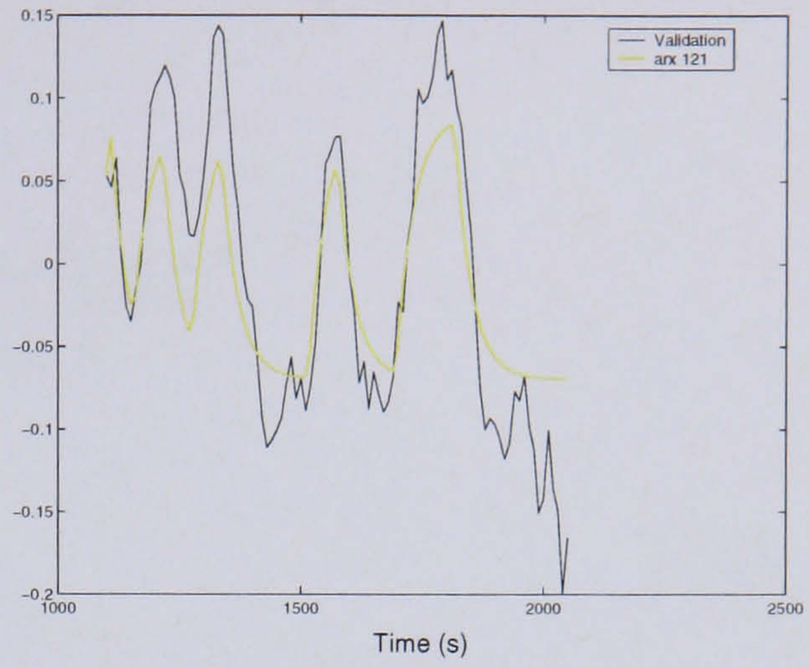

(b) Best fit model.

Figure 5.11: Model identification for model 1.

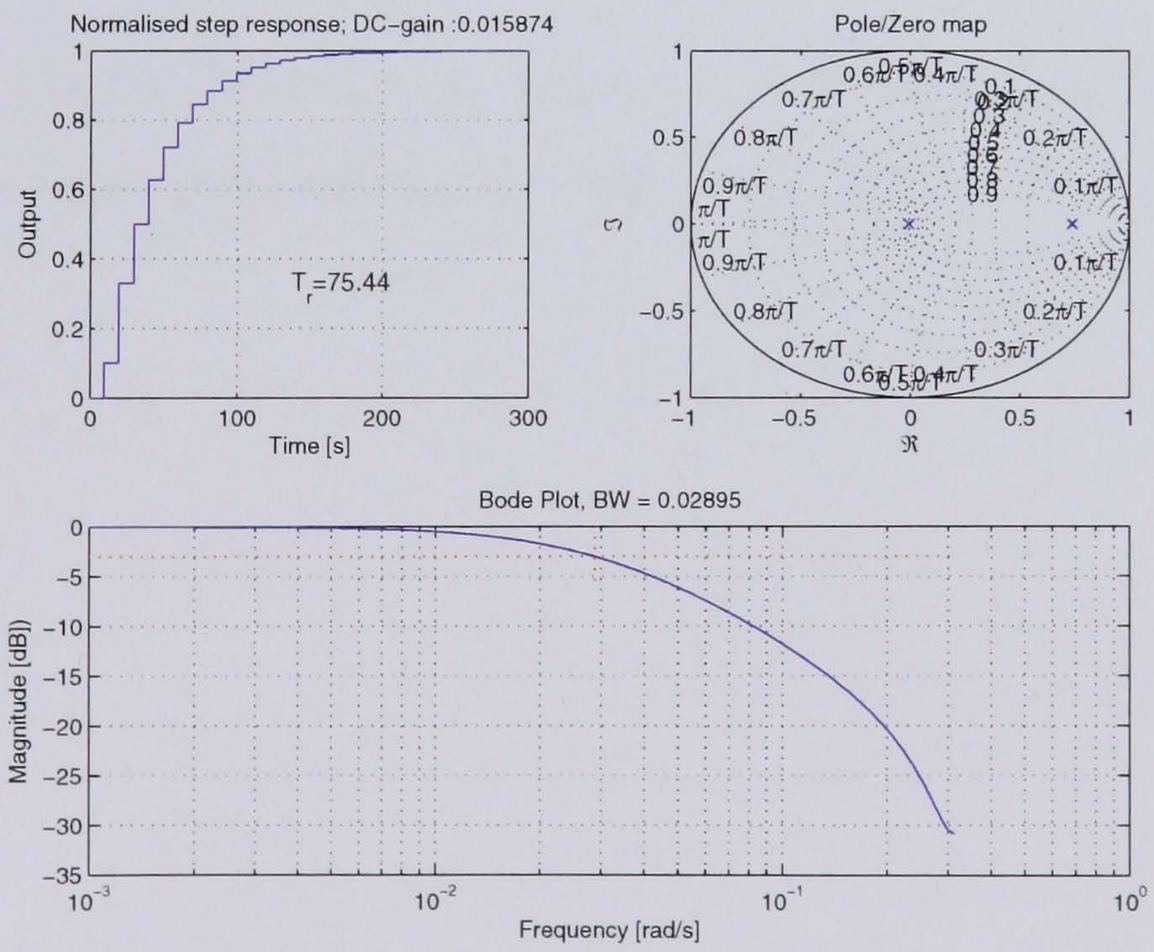

Figure 5.12: Normalised step response, PZ-map and bode plot for Model 1.

Model 2

Figure 5.13(a) shows the working and Validation data for Identification 2 and the corresponding best fit model in Figure 5.13(b). The transfer function for the ARX 121 structure, Model 2 is given as;

$$\frac{0.001331z^{-1} + 0.001538z^{-2}}{1 - 0.8652z^{-1}} \tag{5.3}$$

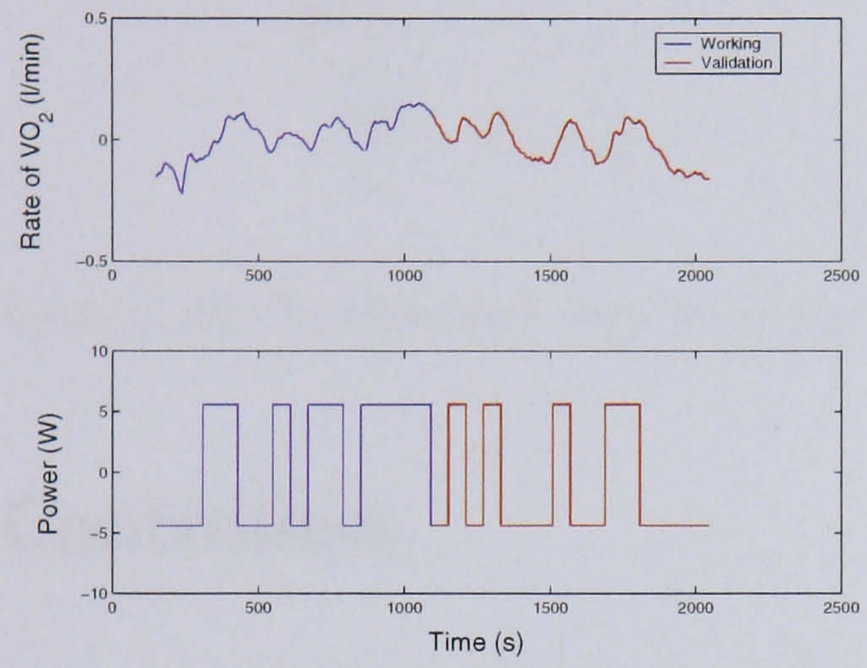

(a) Selected Working and Validation data, with trends and means removed.

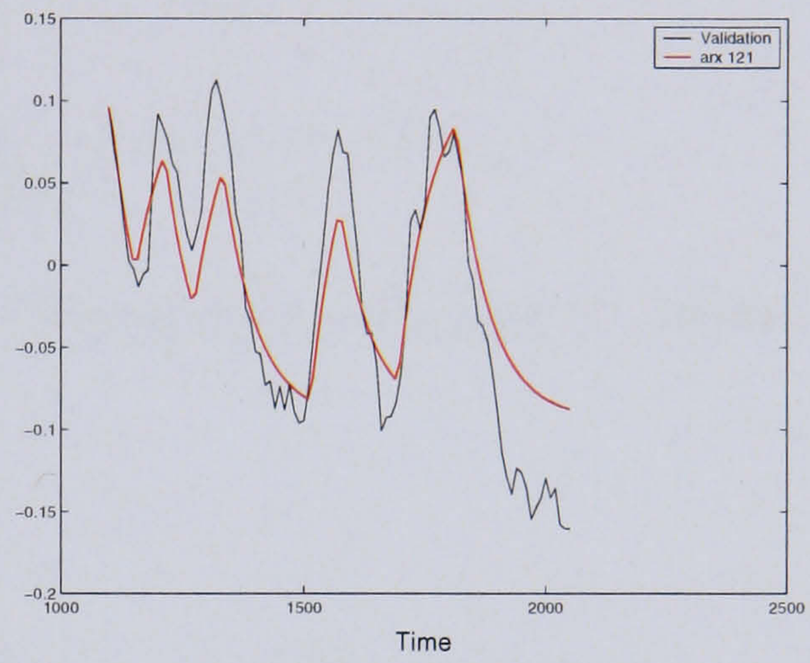

(b) Best fit model.

Figure 5.13: Model identification plots for model 2.

Figure 5.14 shows the normalised step response, bode plot and PZ-map for Model 2. The PZ-map shows both poles within the unit circle, with a pole at the origin.

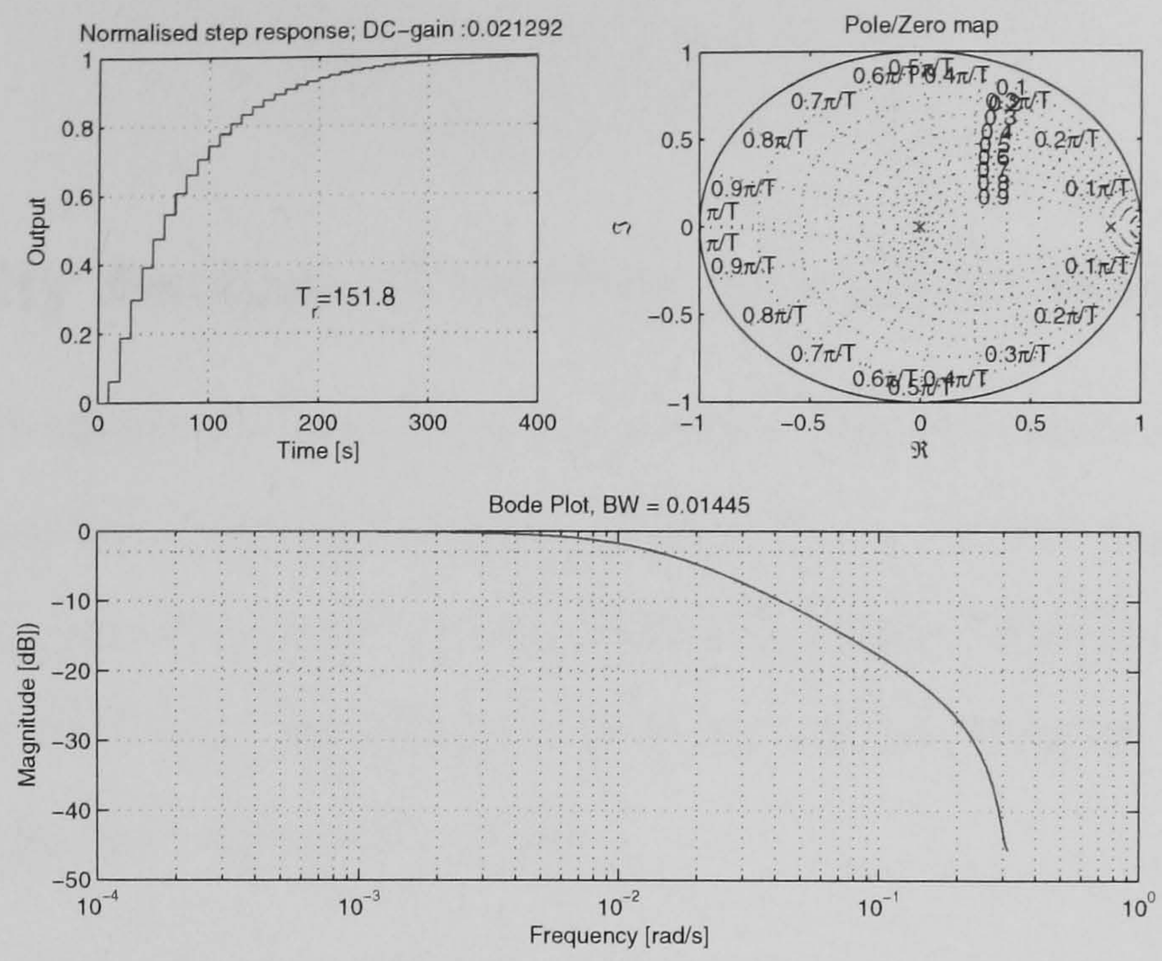

Figure 5.14: Normalised step response, PZ-map and bode plot for Model 2.

5.5 Controllers

Controllers are now designed for the 2 identified models. The controllers are of RST structure, discussed in section 3.6. The controller design includes integral action and plant cancellation. The rise time of the controller is selected to be slightly greater than the rise time of the model. Details of Controllers 1 and 2 are found in Table 5.2.

Controllers	
1	2
Model $T_R = 75.44$ s	Model $T_R = 151.80$ s
Controller $T_R = 80$ s	Controller $T_R = 160$ s
Observer $T_R = 50$ s	Observer $T_R = 100$ s
ARW $T_R = 50$ s	ARW $T_R = 100$ s
T(s) = 10 s	T(s) = 10 s

Table 5.2: Rise times and Controller coefficients for Controllers.

Controller 1 has transfer function,

$$\frac{0.3306z^{-1} + 0.04925z^{-2}}{1 - 1.43z^{-1} + 0.5126z^{-2}} \tag{5.4}$$

and controller 2 has transfer function,

$$\frac{0.01121z^{-1} + 0.01294z^{-2}}{1 - 1.692z^{-1} + 0.7159z^{-2}} \tag{5.5}$$

5.5.1 Sensitivity Analysis of Models and Controllers

The sensitivity (S) and complementary sensitivity (T) are plotted for the 4 different combinations of models and controllers (Figure 5.15). The combinations result in peaking of S, while only the combination of Model 2 and Controller 1 (Figure 5.15(c)) results in peaking of T. As discussed in Section 3.6 peaking of S and T should be avoided, in the cross over region, to avoid:

- overly large sensitivity to disturbances,
- increased influence of measurement noise,
- loss of performance robustness.

The magnitudes of the peaks in S and T do not appear initially significant. The frequencies will be further analysed after testing of the controllers, if any undesirable oscillations are detected.

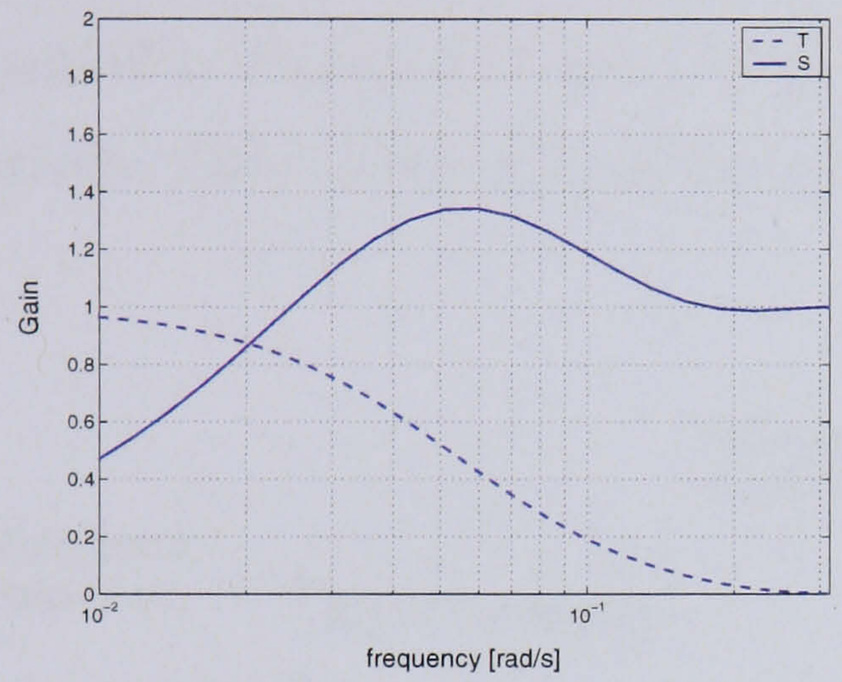

(a) Model 1 and Controller 1.

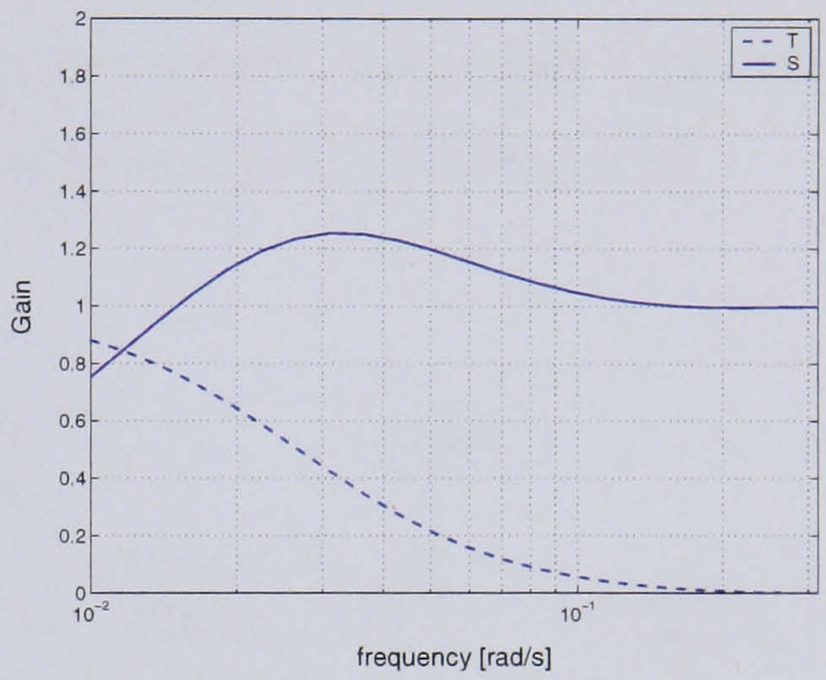

(b) Model 2 and Controller 2.

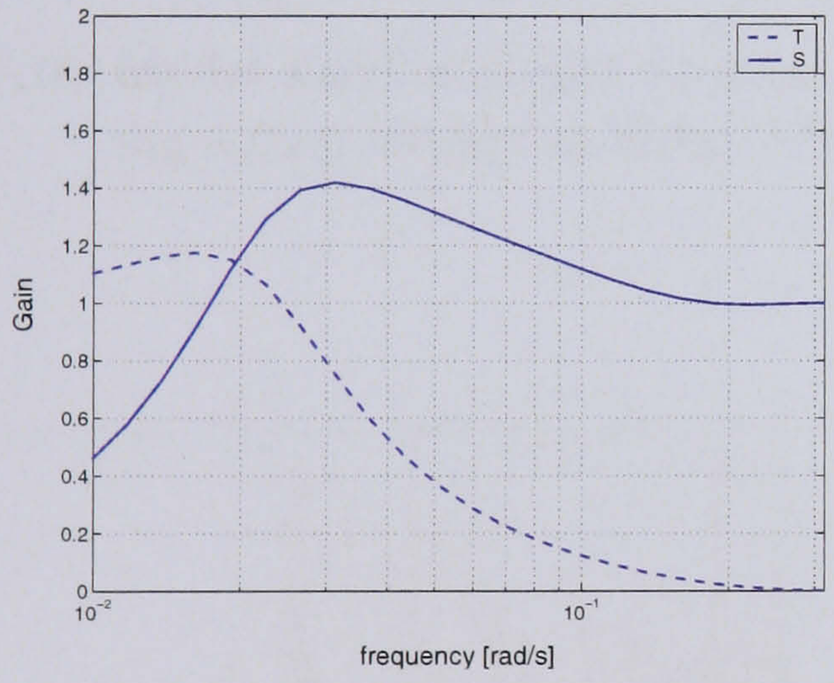

(c) Model 2 and Controller 1.

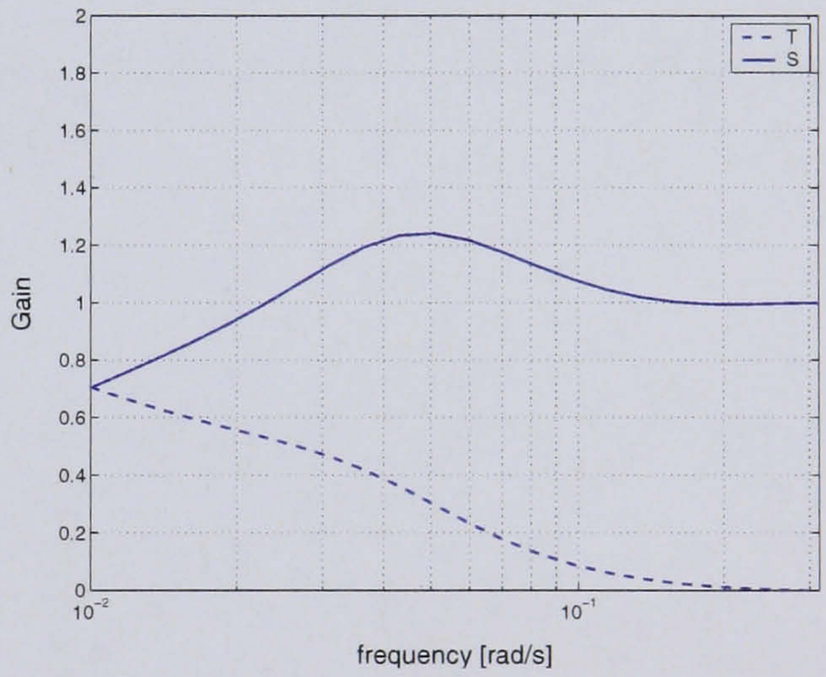

(d) Model 1 and Controller 2.

Figure 5.15: S and T plots for the 4 combinations of Models and Controllers.

5.6 Simulation Study

Prior to implementing the controllers on an able bodied or paraplegic subject, simulations of the controllers are undertaken. These simulations illustrate how the controller will behave with the identified models, an indication of how they may perform with a subject. The model that is simulated is shown schematically in Figure 5.16. A step in reference $\dot{V}O_2$ is applied to the system, 0.25 to 0.7 l/min, after a time of 600 s. The outputs from the model are the $\dot{V}O_2$ and the reference power, the input for the power controller. Figures 5.17 and 5.18 show this step for Controller 1 and Controller 2 respectively, with 3 levels of band-limited white noise (0, 0.05 and 0.25).

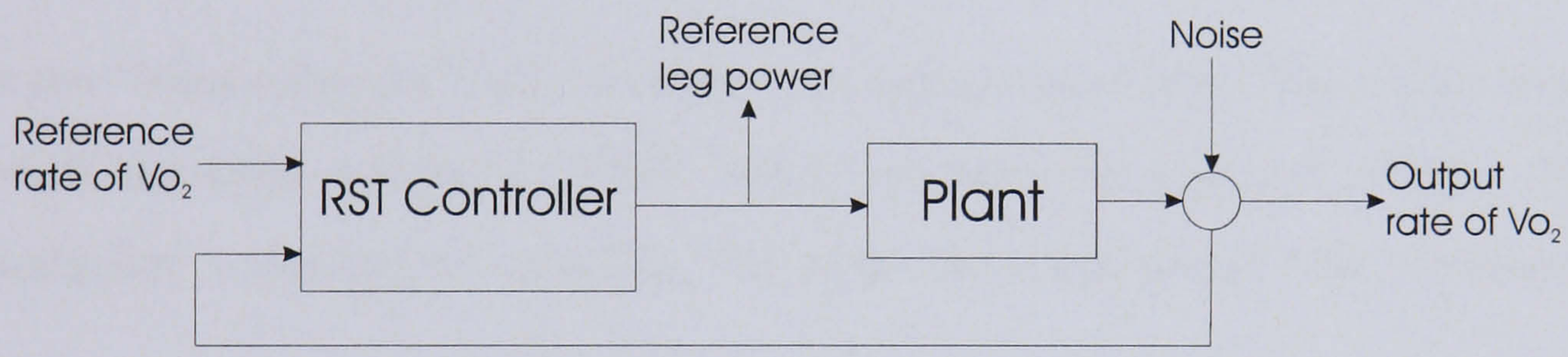

Figure 5.16: Model and Controller system, with noise added to analyse the effects during a step change in input reference.

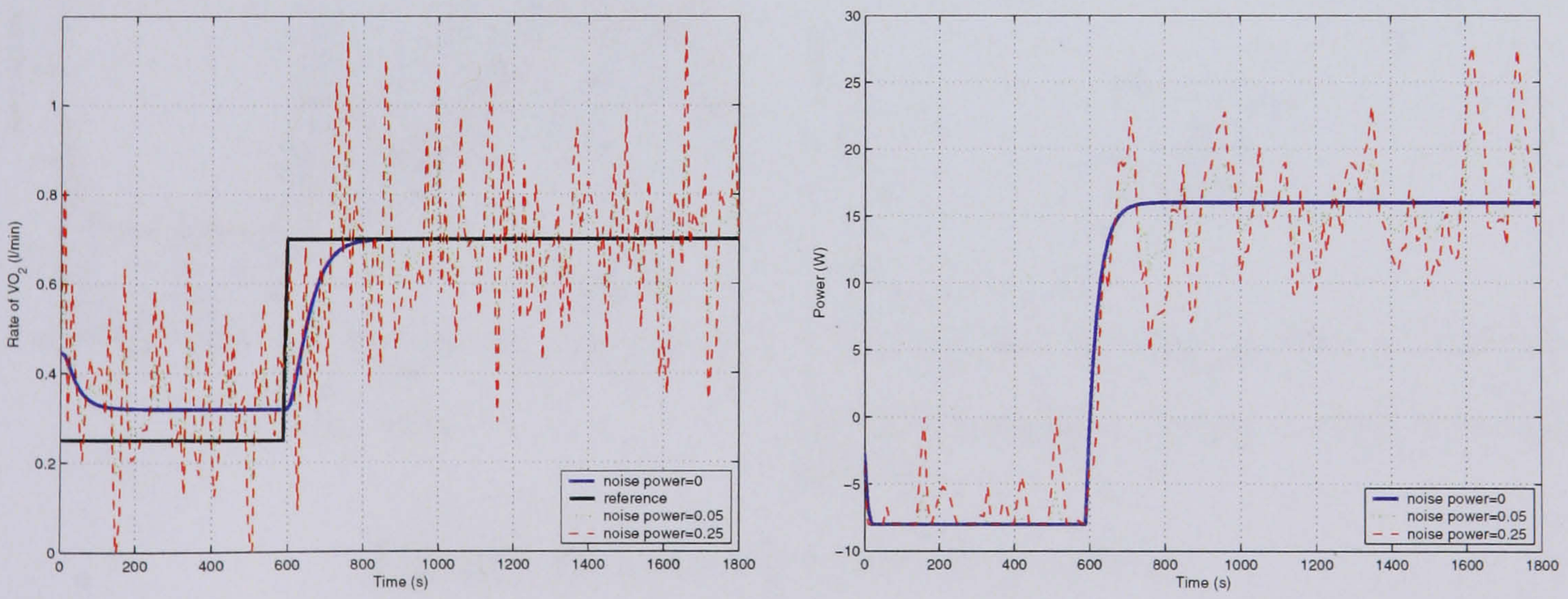

(a) $\dot{V}O_2$ (b) $\dot{V}O_2$ Controller Output - power controller reference

Figure 5.17: Controller 1: Step test with white noise added to the loop.

In practice noise will never be removed from the system. For that reason the zero noise

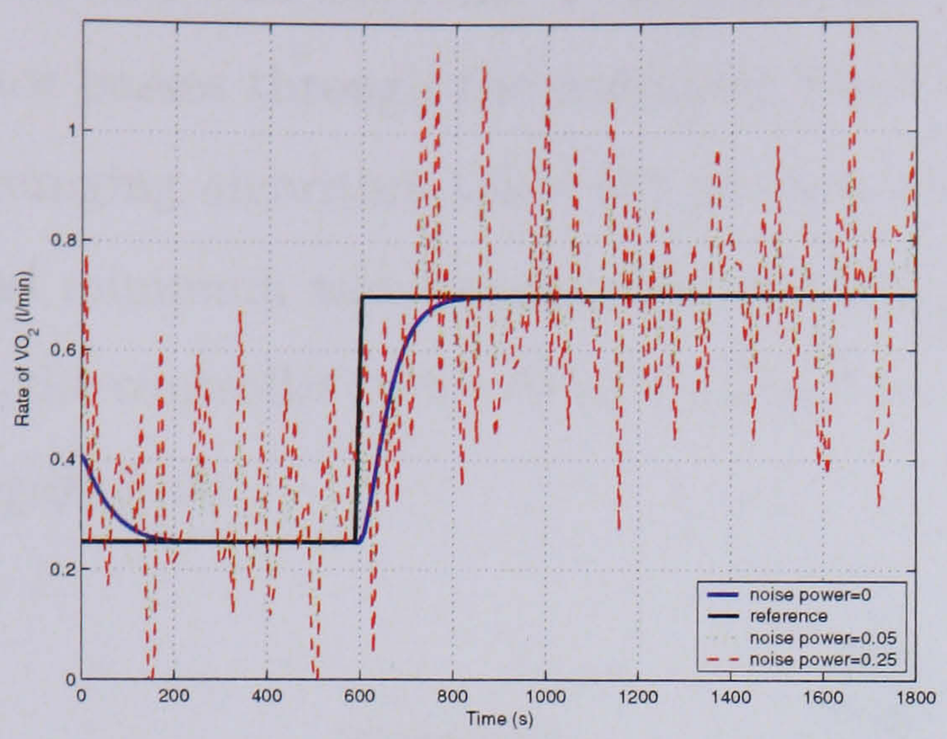

(a) $\dot{V}O_2$

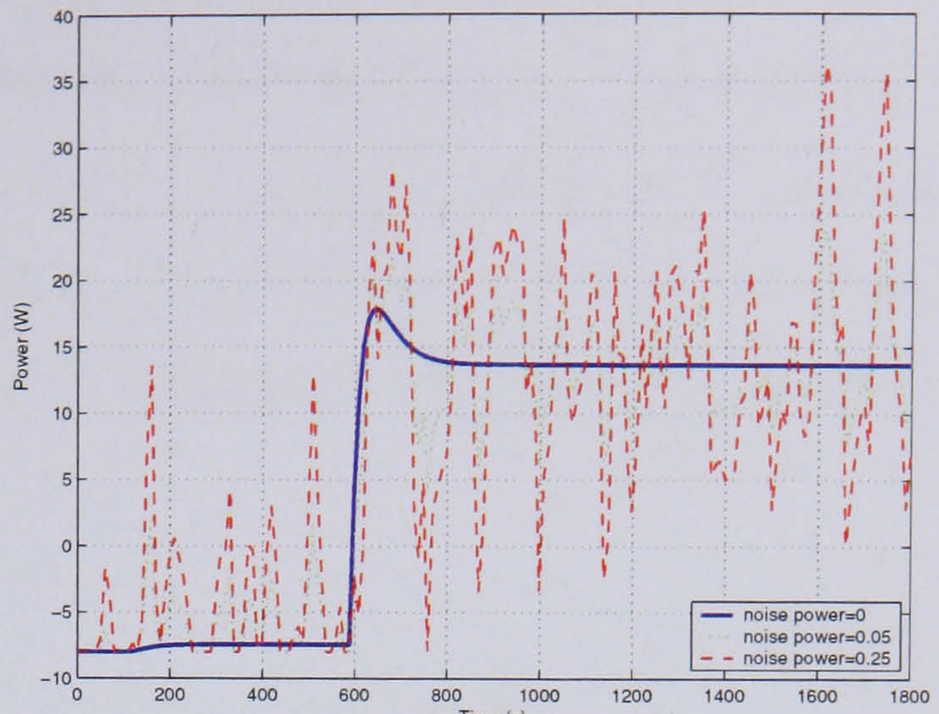

(b) $\dot{V}O_2$ Controller Output - power controller reference

Figure 5.18: Controller 2: Step test with white noise added to the loop.

input is the "ideal response", which would not happen in reality. The realistic response is one with the noise added. In these cases, the controllers do not become unstable, with Controller 1 seeming to attenuate the noise more effectively than Controller 2.

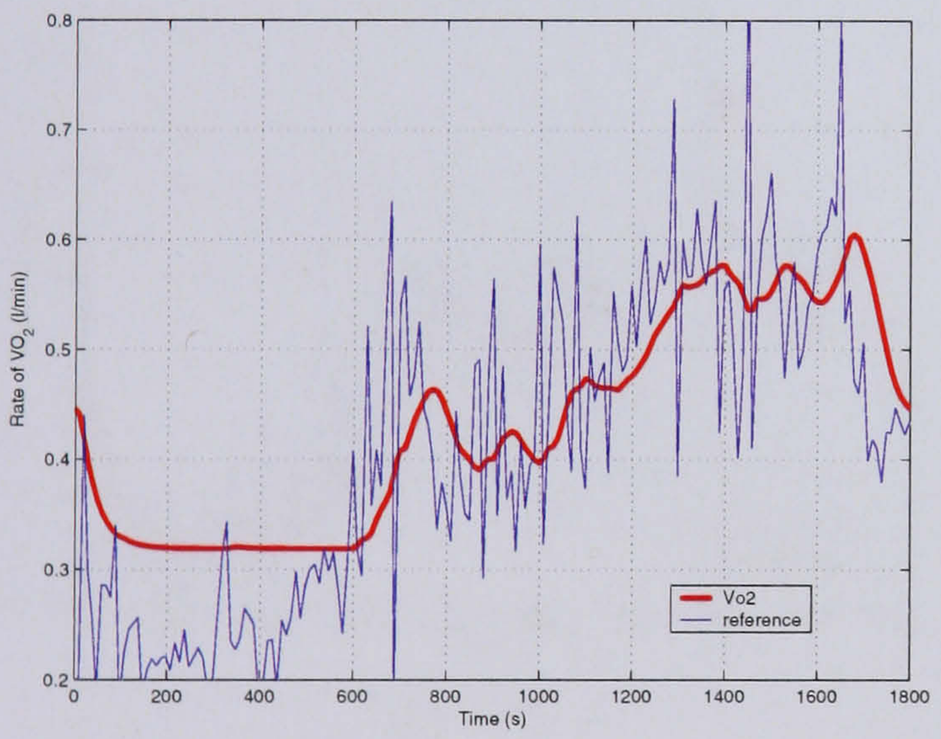

(a) $\dot{V}O_2$

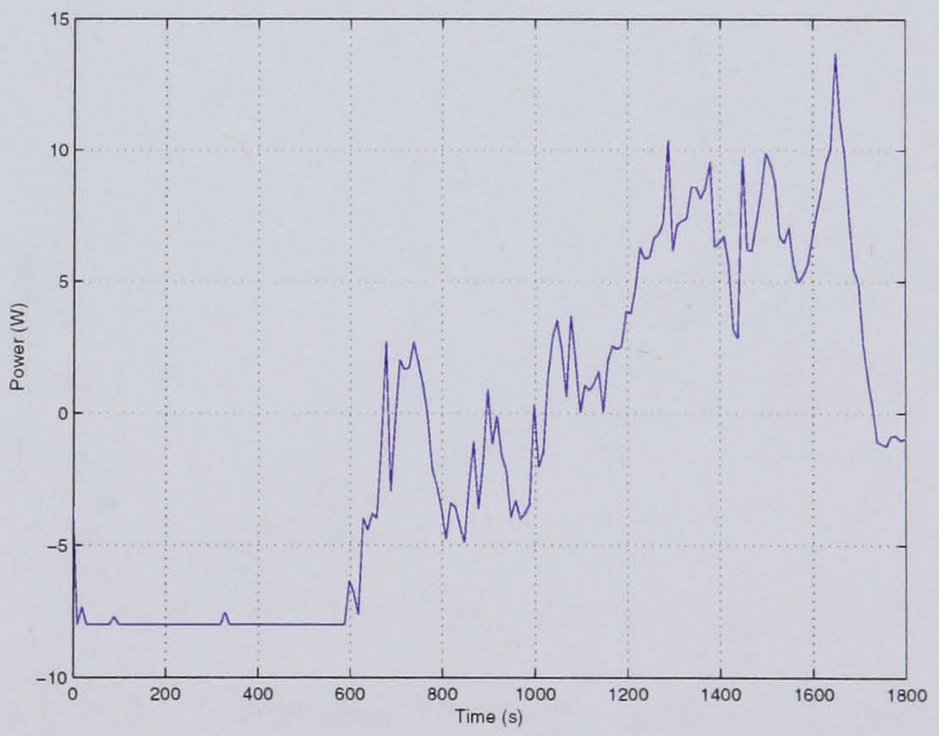

(b) $\dot{V}O_2$ Controller Output - power controller reference

Figure 5.19: Data set 1, with Controller 1.

Next, the original $\dot{V}O_2$ data measured in the two identifications, in Section 5.3, are entered as the reference $\dot{V}O_2$. If the controllers and models were ideal, then the reference power would be the PRBS used for identification (Section 5.2.2). Figures 5.19, 5.21,

5.22, and 5.23 show the 4 combinations of data sets and controllers. The $\dot{V}O_2$ reference passes through the averaging block that will be implemented in real time. The averaging algorithm takes the previous 30 s worth of breaths, removes the maximum and minimum and averages the remaining data. This value for the $\dot{V}O_2$ is outputted to the controller every 10 s, by means of a zero-order-hold. The algorithm is shown in Figure 5.20.

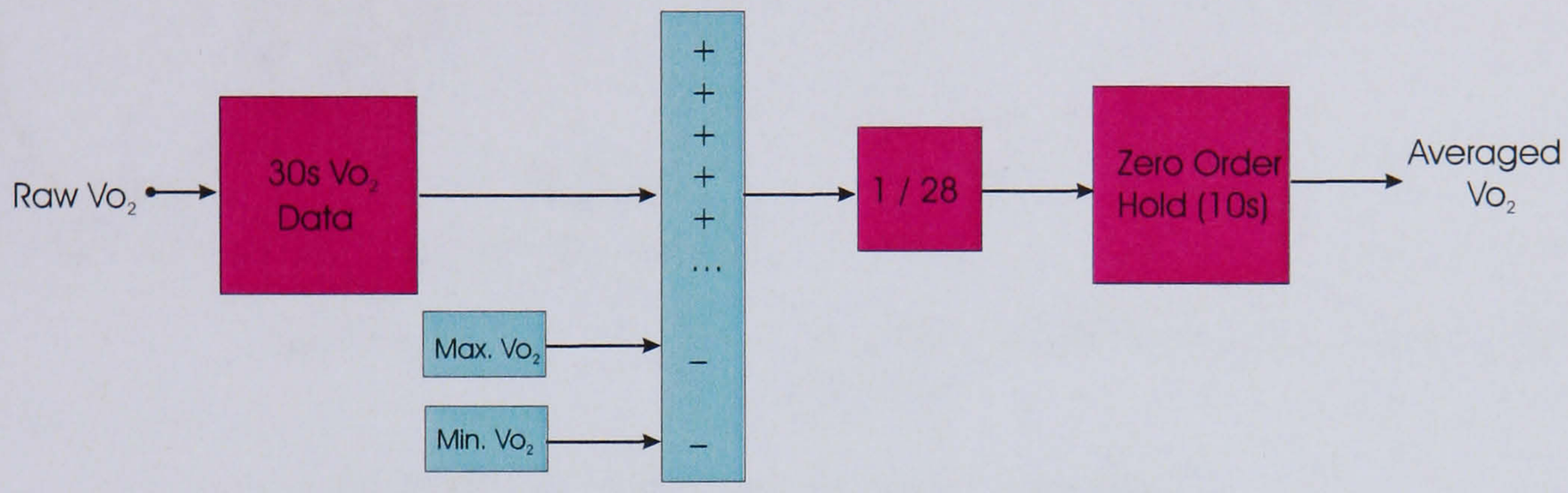

Figure 5.20: Schematic representation of the $\dot{V}O_2$ averaging algorithm.

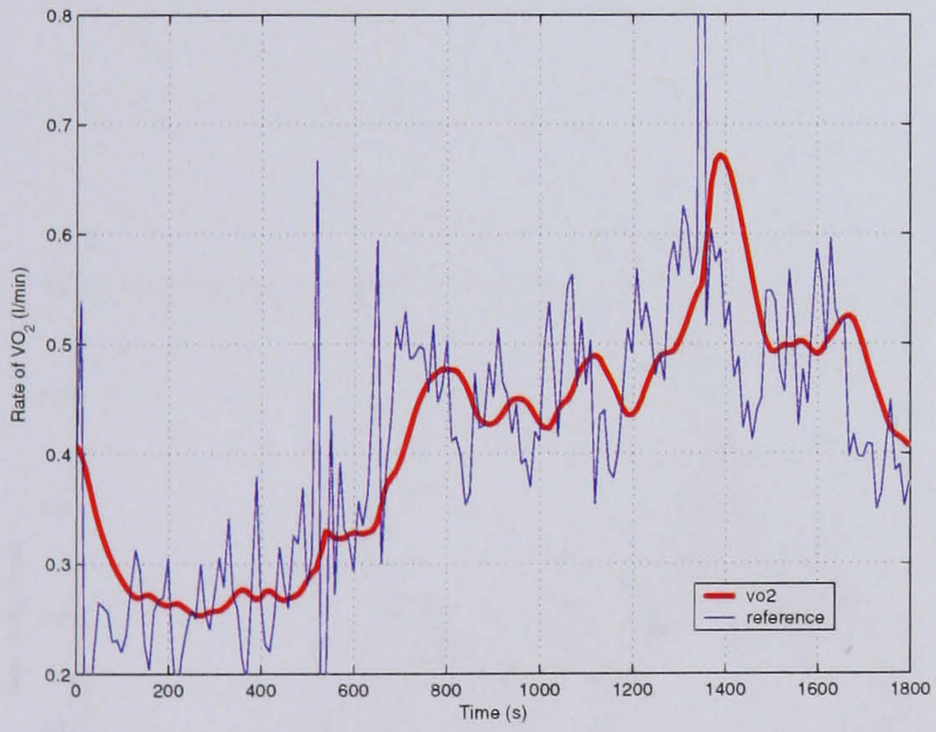

(a) $\dot{V}O_2$

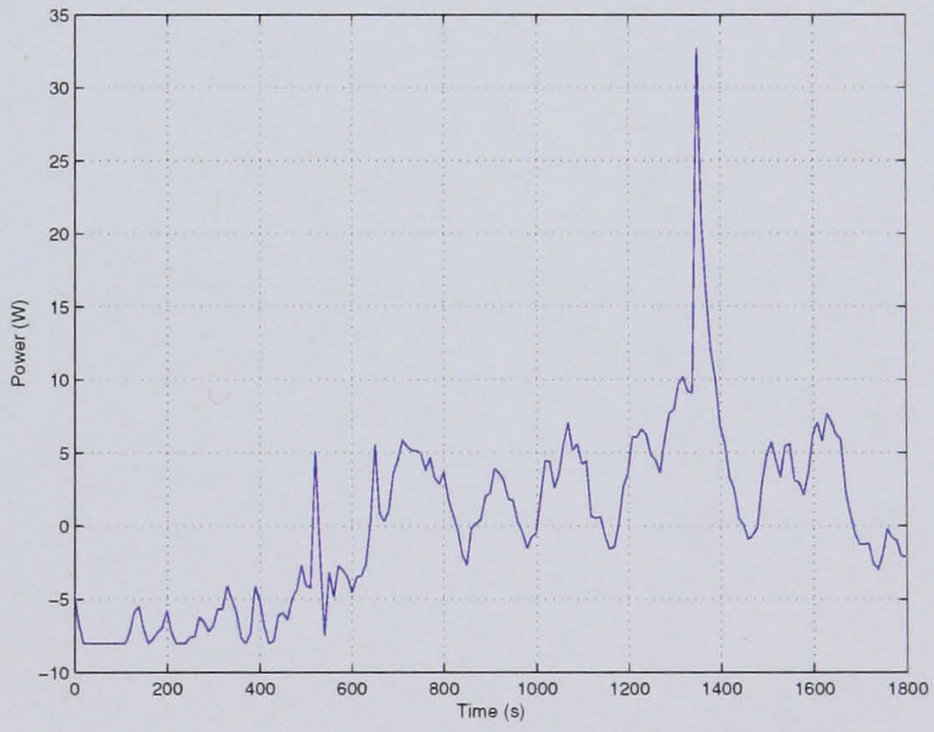

(b) $\dot{V}O_2$ Controller Output - power controller reference

Figure 5.21: Data set 2, with Controller 2.

The $\dot{V}O_2$ reference is noisy, but once averaged, the output $\dot{V}O_2$ from the simulation is more fluent. This indicates that the controller is filtering the noisy $\dot{V}O_2$ data. A small delay can also be seen between the reference and the output $\dot{V}O_2$, due to this averaging. The power reference can be subjectively compared to the input power PRBS.

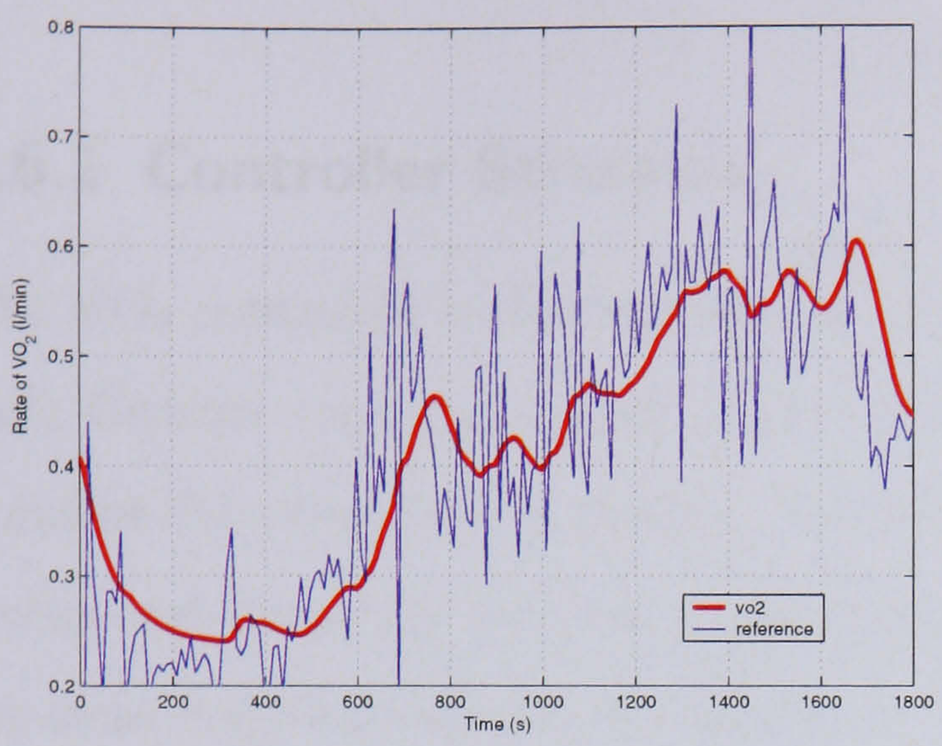

(a) $\dot{V}O_2$

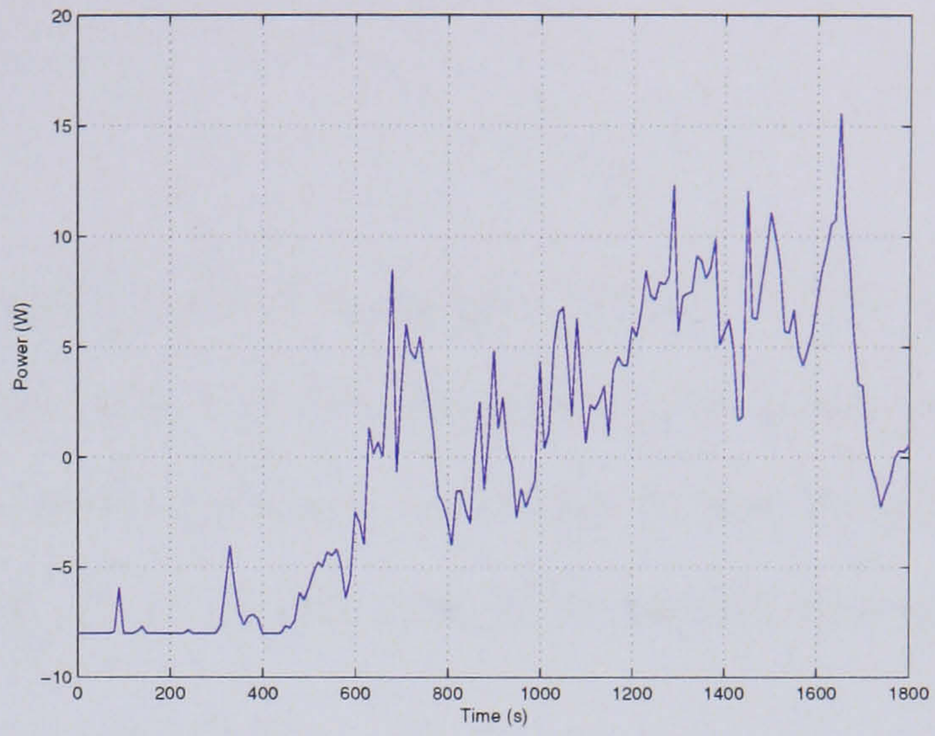

(b) $\dot{V}O_2$ Controller Output - power controller reference

Figure 5.22: Data set 1, with Controller 2.

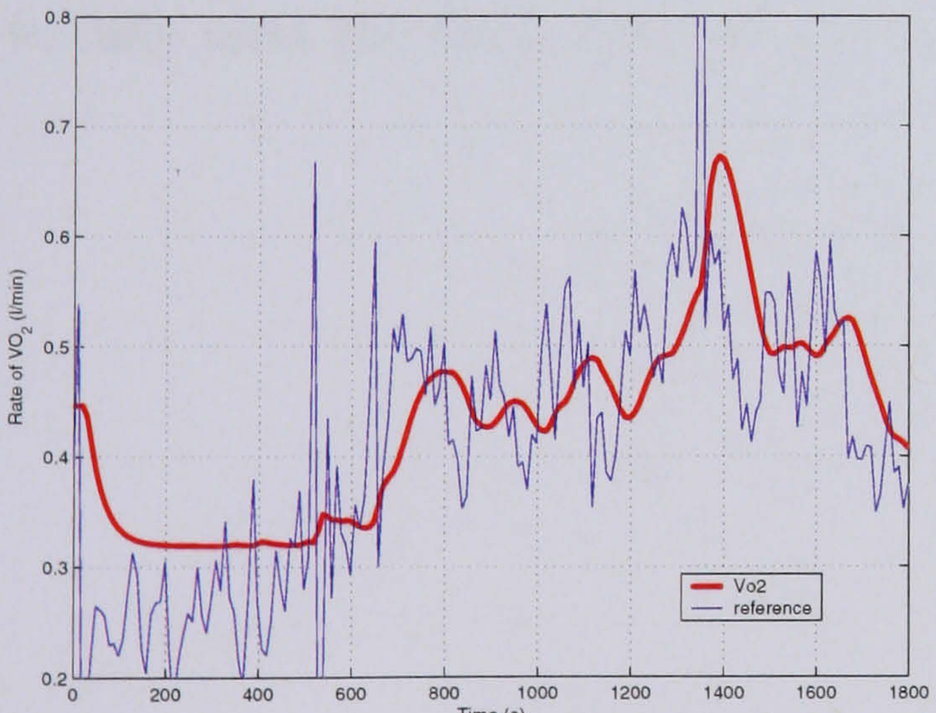

(a) $\dot{V}O_2$

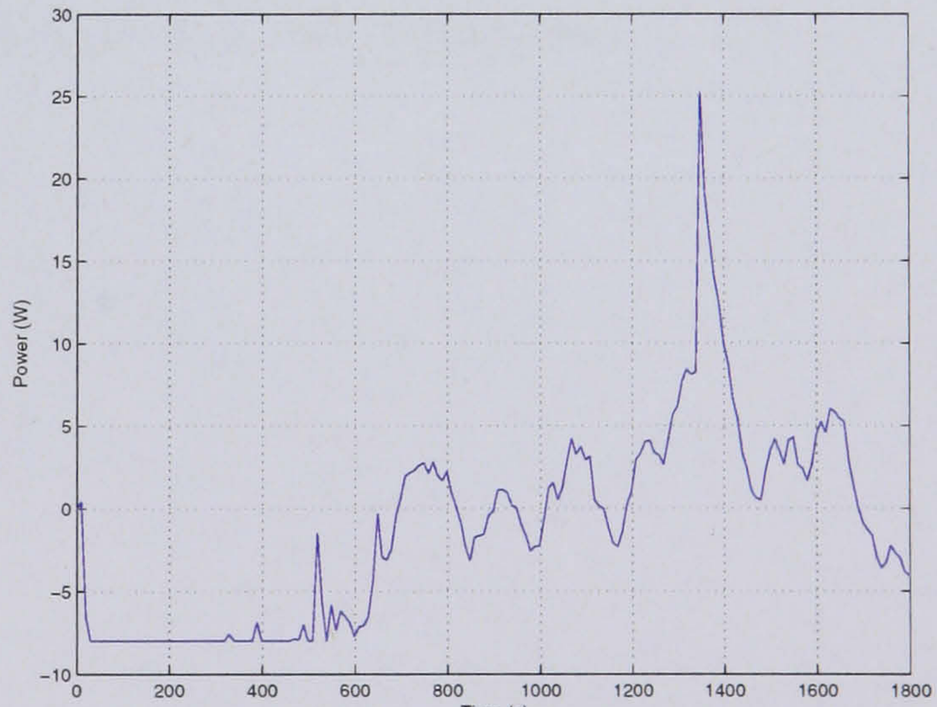

(b) $\dot{V}O_2$ Controller Output - power controller reference

Figure 5.23: Data set 2, with Controller 1.

All 4 power plots tend to roughly follow the overall shape of the PRBS (see Figure 5.22(b)), however they do not accurately reach the magnitudes of the PRBS ($0-10\,W$).

5.6.1 Controller Structure

The $\dot{V}O_2$ controller is implemented in a cascade control structure (Figure 5.24). Cascade Control uses the output of the primary controller to manipulate the operating point of the secondary controller. In this case the primary controller is the $\dot{V}O_2$ controller and the power controller, the secondary. For cascade control to be effective there are some requirements on the system :

- Secondary loop dynamics must be faster than the primary loop dynamics,
- Secondary loop must have influence over the primary loop,
- Secondary loop must be measurable and controllable.

All three of these conditions have been met. The $\dot{V}O_2$ dynamics have been shown to be considerably slower than those of the power controller. The identifications have also shown that the $\dot{V}O_2$ is both measurable and influenced by changes in power. The aim is to fully meet the third condition, to show that $\dot{V}O_2$ is controllable.

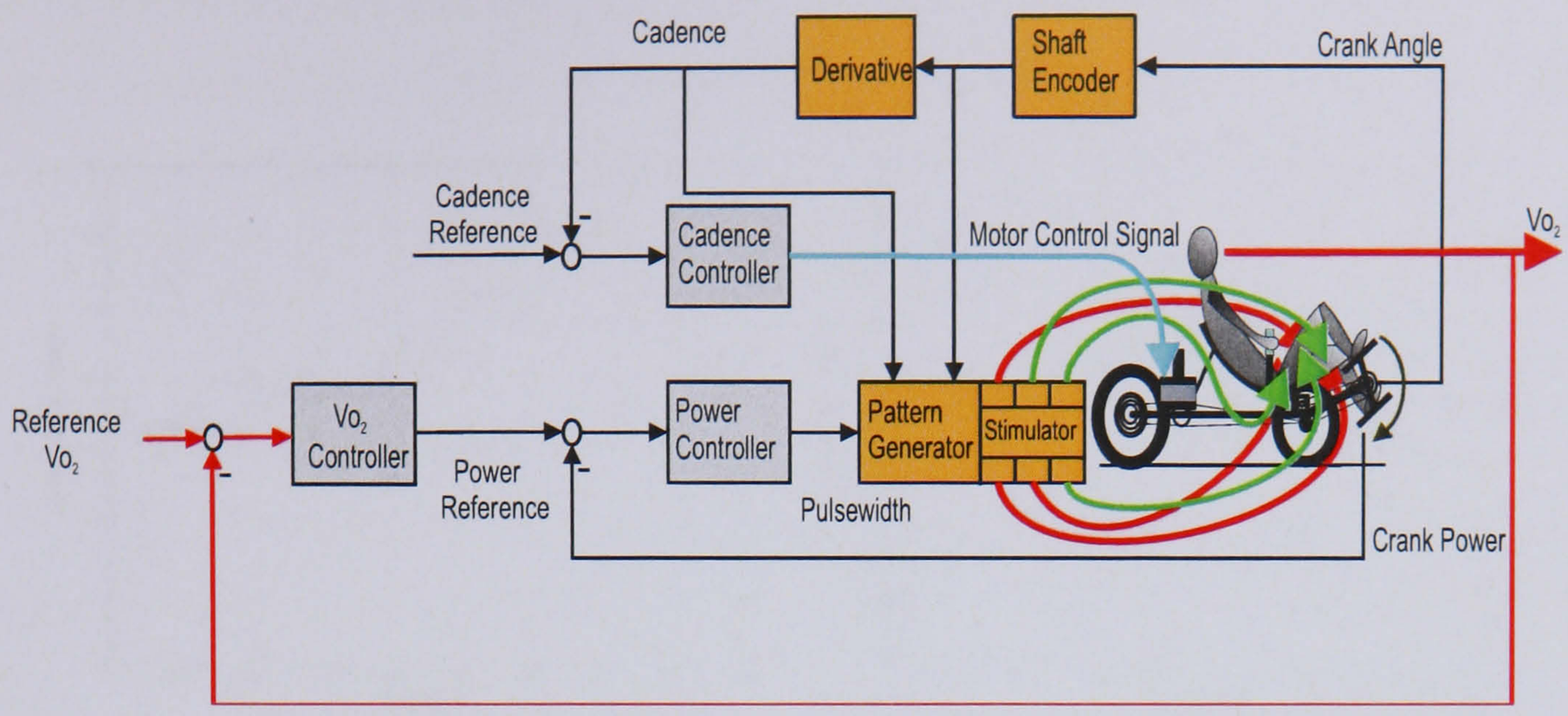

Figure 5.24: Integrated closed-loop control structure. One loop automatically adjusts the motor input to keep the cycling cadence close to a reference. The second loop automatically adjusts the stimulation pulsewidth to keep the leg power close to the reference set by the output of the $\dot{V}O_2$ controller. The $\dot{V}O_2$ controller is implemented in a cascade structure.

5.7 $\dot{V}O_2$ Simulation Tests

Simulation is used to investigate how the $\dot{V}O_2$ controller responds during FES cycling, before it is applied to a paraplegic subject. During these tests, no stimulation is applied, instead dummy loads are fitted to the stimulator. The dummy loads are simply 3 LED's, which illuminate when a stimulation pulse is applied. The simulated subject is asked to follow the reference power, while the motor controller holds the cadence at 50 rpm. The power reference is the output of the $\dot{V}O_2$ controller. Step changes in the $\dot{V}O_2$ are made by the investigator once the reference $\dot{V}O_2$ is achieved.

5.7.1 Simulation Test 1 - Results

Simulation requires following a power reference while cycling at 50rpm. The controller used in this test is Controller 1 and the $\dot{V}O_2$ reference increments in this test are $0.4 \rightarrow 0.6 \rightarrow 0.4$ l/min. The results are shown in Figure 5.25.

Figure 5.25(a) shows the $\dot{V}O_2$ response. The resting $\dot{V}O_2$ is in the region of 0.33 l/min,

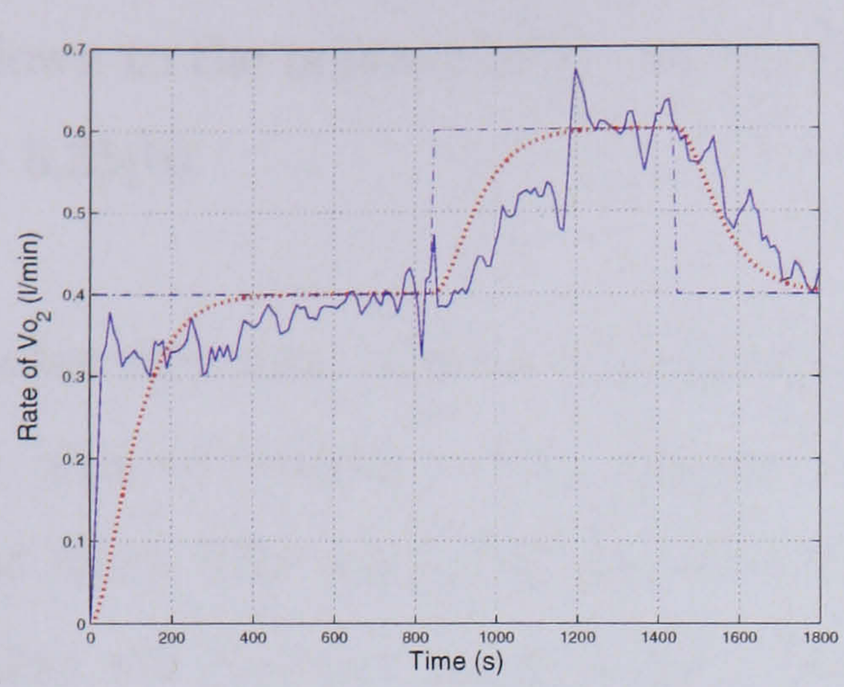

(a)

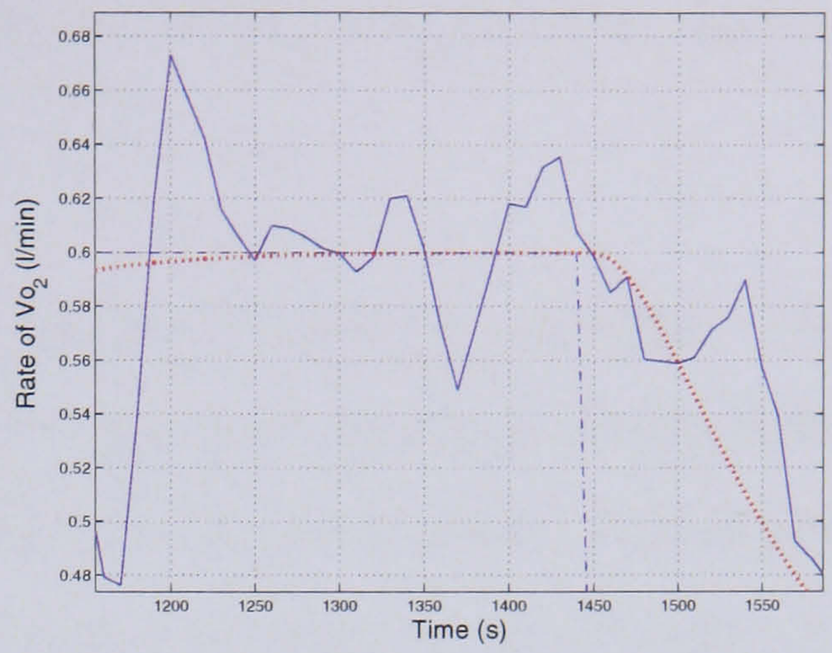

(b)

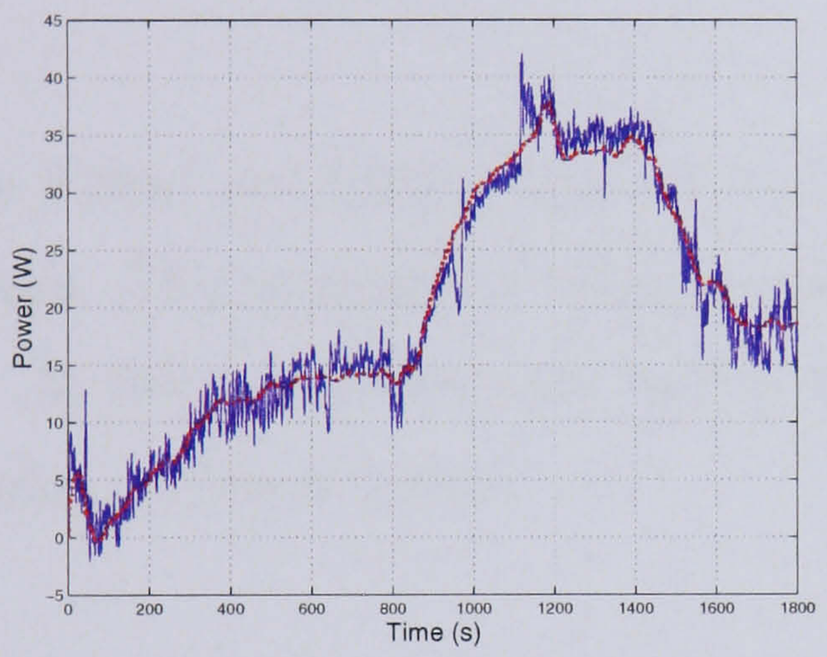

(c)

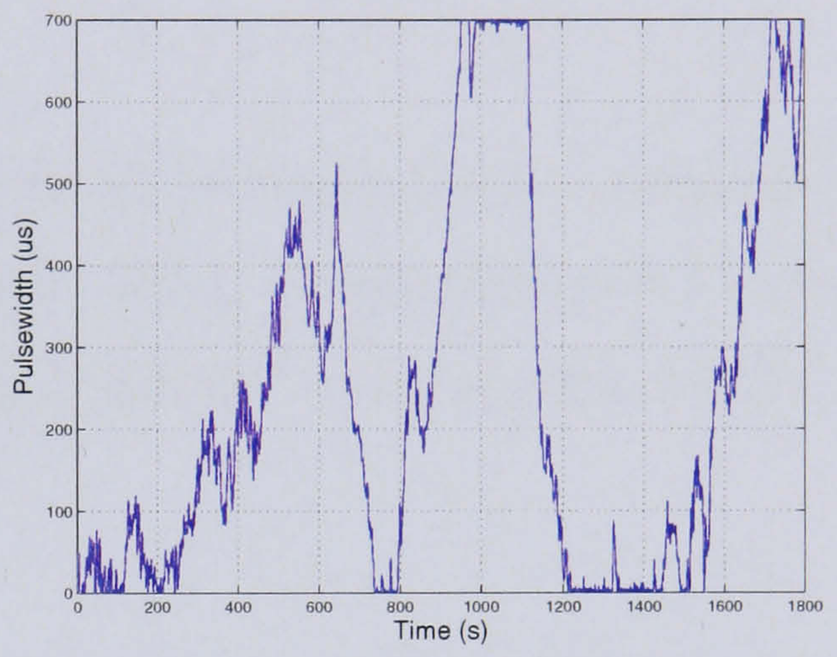

(d)

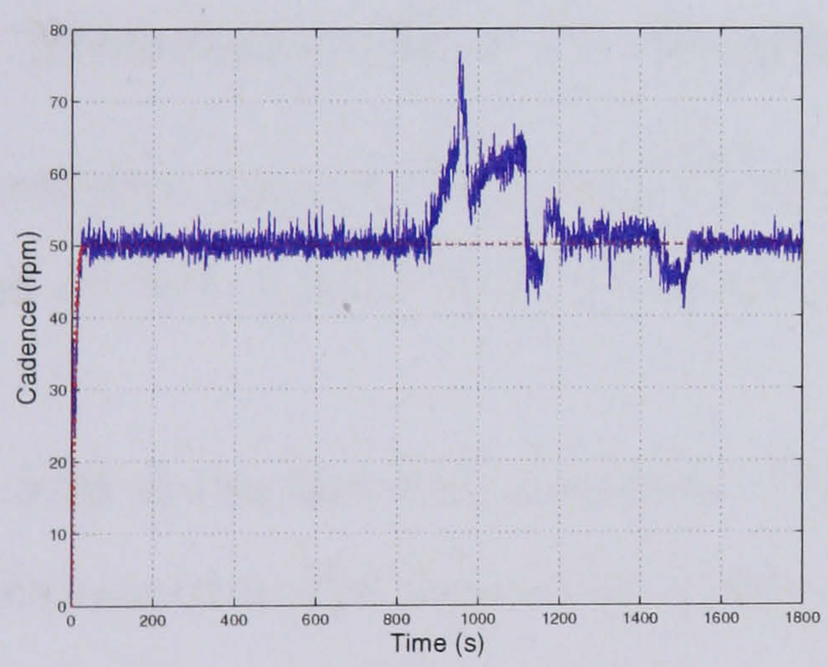

(e)

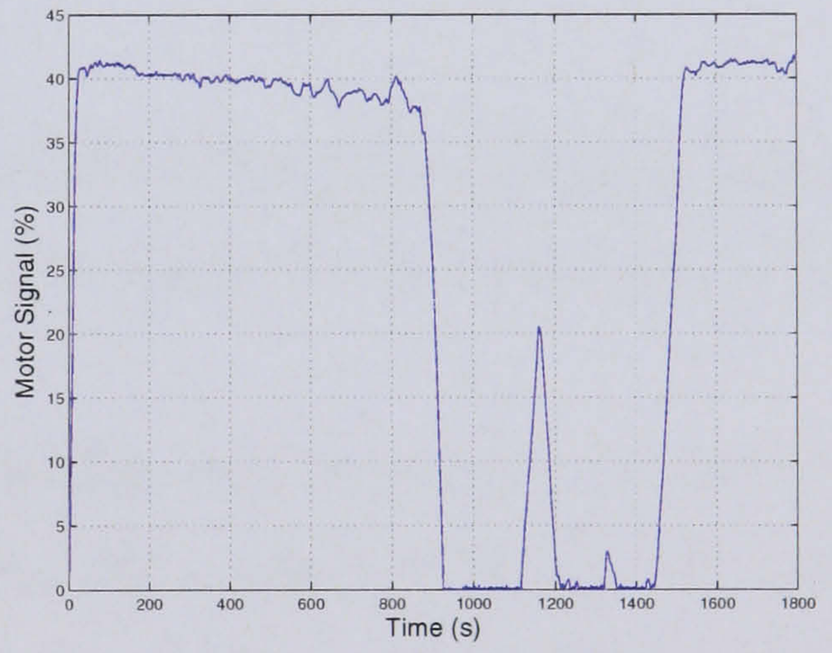

(f)

Figure 5.25: Simulation Test 1: In all graphs the reference is the dashed line, the measured data the solid line and the ideal response the dotted line. The figures show, (a) the $\dot{V}O_2$ controller response, (b) a magnified section of the $\dot{V}O_2$ response, (c) the power controller response, (d) the resulting stimulation from the power controller, (e) the motor controller response and (f) the motor input signal.

and is increased to the desired 0.4 l/min after 800 s (Figure 5.25(a)). The reference is then increased to 0.6 l/min, which is a achieved at 1200 s, thereafter it is stepped back down to the original level. A zoomed section of the $\dot{V}O_2$ response can be seen in Figure 5.25(b).

The power reference (Figure 5.25(c)) is the output of the $\dot{V}O_2$ controller. The power can be seen to respond to the changes in $\dot{V}O_2$, and to achieve a steady state power for that level. The simulated stimulation response (Figure 5.25(d)) indicates that the controller will increase/decrease the stimulation depending on the changes in desired power.

Figures 5.25(e) and 5.25(f) show the response of the motor, with a reference cadence of 50 rpm. This is exceeded at approximately 850 s, corresponding to an increase in power. At this point the motor control signal falls off to compensate for the increase in cadence, in Figure 5.25(f).

5.7.2 Simulation Test 2 - Results

The controller used in this test is Controller 2 and the $\dot{V}O_2$ reference increments in this test are $0.4 \rightarrow 0.6 \rightarrow 0.8 \rightarrow 0.5$ l/min. The results are shown in Figure 5.26.

Figure 5.26 shows the $\dot{V}O_2$ response. The resting $\dot{V}O_2$ is in the region of 0.35 l/min, and is increased to the desired 0.6 l/min after 700 s (Figure 5.26(a)). The reference is then increased to 0.8 l/min, which is a achieved at 1100 s. Thereafter the reference is stepped down to the 0.5 l/min. A zoomed section of the $\dot{V}O_2$ response can be seen in Figure 5.26(b).

Figure 5.26(c) shows the power controller response. The power reference (Figure 5.26(c)) is the output of the $\dot{V}O_2$ controller. The power can be seen to respond to the changes in the $\dot{V}O_2$, and to achieve a mean steady state power for that level. The stimulation response (Figure 5.26(d)) indicates that the power is below the desired

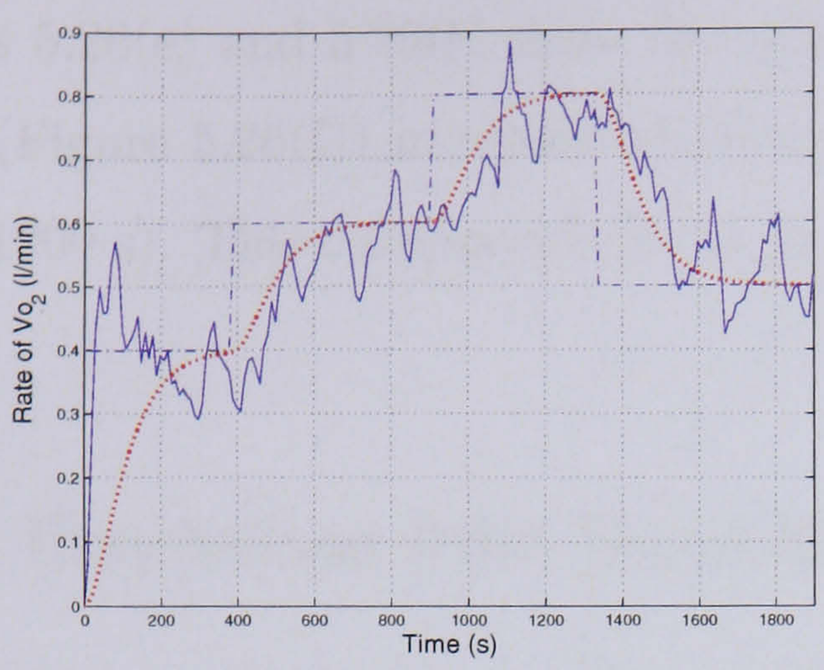

(a)

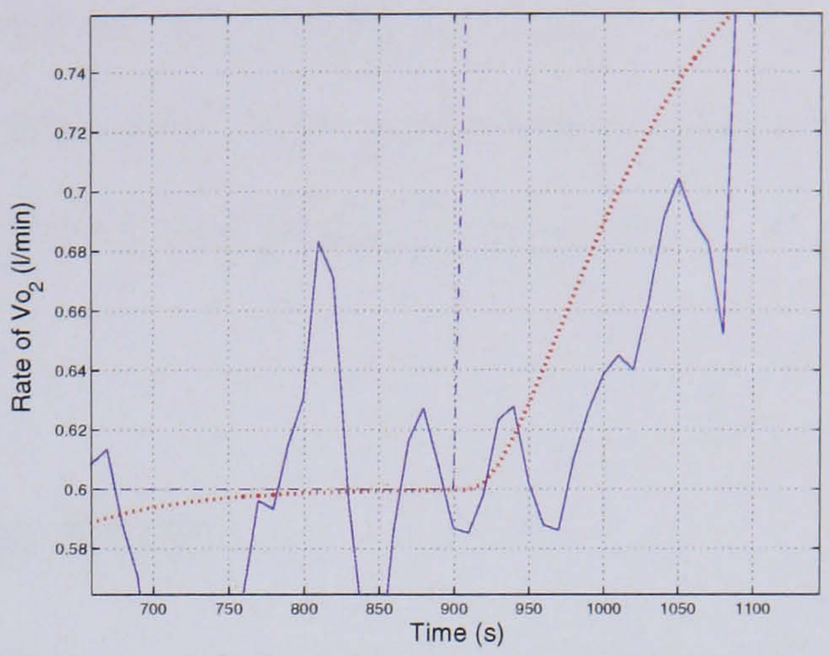

(b)

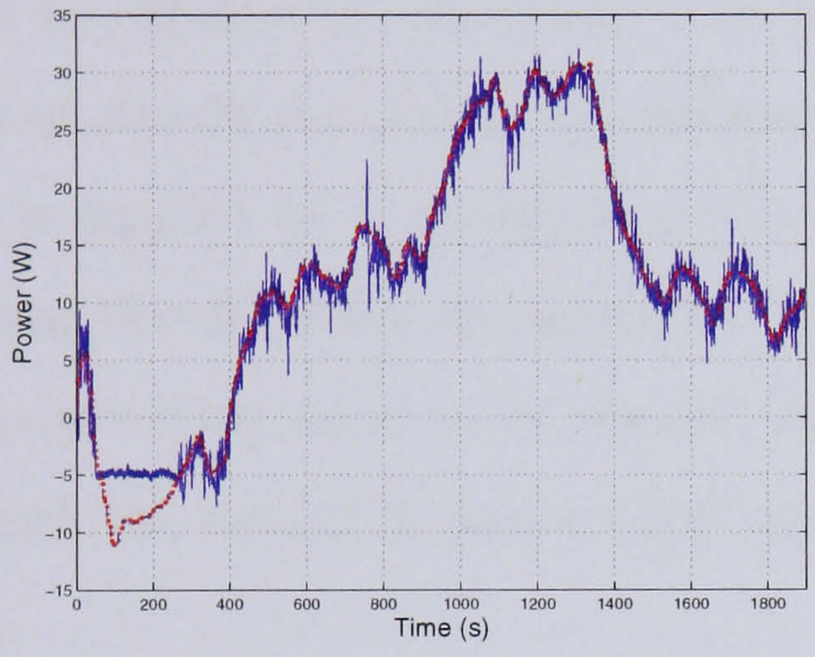

(c)

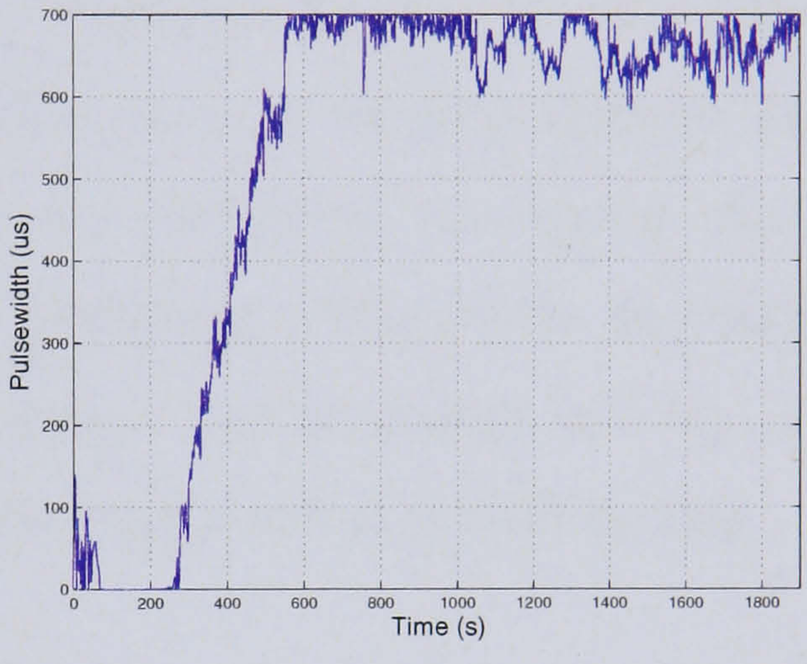

(d)

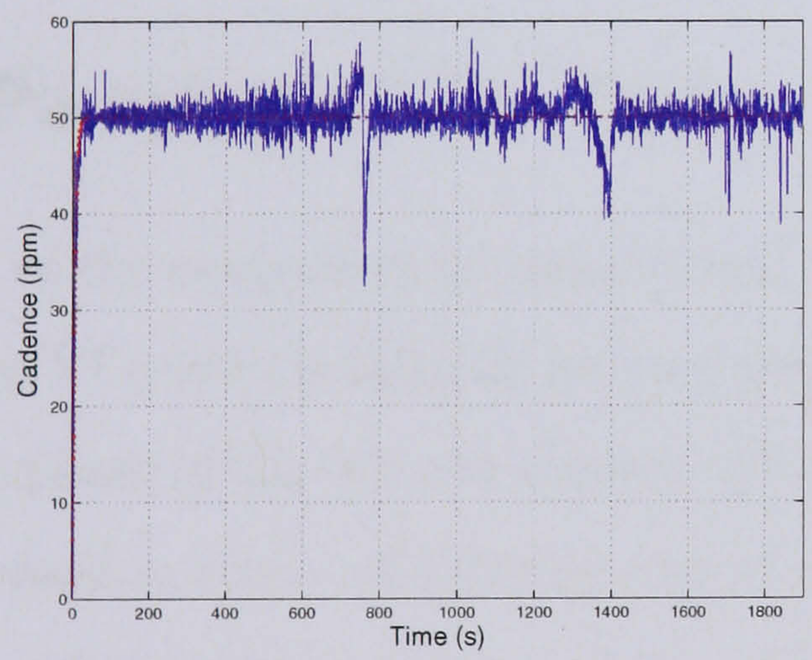

(e)

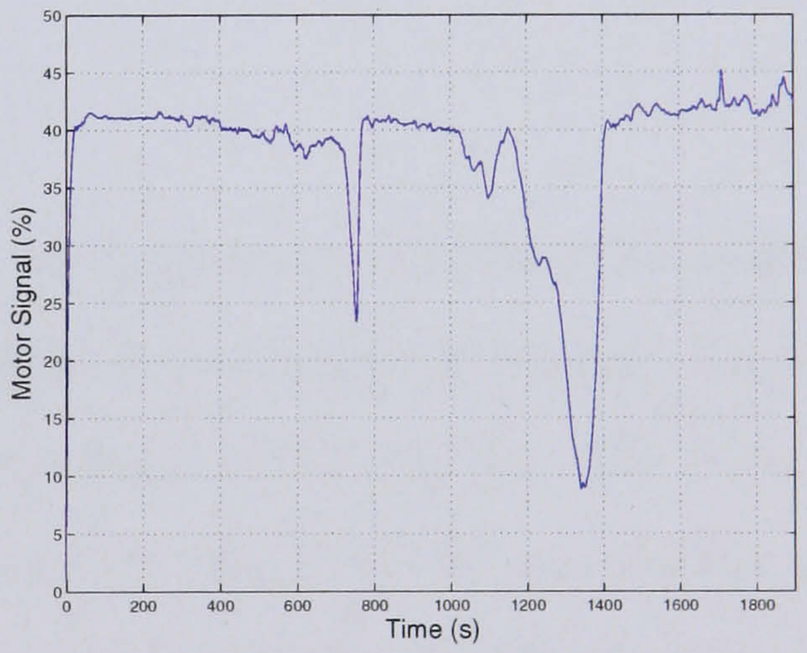

(f)

Figure 5.26: Simulation Test 2: In all graphs the reference is the dashed line, the measured data the solid line and the ideal response the dotted line. The figures show, (a) the $\dot{V}O_2$ controller response, (b) a magnified section of the $\dot{V}O_2$ response, (c) the power controller response, (d) the resulting stimulation from the power controller, (e) the motor controller response and (f) the motor input signal.

power, for the majority of the test, hence the stimulation increases to saturation.

Figures 5.26(e) and 5.26(f) show the response of the motor controller. When the cadence (Figure 5.26(f)) increases above the reference, the motor input can be seen to drop (1000 s). This corresponds to an increase in the power produced.

5.7.3 Conclusions from Simulation Tests

These two tests imply that the three controllers operate correctly together, all responding well to changes in reference. The $\dot{V}O_2$ controller appears to be robust against changes in simulation conditions, however this can only be fully assessed when stimulation is applied on a paraplegic subject. An interesting observation can be made concerning the difference in simulation and paraplegic's $\dot{V}O_2$ levels. In simulation far higher power levels have to be reached to produce a small change in $\dot{V}O_2$. This highlights both the restricted power range and the inefficiencies of FES cycling.

5.8 Paraplegic $\dot{V}O_2$ Tests

Testing of the controllers is implemented on the apparatus described in section 3. The reference $\dot{V}O_2$ level is initially set to a level that is below that of resting. Therefore, for the first phase of the test the subject will cycle without stimulation. The $\dot{V}O_2$ will then be increased in steps, of differing increments. This will show the controllers' ability to react to reference change. One of the additional aims of these initial tests is to identify the level of $\dot{V}O_2$ that is achievable during a test, and how this differs across test days.

For all $\dot{V}O_2$ tests it is desired that the $\dot{V}O_2$ will track within 10 % of the reference level after the initial transient, due to the step in reference. This will be referred to as the steady state.

5.8.1 Test 1

The controller used in this test is Controller 2 and the $\dot{V}O_2$ reference increments in this test are $0.2 \rightarrow 0.3 \rightarrow 0.7 \rightarrow 0.9 \rightarrow 0.3$ l/min. The results are shown in Figure 5.27.

During the first $\dot{V}O_2$ reference level (Figure 5.27(a)), the $\dot{V}O_2$ measured is when the legs are rotated by the motor only. The power decreases to the minimum saturation of the controller, -15 W (Figure 5.27(c)). The reference is then increased to a level slightly above the zero stimulation level of $\dot{V}O_2$. This results in the power increasing and the muscles being stimulated at a low level (Figure 5.27(d)).

Once the $\dot{V}O_2$ stabilises at approximately 0.45 l/min, the reference is changed to 0.5 l/min, resulting in a small increase in power reference and a coinciding increase in the stimulation level. At 1000 s the reference is increased to 0.7 l/min. The $\dot{V}O_2$ is seen to oscillate around the reference level, as shown in Figure 5.27(b). The magnitude of the oscillation begins to reduce, but a steady state is not achieved. The final increase in VO_2 is to 0.9 l/min, where a similar oscillation is again seen, before the reference is reduced to 0.5 l/min. The stimulation (Figure 5.27(d)) throughout the duration of the test remains relatively low (below 250 μs). This indicates that the subject is not close to fatigue.

The results from the motor control loop can be seen in Figures 5.27(e) and 5.27(f). The reference cadence, 50 rpm, is controlled well until the end of the test. After approximately 1000 s the motor control signal increases to its upper saturation level but the cadence is not effected.

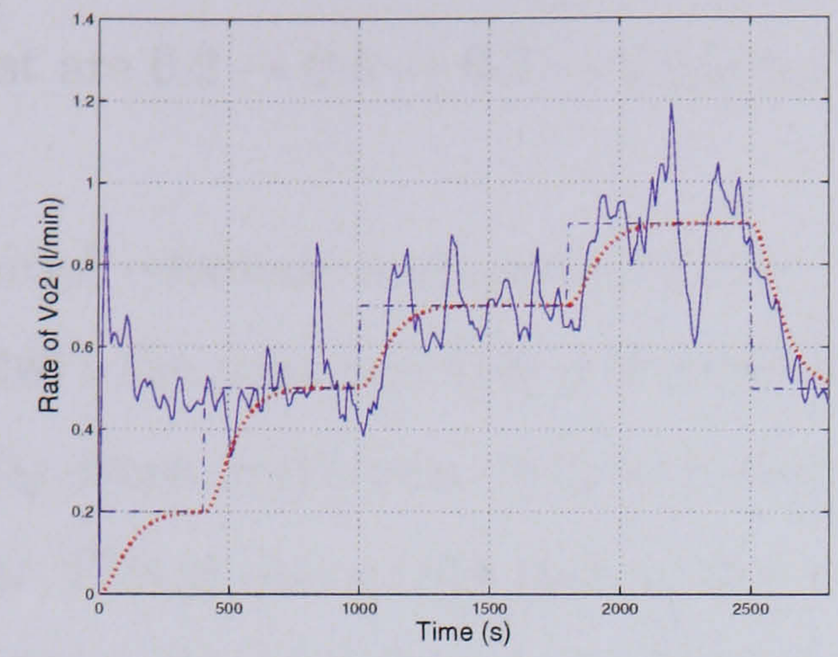

(a)

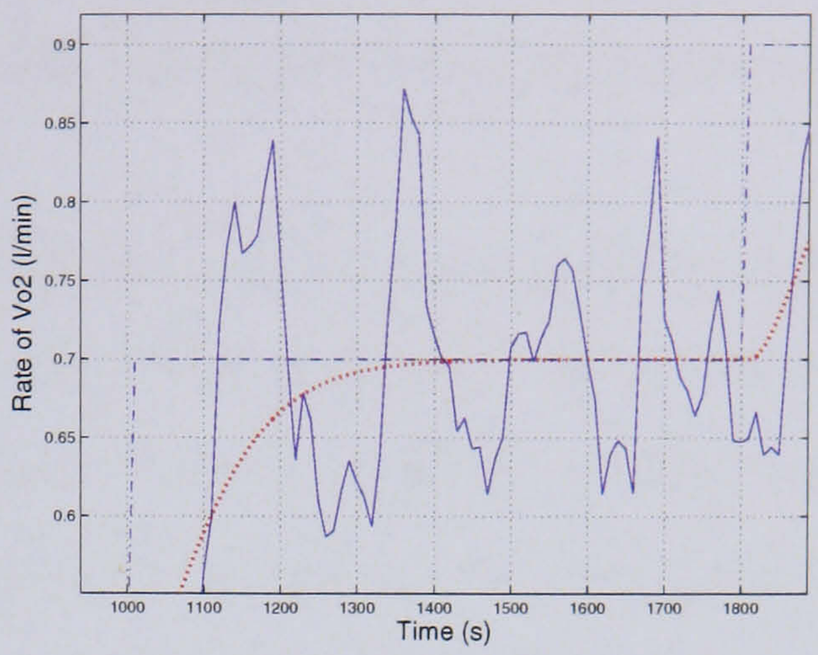

(b)

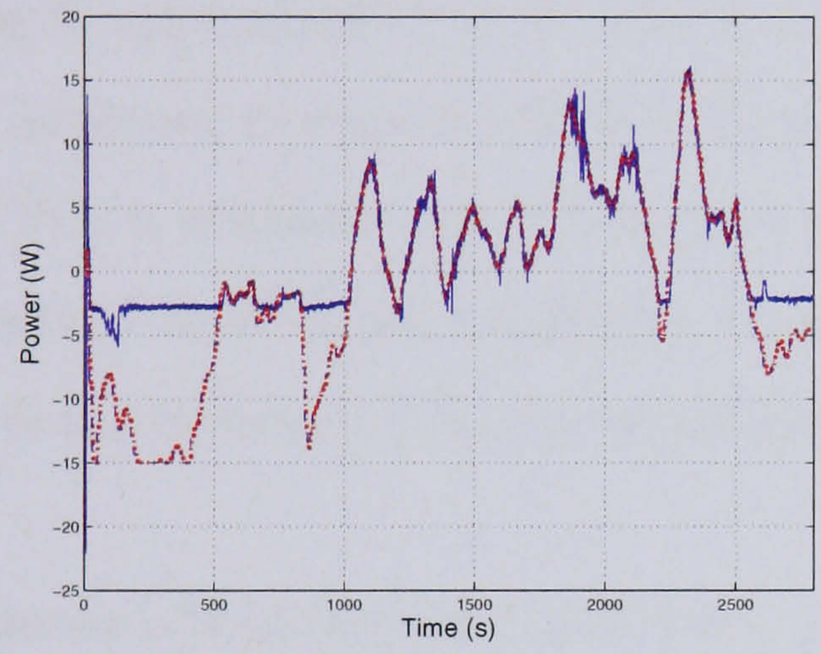

(c)

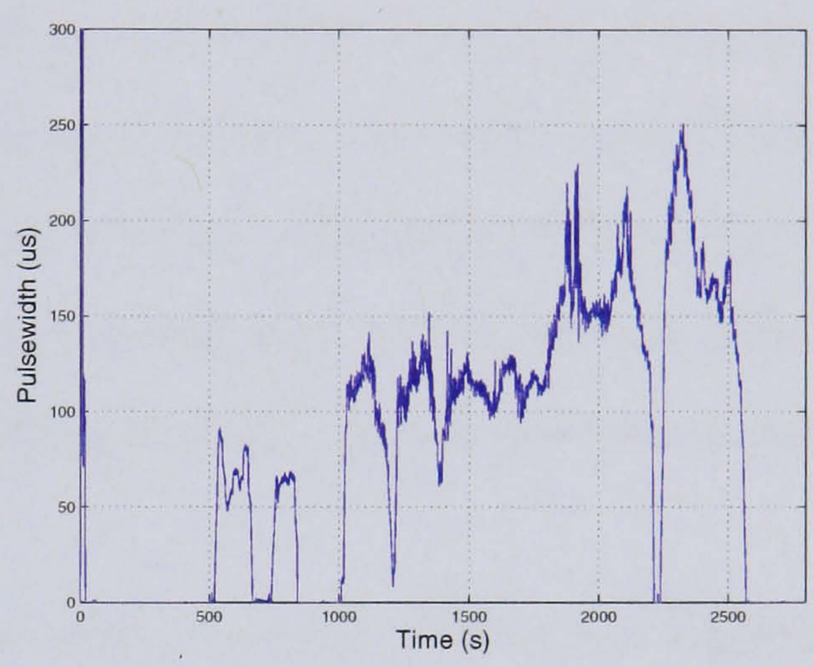

(d)

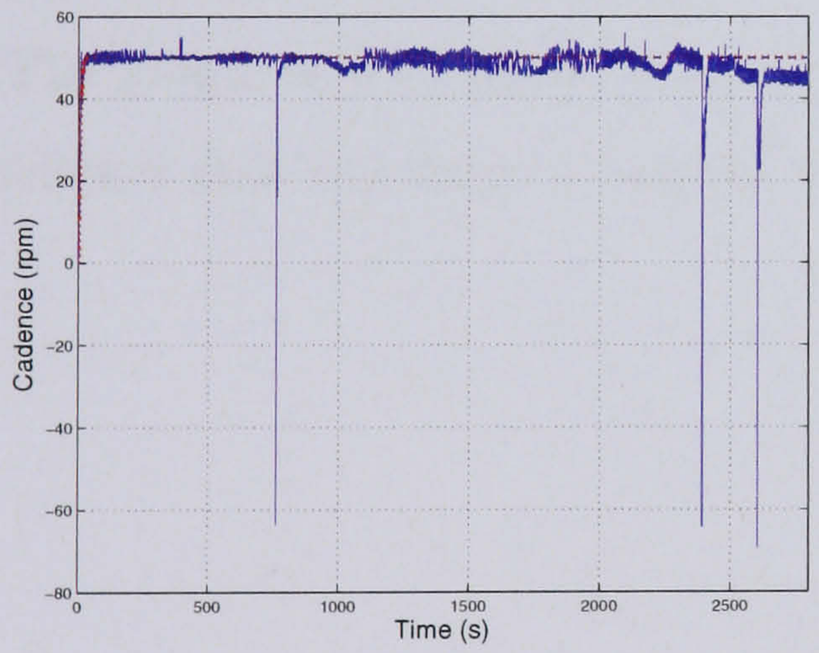

(e)

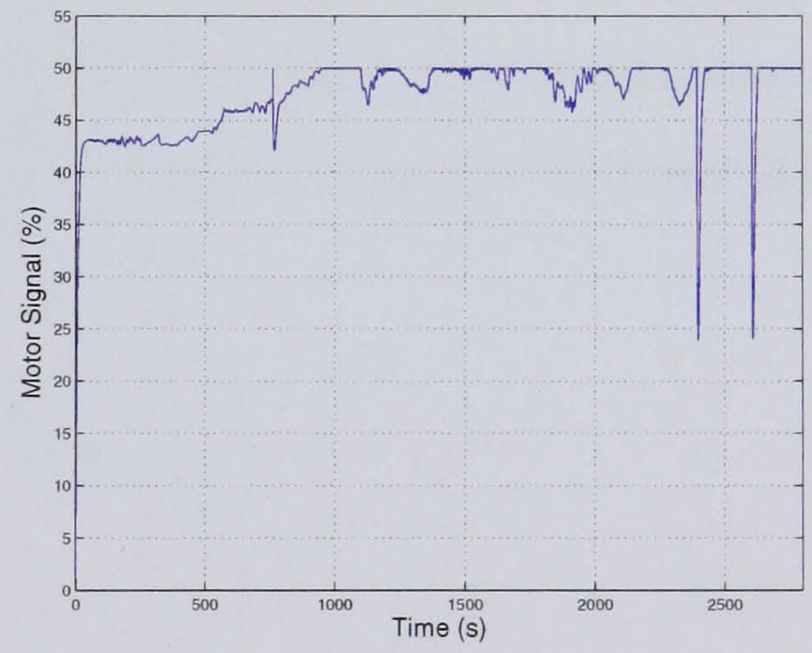

(f)

Figure 5.27: $\dot{V}O_2$ Test 1 : In all graphs the reference is the dashed line, the measured data the solid line and the ideal response the dotted line. The figures show : (a) the $\dot{V}O_2$ controller response, (b) a magnified section of the $\dot{V}O_2$ response, (c) the power controller response, (d) the resulting stimulation from the power controller, (e) the motor controller response and (f) the motor input signal.

5.8.2 Test 2

The controller used in this test is Controller 2 and the $\dot{V}O_2$ reference increments in this test are $0.2 \rightarrow 0.5 \rightarrow 0.7 \rightarrow 0.5$ l/min. The results are shown in Figure 5.28.

The initial reference is set to 0.2 l/min, below the zero stimulation level of the $\dot{V}O_2$. After 420 s the reference $\dot{V}O_2$ is increased to 0.5 l/min, in Figure 5.28(a). At this point the $\dot{V}O_2$ drops to 0 l/min, with a corresponding increase in power, at 500 s, in Figure 5.28(c). This is due to the sample line in the Metamax disconnecting from the face-mask. Once this is replaced, the $\dot{V}O_2$ increases and the power reference responds by reducing to approximately 3 W. The $\dot{V}O_2$ varies between 0.7 and 0.4 l/min at this reference, as shown in Figure 5.28(b). The reference is then increased to 0.7 l/min. This level of $\dot{V}O_2$ is achieved, but at the expense of reaching maximum stimulation (700 μs), at a power of 13 W (Figure 5.28(c)). To avoid the subject cycling at this high stimulation level the reference $\dot{V}O_2$ is stepped down to 0.5 l/min, before the test is terminated.

The cadence is held constant at 50 rpm, until approximately 1700 s, see Figure 5.28(e). The cadence drops below the reference, resulting in an increase in the motor control signal. The motor control signal (Figure 5.28(f)) increases until it saturates at 65%. It is concluded that the drop in cadence is due to a loss in power from the batteries.

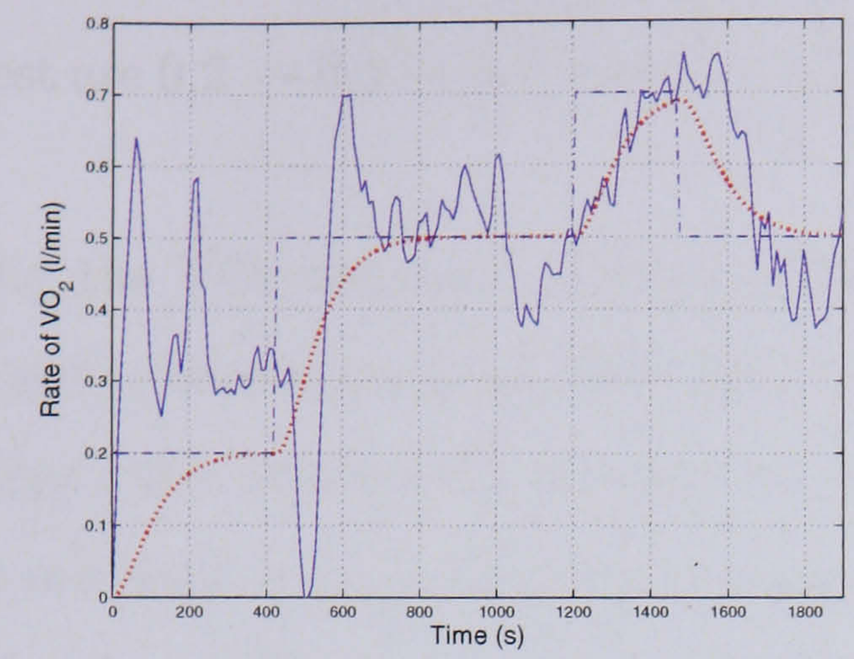

(a)

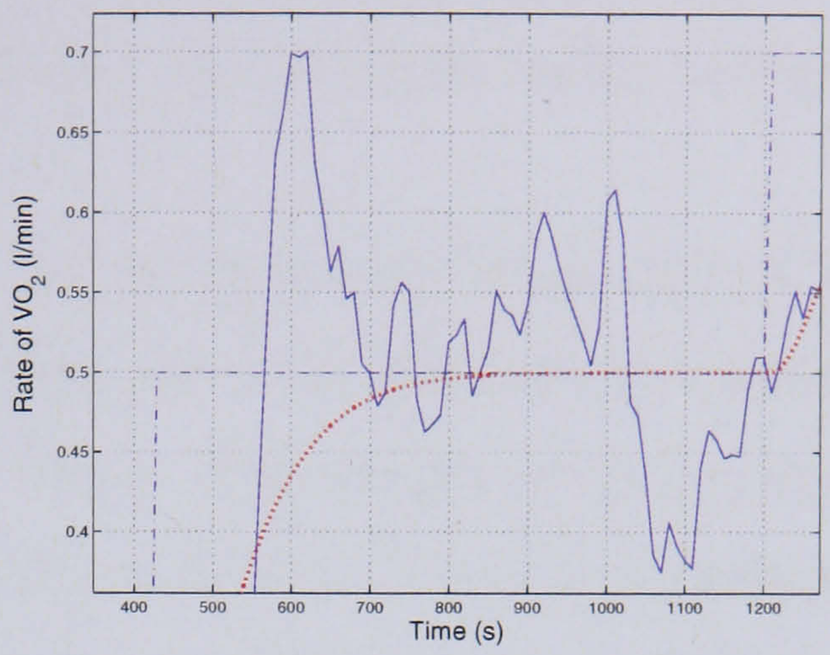

(b)

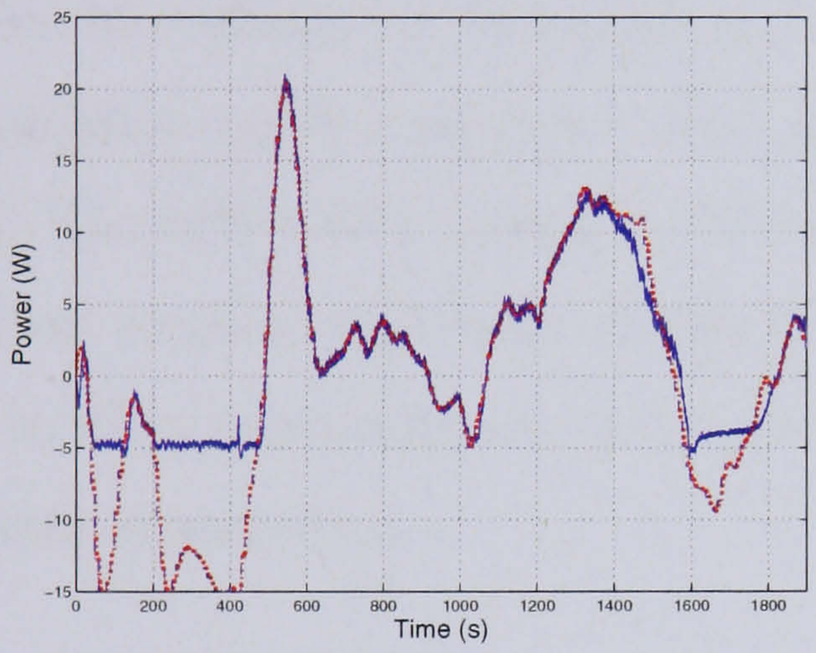

(c)

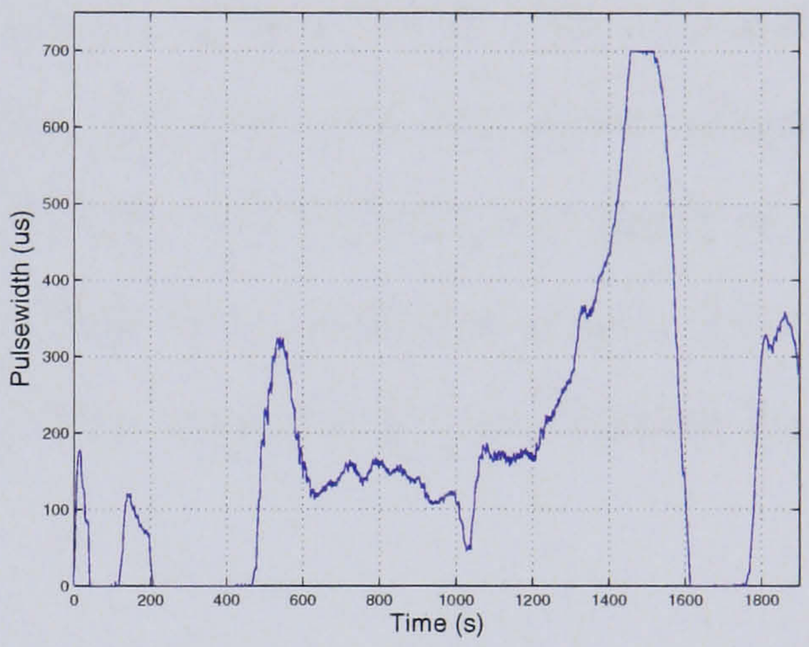

(d)

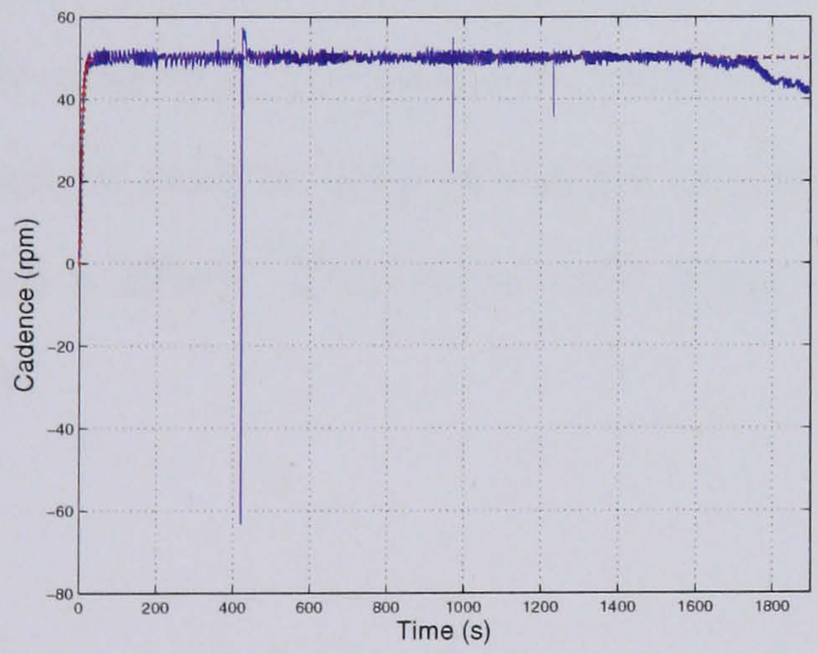

(e)

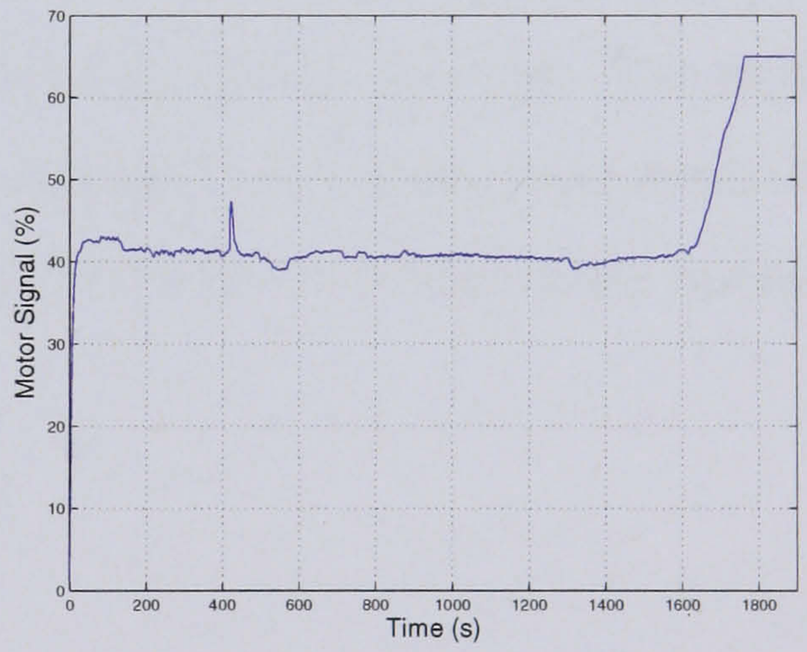

(f)

Figure 5.28: $\dot{V}O_2$ Test 2 : In all graphs the reference is the dashed line, the measured data the solid line and the ideal response the dotted line. The figures show : (a) the $\dot{V}O_2$ controller response, (b) a magnified section of the $\dot{V}O_2$ response, (c) the power controller response, (d) the resulting stimulation from the power controller, (e) the motor controller response and (f) the motor input signal.

5.8.3 Test 3

The controller used in this test is Controller 1 and the $\dot{V}O_2$ reference increments in this test are $0.2 \rightarrow 0.5 \rightarrow 0.7 \rightarrow 0.5 \rightarrow 0.2$ l/min . The results are shown in Figure 5.29.

Initially the $\dot{V}O_2$ reference (Figure 5.29(a)) is set to a level below that of the subject's zero stimulation level (0.3 l/min). When the $\dot{V}O_2$ stabilises at approximately 0.3 l/min, the reference is changed to 0.5 l/min. This results in an increase in the power reference and a coinciding increase in stimulation level, shown in Figures 5.29(c) 5.29(d). The $\dot{V}O_2$, and consequently the power, oscillate around the reference level. At 1200 s the reference is increased to 0.7 l/min. This level of $\dot{V}O_2$ is achieved, but the stimulation reaches saturation, the subject fatigues and the power drops (Figure 5.29(c)). The reference $\dot{V}O_2$ is then decreased back to 0.5 l/min, but again at this level the subject receives maximum stimulation. The $\dot{V}O_2$ oscillates about the reference, similar to when previously set to 0.5 l/min. The reference is then further lowered for zero stimulation cycling.

The results from the motor control loop can be seen in Figures 5.29(e) and 5.29(f). The reference cadence, (50 rpm) is controlled well throughout the test. The motor input signal can be seen to drop when the cyclist is pedalling at a high power level, illustrated in Figure 5.29(e). This is an indication that the three controllers are operating well together.

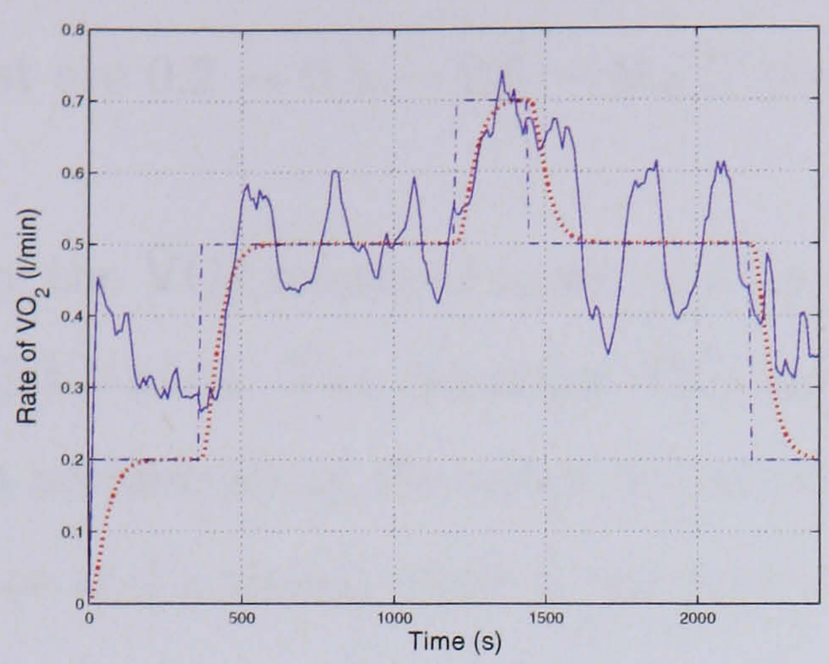

(a)

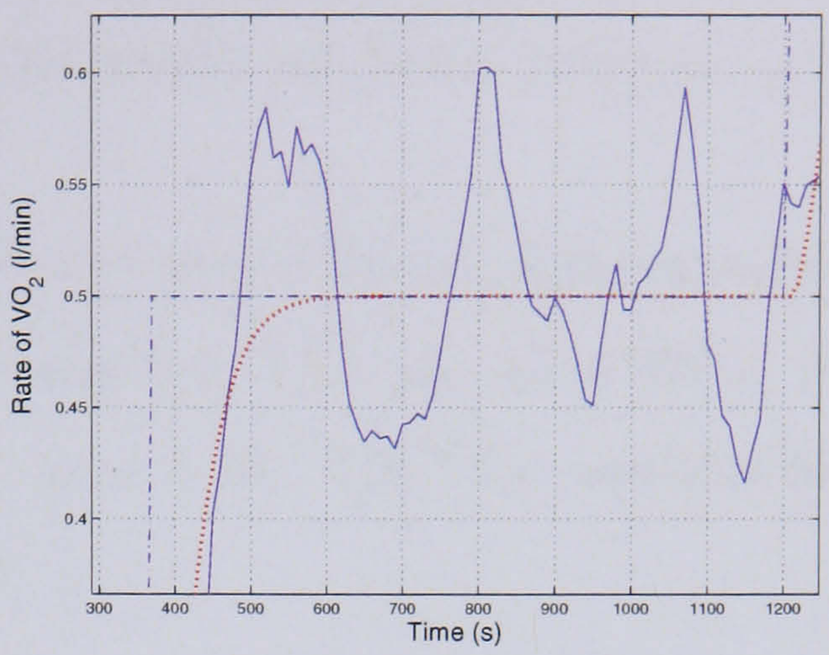

(b)

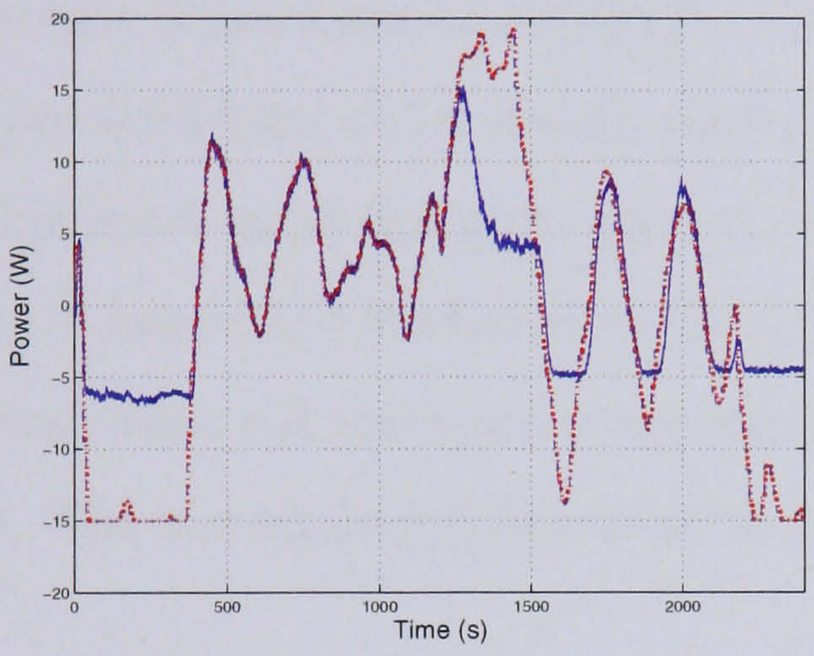

(c)

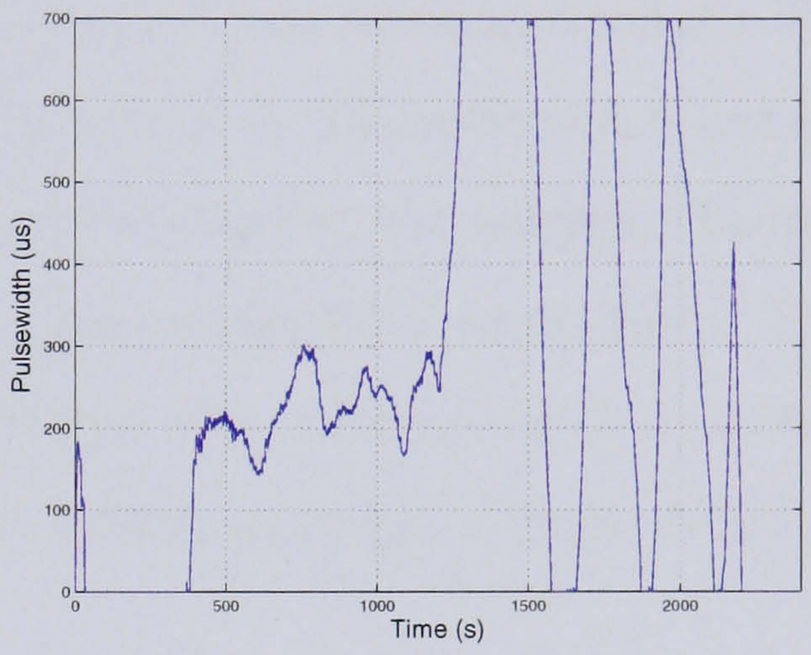

(d)

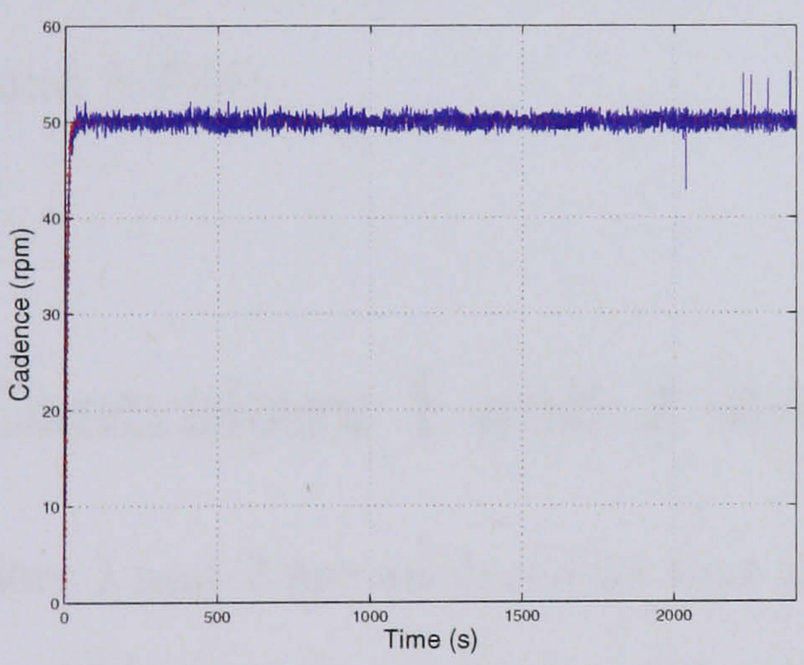

(e)

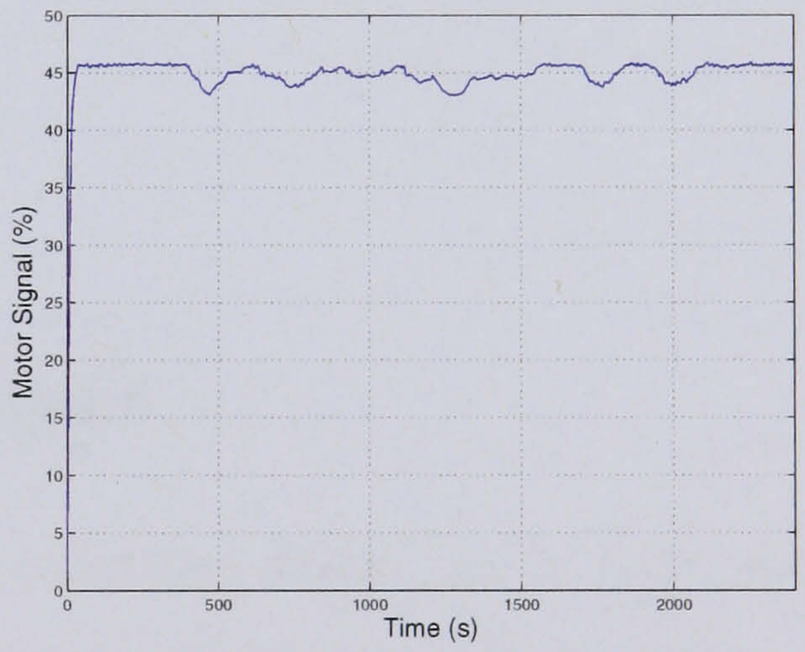

(f)

Figure 5.29: $\dot{V}O_2$ Test 3 : In all graphs the reference is the dashed line, the measured data the solid line and the ideal response the dotted line. The figures show : (a) the $\dot{V}O_2$ controller response, (b) a magnified section of the $\dot{V}O_2$ response, (c) the power controller response, (d) the resulting stimulation from the power controller, (e) the motor controller response and (f) the motor input signal.

5.8.4 Test 4

The controller used in this test is Controller 1 and the $\dot{V}O_2$ reference increments in this test are $0.2 \rightarrow 0.5 \rightarrow 0.6 \rightarrow 0.2$ l/min.The results are shown in Figure 5.30(a).

Initially the $\dot{V}O_2$ reference is set to a level below that of the subjects zero stimulation level (0.3 l/min). The reference $\dot{V}O_2$ is increased to 0.5 l/min after 360 s, which results in an increase in the power reference (Figure 5.30). The $\dot{V}O_2$ oscillates about the reference and a steady state is not achieved.

The reference is increased to 0.6 l/min. As at the previous reference level the $\dot{V}O_2$ oscillates about 0.6 l/min and a steady state is not achieved. The reference is not increased above this level, as in the previous test, to avoid fatiguing the subject. Therefore the reference is reduced to 0.2 l/min to allow for a zero stimulation warm down. The power in this test does not maintain a constant level at any reference level of $\dot{V}O_2$ (Figure 5.30(c)). The corresponding stimulation plot, 5.30(d) oscillates in relation to the power.

As with the previous tests, the cadence is controlled to its reference level in Figures 5.30(e) and 5.30(f).

5.9 Controllers 1 and 2 Analysis

Controllers 1 and 2 are analysed so that the controller design can be improved. This is be means of frequency analysis of the measured signals and analysis of the open loop system.

5.9.1 Frequency Analysis

Sections of data from each of the four paraplegic tests are selected and the frequency content of both the power and the $\dot{V}O_2$ are analysed. Table 5.3 shows the $\dot{V}O_2$ sample

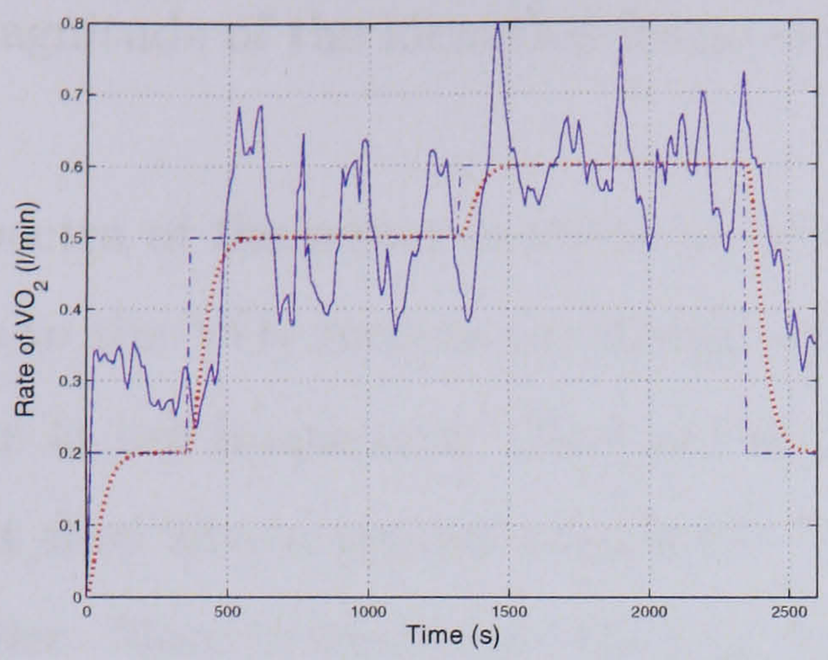

(a)

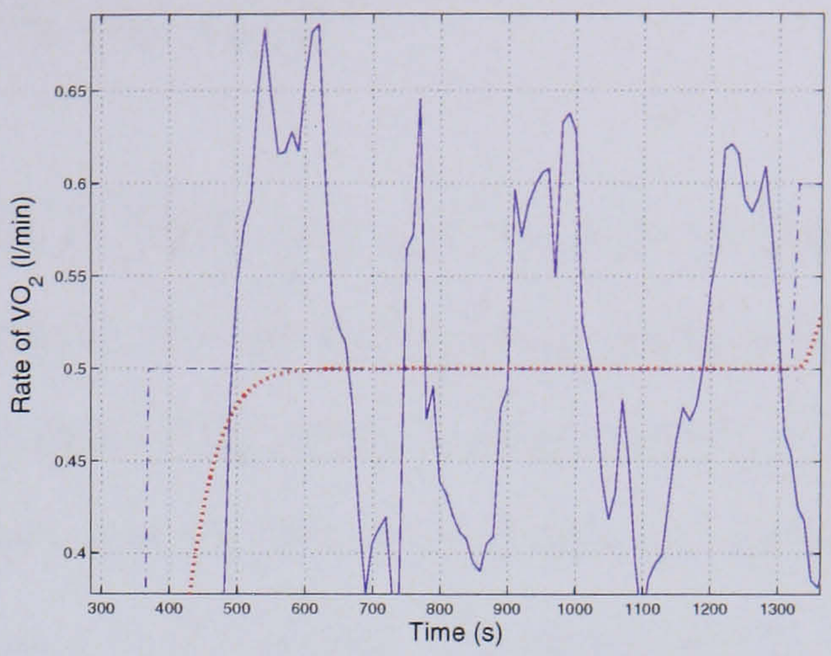

(b)

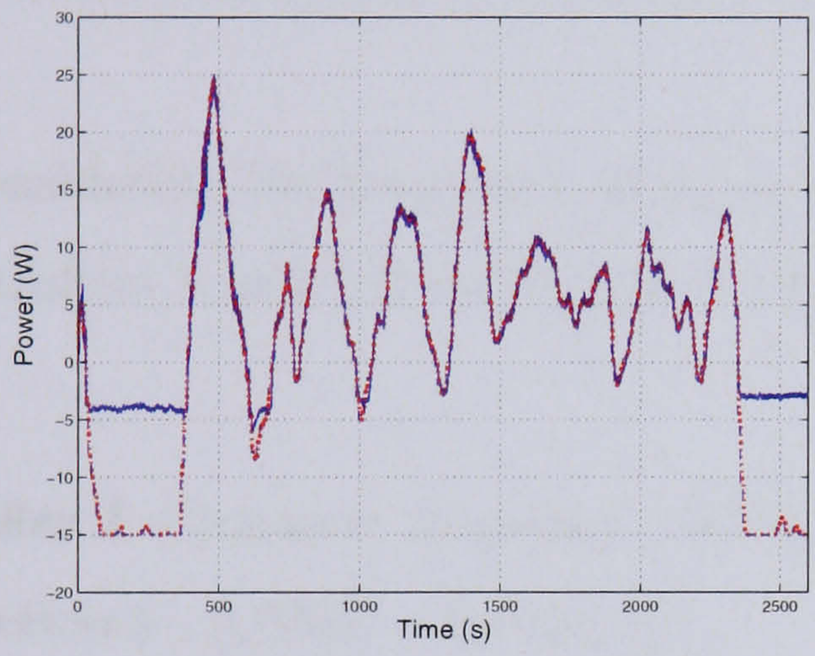

(c)

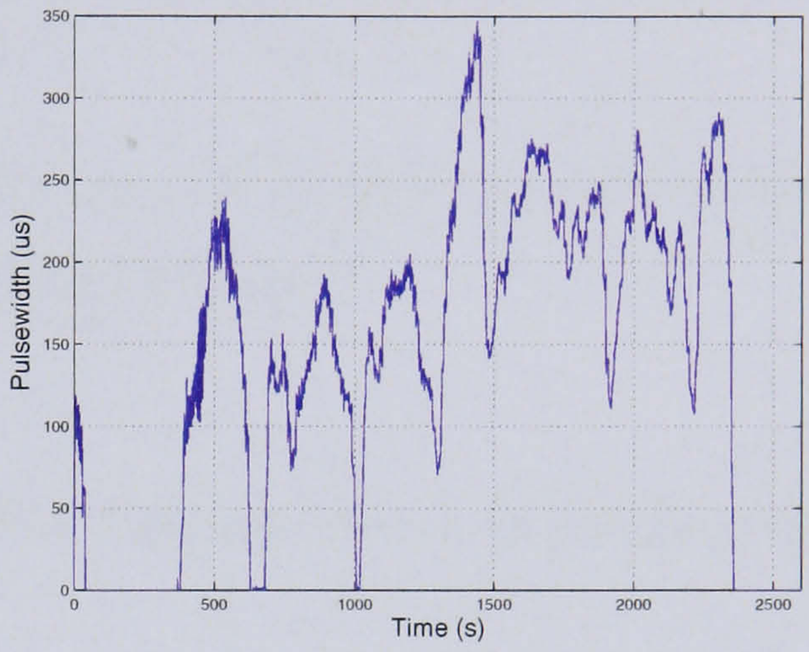

(d)

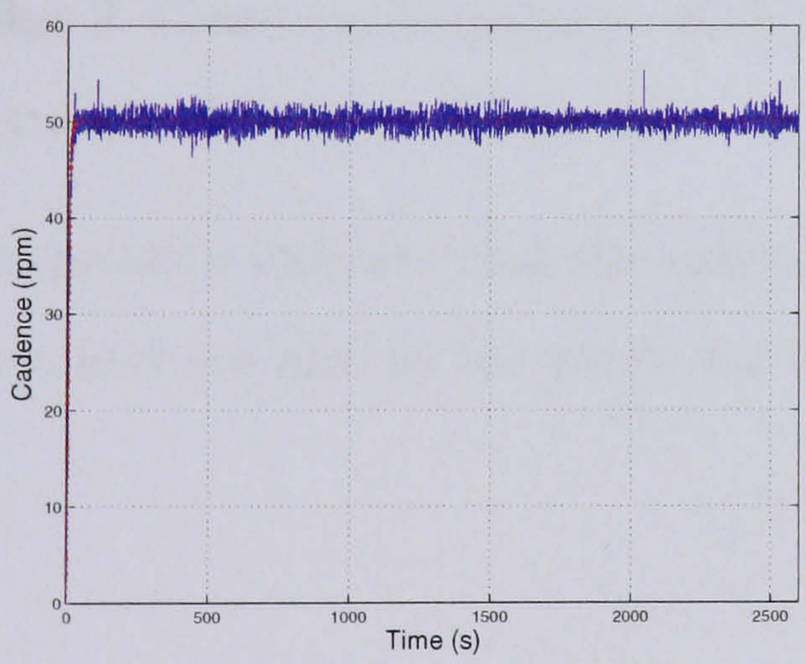

(e)

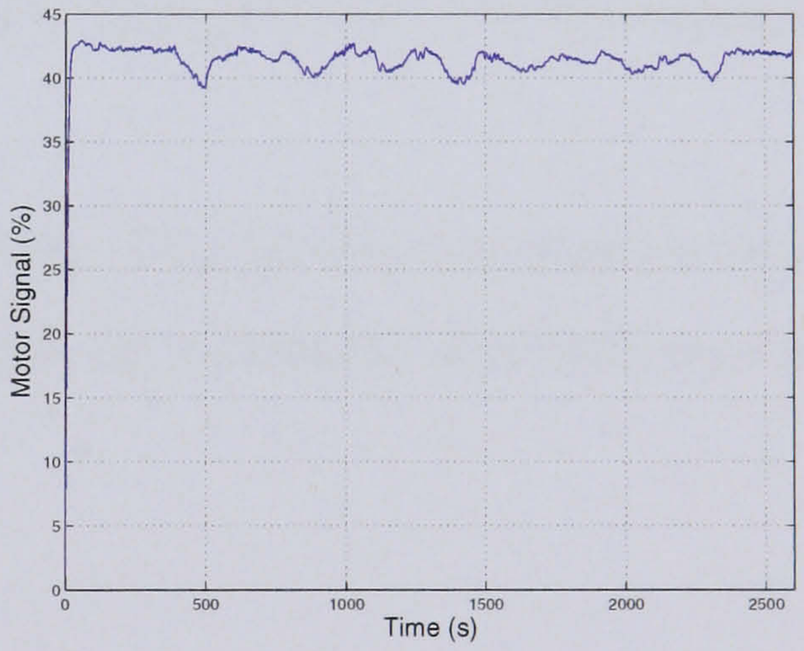

(f)

Figure 5.30: $\dot{V}O_2$ Test 4 : In all graphs the reference is the dashed line, the measured data the solid line and the ideal response the dotted line. The figures show : (a) the $\dot{V}O_2$ controller response, (b) a magnified section of the $\dot{V}O_2$ response, (c) the power controller response, (d) the resulting stimulation from the power controller, (e) the motor controller response and (f) the motor input signal.

for each test. The spectra of these four test indicates that frequencies between 0 and 0.05 Hz, followed by higher frequency harmonics, are measurable within the signal. The magnitude of the identified frequencies is very small.

The spectra of the power analysis are shown in Table 5.4. The section of data corresponds to the $\dot{V}O_2$ spectra previously presented. In all 4 frequency plots clear spikes are seen at low frequencies. They are at the same frequency as those in the VO_2 spectra, but they have a greater magnitude. This increase in power is due to scaling in the controller. More interestingly, the high frequency harmonics are significantly reduced. It can be concluded that both controllers act as a low pass filter.

Now considering the frequency of these spikes in the spectra, the critical frequencies for controllers 1 and 2 from Figures 5.15 are listed below,

Controller 1 Crossover frequency - 0.0032 Hz, S greater than 1 in the frequency range between - $0.0039 \rightarrow 0.0287\ Hz$

Controller 2 Crossover frequency - 0.0019 Hz, S greater than 1 in the frequency range between - $0.0024 \rightarrow 0.0280\ Hz$

These frequencies indicate that the spikes in the $\dot{V}O_2$ spectra are close to the crossover frequency, and are also in the range for which the sensitivity function is greater than 1.

5.9.2 Open Loop Analysis

Examination of the $\dot{V}O_2$'s open loop dynamics will indicate how the $\dot{V}O_2$ behaves when it is not under control. The $\dot{V}O_2$ results from 3 constant load step tests (see Section 3.4.2) are analysed. These tests are from historical data from this subject. An additional test is also implemented so that the subject's current $\dot{V}O_2$ dynamics can be measured. The reasoning for this is to examine how the time between tests affects the dynamics.

Test	$\dot{V}O_2$ Section	Frequency Spectrum
1	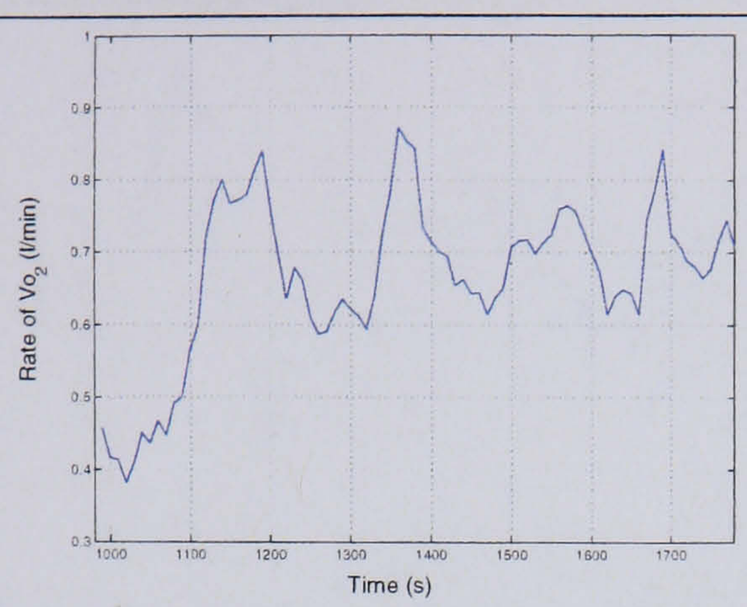	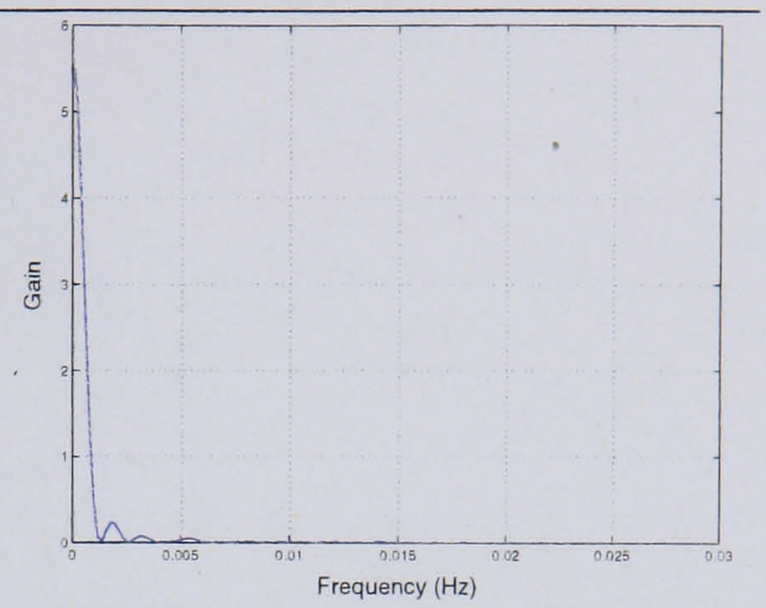
2	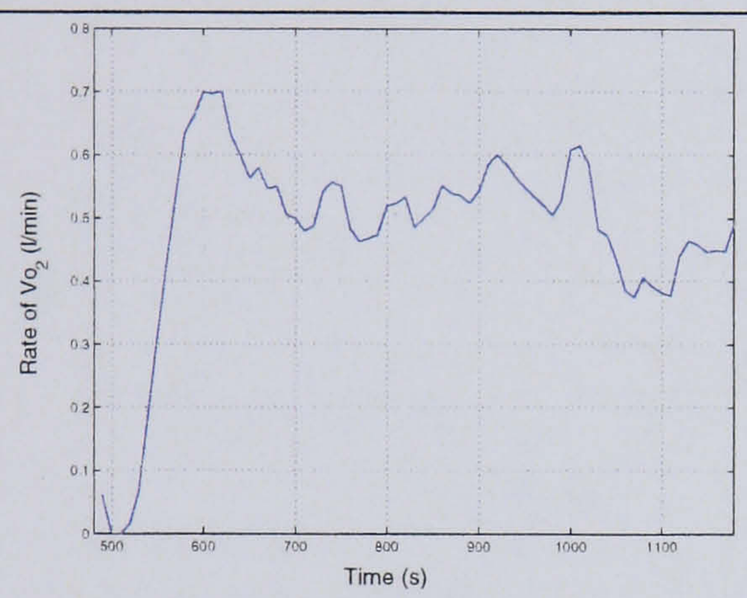	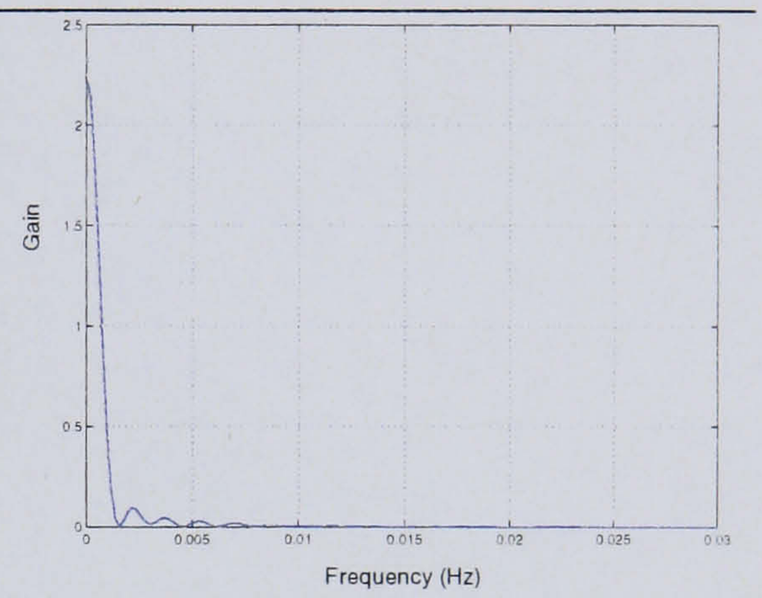
3	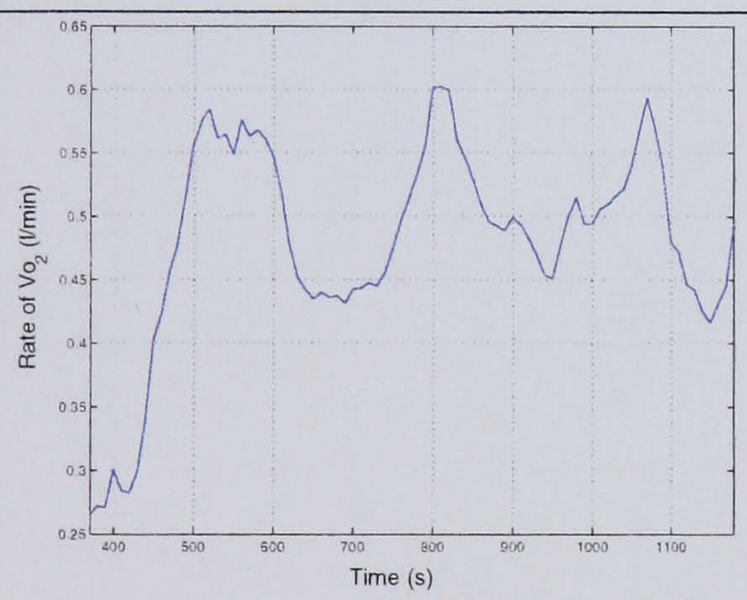	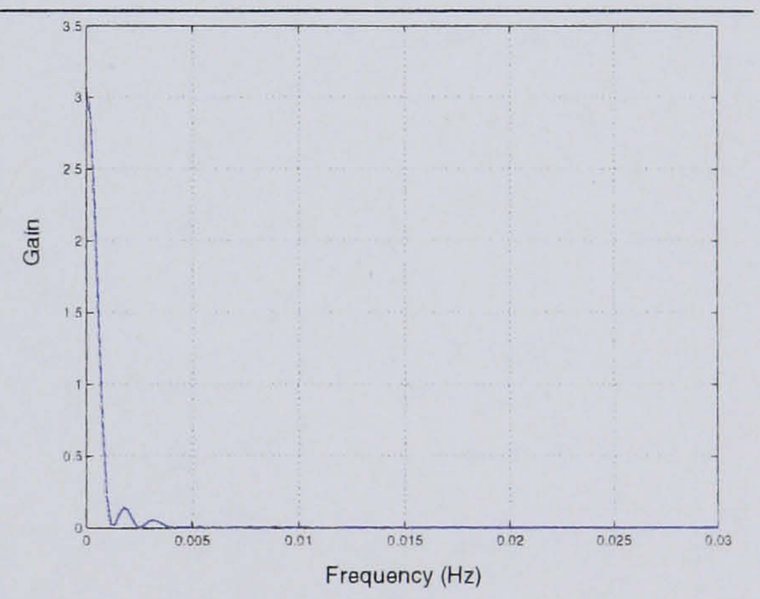
4	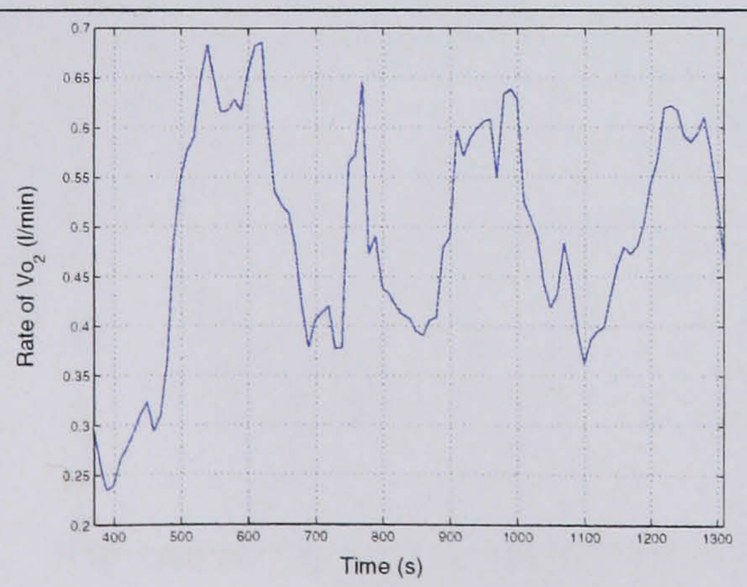	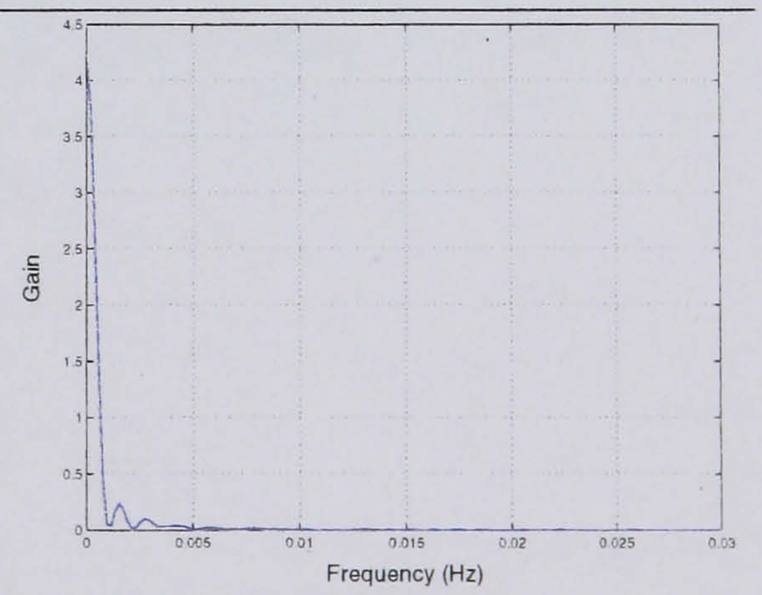

Table 5.3: Sections of $\dot{V}O_2$ data and the resulting spectra from each section of data.

Test	Power Section	Frequency Spectrum
1	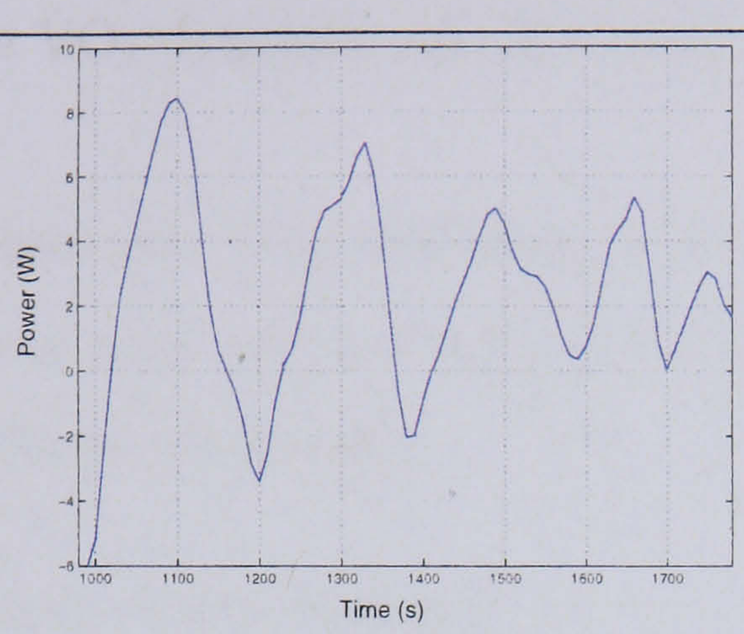	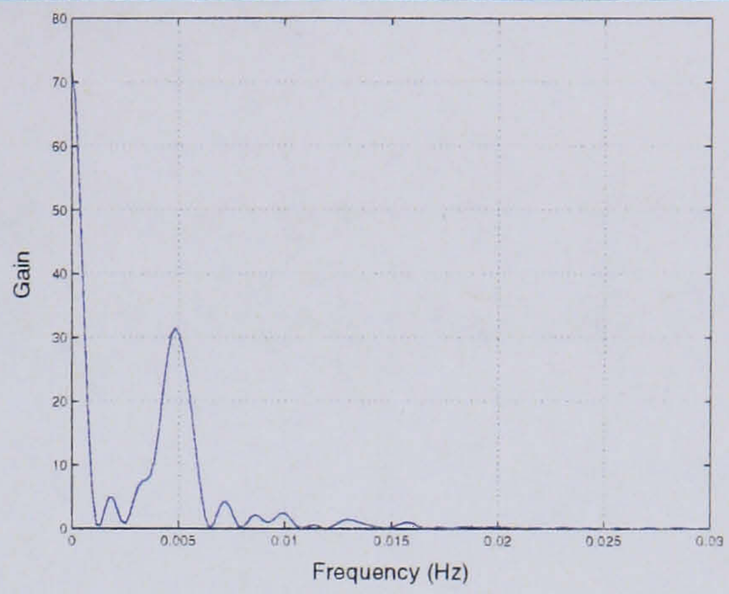
2	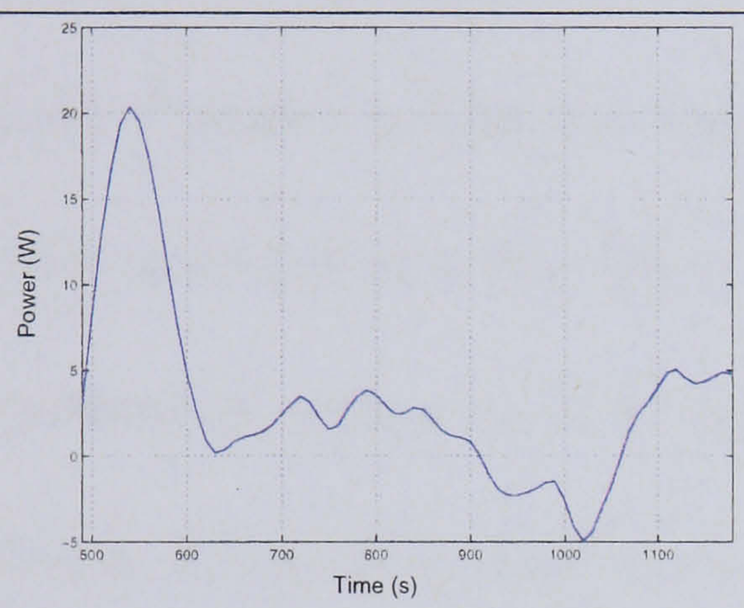	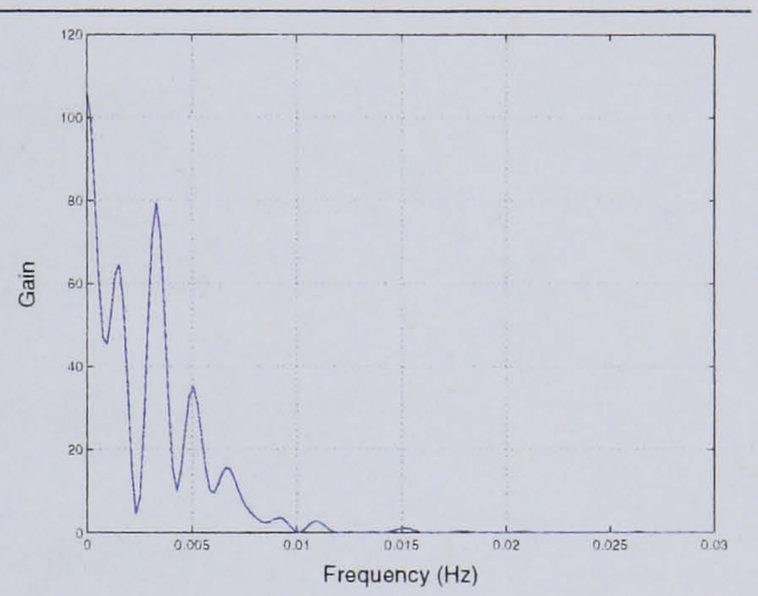
3	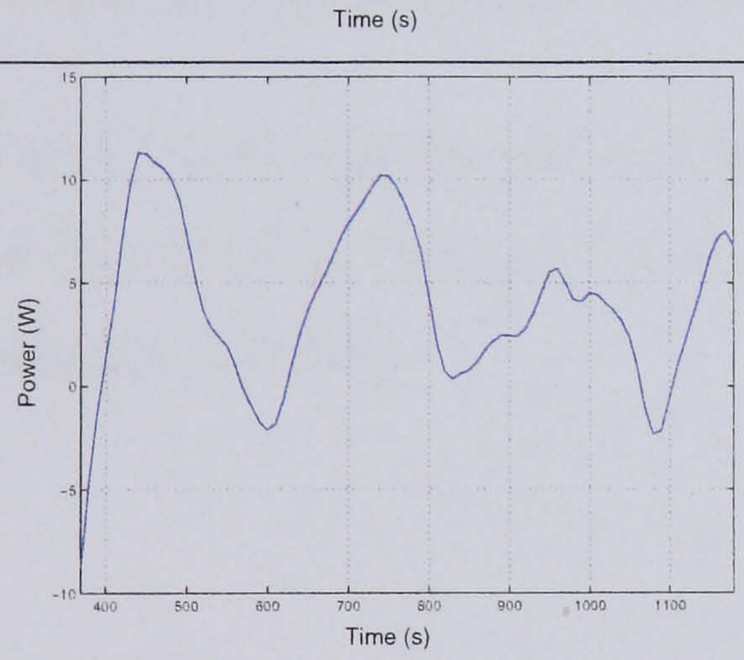	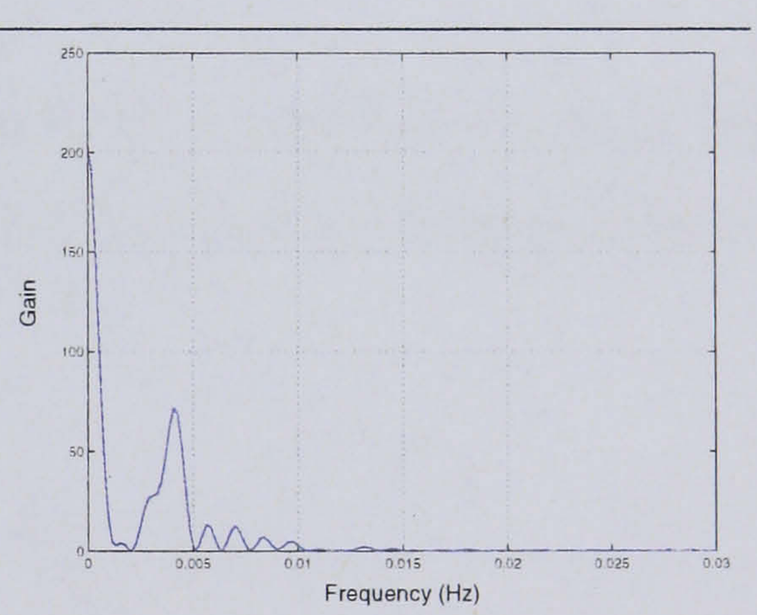
4	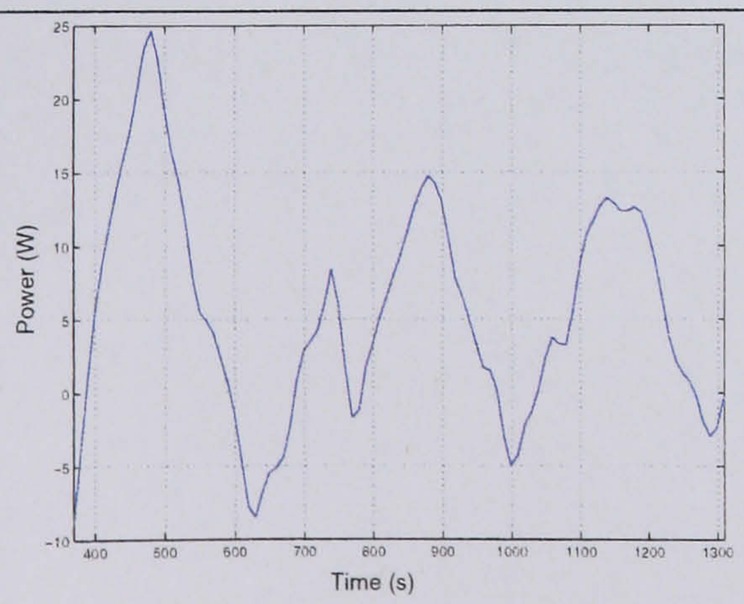	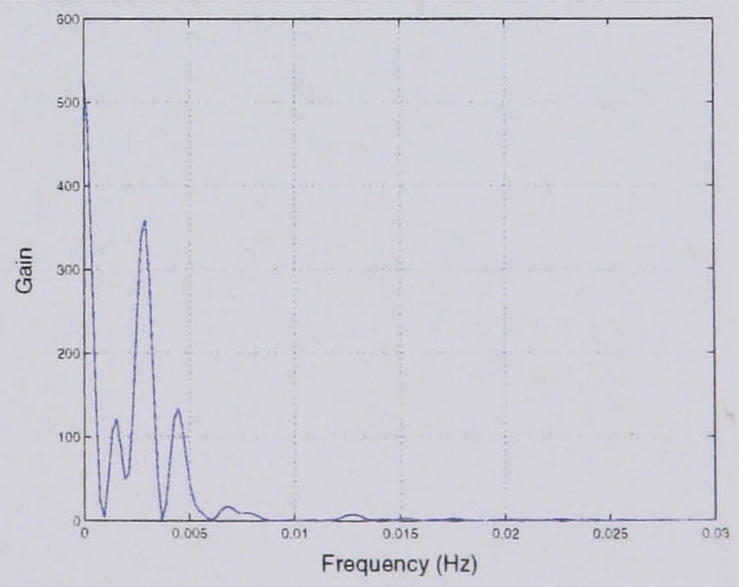

Table 5.4: Sections of power data and the resulting spectra from each section of data.

Previous Tests

These test were undertaken 16 months prior to the $\dot{V}O_2$ identification, and may not be a true reflection of the current dynamics. However, these results demonstrate the variation of the $\dot{V}O_2$ dynamics over a 3 week testing period.

Figure 5.31 shows the $\dot{V}O_2$ responses from the 3 open loop tests. The averaging algorithm that is used online during $\dot{V}O_2$ control is applied to the raw $\dot{V}O_2$. The tests followed the protocol below :

Stage 1 5 minutes of recorded rest

Stage 2 4 minutes of passive cycling (no stimulation)

Stage 3 6 minutes of cycling at 0 W (with stimulation)

Stage 4 12-16 minutes of cycling at 12 W (with stimulation)

Stage 5 6-7 minutes of passive cycling (no stimulation)

Figures 5.31(a) and 5.31(e) indicate the problem of achieving a steady state. Throughout the 12 W period the $\dot{V}O_2$ continues to rise, and only in the final minutes a steady state is approximately achieved.

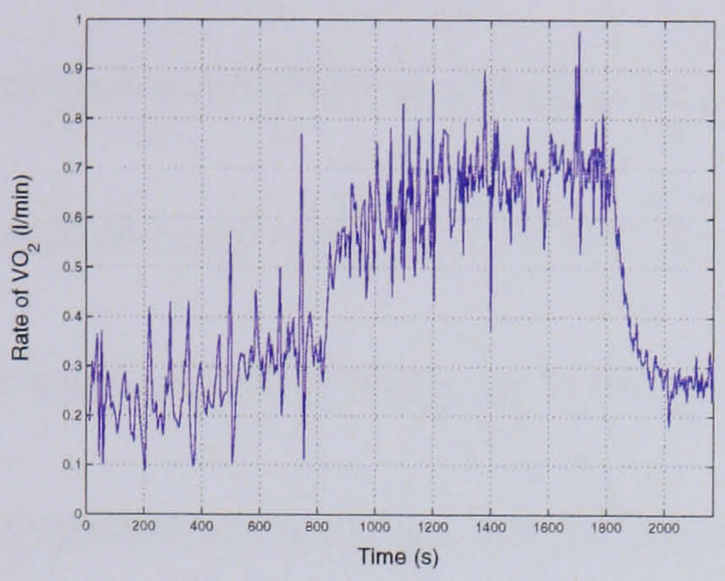

(a) Step Test 1 - Raw $\dot{V}O_2$

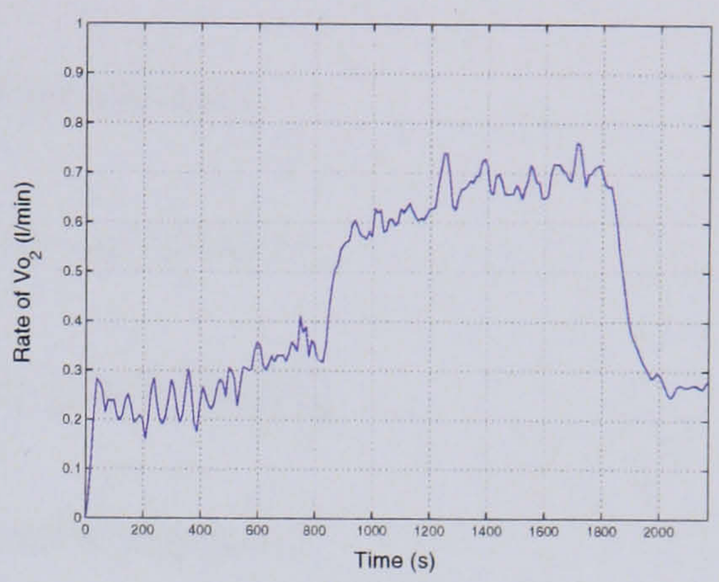

(b) Step Test 1 - Averaged $\dot{V}O_2$

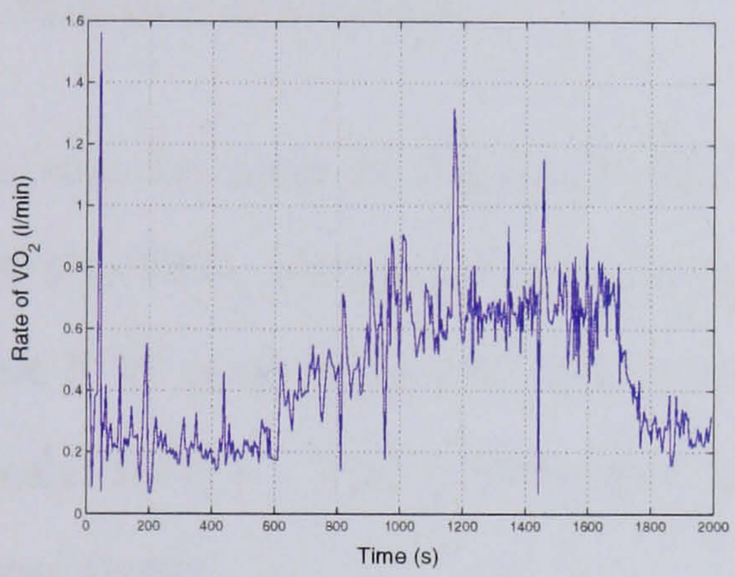

(c) Step Test 2 - Raw $\dot{V}O_2$

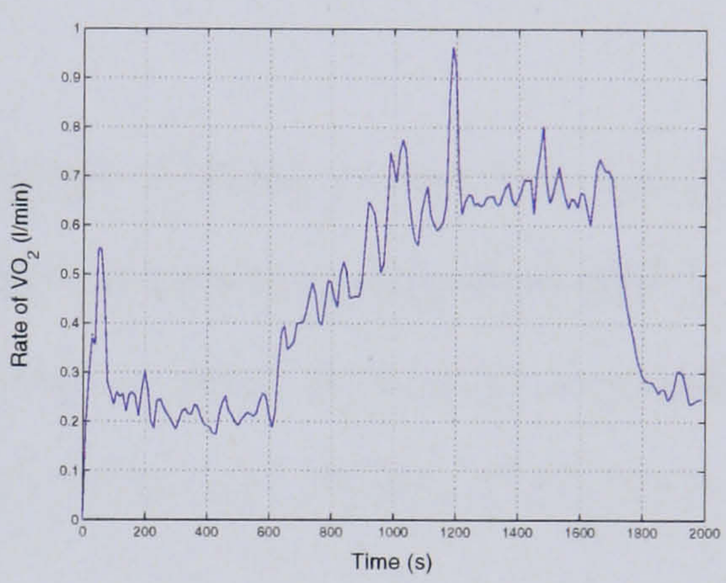

(d) Step Test 2 - Averaged $\dot{V}O_2$

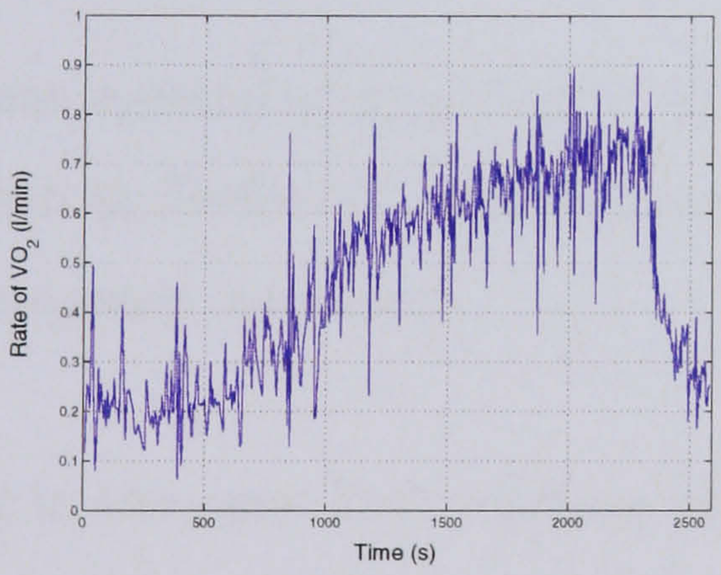

(e) Step Test 3 - Raw $\dot{V}O_2$

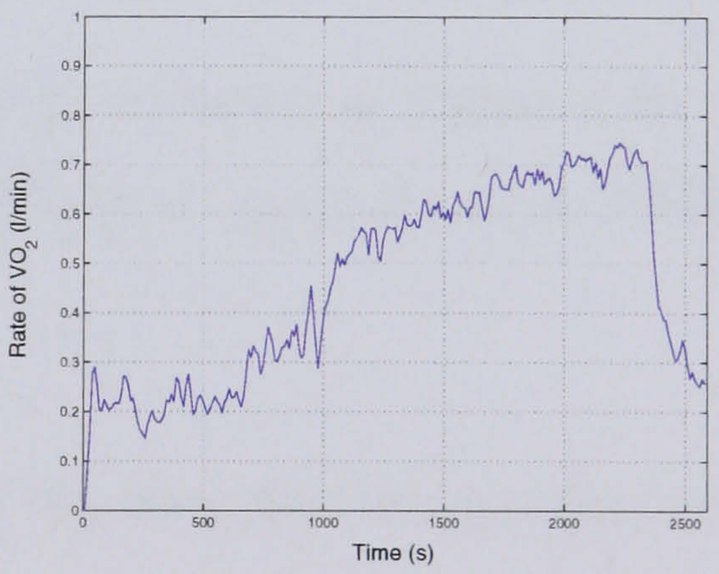

(f) Step Test 3 - Averaged $\dot{V}O_2$

Figure 5.31: $\dot{V}O_2$ responses from 3 step tests.

Open Loop Test

The open loop constant load test is used to identify the subject's current $\dot{V}O_2$ dynamics. The test followed the protocol detailed below :

Stage 1 5 minutes of rest

Stage 2 5 minutes of passive cycling (no stimulation)

Stage 3 5 minutes of cycling at 0 W (with stimulation)

Stage 4 20 minutes of cycling at 8 W (with stimulation)

Stage 5 5 minutes of cycling at 0 W (with stimulation)

Stage 5 2 minutes of recovery

The results can be seen in Figure 5.32. Figure 5.32(a) shows the breath by breath recording of the $\dot{V}O_2$, which are then averaged as shown in Figure 5.32(b). The step in $\dot{V}O_2$, for the 8 W step in power can be clearly be seen, achieving a steady state after approximately 1300 s. The power and stimulation are shown in Figures 5.32(c) and 5.32(d) respectively.

The frequency content of a section of the $\dot{V}O_2$ is shown in Figure 5.33. As with the spectra shown in Table 5.3, spikes are measured at approximately 0.005Hz, followed by higher frequency harmonics.

This finding in the open loop confirms that the identified frequencies are not a result of the control action, but are a physiological factor.

Rise Times and Time Constants

During the controller design process, the rise time of the identified models was used to define the rise time of the controller. The 2 models had rise times of 75.44 s and 151.8 s, which themselves are significantly different. Could the actual rise time of $\dot{V}O_2$

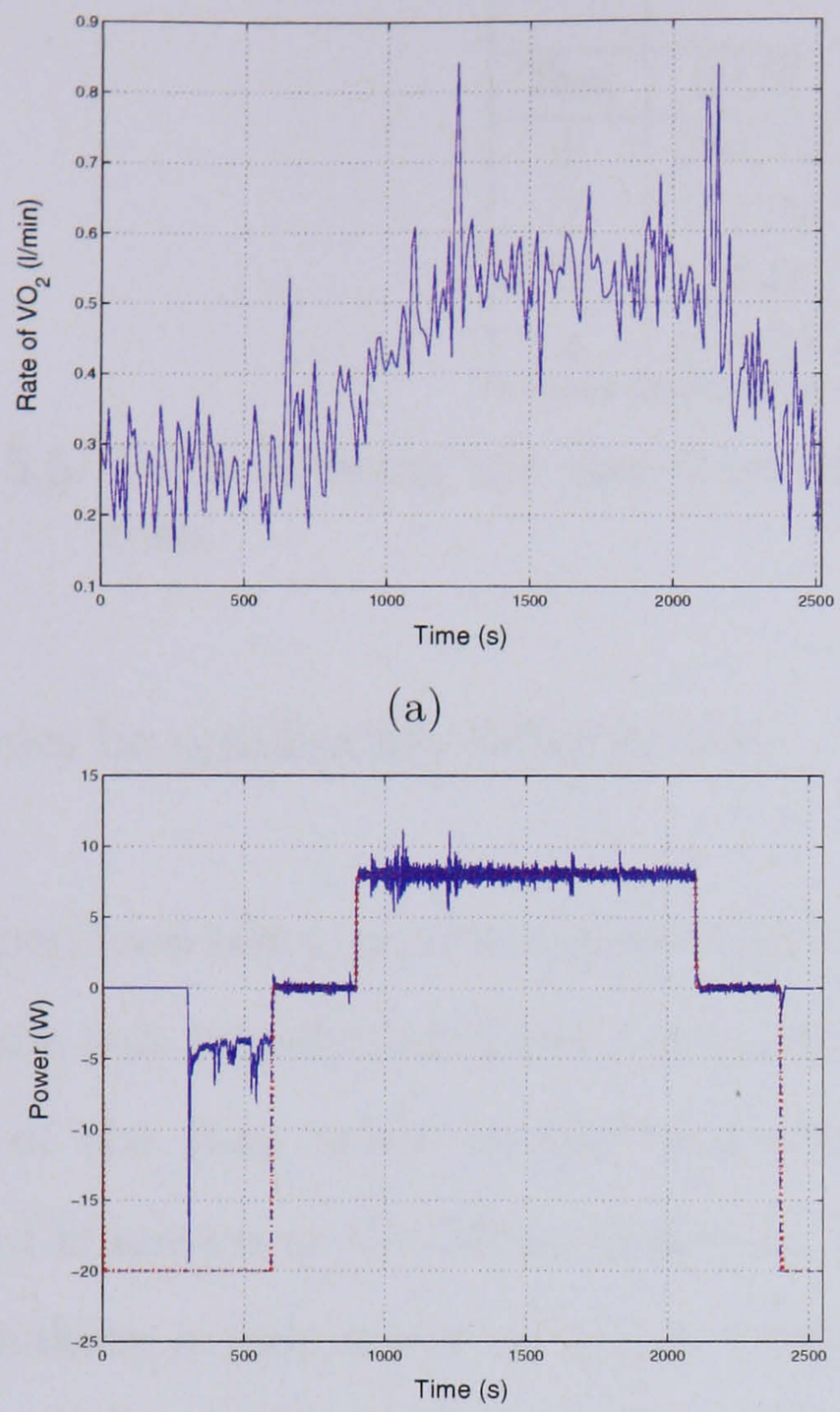

Figure 5.32: Step Test 4. Figures 5.32(a) and 5.32(b) show the raw and averaged $\dot{V}O_2$ respectively. Figures 5.32(c) and 5.32(d) shows the controlled power and the resulting stimulation.

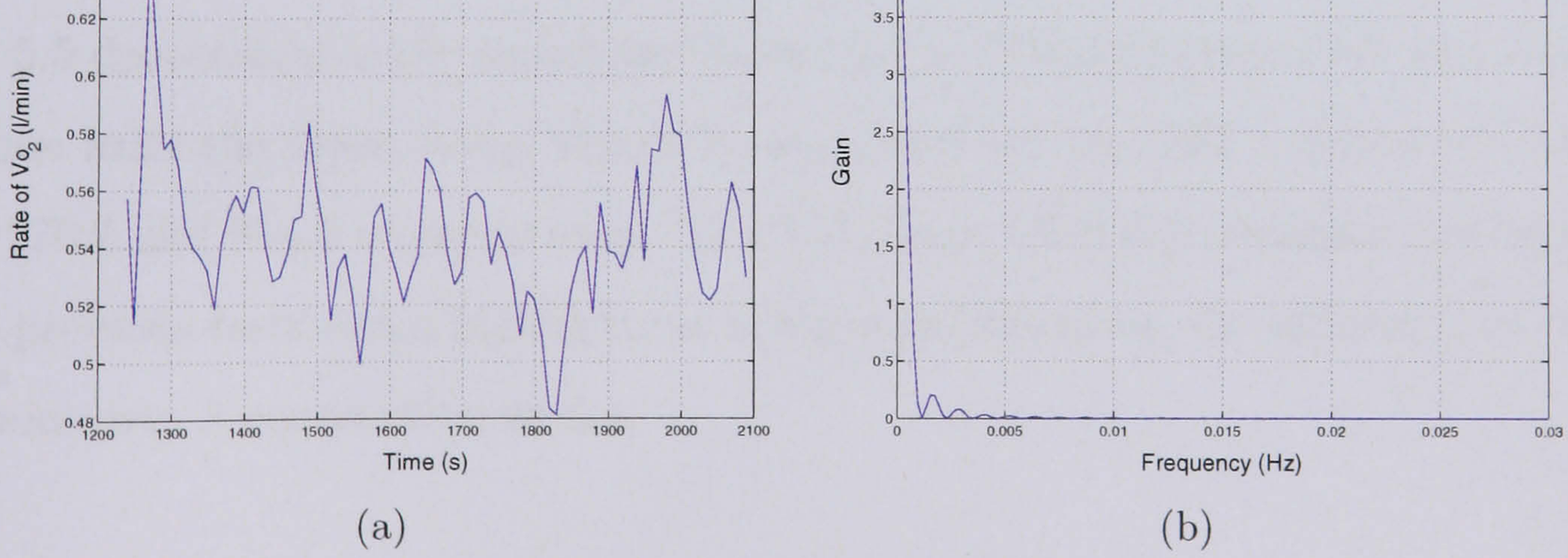

Figure 5.33: A section of the Open Loop $\dot{V}O_2$ is shown in Figure 5.33(a) and the resulting frequency content in Figure 5.33.

	$\tau(s)$	
Test	63 %	ORIGIN
1	284.76	155.45 ± 21.83
2	171.36	38.94 ± 83.13
3	529.00	Not Found
4	270.27	314.93 ± 41.54

Table 5.5: Table showing the rise time via MATLAB and ORIGIN, for 4 open loop tests.

dynamics be significantly different also?

The open loop tests provide a good indication of the $\dot{V}O_2$ rise time for a step test. The rise time can be calculated via a number of methods. The simplest is by calculating 63 % of the time taken in the transition from one steady state to another. This method is known as the Mean Response Time (MRT) [64]. This method relies on the user making a judgement on when a steady state occurs. A more accurate method utilises a statistical software package called ORIGIN[1]. The actual model used is shown as;

$$\dot{V}o_2(t) = P1 + dss(1 - exp(-\frac{t-d}{\tau})) \tag{5.6}$$

where, P1=previous steady state (SS) value, dss=difference between steady state (SS)1 and SS2, d=delay, t=time and τ=Time Constant.

Table 5.5 demonstrates the variability between the $\dot{V}O_2$ dynamics over test days. The rise time from the Open Loop Test 4 is calculated via the 63% method and ORIGIN to be 270.2 and 314.9 s respectively. The $\dot{V}O_2$ from ORIGIN is shown in Figure 5.34. The 3 previous tests again highlight, as in the identifications, the difference in the $\dot{V}O_2$ dynamics over 3 consecutive weeks.

[1]Version 7.5, OriginLab, Massachusetts, US, http://www.OriginLab.com

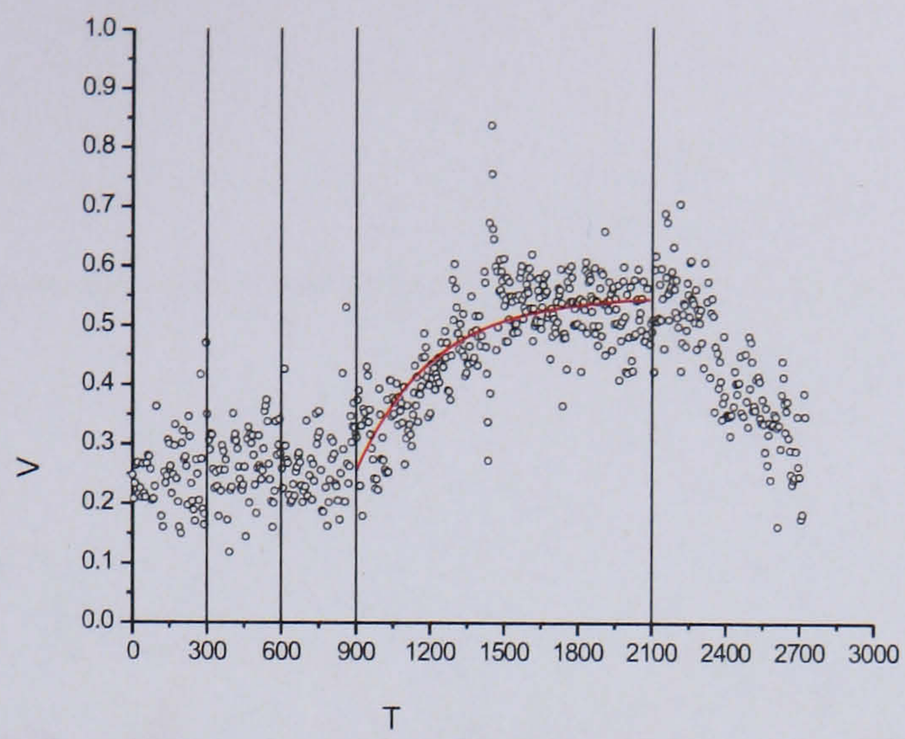

Figure 5.34: Origin calculation of rise time for Open Loop Test 4, presented numerically in Table 5.5. The vertical lines indicate the different phases of the step test as indicated in Section 5.9.2. V = $\dot{V}O_2$ and T = Time (s)

Mean $\dot{V}O_2$

In the 4 closed loop tests, and the open loop test, the $\dot{V}O_2$ has been controlled to or reached a $\dot{V}O_2$ steady state around 0.5 l/min. To compare the effect the controllers are having on the $\dot{V}O_2$, a section of the mean $\dot{V}O_2$ data from each test is plotted. These are shown in Figure 5.35. The 4 controlled tests can be seen to oscillate around a mean of 0.5 l/min, with a similar deviation from the mean. When this is compared to the open loop test, the oscillations are far greater in the closed loop tests.

This can also be seen numerically in Table 5.6. The standard deviation from the mean for the controlled examples is approximately 4 times more than that of the open loop test. For the controlled tests the mean value is approximately the reference value of the controller input, but it is clearly not held constant. The open loop test gives us an indication of the required response under closed loop control.

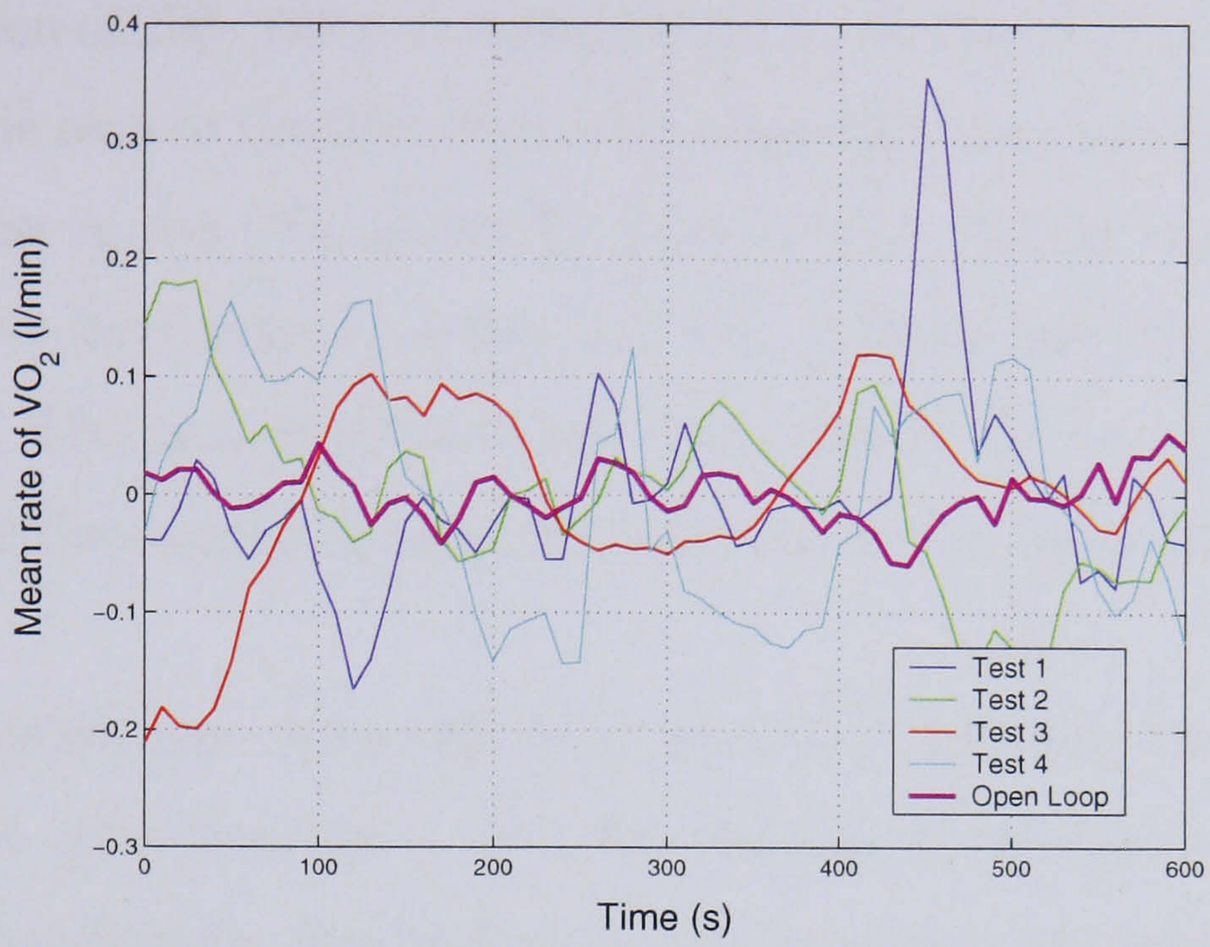

Figure 5.35: Deviation from the mean value for the 4 closed loop tests and the 1 open loop test.

	Test 1	Test 2	Test 3	Test 4	Open Loop
$\triangle$ Time (s)	400 $\rightarrow$ 1000	600 $\rightarrow$ 1200	400 $\rightarrow$ 1000	500 $\rightarrow$ 1100	1400 $\rightarrow$ 2000
Mean $\dot{V}O_2$ (l/min)	0.4982	0.5196	0.4818	0.5199	0.5402
sd	0.0829	0.0763	0.0803	0.0956	0.0227

Table 5.6: Mean values of the $\dot{V}O_2$ during selected sections of the 4 tests. The standard deviations are also presented.

5.10 Conclusions from Analysis

The primary outcome of this analysis is that controllers 1 and 2 are operating too fast and causing the output to oscillate. The open loop test suggests that the dynamic rise time is in the region of 270 - 360 s, compared to 90 - 170 s for controllers 1 and 2 respectively. This can be seen in the four tests. The controller increases the power, resulting in a sharp increase in the $\dot{V}O_2$ above the desired level. As the controller is working too fast, the power then drops to reduce the $\dot{V}O_2$, causing the $\dot{V}O_2$ to oscillate about the desired level. This is best illustrated in the analysis of the mean, in Figure 5.35. The oscillations of the closed loop tests are in the region of 4 times that of the open loop.

The identified models have been shown to have a much lower rise time than those obtained from the open loop tests. This may be due to the relatively low amplitude PRBS used in identification (see Section 5.2.2), in comparison with the large magnitude of step in constant load tests. For future work, a more detailed study into how the PRBS is designed, possibly with larger magnitudes for an increased period may be considered. Alternatively, a simple step test be sufficient for identification and the design of a controller. This may capture the required dynamics of the $\dot{V}O_2$ / power system.

The frequencies contained in the $\dot{V}O_2$ are shown to be present in the power spectrum, but at an increased magnitude. From the frequency analysis of the open loop test, it can be concluded that the frequencies identified are a physiological factor in this subject's $\dot{V}O_2$, and are of such a low frequency that they do not affect the controllers.

In conclusion the next step is to redesign the controllers, increasing the rise time to that identified by the Open Loop Test in section 5.9.2. Two controllers (Controllers 3 and 4) are developed utilising Model 2, with rise times of 270 and 360 s respectively.

6 Further Development of $\dot{V}O_2$ Controllers

In this chapter the findings from the initial 4 tests are collected and used to design new controllers. Primarily, the finding from the Open Loop test that an increased rise time is required, will be utilised. The controllers will again be tested twice and compared against the open loop $\dot{V}O_2$.

6.1 Controller 3

Controller 3 is designed to take into account the findings from the controller analysis. Model 2 is used or the design. Model 2 is chosen as it's rise time is the closest to the rise time measured in the open loop test. The design again includes integral action and plant cancellation. The details of the rise times are given in Table 6.1. The small ARW T_R is due to an input error when designing the controller and was only identified after the $\dot{V}O_2$ control tests had been completed. The sensitivity and complementary sensitivity are shown in Figure 6.1.

Controller 3 has transfer function,

$$\frac{0.004207z^{-1} + 0.004859z^{-2}}{1 - 1.811z^{-1} + 0.8404z^{-2}} \tag{6.1}$$

The overall controller rise time is increased to 270 s, and the Observer and ARW rise times are also altered.

Controller 3
Model $T_R = 151.80$ s
Controller $T_R = 270$ s
Observer $T_R = 150$ s
ARW $T_R = 50$ s
T(s) = 10 s

Table 6.1: Rise times for Controller 3.

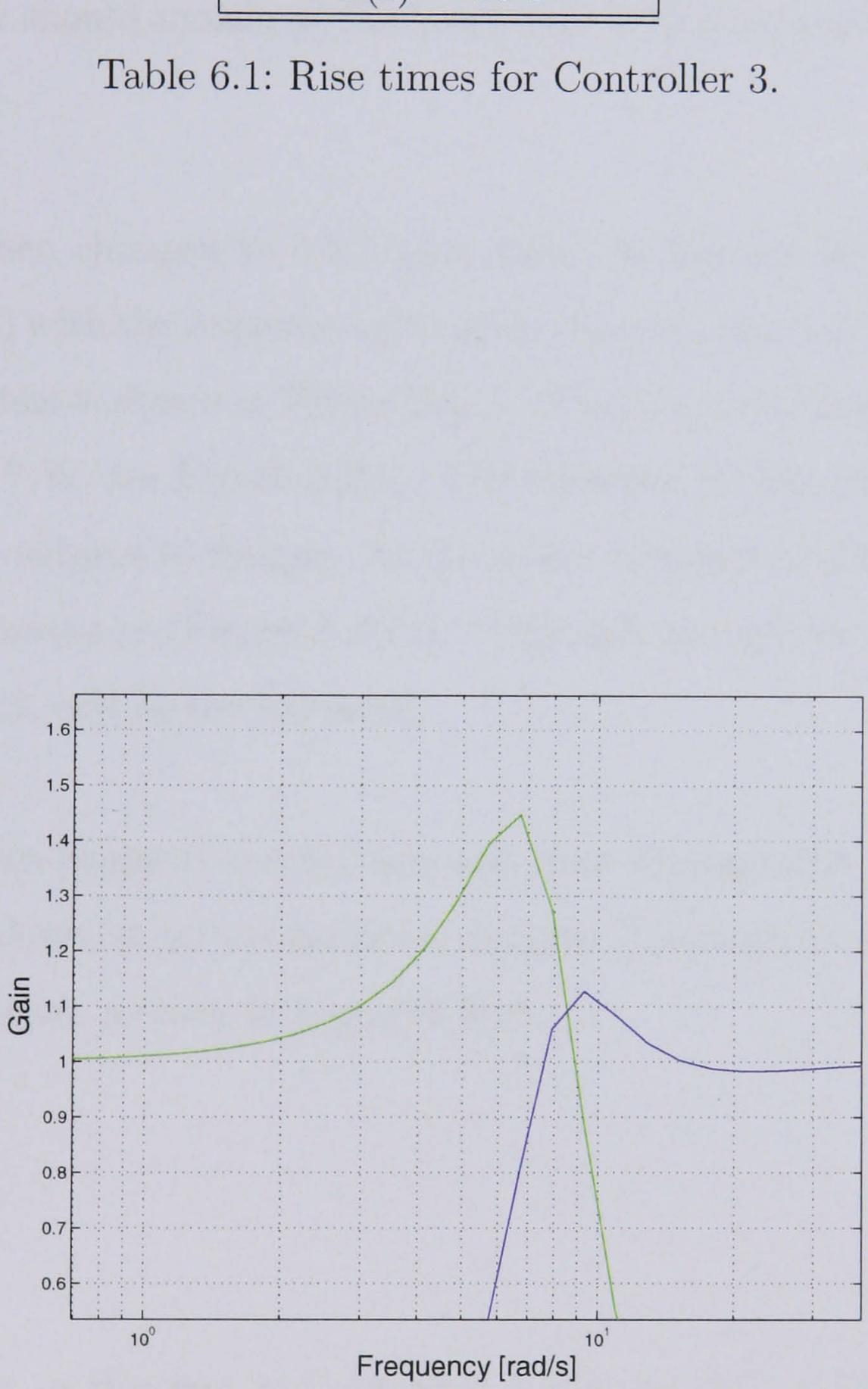

Figure 6.1: Sensitivity (blue line) and Complementary Sensitivity (green line) plots for Controller 3.

6.2 Test 5

Subject 1 follows a power reference while cycling at 50rpm. The controller used in this test is Controller 3 and the $\dot{V}O_2$ reference increments in this test are $0.2 \rightarrow 0.6 \rightarrow 0.5 \rightarrow 0.7 \rightarrow 0.6 \rightarrow 0.2$ l/min . The results are shown in Figure 6.2.

In Figure 6.2(a) the reference $\dot{V}O_2$ is set to 0.2 l/min for the first 500 s. After 400 s, the power response begins to increase without the reference being changed (Figure 6.2(c)). The power should remain at the lower limit of the controller, -15 W. This will be discussed later.

The reference is then changed to 0.5 l/min, which is held for 20 minutes. The $\dot{V}O_2$ tracks well (± 10 %) with the reference value and achieves a mean $\dot{V}O_2$ level of 0.5 l/min. This period of the test is shown in Figure 6.2(b). The power increases to 11 W and then reduces to around 7 W, see Figure 6.2(c). The reference is then changed to 0.7 l/min, but this causes the subject to fatigue. As the power increases to 15 W, the stimulation increases to the maximum (Figure 6.2(d)). Although the subject fatigues, again the $\dot{V}O_2$ is seen to track well to the reference.

The reference is then dropped to 0.6 l/min and then subsequently to 0.2 l/min, where the cyclist warms down at zero stimulation cycling. Throughout the test the cadence is controlled to 50 rpm, as seen in Figure 6.2(e).

6.3 Test 6

The controller used in this test is Controller 3 and the $\dot{V}O_2$ reference increments in this test are $0.2 \rightarrow 0.5 \rightarrow 0.4 \rightarrow 0.5$ l/min. The results are shown in Figure 6.3.

Controller 3 is tested again. The lower limit of the controller increased from -15 W to -10 W. This is to identify any possible problem with this lower limit, and the increase in power seen in Figure 6.2(c). Again the reference is set to 0.2 l/min for zero stimulation

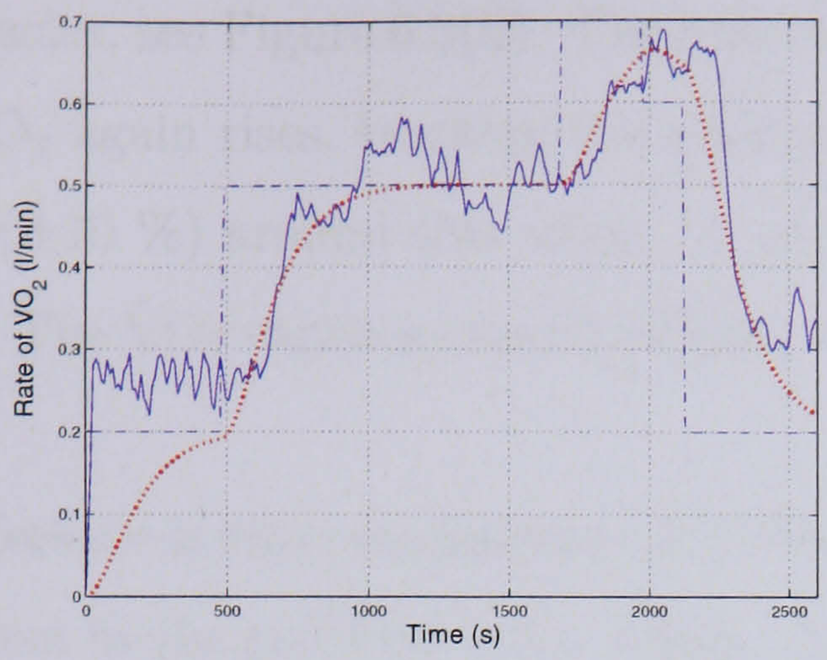

(a)

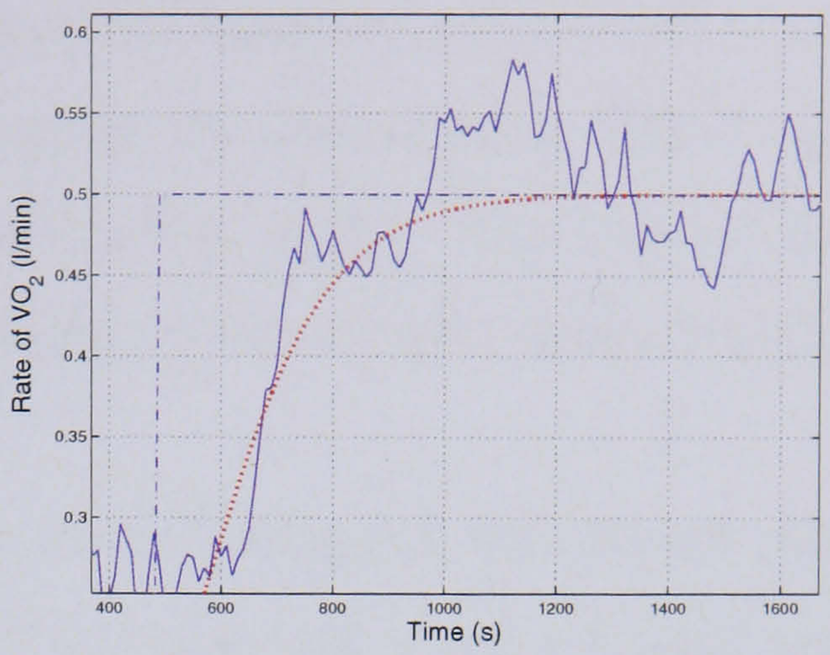

(b)

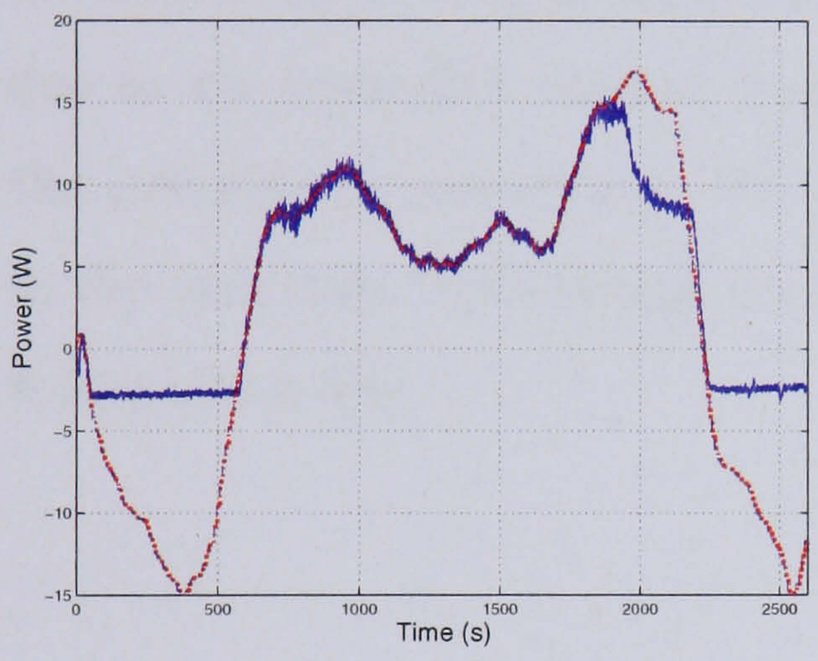

(c)

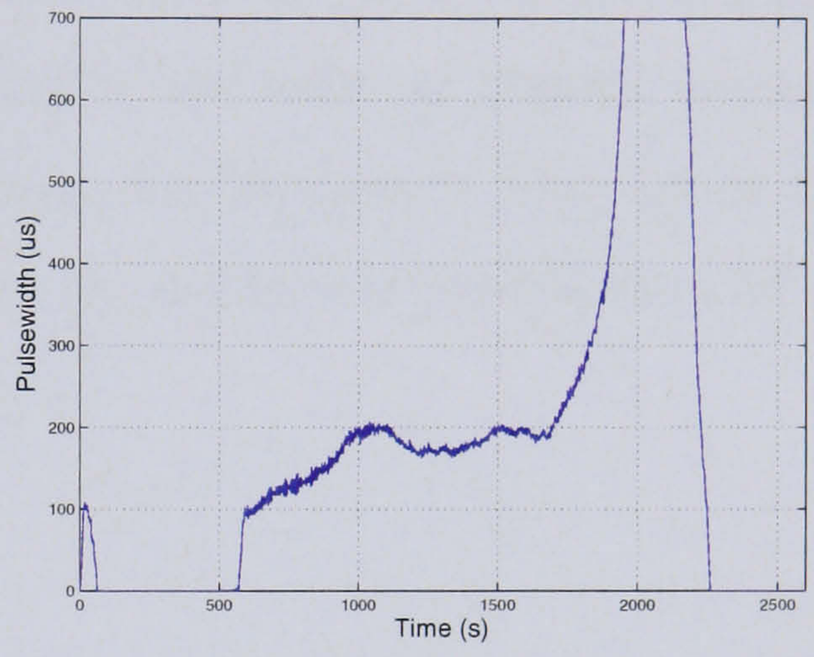

(d)

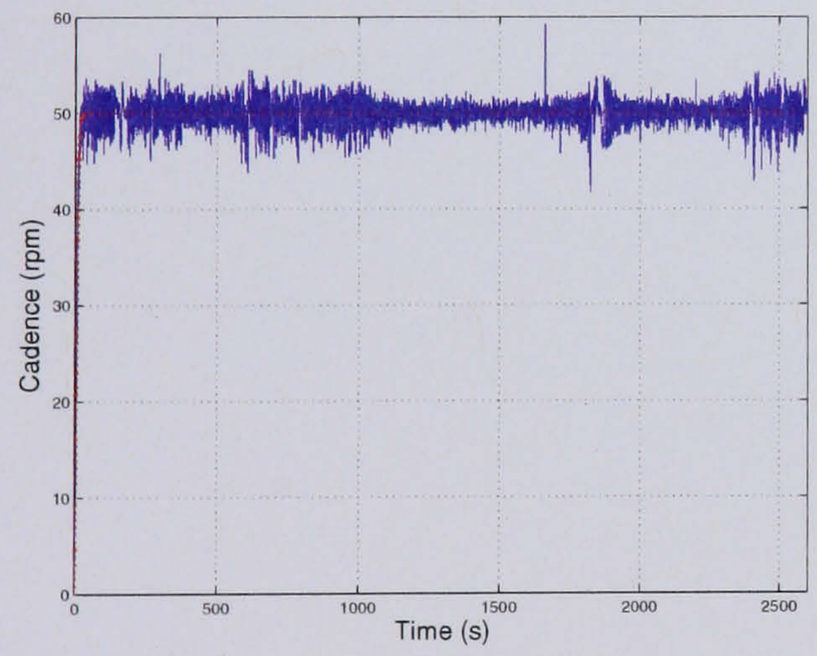

(e)

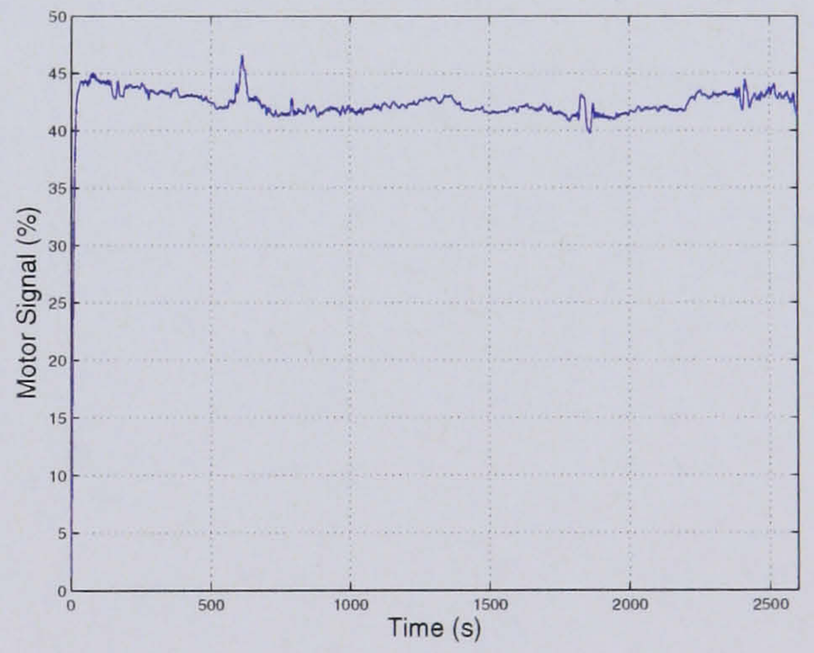

(f)

Figure 6.2: $\dot{V}O_2$ Test 5 : In all graphs the reference is the dashed line, the measured data the solid line and the ideal response the dotted line. The figures show : (a) the $\dot{V}O_2$ controller response, (b) a magnified section of the $\dot{V}O_2$ response, (c) the power controller response, (d) the resulting stimulation from the power controller, (e) the motor controller response and (f) the motor input signal.

cycling. After approximately 200 s the desired power reaches the lower limit of the controller, and begins increasing. The increase in power reference is enough to stimulate the muscles, see Figure 6.3(d). The reference is then increased to 0.5 l/min until 1800 s. The $\dot{V}O_2$ again rises, tracking the reference up to the desired level, with small fluctuations ($\pm$10 %) around this value. A zoomed section of this data is shown in Figure 6.3(b). The $\dot{V}O_2$ varies around 0.5 l/min, and the power averages approximately 6.5 W.

The reference is then decreased to 0.4 l/min, to avoid fatiguing the subject (which was a problem in the previous test). Again, the $\dot{V}O_2$ tracks well to the reference and varies around the desired level. The stimulation can be seen to go to zero, in Figure 6.3(d). This is due to the controller output dropping to the value of passive cycling, -4 W. Finally the reference is increased to 0.5 l/min, and the power steps up to the same level as in the first step. Throughout the test the cadence is controlled to 50 rpm, see Figures 6.3(e) and 6.3(f).

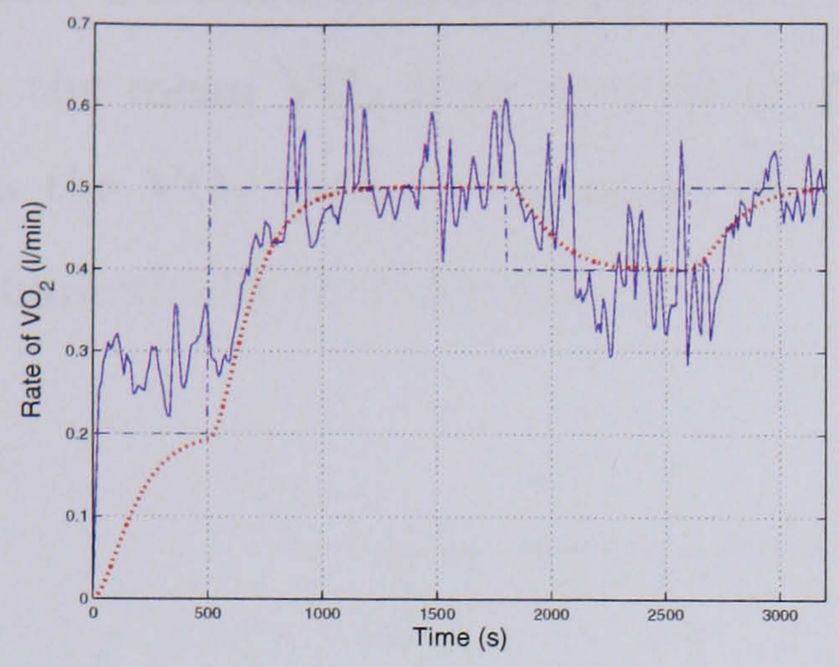

(a)

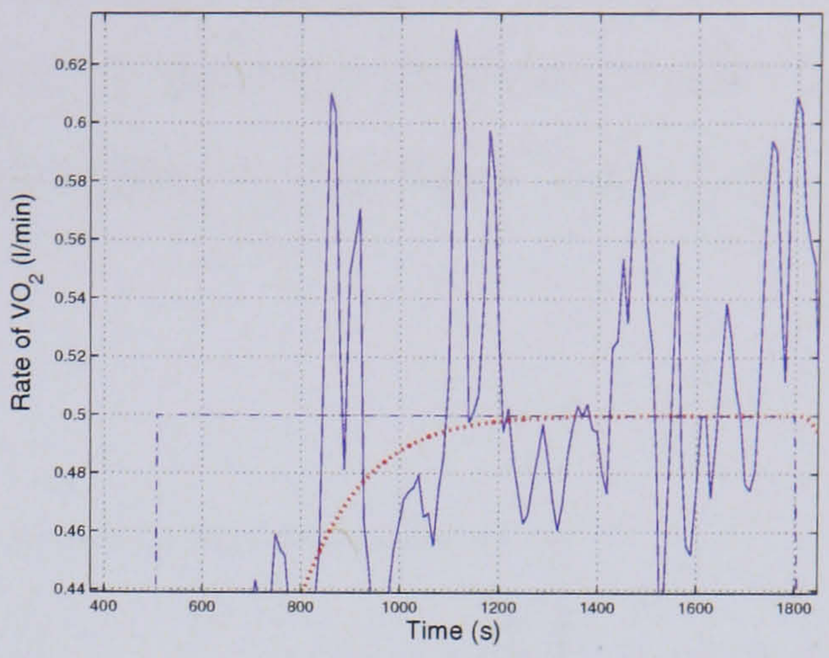

(b)

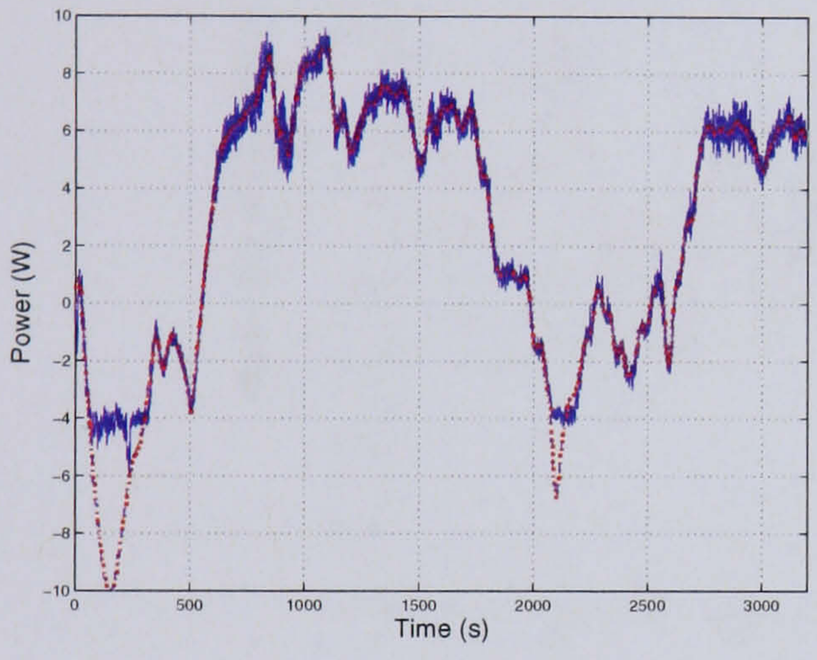

(c)

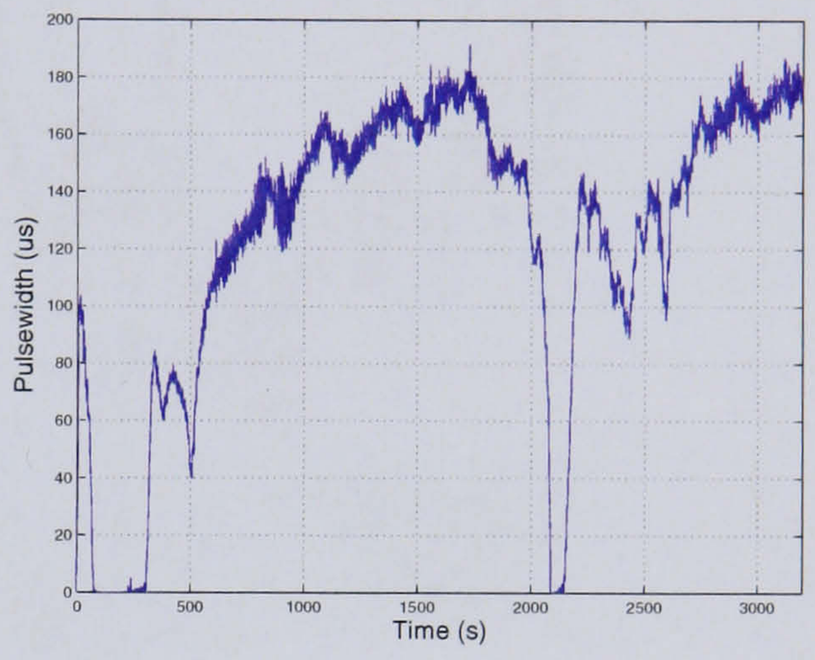

(d)

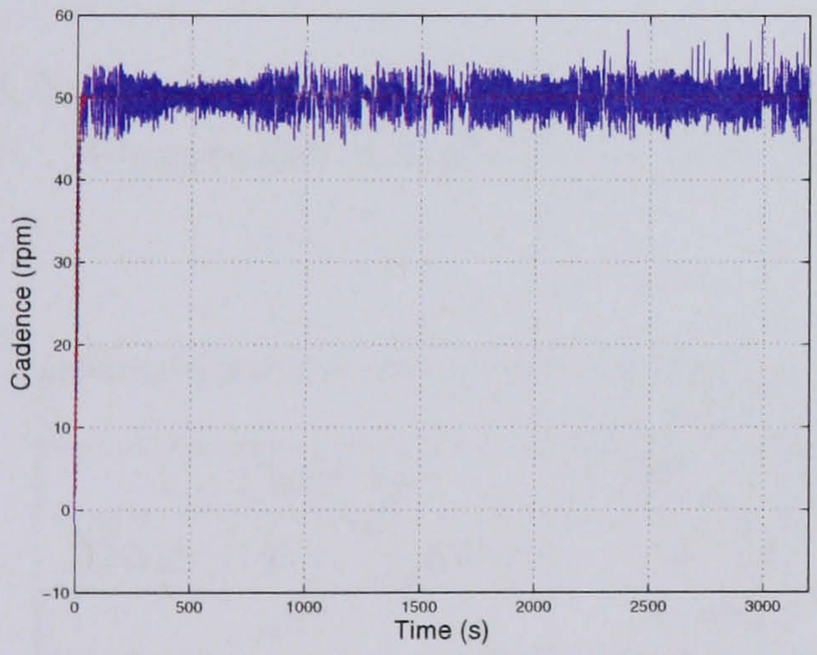

(e)

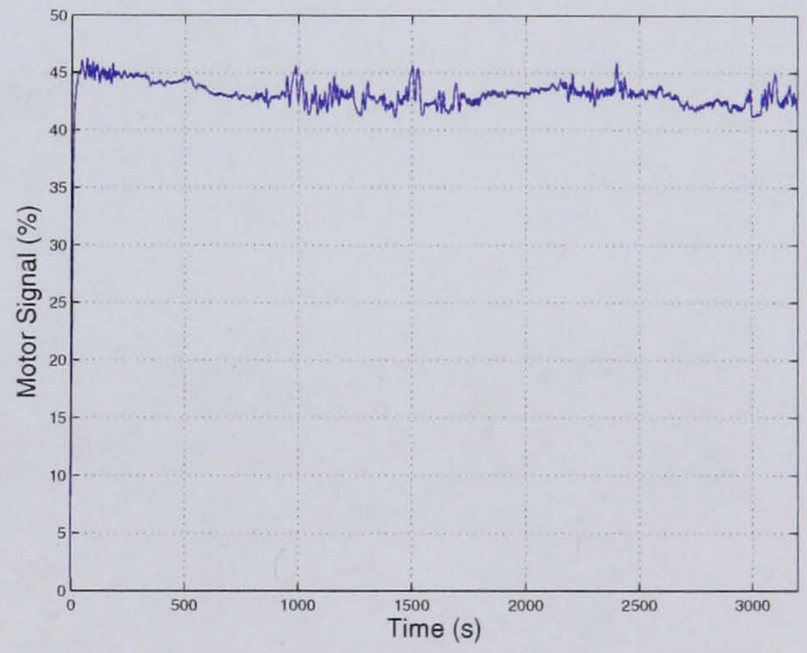

(f)

Figure 6.3: $\dot{V}O_2$ Test 6 : In all graphs the reference is the dashed line, the measured data the solid line and the ideal response the dotted line. The figures show : (a) the $\dot{V}O_2$ controller response, (b) a magnified section of the $\dot{V}O_2$ response, (c) the power controller response, (d) the resulting stimulation from the power controller, (e) the motor controller response and (f) the motor input signal.

6.4 Controller 3 Analysis

As before, a section of mean data is taken from each test at 0.5 l/min and is plotted against the mean $\dot{V}O_2$ from open loop test 4. Figure 6.4 shows that this controller controls the $\dot{V}O_2$ close to the mean $\dot{V}O_2$, identified in the Open Loop test. This is shown numerically in Table 6.2.

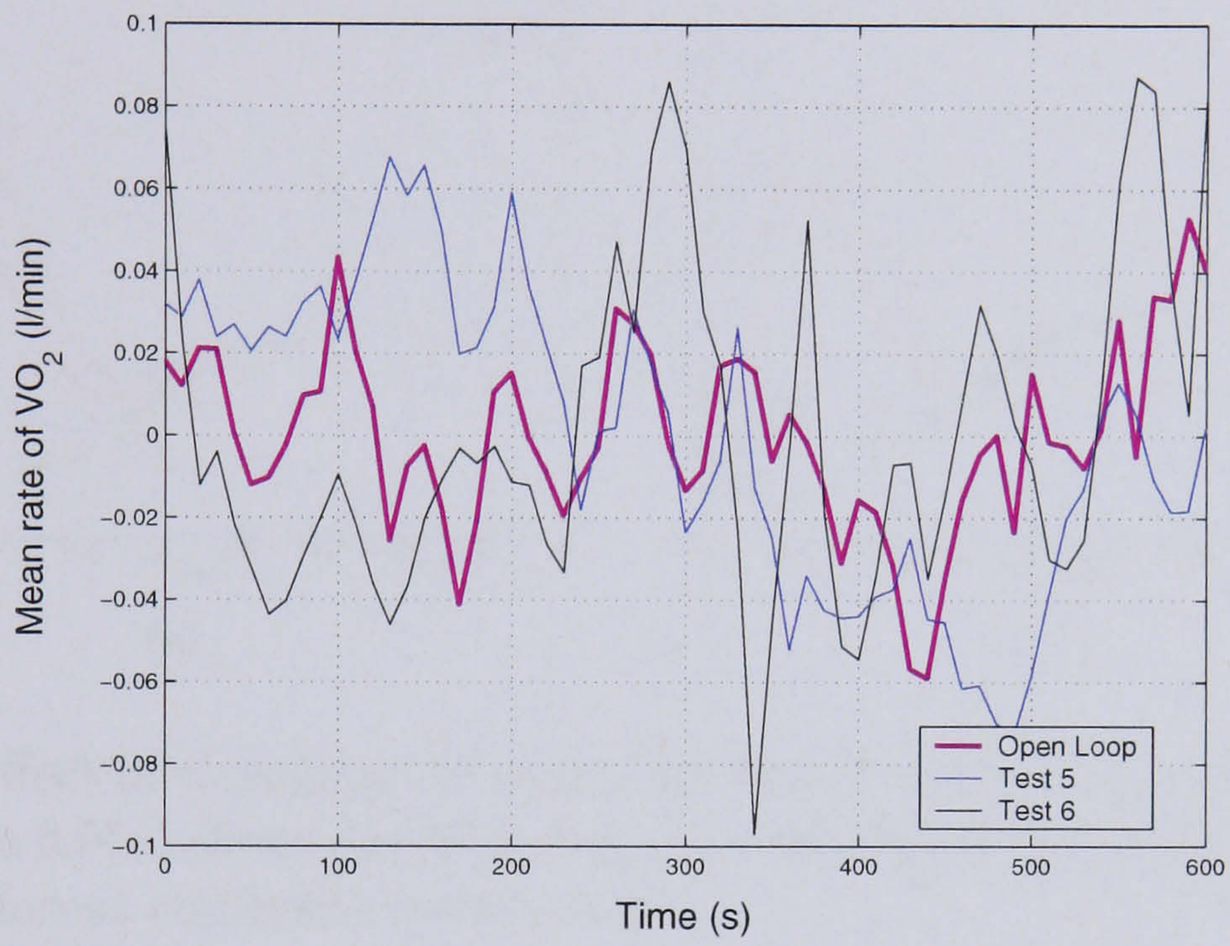

Figure 6.4: Shows the deviation from the mean value for the 2 closed loop tests with Controller 3 and the 1 Open Loop test.

	Test 5	Test 6	Open Loop
$\triangle$ Time (s)	1000 $\rightarrow$ 1600	1200 $\rightarrow$ 1800	1400 $\rightarrow$ 2000
Mean $\dot{V}O_2$ (l/min)	0.5154	0.5065	0.5402
sd	0.0367	0.0401	0.0227

Table 6.2: Mean values of the $\dot{V}O_2$ data during selected sections of tests 5 and 6. The standard deviation are also presented.

6.4.1 ARW Rise Time

In both of the tests with controller 3, a problem with the lower operating limit of the controller has been identified. During zero stimulation cycling the desired power drops

to the lower limit of the controller, and then increases back upwards. In the case of the second test, this results in the muscles being stimulated. The effect of the lower limit can be seen in Figure 6.5. This plot is generated via simulation of the $\dot{V}O_2$ controller. When the controller has a lower limit of -5 W, the fast ARW rise time causes the $\dot{V}O_2$ and power to increase, during the period of zero stimulation.

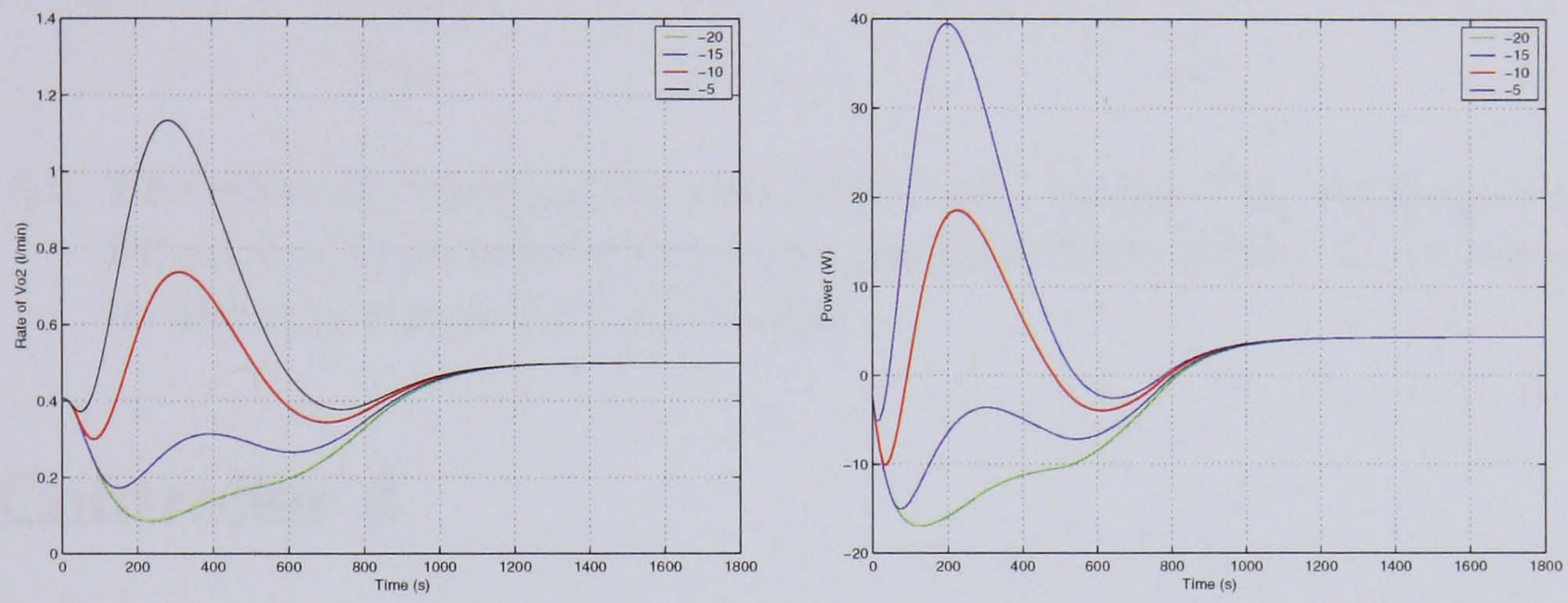

(a) (b)

Figure 6.5: The effect of changing the controller limits on the $\dot{V}O_2$ and power response. Figure 6.5(a) shows the $\dot{V}O_2$ response and Figure 6.5(b) the power response, to different controller lower limits.

When the lower operating limit of the controller is fixed at -10 W, the effect of the ARW rise time is investigated under simulation. As the rise time is increased, when the power reaches the lower limit of the controller, the power remains constant and does not increase. This can be seen in Figure 6.6.

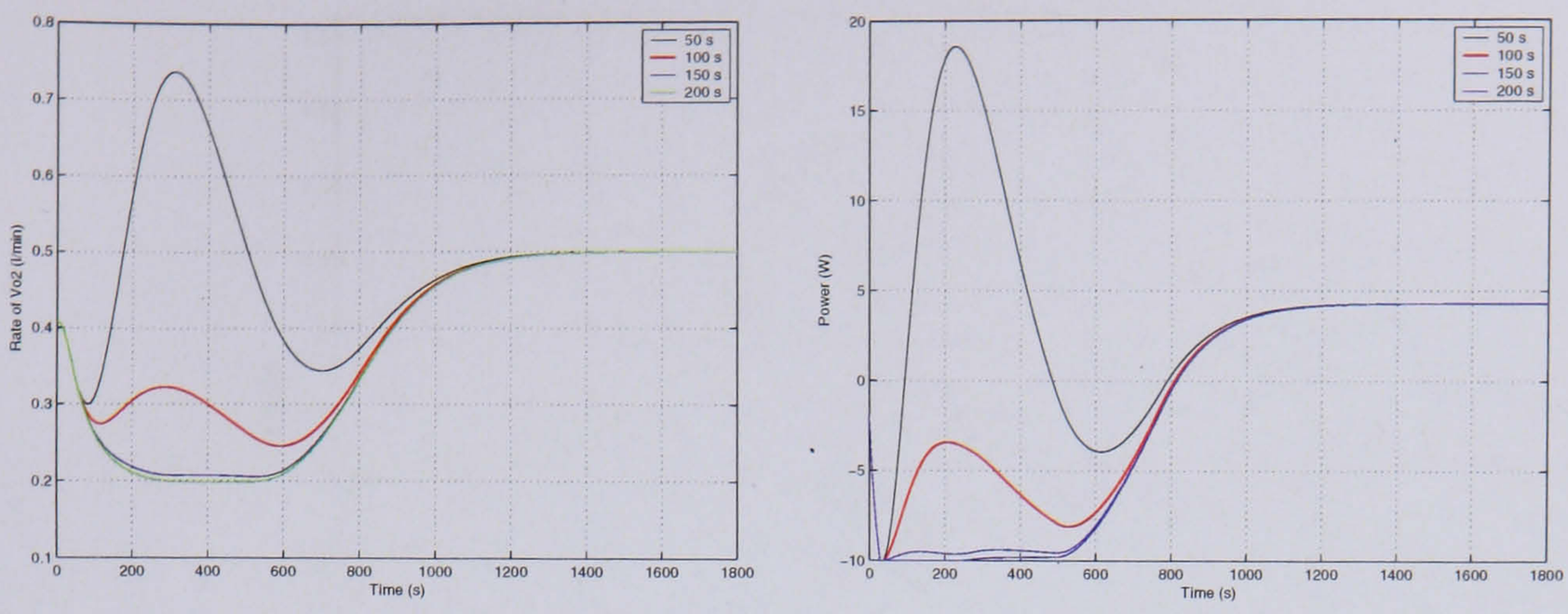

(a) (b)

Figure 6.6: The effect of changing the controller limits on the $\dot{V}O_2$ and power response. Figure 6.5(a) shows the $\dot{V}O_2$ response and Figure 6.5(b) the power response, to different controller lower limits.

6.5 Controller 4

Controller 4 is designed with a slower rise time than Controller 3. Furthermore the ARW rise time is increased to avoid the lower limit problem that was identified in the previous section. The details of the controller are shown in Table 6.3. The sensitivity and complementary sensitivity are shown in Figure 6.7.

Controller 4 has transfer function,

$$\frac{0.002425z^{-1} + 0.002801z^{-2}}{1 - 1.857z^{-1} + 0.862z^{-2}} \tag{6.2}$$

Controller 4
Model $T_R = 151.80$ s
Controller $T_R = 360$ s
Observer $T_R = 150$ s
ARW $T_R = 200$ s
T(s) = 10 s

Table 6.3: Rise times for Controller 4.

Figure 6.7: Sensitivity (blue line)and Complementary Sensitivity (green line) plots for Controller 4.

6.5.1 Test 7

The controller used in this test is Controller 4 and the $\dot{V}O_2$ reference increments in this test are $0.2 \rightarrow 0.5 \rightarrow 0.4 \rightarrow 0.5$ l/min. The results are shown in Figure 6.8.

As with the previous test there is a period of zero stimulation cycling, before a step to 0.5 l/min. The $\dot{V}O_2$ tracks the desired response, in Figure 6.8(a), up to the desired value, where it fluctuates. The power increases to 10 W, during the transition between the two $\dot{V}O_2$ levels and then reduces to 5 W, shown in Figure 6.8(c).

The reference is then changed down to 0.4 l/min and again the controller can be seen to track the desired response, until approximately 2400 s. At this point the motor input signal reaches its maximum level, causing the cadence to drop, see Figure 6.8(e). This results in the power and stimulation to drop in Figures 6.8(c) and 6.8(d). To correct this the battery is connected back to the mains, for the cadence to return to 50 rpm.

Finally the reference is increased back to 0.5 l/min, and this can be seen zoomed in Figure 6.8(b). The $\dot{V}O_2$ follows the reference and the power fluctuates between 4 and 5 W.

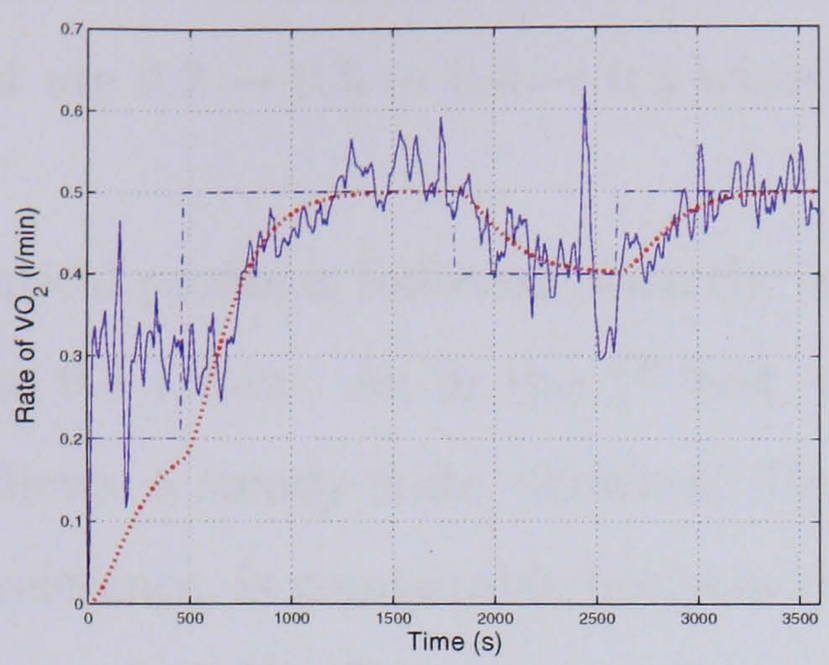

(a)

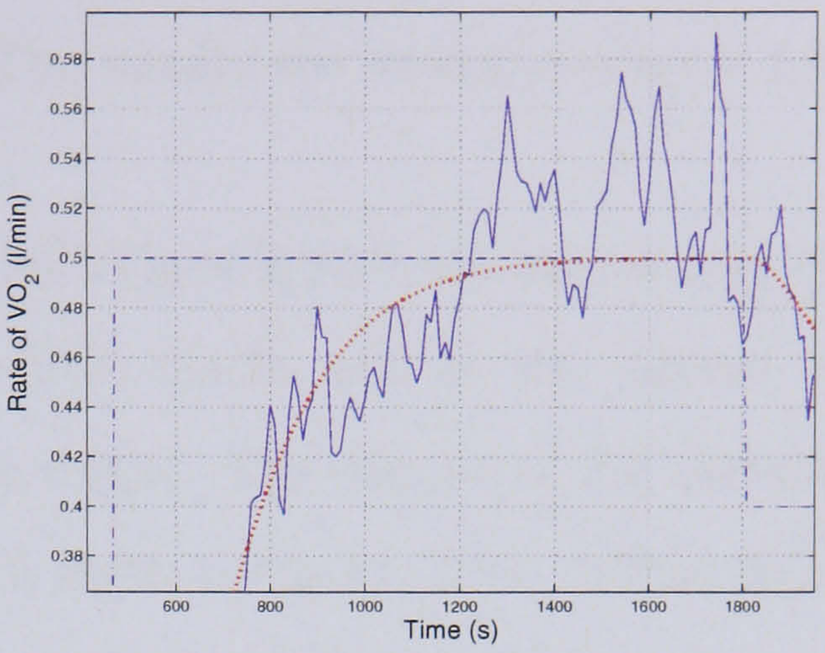

(b)

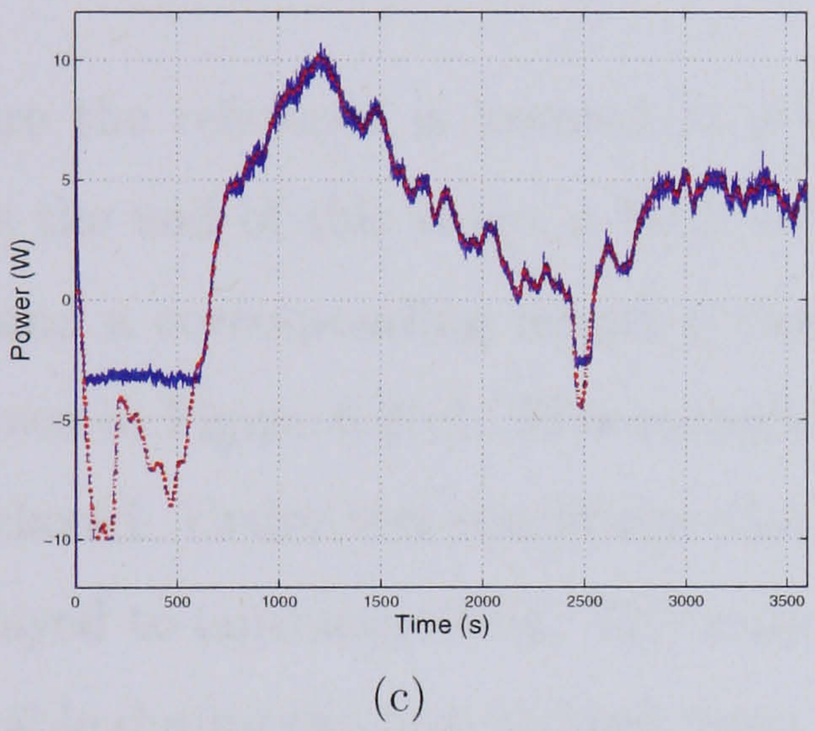

(c)

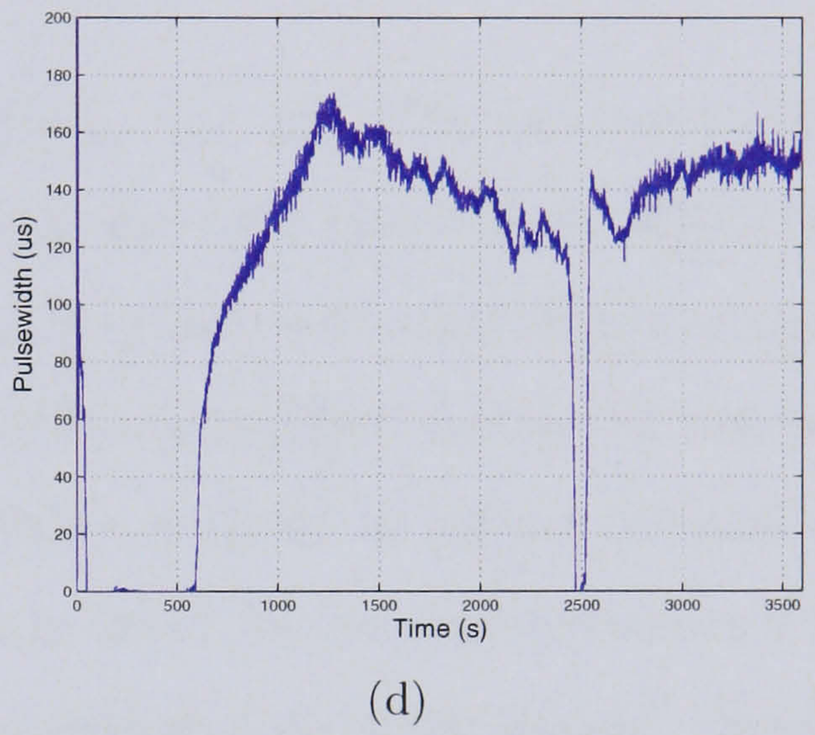

(d)

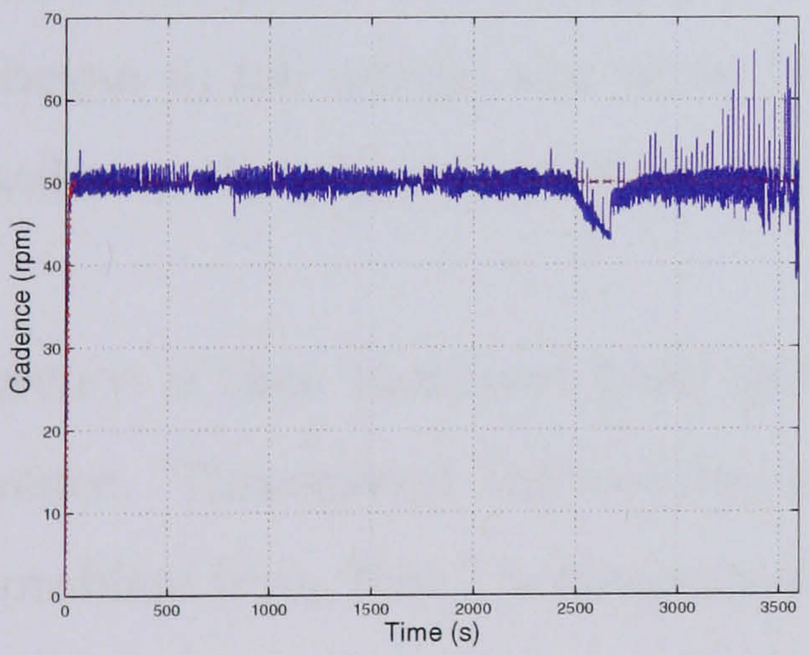

(e)

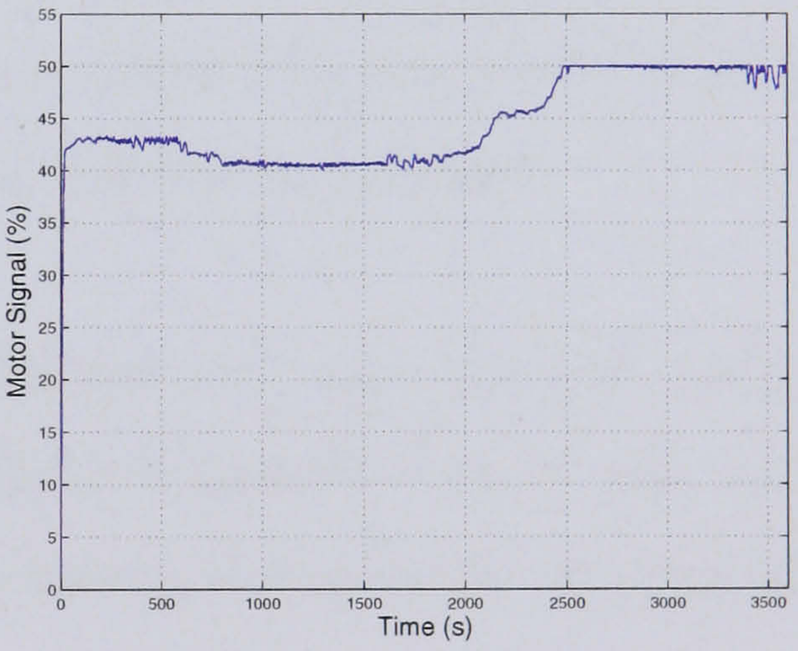

(f)

Figure 6.8: $\dot{V}O_2$ Test 7 : In all graphs the reference is the dashed line, the measured data the solid line and the ideal response the dotted line. The figures show : (a) the $\dot{V}O_2$ controller response, (b) a magnified section of the $\dot{V}O_2$ response, (c) the power controller response, (d) the resulting stimulation from the power controller, (e) the motor controller response and (f) the motor input signal.

6.5.2 Test 8

The controller used in this test is Controller 4 and the $\dot{V}O_2$ reference increments in this test are $0.2 \rightarrow 0.5 \rightarrow 0.4 \rightarrow 0.5$ l/min. The results are shown in Figure 6.9.

An identical profile is followed, with the initial $\dot{V}O_2$ of 0.2 l/min, followed by the transition to 0.5 l/min. As in the 1^{st} test the $\dot{V}O_2$ tracks well to the desired response and achieves a steady state, shown in Figure 6.9(a). The output of the controller, the power reference, is comparable between the 2 tests, rising to 10 W, before reducing to approximately 5 W. This response is shown zoomed in Figure 6.9(c).

As before the reference is lowered to 0.4 l/min, and the $\dot{V}O_2$ reduces to this level. Towards the end of this stage, a large spike in the $\dot{V}O_2$ is recorded, shown in Figure 6.9(a), and a corresponding negative change in power and stimulation to counteract this, shown in Figure 6.9(c). This is explained by the subject during the test becoming "too" relaxed. Under test conditions this subject is asked to remain relaxed, and music is played to encourage this. The subject is asked by the experimenters if they are comfortable during the test, to keep them concentrated on being relaxed. However, the subject began to fall asleep, and when he was asked if he was comfortable, it caused him to wake up sharply and consequently his ventilation increased.

The reference is then increased back to 0.5 l/min and again the $\dot{V}O_2$ tracks well to the reference. Throughout the test the cadence is controlled to 50 rpm and the low battery problem from Test 7 is eliminated by having the batteries charging throughout the test, shown in Figures 6.9(e) and 6.9(f).

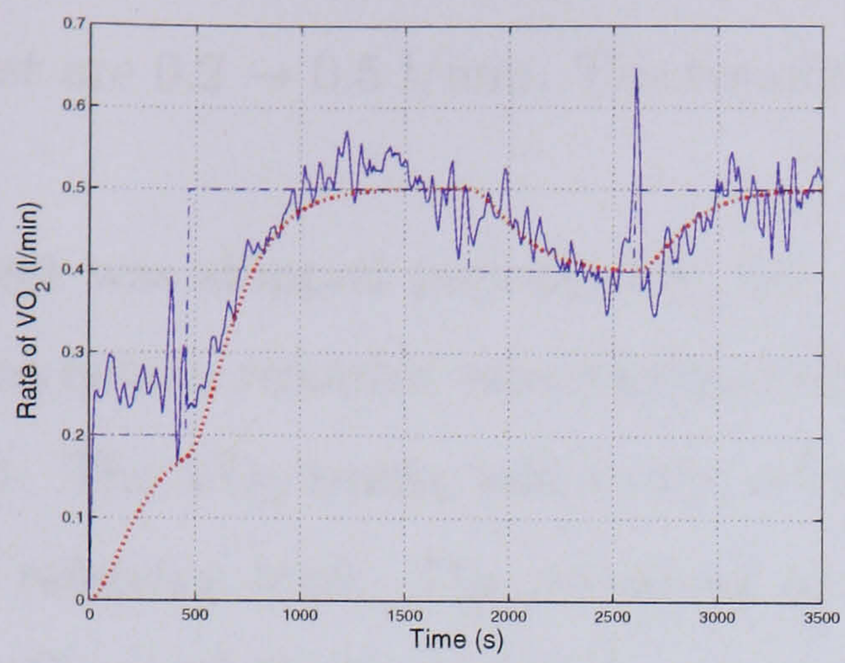

(a)

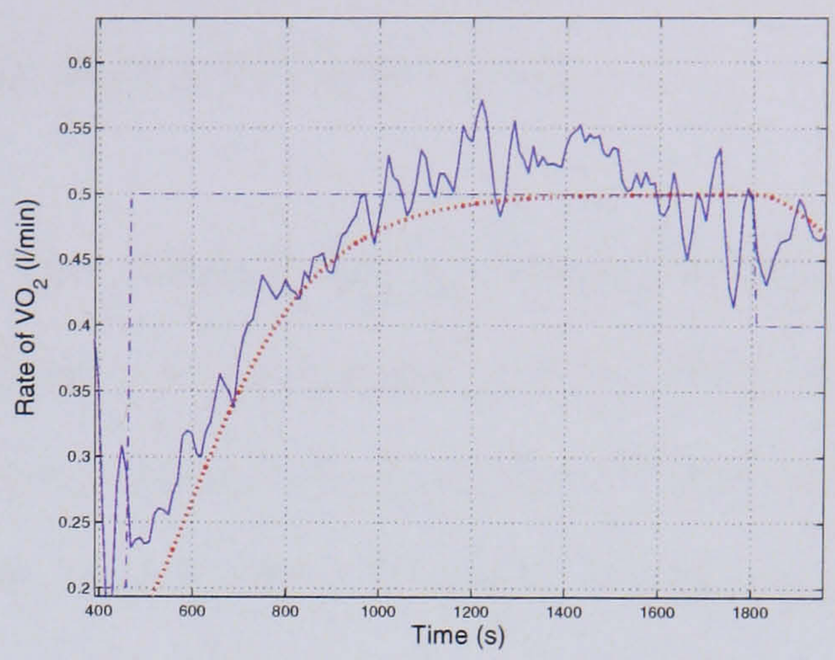

(b)

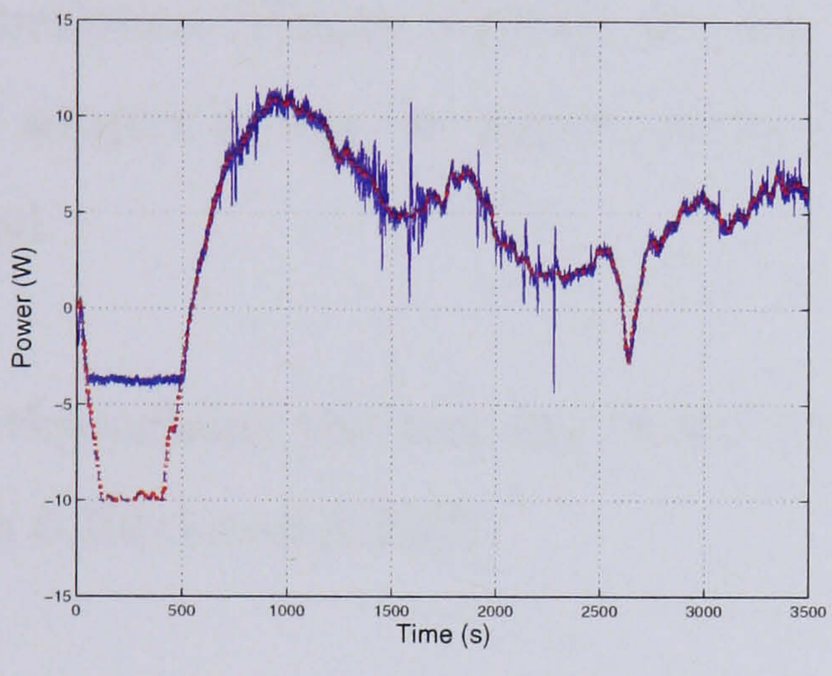

(c)

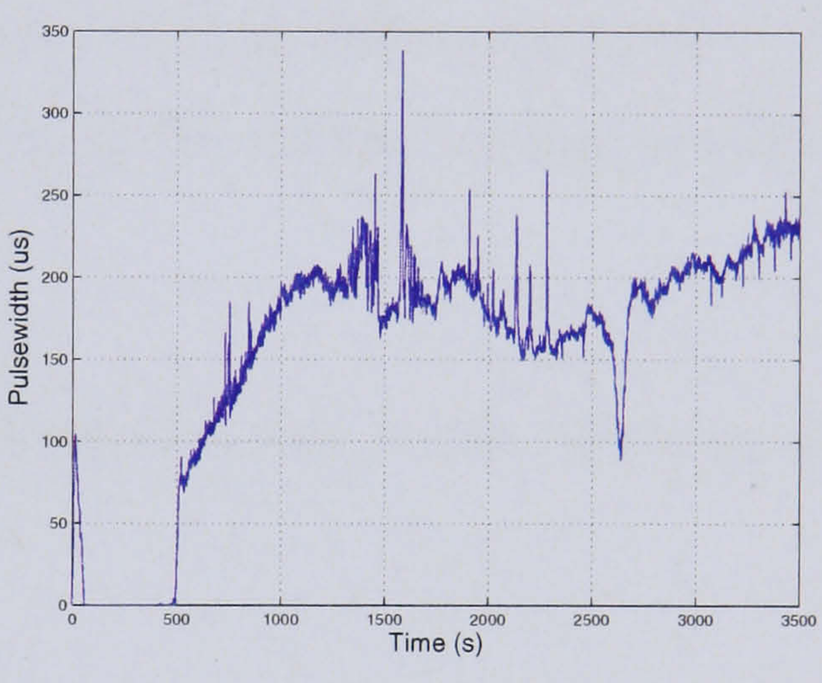

(d)

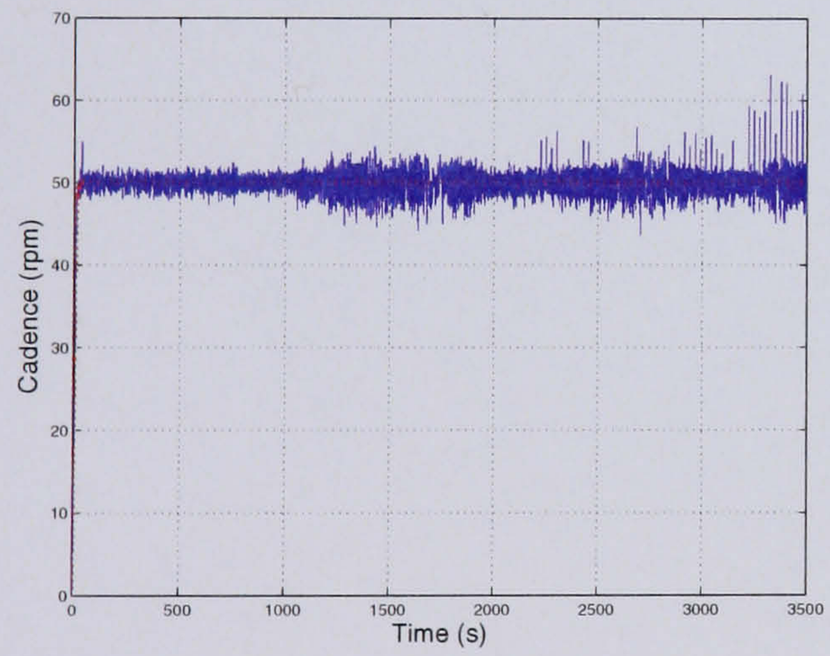

(e)

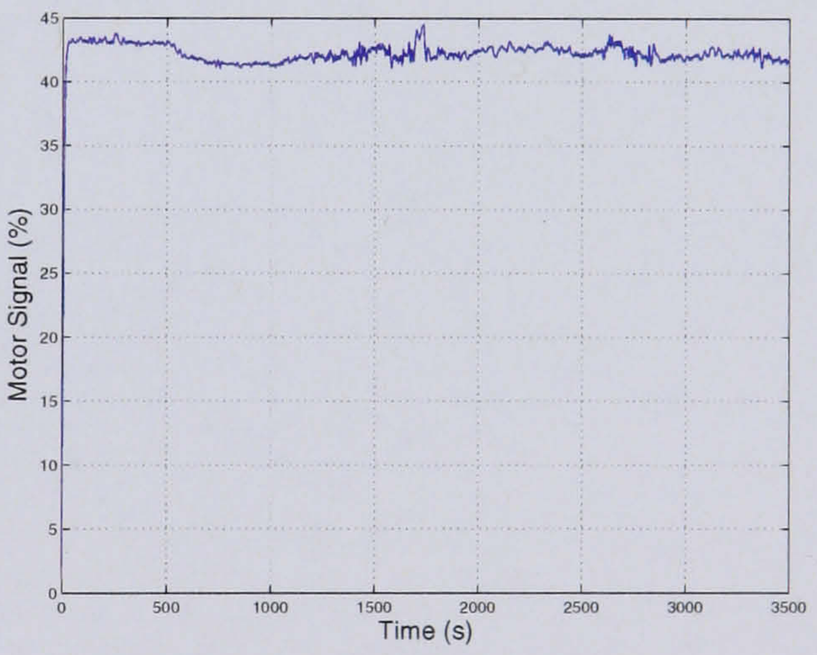

(f)

Figure 6.9: $\dot{V}O_2$ Test 8 : In all graphs the reference is the dashed line, the measured data the solid line and the ideal response the dotted line. The figures show : (a) the $\dot{V}O_2$ controller response, (b) a magnified section of the $\dot{V}O_2$ response, (c) the power controller response, (d) the resulting stimulation from the power controller, (e) the motor controller response and (f) the motor input signal.

6.5.3 Test 9

The controller used in this test is Controller 4 and the $\dot{V}O_2$ reference increments in this test are $0.2 \rightarrow 0.5$ l/min. The results are shown in Figure 6.10.

This test was stopped prematurely, due to the subject feeling uncomfortable. However the results recorded nevertheless still show a step change in $\dot{V}O_2$, seen in Figure 6.10(a). The $\dot{V}O_2$ tracks well to the reference, overshooting slightly before returning to the reference level. The overshoot results in a maximum power of approximately 10 W (Figure 6.10(c)), before it reduces to 5 W. The spikes in both the power and the stimulation (Figure 6.10(d)) are due to the subject shifting position on the seat. As the subject moves, he applies extra power to the pedals, causing the fluctuations recorded.

Again throughout the test the cadence is controlled well to the reference, shown in Figures 6.10(e) and 6.10(f).

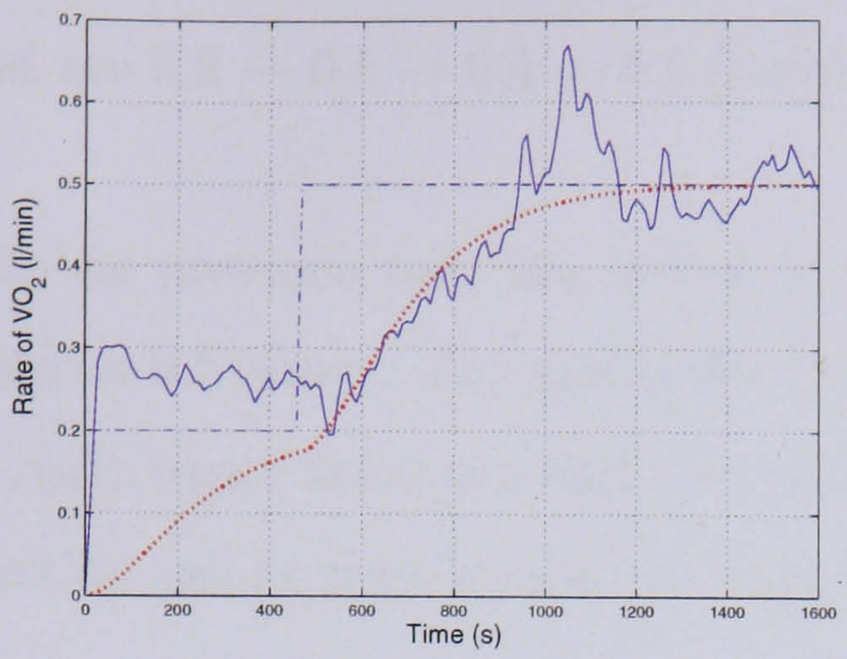

(a)

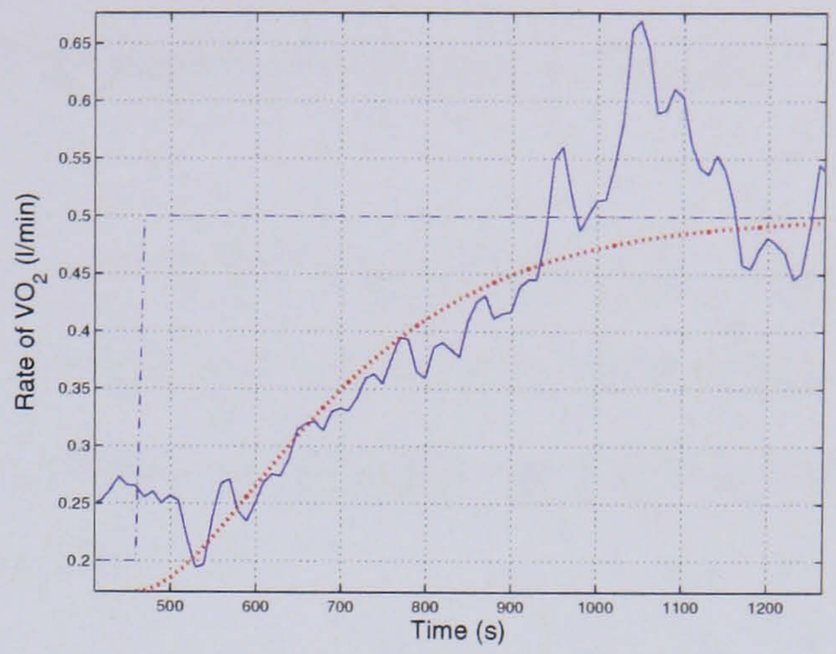

(b)

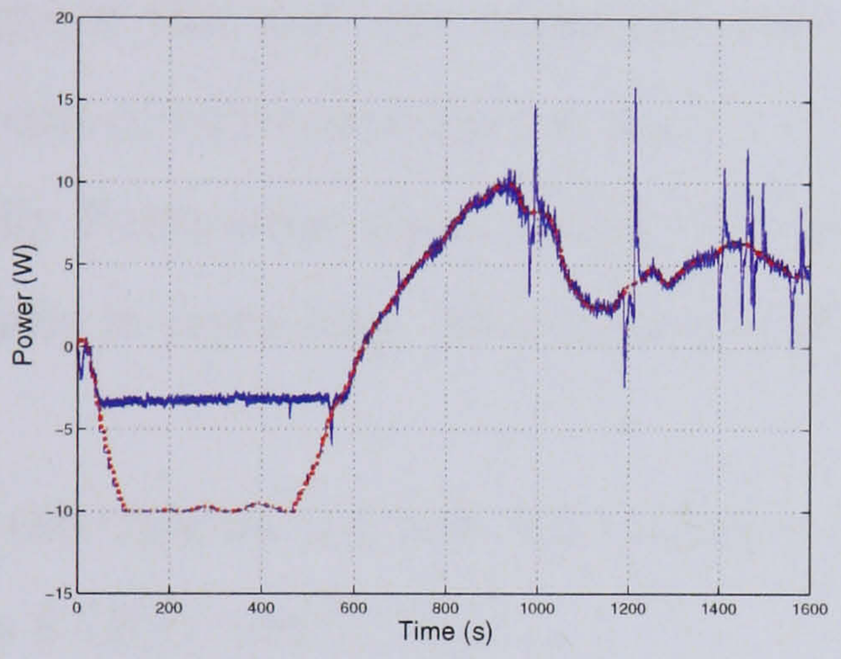

(c)

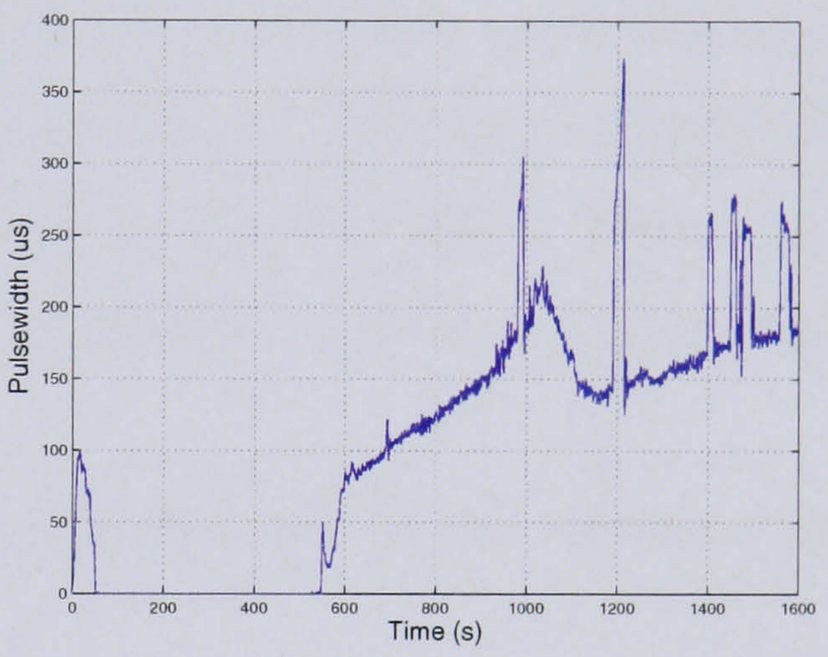

(d)

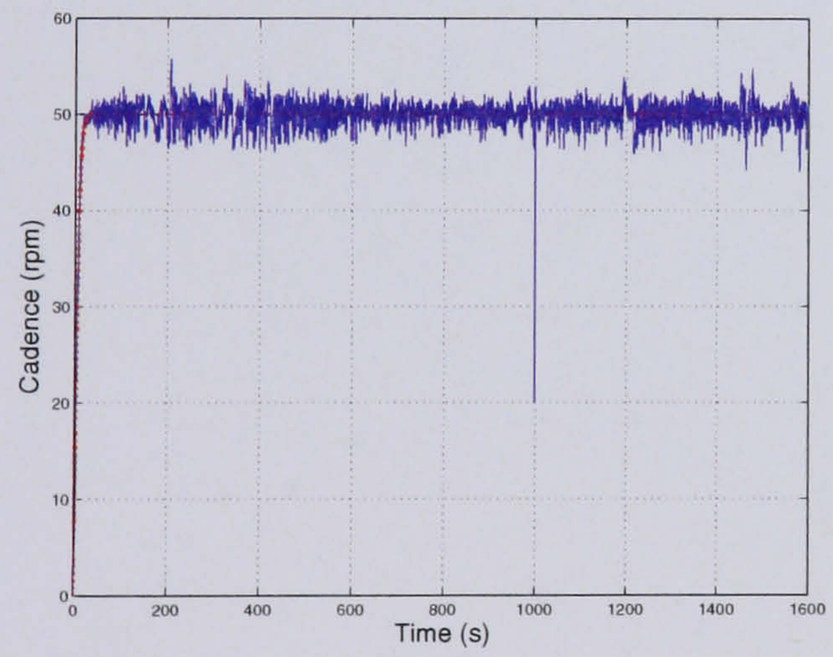

(e)

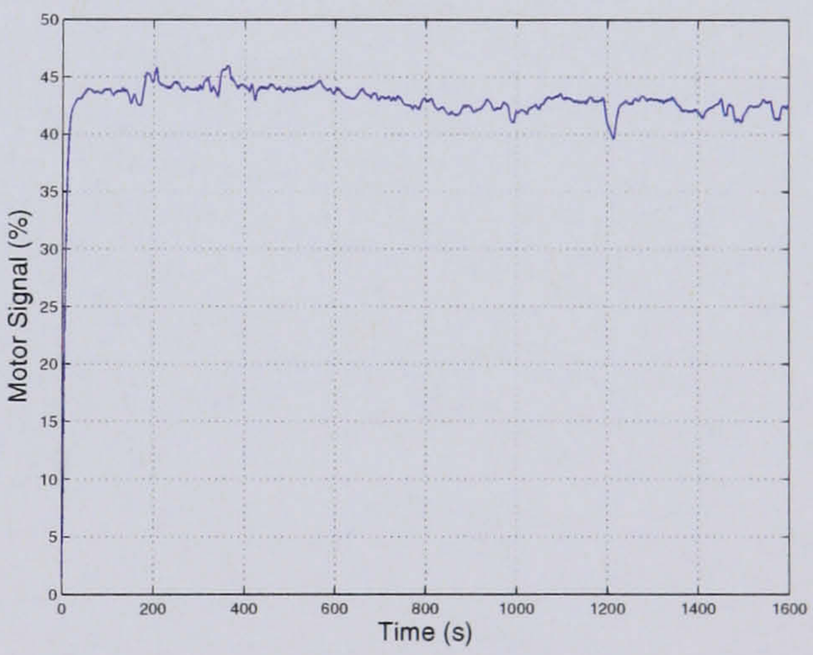

(f)

Figure 6.10: $\dot{V}O_2$ Test 9 : In all graphs the reference is the dashed line, the measured data the solid line and the ideal response the dotted line. The figures show : (a) the $\dot{V}O_2$ controller response, (b) a magnified section of the $\dot{V}O_2$ response, (c) the power controller response, (d) the resulting stimulation from the power controller, (e) the motor controller response and (f) the motor input signal.

6.5.4 Test 10

The controller used in this test is Controller 4 and the $\dot{V}O_2$ reference increments in this test are $0.2 \rightarrow 0.5 \rightarrow 0.4 \rightarrow 0.5$ l/min. The results are shown in Figure 6.11.

As with the previous test, the initial $\dot{V}O_2$ is set at 0.2 l/min before the reference is increased to 0.5 l/min. The measured $\dot{V}O_2$ is seen to track well to the reference (Figure 6.11(a)), again there is a slight overshoot, before it oscillates around the reference. This section can be seen zoomed in Figure 6.11(b).

Throughout this test, the measured power appears to fluctuate more than in the previous tests of this controller, as shown in Figure 6.11(c). This may be due to the $\dot{V}O_2$ naturally fluctuating more, which is noticeable in the first 300 s, where the $\dot{V}O_2$ is essentially in open loop. The corresponding stimulation is show in Figure 6.11(d).

Again throughout the test the cadence is controlled well to the reference, shown in Figures 6.11(e) and 6.11(f).

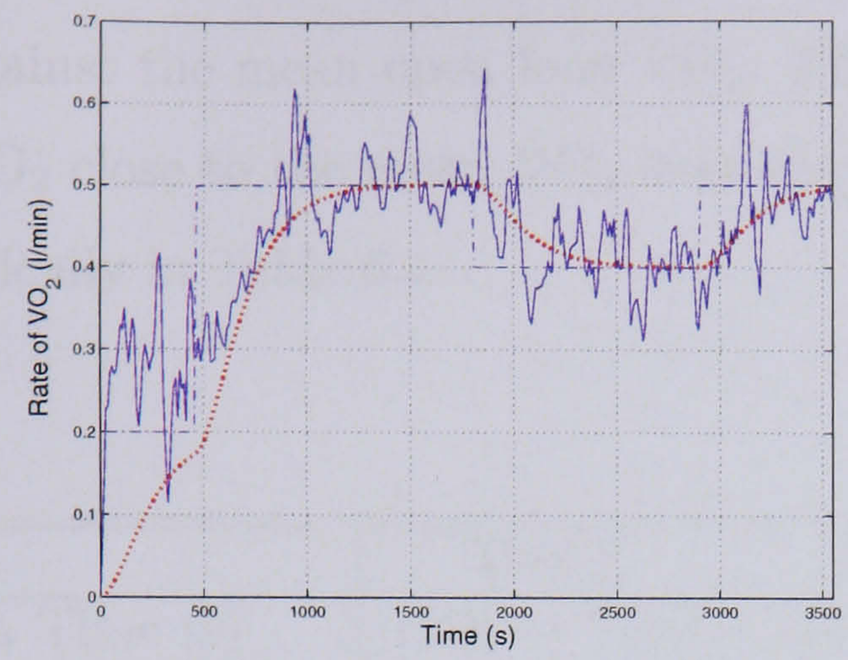

(a)

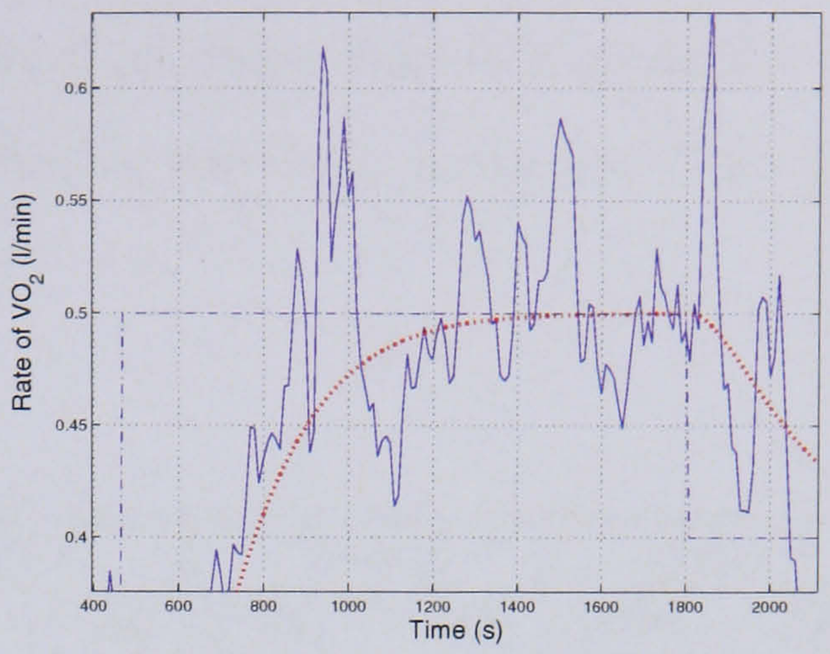

(b)

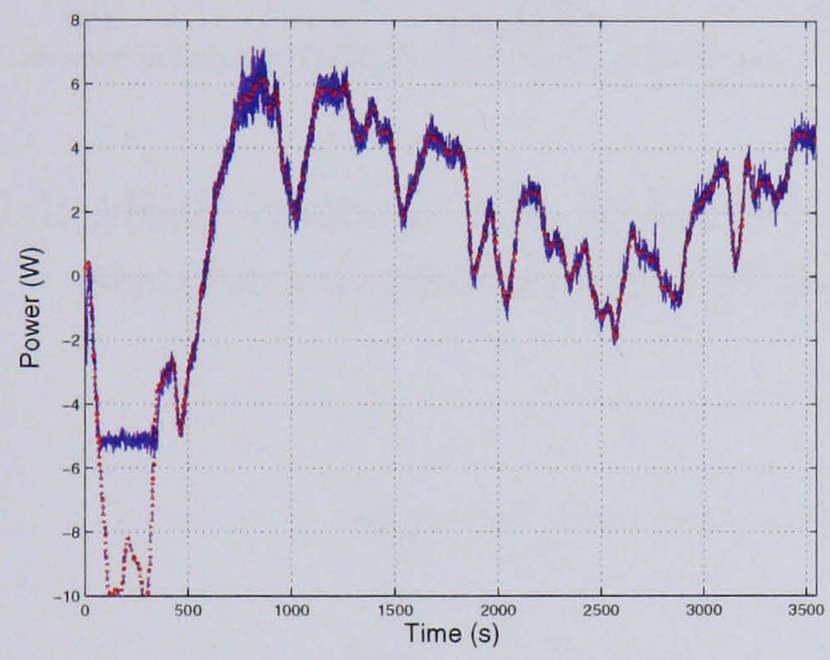

(c)

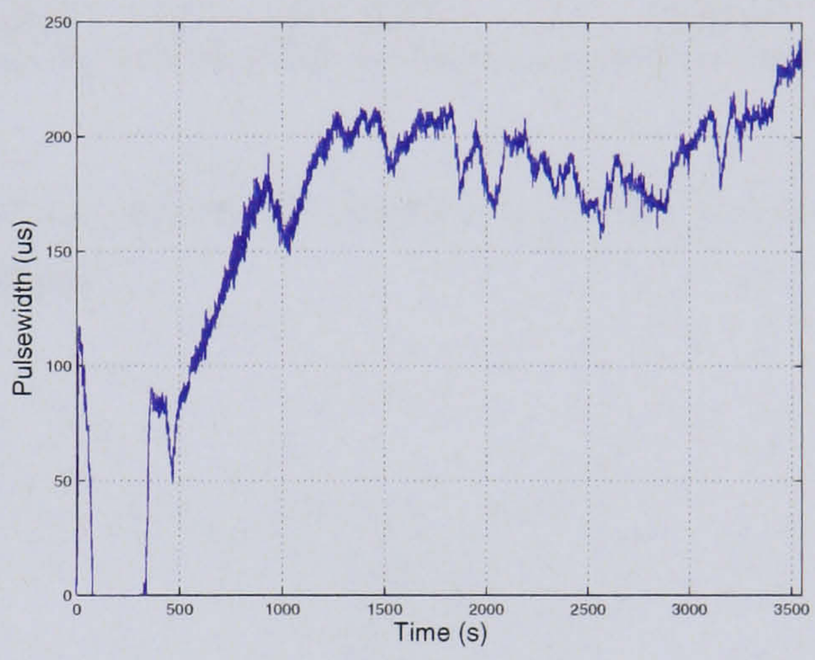

(d)

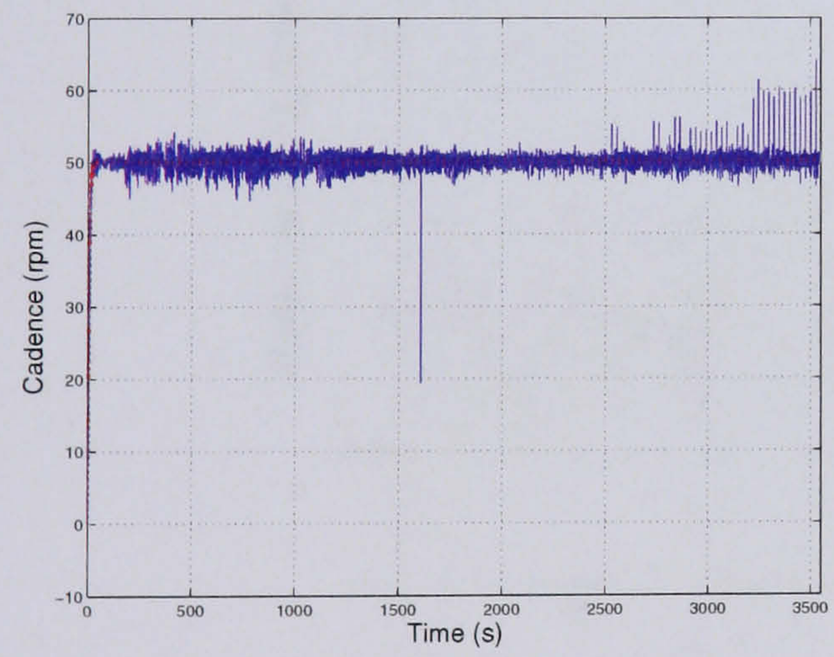

(e)

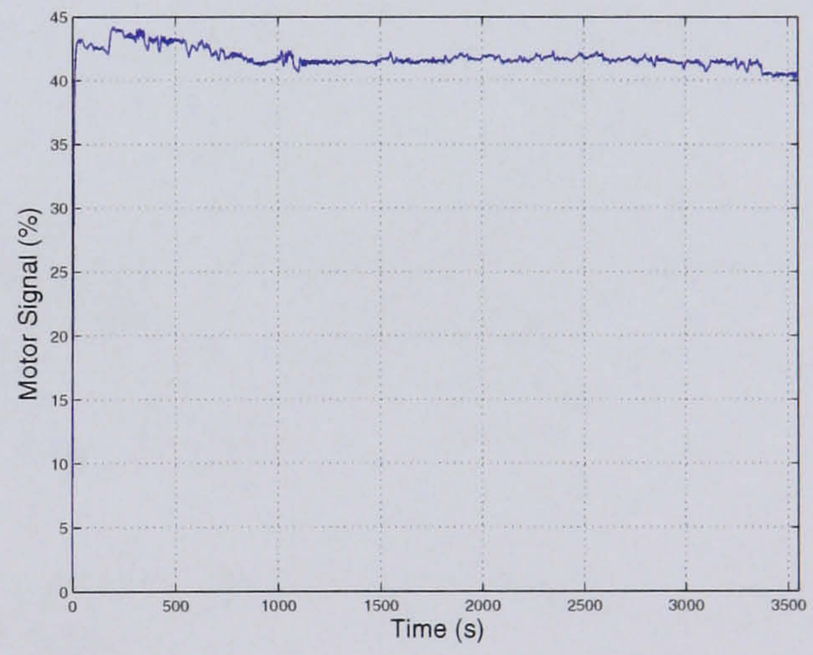

(f)

Figure 6.11: $\dot{V}O_2$ Test 10 : In all graphs the reference is the dashed line, the measured data the solid line and the ideal response the dotted line. The figures show : (a) the $\dot{V}O_2$ controller response, (b) a magnified section of the $\dot{V}O_2$ response, (c) the power controller response, (d) the resulting stimulation from the power controller, (e) the motor controller response and (f) the motor input signal.

6.5.5 Controller 4 Analysis

As before, a section of mean $\dot{V}O_2$ data is taken from each test at 0.5 l/min and is plotted against the mean open loop $\dot{V}O_2$. Figure 6.12 shows that this controller controls the $\dot{V}O_2$ close to the mean $\dot{V}O_2$ level identified in the Open Loop test. This is shown numerically in Table 6.4.

	Test 7	Test 8	Test 9	Test 10	Open Loop
$\triangle$ Time (s)	1100 $\rightarrow$ 1700	1000 $\rightarrow$ 1600	1000 $\rightarrow$ 1600	1000 $\rightarrow$ 1600	1400 $\rightarrow$ 2000
Mean $\dot{V}O_2$ (l/min)	0.5402	0.5215	0.5139	0.4982	0.5219
sd	0.0227	0.0321	0.0528	0.0381	0.0217

Table 6.4: Mean values of the $\dot{V}O_2$ data during selected sections of the 5 tests. The standard deviations are also presented.

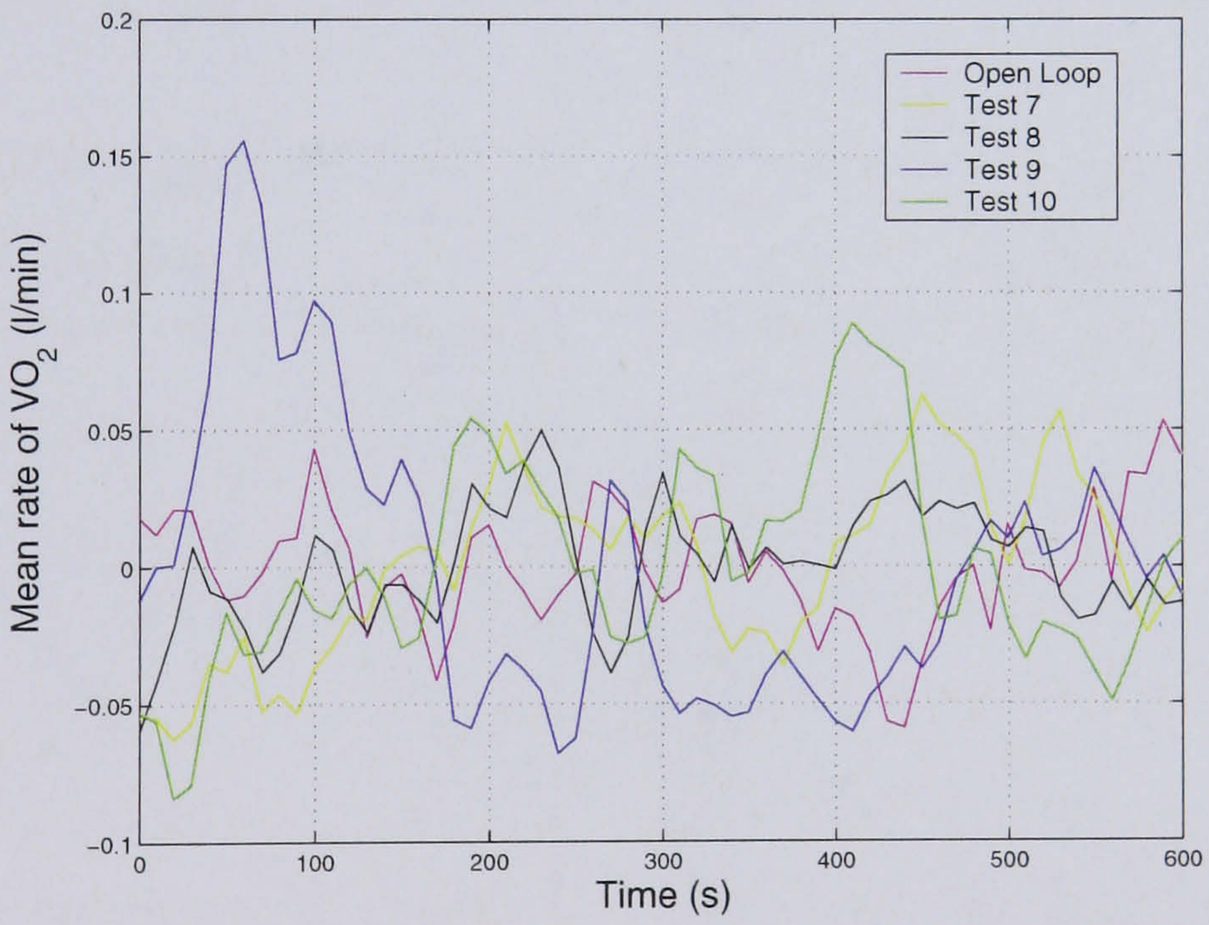

Figure 6.12: Shows the deviation from the mean value and standard deviation for the 4 tests with Controller 4 and the 1 Open Loop test.

6.6 Discussion of $\dot{V}O_2$ Control

6.6.1 Mean $\dot{V}O_2$ Revisited

As previously discussed $\dot{V}O_2$ is not only dependent on the power level; factors such as how the subjects is feeling physically and the environmental conditions can effect the measurements. The mean plots have compared the controllers' performance with one Open Loop test. A more accurate comparison would be for an open loop measurement on the day of each test.

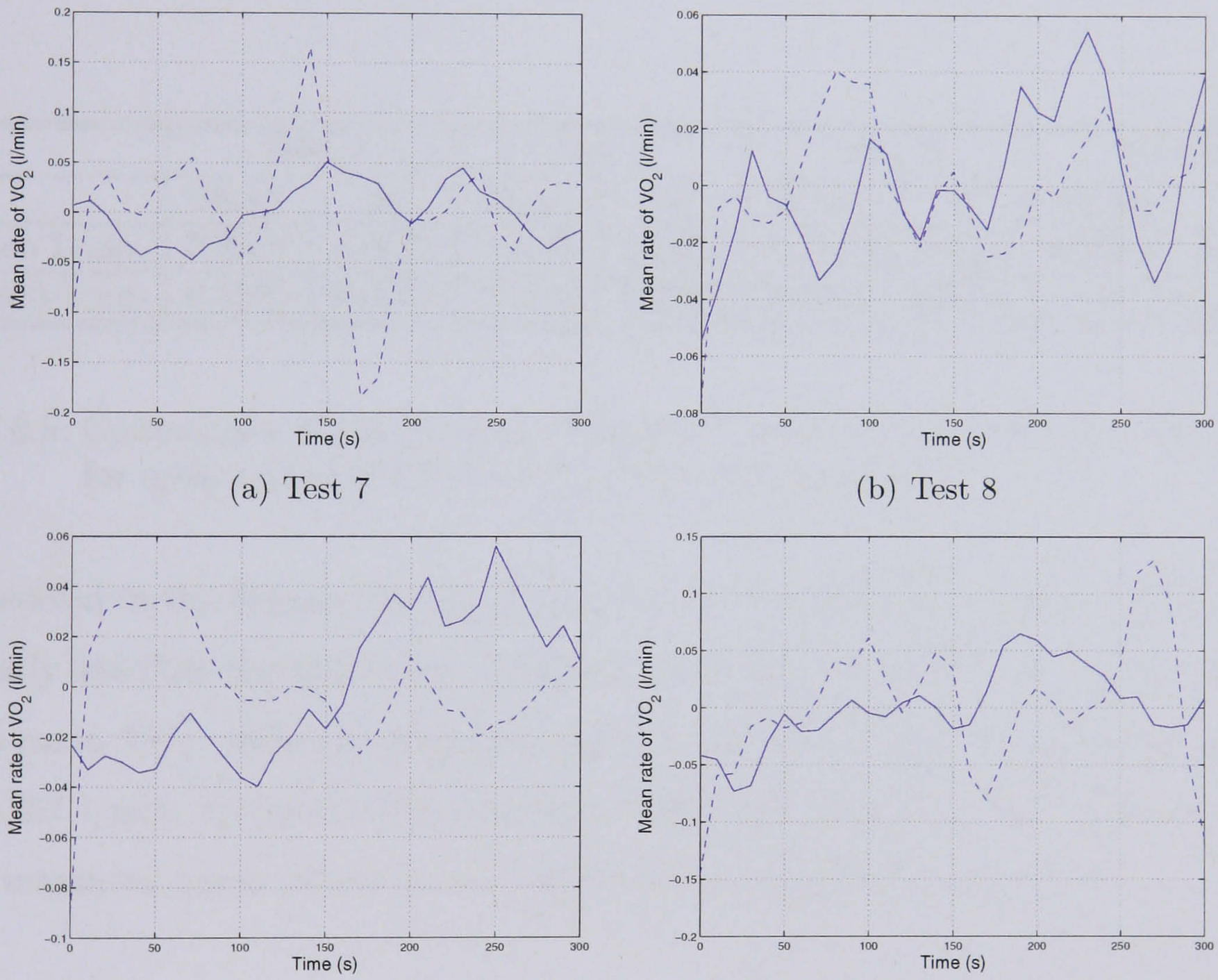

(a) Test 7

(b) Test 8

(c) Test 9

(d) Test 10

Figure 6.13: The figures show the Closed Loop $\dot{V}O_2$ control as the solid line and the Open Loop ($\dot{V}O_2$) as the dashed line

This can be achieved by examining the first 300 s of each test. During this period the reference $\dot{V}O_2$ is set below the level of resting $\dot{V}O_2$, therefore the power references decrease below the stimulation threshold. This means that the $\dot{V}O_2$ is essentially in

open loop control. As before the open loop $\dot{V}O_2$ is compared with a section of closed loop $\dot{V}O_2$, controlled to 0.5 l/min. Figure 6.13 shows both the open and closed loop for Tests 7 to 10.

Figure 6.13 shows that the variation in $\dot{V}O_2$ in both states of control are comparable, and in some cases the closed loop offers a reduction in variation. This is shown in Figures 6.13(a) and 6.13(d), where the open loop visually exceeds the levels of the the closed loop control. In Figures 6.13(b) and 6.13(c) the variation is similar. These observations are reinforced by Table 6.5. This table shows the mean levels for open and closed loop control and the standard deviation from the mean.

	Test 7		Test 8		Test 9		Test 10	
	Mean	sd	Mean	sd	Mean	sd	Mean	sd
Open Loop	0.2998	0.0672	0.2573	0.0227	0.2680	0.0243	0.2876	0.0599
Closed Loop	0.5235	0.0282	0.5170	0.0264	0.4934	0.0293	0.4873	0.0342

Table 6.5: Comparison of the mean and standard deviation (sd) from the mean ($\dot{V}O_2$), for open and closed loop control from the same test.

As observed in the figures, the closed loop standard deviation in Tests 7 and 10 is significantly less than the open loop. A second observation from Table 6.5 is the variation in the mean $\dot{V}O_2$. When in open loop control the $\dot{V}O_2$ is seen to vary between 0.299 and 0.257 l/min, across the four test days. This again indicates the variation in $\dot{V}O_2$ when measured under identical test conditions across different test days.

6.7 Conclusions

The results of this series of tests show that $\dot{V}O_2$ control during FES cycling can be achieved. The subject was able to cycle at various levels of $\dot{V}O_2$ for prolonged periods. The conclusions drawn from these tests are summarised below;

PRBS Design The characteristics of the PRBS identified the fast dynamics of the $\dot{V}O_2$, but failed to capture the overall rise time. The result of this was that the controller was responding too fast to changes in the reference. This was identified after the first 4 tests and when the open loop $\dot{V}O_2$ response was investigated The PRBS therefore should be redesigned to enable the overall dynamics to be identified during one identification test. The PRBS highlighted the variability of the $\dot{V}O_2$ dynamics over identical tests on different test days.

Open Loop Dynamics Measurement of the open loop $\dot{V}O_2$ enabled the overall rise time to be measured. This rise time was used in the controller design process to improve the behaviour of the controller.

Model Variability The two identified models showed the variability in identical tests. The rise times of the models were nearly a factor of 2 different (75 and 130 s). This is believed to be due to the physical condition of the subject on the test day, and how the muscles react differently to stimulation.

Real Time Averaging Measurement of the $\dot{V}O_2$ dynamics in real-time and subsequent averaging and use as a controllable variable proved successful. The $\dot{V}O_2$ was sampled such that the the maxima and minima were removed in a 30 s sample and the remaining $\dot{V}O_2$ samples were averaged. The correlation between the $\dot{V}O_2$ averaging and the sample rate are maintained to avoid problems with the real-time toolbox. The selection of the 30 s averaging, or sample, rate of the $\dot{V}O_2$ has been shown to be of a length such that changes in the $\dot{V}O_2$ are of significant magnitude to be controlled.

Experiment Procedure The length of time involved in the $\dot{V}O_2$ identification and control tests are typically lengthy. Training cycling sessions with this subject

were typically three 20 minute bouts with a rest period between. The $\dot{V}O_2$ tests were typically in the region of one hour, not including the warm-up period. During this time, and a prior rest period, the subject had to wear the facemask for $\dot{V}O_2$ measurements. This may become uncomfortable and will not be enjoyable for the subject. Therefore $\dot{V}O_2$ control should be use intermittently throughout an FES cycling study.

Mean $\dot{V}O_2$ The mean $\dot{V}O_2$ gives a clear indication of the performance of the controller. The variation from the mean, the standard deviation, shows how the controlled $\dot{V}O_2$ differs from the uncontrolled, open loop $\dot{V}O_2$. The variation from the mean varies across test days, but if the controller is successful in reducing the variation from the mean consistently then $\dot{V}O_2$ control could prove to be a significant tool for FES cycling exercise tests .

Test Day Variation Across test days, variation is ideally kept to a minimum. Identical equipment, environment, personnel and procedures are adhered to, and this can be closely controlled. The only variable is the condition or fitness of the subject that undergoes the test. For example, subtle differences such as the subject having increased levels of spasm on the day of the test, may effect the performance. Increased spasm may cause the muscles to tighten, requiring a prolonged warm-up or stretching to be performed before cycling.

These small variabilities will have an effect on the results of a $\dot{V}O_2$ control test. An experienced FES cyclist will be able to judge in a relatively short period of time whether they will be able to cycle for the long period involved in these types of tests. This may result in the test being abandoned, but will result in the session being more enjoyable for the subject.

7 Conclusions and Recommendations for Future Work

In this thesis FES cycling has been developed from the early work by researchers such as Petrofsky through to work by Gföhler and Chen. They identified at an early stage that FES alone may not be a sufficient enough propellant for practical cycling. The integration of an electric motor through gearing and by means of a two loop control strategy overcomes this limitation. The control structure allows for the motor to compensate for a loss of stimulated muscle power, changes in terrain and wind. Thus far the motor has only been utilised in a laboratory environment, therefore it would be advantageous to develop a control strategy that allows for outdoor mobile cycling. This may be achieved by the incorporation of a Heinzmann Hub Motor[1], which is a more compact and lightweight design, in comparison to the motor discussed in this thesis.

Robust control and measurement of the power produced during FES cycling has been demonstrated. The SRM measurement system is integrated to provide accurate power control of the stimulated muscle. In previous studies power has been measured, but little attempt had been made to control it. Previously power has been measured on systems such as the MONARK or ERGYS. These systems measure the power produced at the rear wheel of the system, and therefore are not a true reflection of the power produced by the cyclist, as there are inevitably losses through the system. There is still scope for improvement of the power control. An adaptive control scheme which is based on various stimulation operating points may increase the accuracy of the power

[1] www.heinzmann.de

control. This may involve a control strategy with multiple controllers, which are activated depending on the magnitude of the stimulation required to achieve the desired power. Initial findings have shown that this is a possibility.

Further investigation would be possible into identification of the models and various different types of controllers. A study in the use of nonlinear controllers and models may enhance FES cycling.

The robust control of power and cadence has been developed to provide a stable test bed for exercise testing. While the cadence is held constant, by means of an electric motor, the power can be varied to allow for the implementation of both constant load and incremental exercise tests. Additionally, safety measures are incorporated into the control structure to aid both the experimenter and the subject. The ability to undergo exercise testing safely and with a high accuracy of repeatability under experimental conditions will help to prove the health benefits of FES cycling. Studies are underway in a number of groups to show this.

$\dot{V}O_2$ control is a new and unique concept. In this one subject feasibility study, $\dot{V}O_2$ control has been shown to be a realistic concept. The $\dot{V}O_2$ characteristics of the subject are identified and controllers are designed in relation to the $\dot{V}O_2$ dynamics. However further investigation is required into the identification of $\dot{V}O_2$ dynamics and the PRBS used for identification. A results from this type of investigation may provide information on the delay of the $\dot{V}O_2$ response. Logical steps are followed to develop these controllers, through the results gained in each $\dot{V}O_2$ cycling test. The final controller design is shown to accurately control the subject's $\dot{V}O_2$ while they perform FES cycling. However, this is only a single subject study. In practice these tests are lengthy in time to implement. Therefore a way forward to undertake these tests in a shorter time would be beneficial. A number of subjects are required to determine the applicability of the approach to the wider SCI population. $\dot{V}O_2$ control opens up new methods and approaches to exercise testing. Instead of controlling the power, a $\dot{V}O_2$ level can be defined which can monitored by an experienced experimenter during the

test, as to determine whether the cyclist will be able to maintain the prescribed level. $\dot{V}O_2$ control presents applications outside the paraplegic population. $\dot{V}O_2$ control could be utilised with the AB population in applications such as running, cycling and rowing.

Further recommendations relate to FES cycling moving away from the laboratory. Advancements are required so that FES cycling can be an effective recreational activity, that a subject can participate in without the need for experimenters to be present. Similarly, the introduction of FES cycles into sports centres would open up FES cycling to the general paraplegic population. Under recommendation from the subject's doctor and physiotherapist, they could participate in cycling away from the spinal units, alongside AB persons. The FES cycling system presented within this thesis has been developed for commercialisation by Hasomed GmbH[2] and will soon be released on the market.

[2] www.hasomed.de

List of References

[1] T. Angeli, M. Gföhler, T. Ebetharter, and L. Rinder. Tricycle for paraplegics using functional electrical stimulation. *Med. Biol. Eng. and Comput.*, 37:326–327, 1999.

[2] T.J. Barstow, A.M.E. Scremin, D.L. Mutton, C.F. Kunkel, T.G. Cagle, and B.J. Whipp. Gas exchange kinetics during functional electrical stimulation in subjects with spinal cord injury". *Medicine and science in sports and exercise*, 27:1284–1291, 1995.

[3] T.J. Barstow, A.M.E. Scremin, D.L. Mutton, C.F. Kunkel, T.G. Cagle, and B.J. Whipp. Changes in gas exchange kinetics with training in patients with spinal cord injury. *Med. and Sci. in Sports and Exercise*, 28(10):1221–1128, 1996.

[4] K.K. BeDell, A.M. Scremin, K.L. Perell, and C.F. Kunkel. Effects of FES-induced lower extremity cycling on bone density of spinal cord injured patients. *Amer J. of Phys. Med. and Rehab.*, pages 29–34, 1996.

[5] H.W.A. Berkelmans, M. Arns, and J. Duysens. The development of a hybrid outdoor FES bike. In *8th Annual IFESS Conference*, pages 112–113. IFESS, 2003.

[6] H.W.A. Berkelmans, D.H.J. Thijssen, P. Heesterbeek, B.T.J. Van Ginneken, M.T.E. Hopman, D.H. Van Kuppevelt, and J. Duysens. Physiological responses after 4 weeks training with a hybrid FES tricycle system in spinal cord injured individuals. In *9th Annual IFESS Conference*, pages 174–175. IFESS, 2004.

[7] S.A. Binder-MacLeod and W.B. Scott. Comparison of fatigue produced by various electrical stimulation trains. *Acta. Physiology Scand*, (171):195–203, 2001.

[8] J. Chavarren and J.A.L. Calbet. Cycling efficiency and pedalling rate in road cyclists. *Eur J. Applied Physiology*, 80:555–563, 1999.

[9] J.J. Chen, C. Shih, D. Huang, N. Yu, M. Ju, and T. Huseh. Development of FES-cycling system with closed loop control. *Chinese J. Med Biol. Eng.*, 14(3):195–208, 1994.

[10] J.J. Chen and N.Y. Yu. The validity of stimulus-evoked EMG for studying muscle fatigue characteristics of paraplegic subjects during dynamic cycling movement. *IEEE Trans. on Rehab. Eng.*, 5(2):170–178, 1997.

[11] J.J. Chen, N.Y. Yu, and D. Huang. Applying fuzzy logic to control cycling movement induced by FES. *IEEE Trans. on Rehab. Eng.*, 5(2):158–167, 1997.

[12] M. Cifrek, S. Tonković, and V. Medved. Measurement and analysis of surface myoelectric signals during fatigued cyclic dynamic contractions. *Measurement*, 27:85–92, 2000.

[13] A.M. Edwards, N.V. Challis, and J.H. Chapman. The test-retest reliability of gas exchange kinetics in humans using a pseudo binary sequence exercise test. *Eur. J. Appl Physiol.*, 2001.

[14] P.C. Eser and N. de N. Donaldson. Influence of different stimulation frequencies on power output during fes-cycling in recently injured SCI people. *Trans. Neural Sys. Rehabil. Eng.*, 11(3):236–240, 2003.

[15] P.D. Faghri. Enhancing physical fitness in spinal cord injured individuals through new technology. *CSUN99 Papers, Session 228*, 1998.

[16] P.D. Faghri, R.M. Glaser, and S.F. Figoni. FES leg cycle ergometer exercise: training effects on cardiorespiratory responses of spinal cord injured subjects at rest and during submaximal exercise. *Arch. Phys. Med. Rehab.*, 73:1085–1093, 1992.

[17] C. Ferrario, B. Stone, K.J. Hunt, S.A Ward, A.N. McLean, and M.H.Fraser. Oxygen cost of different stimulation patterns on FES cycling. *9th Annual IFESS Conference*, September 2004.

[18] J.C. Franco, K.L. Perell, Gregor R.J, and A.M.E. Scremin. Knee kinetics during FES induced cycling in subjects with SCI. *J. of Rehab. Research and Development*, 36(3):1–11, 1999.

[19] G.F. Franklin, J.D. Powell, and A. Emami-Naeini. *Feedback Control of Dynamic Systems.* Addison-Wesley, third edition, 1994.

[20] M. Gföhler, T. Angeli, T. Eberharter, P. Lugner, W. Mayr, and C. Hofer. Test bed with force measuring crank for static and dynamic investigations on cycling by means of functional electrical stimulation. *IEEE Trans. on Neural Sys. and Rehabil. Eng.*, 9(2):169–180, 2001.

[21] M. Gföhler, M. Loicht, and P. Lugner. Exercise tricycle for paraplegics. *Med. biol. Eng. Comput.*, 36:118–121, 1998.

[22] M. Gföhler and P. Lugner. Cycling by means of Functional Electrical Stimulation. *IEEE Trans. on Rehab. Eng.*, 8(2):233–243, 2000.

[23] R.M. Glaser, S.F. Figoni, S.R. Collins, M.M. Rodgers, A.G. Suryaprasad, S.C. Gupta, and T. Mathews. Physiological respones of SCI subjects to electricaly induced leg cycle ergometry. *IEEE Engineering in Med. and Bio. Society 10th annual international conference*, 1998.

[24] R.M. Glaser, S.F. Figoni, S.P. Hooker, M.M. Rodgers, B.N. Ezenwa, A.G. Suryaprasad, S.C. Gupta, and T. Mathews. Efficiency of FNS leg cycle ergometry. *IEEE Trans. in Med. and Biol.*, 1989.

[25] R.M. Glaser, J.A. Gruner, S.D. Feinberg, and S.R. Collins. Locomotion via paralysed leg muscles: Feasibility study for leg propelled vehicle. *J. of Rehab. R and D*, 20(1):87–92, 1983.

[26] C.A. Glass. *Spinal Cord Injury, Impact and Coping.* BPS Blackwell, 1999.

[27] Henry Gray. *Gray's Anatomy: The Classic Edition.* Gramercy Books, 1991.

[28] K.W. Hammell. *Spinal Cord Injury Rehabilitation*, volume 1. Chapman and Hall, 1995.

[29] D.W. Hill. The critical power concept - A review. *Sports Medicine*, 16(4):237–254, 1993.

[30] N. Hjeltnes, A.K. Aksnes, and K.I. Birkeland. Improved body composition after 8 wks of electrically stimulated leg cycling in tetraplegic patients. *Amer. J. Physiol.*, 275:1072–1079, 1997.

[31] S.P. Hooker, S.F. Figoni, R.M. Glaser, M.M. Rodgers, B.N. Ezenwa, and P.D. Faghri. Physiologic responses to prolonged electrically stimulated leg cycle exercise in the spinal cord injured. *Arch. Phys. Med. Rehab.*, 71:863–869, 1990.

[32] S.P. Hooker, A.M.E. Scremin, D.L. Mutton, C.F. Kunkel, and G. Cagle. Peak and submaximal physiological responses following electrical stimulation leg cycle ergometer training. *J. of Rehab. R and D*, 32(4):361–366, 1995.

[33] K.J. Hunt, H. Gollee, R.-P. Jaime, and N. de N. Donaldson. Design of feedback controllers for paraplegic standing. *IEE Proc. - Theory Appl.*, 148(2), March 2001.

[34] K.J. Hunt, T. Schauer, and N. Negäard. A pilot study of lower limb FES cycling in paraplegia. *Proc. 7th Ann. Conf. Int. FES Soc., (Ljubljana, Slovenia)*, 2002.

[35] K.J. Hunt, B. Stone, N. Negaard, T. Schauer, M.H. Fraser, A.J. Cathcart, S.A. Ward, and S. Grant. Control strategies for integration of electric motor assist and functional electrical stimulation in paraplegic cycling: utility for exercise testing and mobile cycling. *IEEE Trans. on Neural Sys. and Rehab. Eng*, 12(1):89–101, March 2004.

[36] P.L Nash Jacobs, M.S. Nash, and C.D. Mintz. Assessment of fractional expired gases and air flow by an ambulatory metabolic analyser. *J. of the american society of exercise physiology*, 2(4):20–28, 1999.

[37] K.B. James, R.B. Stein, S.L. Chong, and A.k. Thompson. Design history of a leg propelled wheelchair using FES. In *9th Annual IFESS Conference*, pages 176–178. IFESS, 2004.

[38] T.W.J. Janssen, R.M. Glaser, and D.B. Shuster. Clinical efficacy of electrical stimulation exercise training: Effects on health, fitness and function. *Spinal Cord Inj. Rehab.*, 3(3):33–49, 1998.

[39] M. Kjaer, G. Perko, N.H. Secher, R. Boushel, N. Beyer, S. Pollack, A. Horn, A. Fernendes, T. Mohr, S.F. Lewis, and H. Galbo. Cardiovascular and ventilatory responses to electrically induced cycling with complete epidural anaesthesia in humans. *Acta. Physiol. Scand.*, 151:199–207, 1994.

[40] Frederic Martini. *Fundamentals of Anatomy and Physiology.* Pearson Education, 5^{th} edition, 2001.

[41] K. McLean, P. Jones, and J. Skinner. Exercise prescription for sitting and supine exercise in subjects with quadriplegia. *Med. and Sci. in Sports and Exercise*, 27(1):15–21, 1995.

[42] T.A. Perkins, N. de N. Donaldson, N.A.C. Hatcher, I.D. Swain, and D.E. Wood. Control of leg powered paraplegic cycling using stimulation of the lumbosacral; anterior spinal nerve roots. *IEEE Transactions on Neural Systems and Rehabilitation Engineering*, 10(3):158–164, 2002.

[43] J.S. Petrofsky. Blood pressure and heart rate response to isometric exercise: the effect of spinal cord injury in humans. *Eur. J. Appl. Physiol.*, 85:521–526, 2001.

[44] J.S. Petrofsky. New algorithm to control a cycle ergometer using electrical stimulation. *Med. Biol. Eng. Comput.*, 41:18–27, 2003.

[45] J.S. Petrofsky, H. Heaton, and C.A. Phillips. Outdoor bicycle for exercise in paraplegics and quadriplegics. *J. Biomed. Eng.*, 5:292–295, October 1983.

[46] J.S. Petrofsky, H.H. Heaton III, and C.A. Phillips. Leg exerciser for training of paralysed muscle by closed loop control. *Med. and Biol. Eng. and Comput.*. 22:298–303, 1984.

[47] J.S. Petrofsky, C.A. Phillips, H.H. Heaton, and R.M. Glaser. Bicycle ergometer for paralyzed muscle. *J. of Clinical Eng.*, 9(1):13–19, January 1984.

[48] J.S. Petrofsky and J. Smith. Three-wheeled cycle ergometer for use by men and women with paralysis. *Med. and Biol. Eng. and Comput.*, 30:364–369, 1992.

[49] J.S. Petrofsky and R. Stacy. The effect of training on endurance and cardiovascular responses of individuals with paraplegia during dynamic exercise induced by functional electrical stimulation. *Eur J. of Appl. Physiol.*, 64:487–492, 1991.

[50] J.S. Petrofsky, R. Stacy, and M. Laymon. The relationship between exercise work intervals and duration of exercise on lower extremity training induced by electrical stimulation in humans with spinal cord injuries. *Eur J. of Appl Physiol*, 82:504–509, 2000.

[51] C.A. Phillips, D. Danopulos, P. Kezdi, and D. Hendershot. Muscular, respiratory and cardiovascular responses of quadriplegic persons to a FES bicycle ergometer conditioning program. *Int. J. of Rehab. Res.*, 12(2):147–157, 1989.

[52] D.J. Pons, C.L. Vaugan, and G.G. Jaros. Cycling device powered by the electrically stimulated muscles of paraplegics. *Med. and Biol. Eng. and Computing*, 27, 1989.

[53] Dejan B Popovic and Thomas Sinkjaer. *Control of Movement for the Physically Disabled.* Centre for Sensory Motor Interaction Dept. of Health Science and Technology, 2^{nd} edition, 2003.

[54] S.K. Powers and E.T. Howley. *Exercise Physiology.* Wm. C. Brown, 1990.

[55] K.T. Ragnarsson, W. O'Daniel, J. Petrofsky, and M.S. Nash. Clinical evaluation of computerized functional electrical stimulation after spinal cord injury: A multicenter study. *Arch. Phys. Med. Rehabil.*, 69:672–677, September 1988.

[56] J. Raymond, G.M. Davis, M. Climstein, and J.R. Sutton. Cardiorespiratory responses to arm cranking and electrical stimulation leg cycling in people with paraplegia. *Med. and Sci. in Sports and Exercise*, 31(6):822–828, 1999.

[57] L.M. Schutte, M.M. Rodgers, and F.E. Zajac. Improving the efficacy of electrical stimulation induced leg cycle ergometry: An analysis based on a dynamic musculoskeletal model. *IEEE Transactions on Rehab. Eng.*, 1(2):109–124, 1993.

[58] U. Sekir, F. Ozyener, and H. Gur. Effect of time and day on the relationship between lactate and ventilatory thresholds: A brief report. *J. of Sports Science and Medicine*, 1:136–140, 2002.

[59] P.J. Sinclair, G.M. Davis, R.M. Smith, B.S. Chearn, and J.R. Sutton. Pedal forces produced during neuromuscular electrical stimulation cycling in paraplegics. *Clinical Biomechanics*, 11(1):51–57, 1996.

[60] M.L. Sipski, J.A. Delisa, and S. Schweer. Functional electrical stimulation bicycle ergometry. *Amer J. of Physical Medicine and Rehab.*, pages 147–149, 1989.

[61] K.J. Åstrom and B. Wittenmark. *Computer Controlled Systems - Theory and Design.* Prentice-Hall Inc., third edition, 1997.

[62] D. Tepavac and L. Schwirtlich. Detection and prediction of FES-induced fatigue. *J. of Electromyogr.*, 7(1):39–50, 1997.

[63] D. Thesian, C. Fornusek, J. Raymond, and G.M. Davis. External power output changes during prolonged cycling with electrical stimulation. *J. Rehabil. Med.*, 34:171–175, 2002.

[64] K. Wasserman, J.E. Hansen, D.Y. Sue, B.J. Whipp, and R. Casaburi. *Principles of exercise testing and interpretation.* Lea and Febiger, 2 edition, 1994.

The End (About Time)